Nuclear Science NEA/NSC/DOC(2001)13

Comparison Calculations for an Accelerator-driven Minor Actinide Burner

NUCLEAR ENERGY AGENCY
ORGANISATION FOR ECONOMIC CO-OPERATION AND DEVELOPMENT

ORGANISATION FOR ECONOMIC CO-OPERATION AND DEVELOPMENT

Pursuant to Article 1 of the Convention signed in Paris on 14th December 1960, and which came into force on 30th September 1961, the Organisation for Economic Co-operation and Development (OECD) shall promote policies designed:

- to achieve the highest sustainable economic growth and employment and a rising standard of living in Member countries, while maintaining financial stability, and thus to contribute to the development of the world economy;
- to contribute to sound economic expansion in Member as well as non-member countries in the process of economic development; and
- to contribute to the expansion of world trade on a multilateral, non-discriminatory basis in accordance with international obligations.

The original Member countries of the OECD are Austria, Belgium, Canada, Denmark, France, Germany, Greece, Iceland, Ireland, Italy, Luxembourg, the Netherlands, Norway, Portugal, Spain, Sweden, Switzerland, Turkey, the United Kingdom and the United States. The following countries became Members subsequently through accession at the dates indicated hereafter: Japan (28th April 1964), Finland (28th January 1969), Australia (7th June 1971), New Zealand (29th May 1973), Mexico (18th May 1994), the Czech Republic (21st December 1995), Hungary (7th May 1996), Poland (22nd November 1996), Korea (12th December 1996) and the Slovak Republic (14 December 2000). The Commission of the European Communities takes part in the work of the OECD (Article 13 of the OECD Convention).

NUCLEAR ENERGY AGENCY

The OECD Nuclear Energy Agency (NEA) was established on 1st February 1958 under the name of the OEEC European Nuclear Energy Agency. It received its present designation on 20th April 1972, when Japan became its first non-European full Member. NEA membership today consists of 27 OECD Member countries: Australia, Austria, Belgium, Canada, Czech Republic, Denmark, Finland, France, Germany, Greece, Hungary, Iceland, Ireland, Italy, Japan, Luxembourg, Mexico, the Netherlands, Norway, Portugal, Republic of Korea, Spain, Sweden, Switzerland, Turkey, the United Kingdom and the United States. The Commission of the European Communities also takes part in the work of the Agency.

The mission of the NEA is:

- to assist its Member countries in maintaining and further developing, through international co-operation, the scientific, technological and legal bases required for a safe, environmentally friendly and economical use of nuclear energy for peaceful purposes, as well as
- to provide authoritative assessments and to forge common understandings on key issues, as input to government decisions on nuclear energy policy and to broader OECD policy analyses in areas such as energy and sustainable development.

Specific areas of competence of the NEA include safety and regulation of nuclear activities, radioactive waste management, radiological protection, nuclear science, economic and technical analyses of the nuclear fuel cycle, nuclear law and liability, and public information. The NEA Data Bank provides nuclear data and computer program services for participating countries.

In these and related tasks, the NEA works in close collaboration with the International Atomic Energy Agency in Vienna, with which it has a Co-operation Agreement, as well as with other international organisations in the nuclear field.

© OECD 2002

Permission to reproduce a portion of this work for non-commercial purposes or classroom use should be obtained through the Centre français d'exploitation du droit de copie (CCF), 20, rue des Grands-Augustins, 75006 Paris, France, Tel. (33-1) 44 07 47 70, Fax (33-1) 46 34 67 19, for every country except the United States. In the United States permission should be obtained through the Copyright Clearance Center, Customer Service, (508)750-8400, 222 Rosewood Drive, Danvers, MA 01923, USA, or CCC Online: http://www.copyright.com/. All other applications for permission to reproduce or translate all or part of this book should be made to OECD Publications, 2, rue André-Pascal, 75775 Paris Cedex 16, France.

FOREWORD

Within the framework of the NEA Nuclear Science Committee, an international benchmark exercise for an accelerator-driven system was undertaken. The model chosen for the exercise was a lead-bismuth-cooled subcritical system driven by a beam of 1 GeV protons.

Except for the subassembly geometry, the design of the subcritical core was based on the advanced liquid metal reactor (ALMR) reference design of a sodium-cooled actinide burner. To reduce the high pumping power for the lead-bismuth coolant, the reference subassembly was replaced by a subassembly with a smaller number of pins, and the fission power of the system was proportionally reduced. Lead-bismuth was chosen as the target material to reflect the generally increased interest in this material for high-power spallation target applications.

An interesting role for accelerator-driven systems is to burn actinide waste from nuclear reactors using conventional fuel cycles. The benchmark reactor was therefore assumed to operate as a minor actinide burner in a "double strata" fuel cycle scheme, featuring a fully closed fuel cycle with a top-up of pure minor actinides. Two fuel compositions for a start-up and an equilibrium core were considered, both differing considerably from normal U-Pu mixed-oxide fuel compositions.

Seven organisations (ANL, CIEMAT, KAERI, PSI/CEA, JAERI, RIT and SCK•CEN) contributed to the benchmark exercise. The results were based on deterministic transport as well as Monte Carlo calculations using data from ENDF/B-VI, JENDL-3.2 and JEF-2.2. Significant differences in important neutronic parameters were observed, indicating a need for further investigation of the nuclear data as well as the calculation methods.

Acknowledgement

The Secretariat expresses its sincere gratitude to the participants who kindly devoted their time and effort to this benchmark exercise.

TABLE OF CONTENTS

EXECUTIVE SUMMARY

In nuclear power generation, the treatment of spent fuel produced during the operation of commercial power plants is one of the most important issues not only to the nuclear community but also to the general public. Complementary to the option of long-term geological disposal of spent fuel together with other nuclear waste is that of separating minor actinides (MA) and long-lived fission products from the spent fuel and transmuting them into short-lived or stable radionuclides in appropriate reactor systems for the reduction of the toxic potential into the nuclear waste stream. Various systems, such as existing reactors and fast reactors for minor actinide and fission-product transmutation, have been considered to optimise the transmutation scheme. Recently, many countries have shown interest in accelerator-driven systems because, in the future, these systems may play a role as efficient minor actinide and fission-product burners and/or as energy producers with an enhanced safety potential.

However, the current analysis methods for minor actinide and fission-product burners are not as well established as those for conventionally fuelled reactor systems. Recognising a need for code and data validation in this area, the NEA Nuclear Science Committee, through its Task Force on Transmutation, therefore initiated a first benchmark exercise in 1994. This exercise was based on a transmutation strategy involving light water reactors, fast reactors and an accelerator-driven system (ADS). The latter, a sodium-cooled system with a tungsten target and MA-Pu nitride fuel, was only analysed by three institutions (JAERI, PSI and IPPE). Considerable differences in calculated initial k_{eff} values and burn-up reactivity swings indicated a need for refining the benchmark specification and continuing the exercise with a wider participation.

The present benchmark was therefore launched in July 1999 to resolve the discrepancies observed in the previous exercise and to check the performances of reactor codes and nuclear data for ADS with unconventional fuel and coolant. The choice of lead-bismuth as a coolant and target material reflects the increased interest in this technology.

The ADS is designed to operate as a MA burner in a “double strata” strategy, featuring a fully closed fuel cycle with a top-up of pure MA. Two fuel compositions are prescribed in accordance with this strategy. In the start-up core, MAs are mixed with plutonium from UOX-fuelled LWRs. In the equilibrium core, the fuel represents an asymptotic composition reached after an indefinite number of cycles. Both fuel compositions differ strongly from the usual U-Pu mixed oxide (MOX) composition. The fuel is diluted with zirconium as an inert matrix for the core to give a k_{eff} of about 0.95 at BOL. Since the emphasis is on code and data validation in the energy region below 20 MeV, a predefined spallation neutron source, produced with HETC assuming a proton energy of 1 GeV and a beam radius of 10 cm, was provided to the participants.

Seven institutions (ANL, CIEMAT, KAERI, JAERI, PSI/CEA, RIT and SCK•CEN) have contributed to this exercise using different basic data libraries (ENDF/B-VI, JEF-2.2 and JENDL-3.2) and various reactor calculation methods. The analysis of the results shows significant discrepancies in important neutronic parameters such as one-group microscopic cross-sections, k_{inf}, initial k_{eff}, burn-up

reactivity swing, flux distribution and safety parameters. Strong discrepancies also appear in the estimation of the external neutron source, an important parameter for an ADS because it determines the requested accelerator power.

As demonstrated by a separate parametric study, the discrepancies are mainly due to deficiencies in the nuclear data of actinides which are abundant in minor actinide dominated cores but do not significantly influence the reaction rate balance of conventional MOX cores. However, the impact of the different nuclear data could not fully explain the discrepancies observed in the results. In future benchmark exercises, attention should therefore be paid to both the data processing route and the neutron transport approximations. Concerning the burn-up calculations, attention should be given to the treatment of the fission products and to the actinide decay chains, taking into account that minor actinide burner cores feature unusual fuel compositions.

The causes for many of these discrepancies still require clarification, and efforts in this direction should continue if the calculation tools are to be applied to detailed design calculations for minor actinide dominated ADS cores. A benchmark based on experimental results would be necessary to better understand the origin of discrepancies observed.

Chapter 1

INTRODUCTION

In nuclear power generation, the treatment of spent fuel produced during the operation of commercial power plants is one of the most important issues not only to the nuclear community but also to the general public. Complementary to the option of long-term geological disposal of spent fuel together with other nuclear waste is that of separating minor actinides (MA) and long-lived fission products from the spent fuel and transmuting them into short-lived or stable radionuclides in appropriate reactor systems for the reduction of the toxic potential into the nuclear waste stream. Various systems, such as existing reactors and fast reactors for minor actinide and fission-product transmutation, have been considered to optimise the transmutation scheme. Recently, many countries have shown interest in accelerator-driven systems because, in the future, these systems may play a role as efficient minor actinide and fission-product burners and/or as energy producers with an enhanced safety potential.

However, the current analysis methods for minor actinide and fission-product burners are not as well established as those for conventionally fuelled reactor systems. Recognising a need for code and data validation in this area, the NEA Nuclear Science Committee, through its Task Force on Transmutation, therefore initiated a first benchmark exercise in 1994. This exercise was based on a transmutation strategy involving light water reactors, fast reactors and an accelerator-driven system (ADS). The latter, a sodium-cooled system with a tungsten target and MA-Pu nitride fuel, was analysed by groups from JAERI, PSI and IPPE [1]. Considerable differences in calculated initial k_{eff} values and burn-up reactivity swings indicated a need for refining the benchmark specification and continuing the exercise with a wider participation [2,3].

The present benchmark model is designed to resolve the discrepancies observed in the benchmark exercise of the Task Force on Transmutation and, in general, to check the performance of reactor codes and nuclear data for accelerator-driven systems with unconventional fuels. The benchmark specification was distributed to participants in July 1999. With regard to the first objective, the model is similar to that used previously, except for the target and the coolant. The choices of a liquid metal target and lead-bismuth coolant reflect the generally increased interest in this technology. Since emphasis is on code and data validation in the energy region below 20 MeV, a standard spallation neutron source spectrum and distribution is prescribed.

As in the previous exercise, the ADS is assumed to be a component of a uranium-based advanced nuclear energy system with integrated partitioning and transmutation (P&T). In this context, an obvious role of the ADS is to burn minor actinides in the (fully closed) P&T cycle of a “double strata” fuel cycle scheme [4]. Fuel compositions for a start-up and an equilibrium core are specified in accordance with this strategy.

Seven institutions (ANL, CIEMAT, KAERI, JAERI, PSI/CEA, RIT and SCK•CEN) participated in the benchmark. The final results of these contributions are presented and analysed in this report. Preliminary results from six institutions were presented at the 2nd Workshop on Utilisation and Reliability of High Power Proton Accelerators held on 22-24 November 1999 in Aix-en-Provence, France [5]. To clarify the discrepancies observed in some parameters, a questionnaire on calculation methods and assumptions was circulated in mid-January 2000. In the following some results were revised and an additional solution by was included.

Chapter 2

BENCHMARK MODEL

The detailed benchmark specification can be found in Appendix A and thus only a brief description of the benchmark specification is given here. For the P&T cycle, the appropriate concept is a modular plant which allows the MA burning capacity to be adjusted flexibly to the requirements of the nuclear park. Considering that a MA burner supports some 15 to 17 energy producers of the same thermal power and burner cost-effectiveness is therefore not a primary issue, as the (relatively small) module of the 471 MW_{th} advanced liquid metal reactor (ALMR) reference system has an optimum size. Adopting this system as the basis for the benchmark calculations has the advantage that a detailed plant concept is available and the performance of the plant with normal cores has already been analysed in great detail, including transient and beyond design basis behaviour [6].

For the accelerator-driven ALMR core, a simplified R-Z model was prepared as shown in Figure 2.1. The model comprises a central lead-bismuth target zone, a void zone in the beam duct region, a multiplying region consisting of homogenised fuel and lead-bismuth coolant and an outer steel reflector zone. The core dimensions are those of the ALMR burner reference core. Reflector and radial shield materials consist of an average homogeneous mixture of HT-9 steel (70% by volume) and coolant (remainder). The target top position is a compromise: an optimisation with regard to the neutron source importance and the axial power distribution would give $z_T \cong 120$ cm; in the benchmark model, the target top was set to coincide with the top of the core (i.e. $z_T = 150$ cm) to reduce possible calculation uncertainties due to the presence of a void in the beam duct region.

To reduce the high pumping power for the lead-bismuth coolant, the coolant volume fraction of the subassembly was increased compared with that of the sodium-cooled subassembly. An adequate pitch-to-diameter ratio of 1.6 was achieved by replacing the reference 271-pin subassembly by a 217-pin subassembly. If the pin diameter is preserved, the thermal power reduces proportionally from the 471 MW_{th} of the reference system to 377 MW_{th} for the benchmark reactor.

As for the fuel, dense and non-moderating metals and nitrides are preferable because they improve the neutron economy of the system. Reprocessed by the “dry” technique, they are particularly suitable for the P&T cycle of the double strata concept. With a view to Japanese and French project preferences, nitride fuel was chosen for the benchmark reactor. The nitrogen is assumed to be pure ^{15}N.

Fuel compositions (and hence neutronic characteristics) of MA burner cores differ considerably from those of normal U-Pu mixed-oxide (MOX) cores and also between start-up and equilibrium cores. For determining the composition of the minor actinides transferred to the P&T cycle, the nuclear park was assumed to consist of a mix of uranium-fuelled LWRs (71%), MOX-fuelled LWRs (11%), and CAPRA-type fast reactors (18%) which burn the plutonium in a closed cycle after two recycles in the LWRs [7,8]. From this MA composition, start-up and equilibrium core compositions were determined as follows:

- For the start-up core, the minor actinides are mixed with plutonium from the uranium-fuelled LWRs using a fixed mixing ratio which gives a k_{eff} of about 0.95 at the beginning of life (BOL).

- For the equilibrium core (fully closed cycle with MA top-up or "feed"), the cycle averaged equilibrium composition was calculated directly using the algorithm described in Ref. [9], and a BOL correction based on an evolution calculation was applied.

Because an equilibrium core with undiluted fuel is too reactive, an actinide-zirconium mixture in the form of mononitrides is used. The actinide-to-zirconium ratio was set to give a k_{eff} of about 0.95 at BOL. This (fixed) actinide-to-zirconium ratio is also used for the start-up core. Diluting the actinides in an inert matrix has the additional benefit of reducing the activity of the irradiated fuel. The operating temperature of the fuel is 980 K. The target and reflector temperature is 650 K.

The fuel is assumed to be irradiated during five years at an average thermal power of 320 MW, corresponding to a load factor of 0.85; at the end of life (EOL), it reaches a burn-up of approximately 200 GWd/t_{HM}.

The spallation neutron source was produced with the PSI version of HETC assuming a proton energy of 1 GeV and a beam radius of 10 cm. To ensure consistence between different calculations, the participants were provided with a fine group source with lethargy width 0.1 and a collapsing program, developed by JAERI, which enables the user to produce broad group sources for different group structures.

From homogenous cell calculations, one-group fission and capture microscopic cross-sections, k_{inf}, B_c^2 and M^2 are requested. The requested results from reactor calculations are: reaction rate balance components for the fuel zone at BOL, axial and radial neutron flux distributions, neutron spectrum and reaction rate ratios relative to ^{239}Pu at the core centre, burn-up, k_{eff}, with and without fission products, source strength for five burn-up steps, fuel isotopic composition at EOL, coolant void and fuel Doppler reactivity effects at BOL and EOL, β_{eff} at BOL, etc.

Chapter 3

PARTICIPANTS, CODES AND DATA

Seven institutions participated in the benchmark. The complete list of participants, basic libraries and codes used are presented below and summarised in Table 3.1. Calculation details provided by the participants can be found in Appendix B.

1. ***ANL, USA***
   Participants: W.S. Yang and C.G. Stenberg
   Basic library: ENDF/B-VI and ENDF/B-V for lumped fission products
   Codes used: MC^2-2, TWODANT, REBUS-3

2. ***CIEMAT, Spain***
   Participants: M. Embid, J.M. García-Sanz, E. González, D. Cano-Ott and D. Villamarín
   Basic library: JENDL-3.2, EAF-3.1 (burn-up) and ENDF/B-VI (fission yields)
   Codes used: EVOLCODE system (NJOY, MCNP-4B and ORIGEN-2.1)

3. ***KAERI, Korea***
   Participants: Won Seok Park and Yong Nam Kim
   Basic library: JEF-2.2 and JENDL-3.2 for Pb_{nat} and ^{242m}Am
   Codes used: TRANSX-2.15, TWODANT, DIF3D-7.0 and REBUS-3
   Remarks: Diffusion approximation

4. ***PSI/CEA, Switzerland/France***
   Participants: M. Cometto (CEA/PSI), P. Wydler (PSI) and J-C. Bosq (CEA)
   Basic library: JEF-2.2 (ERALIB1 library)
   Codes used: ERANOS and ORIHET (activity and decay heat calculations)

5. ***JAERI, Japan***
   Participants: K. Nishihara, K. Tsujimoto, H. Takano
   Basic library: JENDL-3.2
   Codes used: ATRAS (SCALE, TWODANT, BURNER, ORIGEN-2)

6. ***RIT, Sweden***
   Participants: K. Tucek, J. Wallenius and W. Gudowski
   Basic library: JEF-2.2
   Codes used: NJOY, MCNP-4B, MCB (burn-up) ORIGEN-2

7. ***SCK•CEN, Belgium***
   Participants: H. Wienke, Ch. De Raedt, H. Ait Abderrahim, Th. Aoust and E. Malambu
   Basic library: JEF-2.2 (except for Pb and ^{233}U which are from ENDF/B-6)
   Codes used: NJOY97.95, MCNP-4B, ORIGEN-2, BATEMAN2

Chapter 4

RESULTS AND DISCUSSION

Originally, six institutions (ANL, CIEMAT, KAERI, JAERI, PSI/CEA and RIT) contributed preliminary results. The analysis of these revealed significant differences in important neutronic parameters such as initial k_{eff}, burn-up reactivity swings, safety parameters and flux distributions. The results were presented at the OECD/NEA Workshop on Utilisation and Reliability of High Power Proton Accelerators, in Aix-en-Provence, France, in November 1999 [5].

To clarify the origin of the discrepancies, a questionnaire on calculation methods and assumptions was distributed to the participants in mid-January 2000. The questionnaire is provided in Appendix C. Following the replies to the questionnaire, some results were revised. Table C.1 in Appendix C summarises the answers of the participants to the questionnaire. SCK•CEN joined in the benchmark activity afterwards.

Therefore, a total of seven final contributions are presented and analysed in this report.

Homogeneous cell calculations

One-group fission and capture microscopic cross-sections

The benchmark specification asked for one-group cross-sections produced by means of a cell code which calculates the fundamental mode neutron spectrum of the cell and averages the cross-sections with this spectrum. Two separate sets of values were requested, one for the start-up core and one for the equilibrium core. Whereas ANL, KAERI and PSI/CEA performed the fundamental mode cell calculations, the other organisations derived one-group microscopic cross-sections from the reactor calculations. The latter cross-sections represent averages over the core fuel zone and, therefore, differ from those obtained from cell calculations. PSI/CEA carried out an additional calculation to derive the core-averaged cross-sections for comparison, and SCK•CEN submitted a second series of cross-sections obtained from a Monte Carlo calculation for a homogeneous critical sphere. The results, including the complementary results from PSI/CEA and SCK•CEN, are presented in Tables 4.1.1 to 4.1.6 and plotted in Figures 4.1.1 to 4.1.16.

The cross-sections show some correlation with the basic data used. The results reported by CIEMAT and JAERI using JENDL-3.2 can easily be compared because both refer to a core calculation; their results are very close for both capture and fission cross-sections. When analysing JEF-based results, it should be taken into account that KAERI and RIT results cannot be directly compared because of the difference in the averaging method. Furthermore, the JEF library used by KAERI includes Pb_{nat} and ^{242m}Am data from JENDL, and the ERALIB1 library used by PSI/CEA has been adjusted from the original JEF-2.2 data. Comparing the JEF-based cross-sections obtained by an average over the core, RIT and SCK•CEN results are in very good agreement, but deviate from the PSI/CEA result by more than 5% for the majority of the isotopes. The JEF-based cross-sections obtained from a cell calculation show a less clear trend: KAERI and PSI/CEA values are close for U,

the majority of Cm isotopes and for the captures of ^{237}Np, ^{238}Pu, ^{239}Pu, ^{241}Am, ^{243}Am, whereas the SCK•CEN values are considerably different. In other cases (^{240}Pu, ^{242}Pu, fission cross-sections of ^{237}Np, ^{238}Pu, ^{241}Am and ^{243}Am) SCK•CEN and PSI/CEA results are closer, but different from those submitted by KAERI.

In order to investigate the differences between the one-group cross-sections obtained from the fundamental mode cell calculation and those averaged over the whole core, the two series of results provided by PSI/CEA and SCK•CEN for the equilibrium core are compared in Figures 4.1.17 to 4.1.20. Both PSI/CEA and SCK•CEN show the same trends: the capture cross-sections of all isotopes and the fission cross-sections of fissile nuclides are always larger when condensed with the core-averaged spectrum. However, the fission cross-sections of fertile nuclides show an opposite trend. This indicates that the spectrum in the core is softer than that in the cell. The differences due to the averaging methods are between 4.5% and 13% for the one-group capture cross-sections and between -6% and 5% for the one-group fission cross-sections, indicating that the comparison of the cross-sections obtained with different averaging methods require caution.

Nevertheless, the following comments concerning individual actinides can be made:

- Uranium cross-sections are found to be in good agreement except for some differences in the capture cross-sections of ^{234}U and ^{236}U.

- For neptunium, a maximum difference of 13% in the ^{237}Np capture cross-section and very large differences in ^{238}Np capture and fission cross-sections are found. Due to the low concentration of ^{238}Np in the fuel, however, cross-sections for this nuclide do not significantly influence the reaction rate balance of the core.

- Plutonium exhibits differences particularly in the capture cross-sections, ENDF/B-VI giving the highest value for the isotope 238 (+25% relative to JENDL and +48% relative to JEF) and always the lowest values for the other isotopes. JEF-2.2 and JENDL-3.2 capture cross-sections are closer, but there are systematic discrepancies for the isotopes 238 (JENDL 17% above JEF) and 241 (JEF 14% above JENDL).

- For americium, significant differences in capture cross-sections are found for all isotopes, ENDF/B-VI giving lower values than JENDL-3.2 for the isotopes 241 (-12%), 242m (-40%) and 243 (-16%), and JEF-2.2 giving consistently higher values than JENDL for the isotopes 241 (+10%) and 243 (+6%). A striking feature is the high ENDF ratio for fission-to-capture in ^{242m}Am which exceeds the respective ratio derived from the other libraries by a factor of two.

- Considerable deviations of ENDF/B-VI from the other libraries can also be noticed for curium, especially for ^{242}Cm (capture two times and fission more than three times smaller). Relative to JENDL-3.2, the ^{244}Cm capture cross-section is large for ENDF (+15%) and small for JEF (-28%); for all other isotopes, JENDL gives consistently the highest capture cross-section.

Infinite multiplication factor (k_{inf}), buckling and migration area

The results of k_{inf}, critical buckling and migration area are presented in Table 4.2.

ANL, PSI/CEA, KAERI and JAERI obtained k_{inf} by a cell calculation and the other three participants by a separate Monte Carlo calculation for the fuel zone with reflective boundary conditions.

The k_{inf} results show a considerable spread: the difference between the highest and the lowest values is about 2.5% for the start-up core and about 3% for the equilibrium core. No clear correlation with the cross-sections used can be observed. Significant discrepancies are observed between the two JENDL-based results (about 2.0%). The four JEF-based results can be grouped into two classes characterised by high (RIT and SCK•CEN) and low (PSI/CEA and KAERI) k_{inf} values. Another interesting effect is that JEF predicts similar k_{inf} values for both core configurations, whereas ENDF and JENDL predict a k_{inf} difference of about 1.5% between the start-up and the equilibrium cores.

Only four participants provided the results of the critical buckling and migration area. The results are rather discrepant depending on k_{inf} and the transport cross-section calculated.

Reactor calculations

Tables 4.3.1 and 4.3.2 summarise the main results of the reactor calculations for the start-up and the equilibrium core. Before discussing these results, it is necessary to dwell on the reactor calculation methods used by the participants. In evaluating the nuclear power, ANL, PSI/CEA, CIEMAT and KAERI took into account the energy coming from both fission and neutron capture, JAERI and SCK•CEN considered only the energy coming from fission and RIT neglected both the energy from capture and from delayed gamma. An additional calculation performed by PSI/CEA using ERANOS shows that the neutron capture contribution to the total power is about 4%; RIT estimates that the energy coming from capture and from the delayed gamma together is about 9% of the total.

Neglecting some reactions in the power calculation increases the absolute value of the neutron flux (which is normalised to a total power of 377 MW) and hence affects reaction rates, neutron flux distributions and burn-up calculations. It is easy to appropriately scale the results for the BOL cores; however it is more difficult to estimate the impact of the flux-to-the-power adjustment on the results involving a burn-up calculation, as the k_{eff} variation and the isotopic composition at EOL.

k_{eff} at beginning of life

For the k_{eff} of the start-up core at beginning of life, RIT provided in addition to the JEF-2.2 value an ENDF and a JENDL value.

The k_{eff} at beginning of life (Tables 4.3.1 and 4.3.2) show a maximum discrepancy of 4% for the start-up core; the spread in the k_{eff} values is slightly reduced for the equilibrium core. The k_{eff} values do not show a clear correlation with the library used, indicating that the sensitivity of the results to the data processing route and/or the neutron transport approximation should also be investigated. Relatively large k_{eff} differences of more than 1% arise in the two ENDF/B-VI calculations and a maximum of 0.8% is observed between the three JENDL-3.2 based results. The multiplication factors calculated with JEF-2.2 and MCNP (RIT and SCK•CEN) agree well, but exceed the JEF-based values from KAERI and PSI/CEA by about 1.0%. However, interpreting these results is difficult, because only RIT used a pure JEF-2.2 library. PSI/CEA used the adjusted ERALIB1 library and KAERI and SCK•CEN used lead data from JENDL and ENDF, respectively.

KAERI performed a systematic sensitivity analysis for the start-up core in order to assess the impact of the nuclear data for the important actinides, lead, bismuth and nitrogen on k_{eff} values and reaction rates. For this purpose, the code ONEDANT (P_3 and S_8 approximation) was applied to a one-dimensional spherical core model which preserves the volume of the 2-D R-Z model. The library ENDF/B-VI was used for all nuclides as the reference, and JEF-2.2 and JENDL-3.2 cross-sections

were generated for actinides and other important nuclides. NJOY was used to produce 175-group (Vitamin-J) cross-sections in MATXS-format. The sensitivities were examined by exchanging the isotopes one after another.

Table 4.4 summarises the results for k_{eff}, and the complete set of results can be found in Appendix D. Taking the ENDF-based k_{eff} as the reference, the substitution of Np, Am, ^{239}Pu and ^{240}Pu isotopes JEF or JENDL always has a negative effect, while the substitution of ^{238}Pu and Cm isotopes results in a positive effect. The absolute differences in k_{eff} when exchanging all the actinides sum to more than 4 000 pcm for JEF and 2 000 pcm for JENDL; however, due to the compensation of positive and negative effects, the total differences in k_{eff} reduce to 2 250 pcm for JEF and 1 160 pcm for JENDL. The substitution of ^{15}N from JEF and JENDL decreases the reference k_{eff} by 423 and 450 pcm, respectively. Similar sensitivities for JEF and JENDL are also obtained when replacing the bismuth nuclear data: the k_{eff} decreases by approximately 75 pcm. The biggest discrepancies between libraries arise from the lead data: the k_{eff} changes are +680 pcm for JEF and -1 108 pcm for JENDL. The effect of all nuclides together is about -2 070 pcm for JEF and -2 800 pcm for JENDL. For JEF and JENDL, the largest contributions arise from heavy metals, lead and ^{15}N while the contribution of bismuth is smaller.

In a contribution to the 1999 Winter Meeting of the ANS, W.S. Yang, *et al*. reported a strong dependence of k_{eff} on lead and bismuth cross-sections, substitution of JENDL-3.2 data for lead and bismuth reducing k_{eff} by about 1.0% [10]. It is interesting to note that the JEF library used by KAERI contains lead data from JENDL, and that the k_{eff} difference between KAERI and RIT/SCK•CEN agrees with the bias observed by Yang. A sensitivity calculation showed that the adjustments in ERALIB1 lower k_{eff} by 0.3% and are therefore not sufficient to explain the deviation of the k_{eff} calculated by PSI/CEA.

Complementary information can be obtained by comparing the three RIT values for the k_{eff} of the start-up core. The highest k_{eff} is obtained with ENDF data; the values obtained with JEF and JENDL data are 3.9% and 3.5% lower. For JEF, the difference is bigger than that predicted by the sensitivity analysis of KAERI.

The multiplication factors for the start-up and the equilibrium core do not exhibit consistent biases. This can be explained by the fact that the reaction rates in the two cores are not dominated by the same producers and absorbers (see Figures 4.6.3 to 4.6.6). The reaction rate balances show that the neutron production is dominated by ^{239}Pu (about 40% of the total production) in the start-up core, and by ^{238}Pu (about 25% of the total production) in the equilibrium core. The most important absorber is ^{241}Am, followed by ^{239}Pu and ^{243}Am in the start-up core, and by ^{243}Am and ^{238}Pu in the equilibrium core. The unusual reaction rate balance of the equilibrium core means that the neutronic characteristics of this core are sensitive to nuclear data that do not play an important role in normal MOX-fuelled cores.

The reduction in the spread of initial k_{eff} values arising from the substitution of the more conventional start-up by the unusual equilibrium core must be due to compensation effects. It appears that, thanks to these compensation effects, the move from a start-up core to an equilibrium core does not introduce additional uncertainties in the multiplication factor.

k_{eff} variation with burn-up

The k_{eff} variations with burn-up are shown in Figures 4.2.1 and 4.2.2, and the respective burn-up reactivity drops, k_{BOC}-k_{EOC}, including decompositions of the global reactivity drop into actinide and fission product components, are given in Table 4.5.

The burn-up reactivity drop, k_{BOC}-k_{EOC}, ranges from 0.036 to 0.069 in the start-up core, and from -0.004 to 0.036 in the equilibrium core, ANL predicting, in both cases, by far the highest reactivity drop. For the start-up core, CIEMAT, KAERI, JAERI, RIT (JEF) and SCK•CEN calculate similar values between 3 900 and 4 100 pcm, but this is due to compensating effects between fission product and heavy metal contributions and is, therefore, fortuitous. The results are more spread out for the equilibrium core.

Three of the four JEF-based actinide components of the burn-up reactivity drop are consistent; otherwise neither the actinide nor the fission-product components are well correlated with the data library used. It is important to note that three participants (CIEMAT, RIT and SCK•CEN) used explicitly represented fission products whereas all the other participants used lumped fission products. PSI/CEA used lumped fission products representing only solid nuclides. The impact of the different fission-product treatments was examined by PSI/CEA for the equilibrium core. Using lumped fission products that include solid and gaseous isotopes increases the reactivity drop due to the fission products by 440 pcm or about 10%.

Possible causes of the discrepancies observed in the reactivity drops are differences in the actinide burn-up chains and the treatment of fission products (fission-product chains, lumped fission products and fission yields); they should be investigated thoroughly. It is, for example, questionable whether lumped fission products generated from U and Pu are representative for a system where a non-negligible fraction of the fission (about 30% in the start-up core and about 40% in the equilibrium core) arises from minor actinides with a higher mass number such as Am and Cm. However, no obvious correlation related to the use of individual or lumped fission products can be observed.

The spectrum change and possible variation of the power during burn-up are other potential causes of discrepancies in the reactivity loss per cycle and the power shapes. As demonstrated in a sensitivity study by RIT, significant differences in burn-up reactivity drop arise from inadequate choices of the burn-up interval after which the neutron spectrum is recalculated and/or the power re-normalised (Figure 4.2.3): 73 day steps give a steeper reactivity loss than 1 year steps ($39 \cdot 10^3$ Δk against $22 \cdot 10^3$ Δk).

Neutron spectrum

The participants provided the neutron spectrum for both the start-up and the equilibrium cores at R = 56 cm and Z = 100 cm; this point corresponds to the centre of the fuel region where the neutron spectrum is dominated by fission neutrons.

Neutron spectra per unit lethargy are presented in Figures 4.3.1 to 4.3.4. The spectra are normalised to a total flux of 1. The “hardness” of the spectrum may be characterised by its median energy. From the submitted neutron spectra, median energies have therefore been calculated. The median energies, shown in Tables 4.3.1 and 4.3.2, indicate that the spectrum in the equilibrium core is always softer than that in the start-up core, and that, for both cores, the spectra are in good agreement except for the JAERI spectrum which is clearly softer. For the start-up core, the median energy of the KAERI, RIT and SCK•CEN spectra is only about 4% higher than that of ANL, CIEMAT and PSI/CEA spectra. For the equilibrium core the highest values are those of the CIEMAT, RIT and ANL spectra; the values for the PSI/CEA, SCK•CEN and KAERI spectra are about 3% lower. For both cores the median energy of the JAERI spectrum is about 20% lower then that of the other spectra.

A comparison of the spectra themselves is more difficult because the participants used different group structures; however the spectra of KAERI, RIT, ANL, CIEMAT, PSI/CEA and SCK•CEN are in good agreement especially in the energy range above 5-10 keV which covers approximately 95% of

the neutrons. Only in the lower resonance region (between 100 eV and 1 keV) do the differences between the results become pronounced. The fraction of neutrons in this energy range is larger for PSI/CEA, JAERI and CIEMAT than for ANL, RIT and SCK•CEN.

Neutron flux distributions

One radial neutron flux distribution corresponding to the mid-plane (Z = 100 cm) and two axial flux distributions corresponding respectively to the centre of the target and the fuel zone (R = 0 and 56 cm) were requested. The neutron flux distributions had to be normalised to the maximum reactor power of 377 MW. The results are compared in Figures 4.4.1 to 4.4.6.

Except for two calculations which feature very low (ANL) and very high (KAERI) target fluxes, the radial flux distributions in the start-up core are in reasonable agreement. In the equilibrium core, the flux distributions are more spread and the ANL and KAERI distributions deviate less from the others.

The axial flux distribution along the target shows particularly large discrepancies, the ENDF-based results (ANL and RIT) giving by far the lowest neutron flux. The other results are closer, but the differences are nevertheless significant. Other big discrepancies arise when analysing the shape of the flux distributions: the CIEMAT result shows a distinct shape in the lowest part of the target region and the KAERI result has a vanishing flux in the zone corresponding to the duct (void region). The shape reported from CIEMAT can be explained by the fact that they used a symmetric geometry model in which the lowest part of the target (first 50 cm) was replaced by a void region. Therefore, the leakage increases and the neutron flux gradient is steeper. The shape obtained by KAERI is probably due to the diffusion approximation not being valid in the duct.

In the axial flux distributions in the fuel zone, differences in flux levels and peak flux positions appear; the PSI/CEA result shows the lowest and RIT (JEF) the highest flux. In the latter case, no correlation with the library used can be observed.

The discrepancies in the flux distributions can partially be explained by different subcriticality levels. A system with a lower k_{eff} needs more external neutrons in order to maintain the chain reaction, and this results in:

- More peaked radial and axial flux distributions in the centre of the reactor (target region).
- A displacement of the peak of the axial neutron flux in the fuel region towards the upper part of the core.

The effects are particularly important for the ENDF-based flux distributions which correspond to a significantly higher k_{eff} and therefore a much smaller number of spallation neutrons than the other solutions. For example, in the start-up core the total number of spallation neutrons of the ANL solution is only about 27% of that of the PSI/CEA solution.

In the axial flux distributions at R = 56 cm the effect is mitigated since most of the neutrons in this region come from fission reactions. However, at R = 0 cm, the ANL flux level is much lower than the others. For the same reason, the radial distribution of ANL is the lowest in the centre region.

The RIT flux distributions in the equilibrium core, which are also based on ENDF/B-VI, show behaviour similar to that of the ANL distributions. The fact that the ratios of RIT fluxes to ANL fluxes are fairly constant (about 1.2) indicates that the differences between the two distributions are mainly due to the different power normalisation.

Additional ERANOS calculations for the equilibrium core were performed by PSI/CEA to quantitatively assess the impact of the subcriticality on the neutron flux distribution. By modifying the ν values to reproduce the k_{eff} values submitted by the participants, k_{eff}-dependent ERANOS neutron flux distributions were calculated. From these distributions, spatially dependent correction factors were obtained. Finally, the neutron flux distributions supplied by the participants were adjusted to the reference k_{eff} value of 0.95 using the spatially dependent correction factors. The adjusted neutron flux distributions are presented in Figures 4.4.7 to 4.4.9.

In the fuel region, the shape of the axial neutron flux distributions is now in good agreement for most participants. However, the peak position reported by KAERI is shifted to the core centre (Z = 100 cm). The spread in the absolute value of the flux is still significant and the difference between the highest and the lowest value (obtained by RIT and PSI/CEA respectively) is about 20%. As expected, the discrepancies of the axial neutron distributions in the target region become considerably smaller after the adjustment. The shapes of the flux distributions have a similar trend and the values are less spread. Similar observations apply to the radial neutron flux distribution corresponding to the mid-plane. It is interesting to note that, after the k_{eff} adjustment, the neutron flux distributions evaluated by PSI/CEA and ANL become very close.

As to the flux-to-power normalisation mentioned earlier, the neutron flux values provided by RIT, SCK•CEN and JAERI are overestimated relative to the other participants and should be reduced by 9%, 4% and 4%, respectively.

Even after the k_{eff} and the flux-to-power adjustment there still remain discrepancies in both the absolute value of the flux and its shape. Large discrepancies are observed in the shape of the axial flux in the target calculated by CIEMAT and KAERI. The CIEMAT result for the equilibrium core shows a unique radial distribution within the target region, with a local minimum at R = 0. The KAERI result exhibits a particular trend for the radial flux at the interface between the target and fuel region, and the peak position of the axial flux in the fuel is shifted to the core centre in comparison with the other results. Finally, the RIT result with ENDF data exhibits a “reflector effect” at the interface between fuel and reflector (radial distribution) and features that are not understood in axial distributions along target and fuel regions, neither of which are present in the JEF-based results.

Burn-up

Unexpected discrepancies arise between burn-up values as a function of irradiation time (Tables 4.3.1 and 4.3.2). The burn-up, defined as the total energy released from the fuel divided by the mass of heavy metal at BOL, can be directly derived from the specification using the given thermal power and irradiation time and the calculated burn-up was expected to be close.

For the start-up core, four participants (CIEMAT, KAERI, PSI/CEA and RIT) quoted the value of 185.7 GWd/t_{HM}. The value obtained by JAERI is slightly higher (+0.9%), and the value provided by ANL is considerably lower (-5.5%). The values supplied for the equilibrium core are close to those of the start-up cores with the exception that RIT reports a burn-up of 193.7 GWd/t_{HM}, i.e. +4% compared with the start-up core.

In the ANL case, the burn-up value in the table only considers the energy released by fission. However, in the flux normalisation and in the depletion calculation the energy released from radioactive capture was correctly included. ANL estimated that about 94.8% of the total power was due to the fission, thus explaining the above deviation of -5.5%.

It should be noted that some codes could not compute the total thermal energy release. In these cases, the burn-up was derived from the specified thermal power and irradiation time.

Another important aspect concerning the burn-up calculation is that some calculation routes cannot perform burn-up calculations at constant power but use a constant flux. In these cases, the burn-up depends on the number of time steps between the flux re-normalisation and on the method used to simulate a constant power depletion.

Source strength

The source strength, i.e. the number of neutrons per second that the subcritical reactor needs to maintain the chain reaction, is an important parameter in an ADS calculation because it is directly proportional to the required accelerator power. Its value is given by the following equation [11]:

$$N = \frac{P_{th} \cdot \nu_k}{E_f} \cdot \left(\frac{1}{k} - 1 \right) \cdot \frac{1}{\varphi^*}$$

where N is the number of neutrons/s, P_{th} the thermal power, ν_k and E_f the averaged number of neutrons and the averaged energy released per fission in the fuel, k the multiplication factor of the system without source and φ^* the importance of spallation neutrons relative to fission neutrons. The variations of the spallation neutrons with the burn-up are showed in Figures 4.5.1 and 4.5.2.

The neutron source strengths at BOL and EOL presented in Tables 4.3.1 and 4.3.2 show quite a spread. At BOL, the ratio between the highest and the lowest values is about 7 for the start-up core and 3 for the equilibrium core. Consistent with the k_{eff} values, ANL predicts the lowest value at BOL. KAERI predicts by far the highest value for both start-up and equilibrium core. The other three JEF-based results lie in a similar range (maximum difference of about 10%) and the two JENDL-based results show a difference of about 30% for both core configurations. A correlation with the libraries can be observed: JEF predicts the highest number of spallation neutrons, followed by JENDL and ENDF.

As the above equation indicates, the required number of spallation neutrons is strongly dependent on the multiplication factor of the subcritical system. It may be interesting to isolate that effect by dividing the source strength value by $(1/k - 1)$, in order to remove the differences due to the multiplication factor (keeping in mind that φ^* is also dependent on k). The numerical value obtained in this way is dependent only on P_{th}, E_f, ν_k and φ^*, and the results should be closer. The k_{eff}-corrected neutron source strengths for the start-up core are presented in Figure 4.5.3.

Surprisingly, the values obtained are quite discrepant, KAERI presenting by far the highest value, and the correlation between the three other JEF-based results turns out to be fortuitous. RIT and SCK•CEN results are closer and the PSI/CEA value is similar to that obtained by ANL. The two JENDL-based results lie in a similar range. The ratio between the highest and the lowest values is about 2 and is too big to be explained only by differences in libraries and calculation methods.

Reaction rate balance components

The production and absorption reaction rates at BOL were reported for the fuel zone and for a total power of 377 MW. The absorption reaction rates take into account only the capture and fission contributions and the production reaction rates refer only to the neutrons from fission; no correction for (n,Xn) reaction is made. The results are given in Tables 4.6.1 to 4.6.6.

From the reaction rates provided by the participants for both core configurations, the total production and absorption reaction rates are computed by summing the contributions of all heavy nuclides and the production-to-absorption (P/A) ratio is also calculated. The P/A values are given in Tables 4.3.1 and 4.3.2, and the total reaction rates and the P/A ratios are presented in Figures 4.6.1 and 4.6.2.

The results for the total production and absorption reaction rates can be grouped in three classes characterised by high (RIT, SCK•CEN and JAERI), medium (ANL and PSI/CEA) and low values (KAERI and CIEMAT). The difference between these classes is significant. The capture and the production rates estimated by the first group exceed the ones calculated by the second group by 10-15% (RIT and JAERI) and 6-7% (SCK•CEN), and the results provided by KAERI and CIEMAT are always between 9-14% lower then those provided by ANL and PSI/CEA. According to different normalisations of the neutron flux to the power, discussed earlier, the reaction rates provided by RIT, JAERI and SCK•CEN should be reduced by about 9% (RIT) and 4% (JAERI and SCK•CEN). This would reduce the differences among the results.

The P/A ratios are not sensitive to different normalisations of the neutron flux. ANL (ENDF) predicts by far the highest P/A ratios for both core configurations, whereas the other results are closely grouped. The two JENDL-based results are similar and, among the four JEF-based results, SCK•CEN gives the highest value and RIT the lowest value for both core configurations. The P/A in the start-up and the equilibrium core are similar for ENDF and JENDL. However, JEF gives systematically larger values (+2.5%) for the equilibrium core than for the start-up core. Interestingly, the k_{eff} values are not correlated in a systematic way with the P/A ratios as one would expect. In particular, all four JEF-based results give a lower P/A ratio but a higher k_{eff} in the start-up core. ANL, CIEMAT and JAERI calculated similar P/A values but different multiplication factors for both cores.

The two cores are not dominated by the same producers and absorbers, as seen in Figures 4.6.3 to 4.6.6. The majority of fission neutrons come from ^{239}Pu, ^{241}Pu and ^{241}Am in the start-up core and from ^{238}Pu, ^{245}Cm, ^{240}Pu and ^{244}Cm in the equilibrium core. The majority of absorptions are due to ^{241}Am, ^{239}Pu and ^{243}Am (about 28%, 20% and 17%, respectively) in the start-up core, and to ^{241}Am, ^{243}Am and ^{238}Pu (about 20%, 15% and 15%) in the equilibrium core.

Figures 4.6.7 to 4.6.10 present reaction rates per nuclide normalised to the total reaction rate. There is a strong correlation with the nuclear data for the absorption rates but not for the production rates. For JENDL, the absorption reaction rates are in good agreement, the maximum difference being always less than 1% for all the important nuclides. Interestingly this is not the case for the production reaction rates for which the differences are pronounced. For JEF both absorption and production rates are very close, taking into account that the JEF library used by KAERI includes ^{242m}Am from JENDL, and that the ERALIB1 library used by PSI/CEA has been adjusted, especially for Pu isotopes.

As already noted when analysing the microscopic cross-sections, there are large discrepancies for some important isotopes. The ^{238}Pu and ^{244}Cm absorption rates calculated with ENDF data are considerably higher than JEF-based (+25% and +30% respectively) and JENDL-based absorption rates (+15% for both nuclides). The JEF-based absorption rates for ^{241}Am and ^{243}Am are larger than those obtained from ENDF (+12% for both) and JENDL (+8% and +6%). Compared with the other results, JENDL predicts a higher ^{237}Np absorption rates for the equilibrium core (+6%).

It is interesting to note that the normalised production rates for the two JENDL solutions differ considerably, although the respective one-group fission cross-sections are in good agreement.

Reaction rate ratios relative to ^{239}Pu fission

The reaction rate ratios relative to ^{239}Pu fission are presented in Table 4.7.1 (start-up core) and in Table 4.7.2 (equilibrium core) and in Figures 4.7.1 to 4.7.4. In general, the ratios for capture are more discrepant than those for fission. The agreement among the results is better for the start-up core than for the equilibrium core.

With regard to fission ratios, all four JEF-based results generally show a good agreement whereas the discrepancies between the two JENDL-based fission ratio results are quite large. Compared to the JAERI results, CIEMAT obtains higher fission rate ratios for most isotopes (between +5% and +17%) and lower fission rate ratios for ^{241}Pu, ^{242m}Am, ^{243}Cm and ^{245}Cm (between -3% and -4%) in the start-up core. A similar trend is observed in the equilibrium core. The CIEMAT results are more consistent with those obtained using JEF data, except for ^{242}Cm (20%). These discrepancies are probably related to the softer spectrum calculated by JAERI.

In comparison with the results obtained with JENDL or JEF data, ANL ENDF-based results report higher fission ratios in both cores for ^{242m}Am and ^{243}Am (between 10% and 20%) and lower fission ratios for ^{242}Cm, ^{243}Cm and ^{245}Cm. Large discrepancies are observed for ^{238}Np in the equilibrium core: the ANL value is 9 times smaller than those reported by PSI/CEA, RIT and SCK•CEN and is five times smaller than those obtained by CIEMAT, JAERI and KAERI.

Concerning capture ratios, the difference between the two JENDL-based results are pronounced in both cores (more than 6% for all isotopes). The agreement among the four JEF-based results is good for most nuclides (less than 6%) except for ^{243}Cm (10%) and the Pu isotopes (up to 20%), for which the PSI/CEA results deviate from the others. The ^{238}Np capture ratio reported by KAERI is similar to the value from CIEMAT, i.e. 140% larger than that from other JEF-based results. Large discrepancies between JEF- and JENDL-based results are observed, especially for ^{234}U, ^{236}U, ^{238}Pu, ^{240}Pu and Cm isotopes. ANL ENDF-based results are closer to the JEF-based results for ^{234}U, ^{235}U, ^{237}Np, ^{240}Pu, ^{242}Pu and Cm isotopes (except for ^{244}Cm) whereas they differ strongly from both JEF and JENDL results for the ^{238}Pu, ^{241}Pu, ^{244}Cm and all Am isotopes.

Isotopic composition at EOL

The isotopic composition at EOL for both the start-up and the equilibrium core are given in Tables 4.8.1 and 4.8.2, respectively. Significant discrepancies in the results are observed. The results are only partially correlated with the nuclear data libraries used.

Before discussing the isotopic composition of the irradiated fuel, it is interesting to compare the fractions of heavy metal that fissioned during the five years of irradiation. Surprisingly these fractions are strongly different and can be grouped into two classes characterised by a high “burn-up” (KAERI, RIT and SCK•CEN, all using the JEF library) and a low “burn-up”. For the start-up core, the high values are between 21.3% (RIT) and 22.0% (SCK•CEN) and the low values between 18.5% (PSI/CEA) and 18.8% (ANL). Similar observations apply to the equilibrium core. The difference in the “burn-up” between the two “classes” is large (more than 15%) and cannot be fully understood.

As mentioned earlier, the differences in power calculation have consequences on the fraction of heavy metal that fissioned. RIT, JAERI and SCK•CEN did not take into account some reactions when calculating the power and therefore they obtained higher neutron fluxes and higher reaction rates which increase the fraction of fissioned heavy metals. The magnitude of this effect (about 9% for RIT and 4% for SCK•CEN and JAERI), however, is not sufficient to explain the discrepancies observed in the total concentration of heavy nuclides at EOL.

The nuclide densities at EOL reported by the participants are plotted in Figures 4.8.1 to 4.8.2 together with the prescribed densities at BOL. As expected, a strong dependence of the isotopic composition on the "burn-up" is observed. In comparison with the other participants, RIT, JAERI and SCK•CEN (high burn-up) report lower densities for burnt isotopes, such as ^{237}Np, ^{239}Pu, ^{241}Pu, ^{241}Am and ^{243}Am and higher densities for built-up isotopes, such as ^{238}Pu, ^{242}Cm and ^{244}Cm.

The analysis of the uranium composition at EOL shows a different trend for the two cores. The discrepancies are considerably higher in the start-up than those in the equilibrium core. In the start-up core, SCK•CEN and KAERI obtained a significantly lower concentration of ^{236}U at EOL compared to that obtained by the other participants (the values are about 6 and 16 times smaller). Interestingly, SCK•CEN gives a very low ^{235}U concentration (-25% compared to the average of all the participants), whereas KAERI reports a high concentration of this isotope (+13%). When considering the equilibrium core, the results provided by SCK•CEN and KAERI are closer to the other results except for ^{236}U, for which KAERI obtains a value that is 15% above the average. These discrepancies may be due to a different treatment of the (n,2n) reaction for ^{237}Np which generates ^{236}U. In the start-up core, the uranium is not present at BOL and the majority of ^{236}U is therefore generated from Np, whereas in the equilibrium core the concentration of uranium at BOL is significant and the production of ^{235}U and ^{236}U is mainly due to the capture reactions in ^{234}U and ^{235}U (the capture reaction rates at BOL for the equilibrium core were found to be in a good agreement).

The differences for ^{237}Np are similar for both cores. The maximum deviation from the average is about 6%. Higher discrepancies arise for the plutonium compositions at EOL. In particular the values for ^{238}Pu show a considerable spread, SCK•CEN and ANL reporting the extreme values (+10% and -9.5% relative to the average for the equilibrium core). The results for the two other fertile isotopes, ^{240}Pu and ^{242}Pu, are more closely grouped, with the exception of SCK•CEN which predicts far lower values (-15% and -26% respectively in the start-up core).

The densities of the fertile Am isotopes show a correlation with the cross-section data used, ENDF and JEF giving the highest and the lowest concentrations, respectively. Some discrepancies in the results are related to differences in branching ratios or to a different treatment of some reactions. For example, the differences observed in the ^{242m}Am and ^{242}Cm concentrations are due to discrepancies in the branching ratios for the (n,γ) reaction of ^{241}Am. Most participants used the 0.2/0.8 value for ^{242m}Am/^{242}Am, whereas RIT used 0.225/0.775, PSI/CEA used 0.15/0.85 and SCK•CEN used 0.09/0.91. Consequently RIT obtains the highest and PSI/CEA and SCK•CEN obtain the lowest concentration of ^{242m}Am. As expected, the opposite effect is observed for ^{242}Cm.

Regarding the Cm isotopes, large discrepancies are observed for ^{244}Cm and ^{245}Cm. The results seem to be correlated with the library used. JEF gives the highest ^{244}Cm and the lowest ^{245}Cm concentration. Good agreement is observed for ^{246}Cm, especially for the equilibrium core.

Safety parameters

The results for the coolant void reactivity effect, the fuel Doppler effect and the effective delayed neutron fraction (β_{eff}) are given in Tables 4.3.1 and 4.3.2.

Coolant void reactivity calculations are traditionally difficult. Only integral values for the coolant void reactivity from k_{eff} difference calculations are available. The JENDL-based calculations by CIEMAT and JAERI give similar results (agreement within about 10%). Assuming that the Monte Carlo calculations by CIEMAT and RIT can be considered as reference calculations which are only sensitive to differences in nuclear data, the decrease in the BOL coolant void reactivity arising

from the substitution of JENDL-3.2 by JEF-2.2 is about 30% (26% for the start-up core and 32% for the equilibrium core). For the other JEF-based coolant void reactivity predictions, one observes a maximum deviation of 30% with respect to the RIT prediction. It is interesting to note that in the ANL and JAERI cases, the voided core becomes supercritical.

A general observation regarding the fuel Doppler reactivity and β_{eff} values is that they are small compared with typical values of MOX-fuelled fast reactor cores due to the absence of ^{238}U and due to the harder neutron spectrum. The results of the β_{eff} calculations depend mainly on the delayed neutron data.

The calculated Doppler reactivities are almost zero. The ability to predict the magnitude of the Doppler reactivity in more conventional fast reactors was demonstrated with an uncertainty of ±15%, which corresponds to an uncertainty of about ±100 pcm. It is therefore difficult to compare the values in the tables, all very small and dispersed around zero. Since the Doppler reactivity comes essentially from capture and fission reactions in the resonance energy region, a more thorough insight into the calculation procedures used by the participants, especially the resonance self-shielding treatment, would be necessary to understand the discrepancies. In the case of Monte Carlo calculations, attention should be paid to statistical uncertainties in the safety parameters (in the case of CIEMAT, statistical errors reported are about ±100%).

The β_{eff} values lie in the expected range; they are smaller than typical values for normal, MOX-fuelled fast reactor cores by about a factor of 2. Group and isotopic component-wise β_{eff} values predicted by ANL, PSI/CEA and JAERI are presented in Tables 4.9.1 and 4.9.2. ANL and JAERI applied the ENDF/B-VI library for their calculations, while PSI/CEA used the JEF-2.2 library. Both libraries give similar isotopic components of β_{eff}. However, ANL (ENDF/B-VI) gives a total value smaller than that of JAERI because the β_{eff} contributions of ^{242m}Am, ^{243}Am and Cm were not taken into account (the respective delayed neutron data are not available in the ENDF/B-VI version of ANL). JAERI used the delayed neutron data of ^{242m}Am, ^{243}Am and ^{245}Cm isotopes from JENDL-3.2. PSI/CEA took into account the contribution of all the isotopes. Therefore, PSI/CEA predicts larger β_{eff} values than ANL and JAERI. It is interesting to observe that the Monte Carlo calculations give even larger β_{eff} values, although RIT used the delayed neutron data from ENDF/B-VI and did not consider ^{242m}Am, ^{243}Am and Cm isotopes (CIEMAT used the delayed neutron data based on JENDL-3.2).

Activity, decay heat, neutron source

Five participants provided partial results for the activity from actinides, fission products and activation products, the decay heat, and the neutron source due to spontaneous fission and (α,n) reactions. They are summarised in Tables 4.10.1 to 4.10.5 and shown in Figures 4.9.1 to 4.9.10.

Activity

Only JAERI and PSI/CEA provided the results for the activity of the activation products. The results are close at the end of irradiation but the difference increases with cooling time. JAERI predicts a faster drop of the activity with the cooling time than PSI/CEA. Both participants predicted a higher activity in the equilibrium core than in the start-up core.

Four participants provided results for the activity of the heavy metals. The results reported by CIEMAT and JAERI are close and those obtained by PSI/CEA are lower at the end of irradiation (-40% for the start-up core and -10% for the equilibrium core). The results from SCK•CEN are more

than 6 orders of magnitude lower. Interestingly, the activity calculated by PSI/CEA becomes larger than that calculated by CIEMAT and JAERI after two years of cooling time; the discrepancy between the results is always lower than 6% for the following time steps.

Only JAERI and CIEMAT performed the calculation for the fission product activity. The variation of the activity during the cooling time is similar, but the initial values differ considerably, JAERI predicting an activity about 2.5 times higher than CIEMAT (it should be noted that JAERI used lumped fission products in the burn-up calculation).

RIT provided only the total activity, without a breakdown into the different components. Activity at the end of irradiation is lower than that obtained by CIEMAT and JAERI, but the difference becomes smaller with increasing cooling time. The largest discrepancies in the activity calculation arise from the fission products and, therefore, the results are more spread at short cooling times. Activity from heavy metals, which dominates at longer cooling times, is calculated more accurately.

Decay heat

Decays of heavy metals, fission products and activation products contribute to the decay heat. PSI/CEA did not calculate the contribution due to the fission products, which is dominant at the end of irradiation, and CIEMAT did not consider the contribution due to the activation. It is therefore difficult to make a direct comparison of the results. As expected, the four results show large discrepancies at the beginning of the cooling time. JAERI reports the highest and PSI/CEA the lowest value. The results show a better agreement after two years of cooling when the maximum difference is about 13%. As for the activity, the decay heat calculated by PSI/CEA and RIT becomes larger than those calculated by JAERI and CIEMAT after two years of cooling.

Neutron production

RIT, JAERI and CIEMAT provided the neutron production from (α,n) reactions. The results are very close between CIEMAT and JAERI. RIT predicts a slightly higher value (+15% at the beginning of cooling time). The values are even closer when the cooling time increases. At the end of cooling time, the difference among the results is less than 4%. The number of neutrons produced by (α,n) reactions in the start-up core is about 28% higher than that in the equilibrium core.

RIT, JAERI, PSI/CEA and CIEMAT reported the neutron production due to spontaneous fissions. Except for the results from PSI/CEA, which are considerably higher than the other results, there is a relatively good agreement. RIT obtains a higher value than JAERI and CIEMAT. The difference is about 10% for both core configurations and is approximately constant during the cooling time.

^{210}Po activity of target

The calculated activity of the ^{210}Po in the target region for the start-up core is given in Table 4.11. Only RIT and JAERI provided the results. The two results are relatively close. However, the value reported by JAERI is higher by 23%.

Chapter 5

CONCLUSIONS

An international benchmark exercise for an accelerator-driven minor actinide burner was undertaken in the framework of the OECD/NEA. Seven organisations contributed to this benchmark exercise using different basic data libraries and reactor analysis codes and applying both deterministic and Monte Carlo methods. The analysis of the results shows significant discrepancies in important neutronic parameters such as one-group microscopic cross-sections, k_{inf}, initial k_{eff}, burn-up reactivity swing, flux distribution and safety parameters. Strong discrepancies also appear in the estimation of the external neutron source, an important parameter for an ADS because it determines the requested accelerator power.

As demonstrated by a separate parametric study, the discrepancies are mainly due to deficiencies in the nuclear data of actinides which are abundant in cores dominated by minor actinides but do not significantly influence the reaction rate balance of conventional MOX cores. However, the impact of the different nuclear data could not fully explain the discrepancies observed in the results. In future benchmark exercises, attention should therefore be given to both the data processing route and the neutron transport approximations.

Concerning the burn-up calculations, attention should be paid to the treatment of the fission products and to the actinide decay chains, taking into account the unusual fuel compositions featured by minor actinide burner cores.

The causes for many of these discrepancies still require clarification, and efforts in this direction should continue if the calculation tools are to be applied to detailed design calculations for ADS cores dominated by minor actinides. A benchmark based on experimental results would be necessary to better understand the origin of discrepancies observed.

REFERENCES

[1] OECD/NEA NSC Task Force on Physics Aspects of Different Transmutation Concepts, "JAERI Proposal of Benchmark Problem on Method and Data to Calculate the Nuclear Characteristics in Accelerator-based Transmutation System With Fast Neutron Flux" (NSC/DOC(96)10).

[2] H. Takano, *et al.*, Proc. Int. Conf. on the Physics of Nuclear Science and Technology, 5-8 October 1998, Long Island, USA, 1 462.

[3] "Calculations of Different Transmutation Concepts: An International Exercise", OECD/NEA report, February 2000.

[4] T. Mukaiyama, *et al.*, "R&D Strategy for Partitioning and Transmutation under OMEGA Program and Neutron Science Project of JAERI", 5th OECD/NEA Information Exchange Meeting on Actinide and Fission Product Partitioning and Transmutation, 25-27 November 1998, Mol, Belgium.

[5] B.C. Na, P. Wydler and H. Takano, "OECD/NEA Comparison Calculations for an Accelerator-driven Minor Actinide Burner: Analysis of Preliminary Results", 2nd OECD/NEA Workshop on Utilisation and Reliability of High Power Accelerators, 22-24 November 1999, Aix-en-Provence, France.

[6] Utility Industry Review of the ALMR Plant Design Program, 20-21 May 1993, San Jose, California, USA.

[7] M. Salvatores, "Advanced Options for Transmutation Strategies", 5th OECD/NEA Information Exchange Meeting on Actinide and Fission Product Partitioning and Transmutation, 25-27 November 1998, Mol, Belgium.

[8] J. Tommasi, CEA Cadarache, private communication.

[9] P. Wydler and Y. Kadi, Proc. 3rd OECD/NEA Information Exchange Meeting on Actinide and Fission Product Partitioning and Transmutation, 12-14 December 1994, Cadarache, France, 298 (NEA/P&T Report No. 13).

[10] W.S. Yang, H.S. Khalil and C.G. Stenberg, "Effects of Lead and Bismuth Cross-sections on ATW Subcriticality Predictions", 1999 Winter Meeting Transactions of the ANS, Volume 81, TANSAO 81 1-374 (1999), ISSN 0003-081X, pp. 273-275, 14-18 November 1999, California, USA.

[11] H. Takahashi and H. Rief, "Concepts of Accelerator-based Transmutation Systems", Proc. of the Specialists Meeting on Accelerator-based Transmutation, 24-26 March 1992, PSI Villigen, Switzerland, 2-26.

TABLES

Table 3.1. Participating organisations, data libraries and codes

Organisation (country)	Basic data libraries	Codes/code systems
ANL (USA)	ENDF/B-VI ENDF/B-V (lumped fission products)	MC^2-2 TWODANT REBUS-3
CIEMAT (Spain)	JENDL-3.2 EAF-3.1 (burn-up) ENDF/B-VI (fission yields)	EVOLCODE system (NJOY, MCNP-4B, ORIGEN-2.1)
KAERI (Korea)	JEF-2.2 JENDL-3.2 (Pb_{nat}, ^{242m}Am)	TRANSX-2.15 and TWODANT DIF3D-7.0 REBUS-3
PSI/CEA (Switzerland/France)	JEF-2.2 (based ERALIB1)	ERANOS ORIHET (activity and decay heat)
JAERI (Japan)	JENDL-3.2	ATRAS (SCALE, TWODANT, BURNER, ORIGEN-2)
RIT (Sweden)	JEF-2.2	NJOY, MCNP-4B, MCB (burn-up) ORIGEN-2
SCK•CEN (Belgium)	JEF-2.2 (except for Pb and ^{233}U which are from ENDF/B-VI)	NJOY97.95, MCNP-4B, ORIGEN-2, BATEMAN2

Table 4.1.1. One-group fission microscopic cross-sections (barn) in start-up core

	ANL (cell)	KAERI (cell)	PSI/CEA (cell)	SCK•CEN (cell)	CIEMAT (core)	JAERI (core)	RIT (core)	PSI/CEA (core)	SCK•CEN (core)
	ENDF	JEF	JEF	JEF	JENDL	JENDL	JEF	JEF	JEF
^{234}U	–	0.358	0.402	–	0.351	0.360	0.384	–	–
^{235}U	–	1.688	1.679	–	1.697	1.701	1.680	–	–
^{236}U	–	0.102	0.119	–	0.103	0.106	0.111	–	–
^{237}Np	0.400	0.345	0.390	0.392	0.365	0.374	0.372	0.362	0.374
^{238}Np	–	1.956	3.067	–	1.977	1.983	3.107	–	–
^{238}Pu	1.198	1.119	1.168	1.162	1.133	1.146	1.149	1.150	1.150
^{239}Pu	1.673	1.708	1.726	1.691	1.702	1.710	1.721	1.761	1.717
^{240}Pu	0.450	0.401	0.430	0.444	0.398	0.407	0.426	0.404	0.428
^{241}Pu	2.172	2.248	2.208	2.157	2.282	2.282	2.239	2.311	2.230
^{242}Pu	0.329	0.285	0.307	0.324	0.286	0.294	0.308	0.284	0.309
^{241}Am	0.332	0.275	0.318	0.315	0.289	0.297	0.299	0.293	0.301
^{242m}Am	3.296	2.782	2.803	2.688	2.807	2.810	2.795	2.947	2.784
^{243}Am	0.263	0.214	0.251	0.248	0.210	0.215	0.234	0.229	0.235
^{242}Cm	0.190	0.620	0.672	0.674	0.762	0.776	0.650	0.638	0.653
^{243}Cm	2.257	2.945	2.931	2.836	2.713	2.720	2.933	3.054	2.922
^{244}Cm	0.515	0.454	0.511	0.510	0.456	0.468	0.487	0.478	0.489
^{245}Cm	2.031	2.388	2.400	2.296	2.399	2.404	2.383	2.513	2.374
^{246}Cm	0.334	0.281	0.327	0.324	0.289	0.297	0.306	0.300	0.308
^{247}Cm	–	1.927	1.931	–	2.144	2.150	1.935	–	–
^{248}Cm	–	0.320	0.366	–	0.317	0.326	0.345	–	–

Table 4.1.2. One-group capture microscopic cross-sections (barn) in start-up core

	ANL (cell)	KAERI (cell)	PSI/CEA (cell)	SCK•CEN (cell)	CIEMAT (core)	JAERI (core)	RIT (core)	PSI/CEA (core)	SCK•CEN (core)
	ENDF	JEF	JEF	JEF	JENDL	JENDL	JEF	JEF	JEF
^{234}U	–	0.479	0.483	–	0.422	0.428	0.482	–	–
^{235}U	–	0.432	0.447	–	0.446	0.446	0.424	–	–
^{236}U	–	0.454	0.454	–	0.362	0.365	0.454	–	–
^{237}Np	1.164	1.250	1.226	1.128	1.330	1.330	1.225	1.356	1.215
^{238}Np	–	0.352	0.133	–	0.358	0.360	0.131	–	–
^{238}Pu	0.699	0.434	0.428	0.391	0.530	0.532	0.428	0.476	0.424
^{239}Pu	0.331	0.387	0.394	0.343	0.393	0.396	0.384	0.450	0.379
^{240}Pu	0.374	0.438	0.395	0.395	0.470	0.470	0.435	0.449	0.431
^{241}Pu	0.300	0.477	0.388	0.453	0.403	0.401	0.475	0.416	0.472
^{242}Pu	0.327	0.381	0.331	0.342	0.395	0.395	0.375	0.371	0.371
^{241}Am	1.261	1.625	1.588	1.496	1.423	1.426	1.594	1.719	1.584
^{242m}Am	0.260	0.462	0.416	0.402	0.468	0.468	0.421	0.442	0.419
^{243}Am	1.079	1.386	1.345	1.258	1.281	1.281	1.357	1.473	1.347
^{242}Cm	0.205	0.387	0.382	0.339	0.408	0.408	0.380	0.437	0.376
^{243}Cm	0.165	0.162	0.163	0.142	0.310	0.311	0.160	0.187	0.158
^{244}Cm	0.643	0.446	0.436	0.415	0.563	0.558	0.442	0.480	0.439
^{245}Cm	0.243	0.260	0.256	0.234	0.301	0.300	0.255	0.284	0.253
^{246}Cm	0.166	0.180	0.180	0.163	0.271	0.272	0.180	0.201	0.178
^{247}Cm	–	0.266	0.255	–	0.420	0.417	0.259	–	–
^{248}Cm	–	0.192	0.190	–	0.215	0.216	0.195	–	–

Table 4.1.3. One-group capture to fission microscopic cross-sections (barn) in start-up core

	ANL (cell)	KAERI (cell)	PSI/CEA (cell)	SCK•CEN (cell)	CIEMAT (core)	JAERI (core)	RIT (core)	PSI/CEA (core)	SCK•CEN (core)
	ENDF	JEF	JEF	JEF	JENDL	JENDL	JEF	JEF	JEF
^{234}U	–	1.338	1.201	–	1.202	1.190	1.257	–	–
^{235}U	–	0.256	0.266	–	0.263	0.262	0.253	–	–
^{236}U	–	4.459	3.812	–	3.509	3.442	4.098	–	–
^{237}Np	2.909	3.625	3.143	2.878	3.641	3.555	3.297	3.748	3.251
^{238}Np	–	0.180	0.043	–	0.181	0.181	0.042	–	–
^{238}Pu	0.583	0.388	0.366	0.336	0.468	0.464	0.372	0.414	0.368
^{239}Pu	0.198	0.227	0.229	0.203	0.231	0.232	0.223	0.255	0.221
^{240}Pu	0.831	1.095	0.919	0.890	1.183	1.154	1.022	1.112	1.006
^{241}Pu	0.138	0.212	0.176	0.210	0.177	0.176	0.212	0.180	0.212
^{242}Pu	0.995	1.338	1.081	1.055	1.379	1.341	1.218	1.306	1.200
^{241}Am	3.796	5.903	4.997	4.744	4.920	4.802	5.331	5.869	5.264
^{242m}Am	0.079	0.166	0.148	0.149	0.167	0.167	0.151	0.150	0.150
^{243}Am	4.097	6.468	5.368	5.082	6.106	5.948	5.805	6.424	5.724
^{242}Cm	1.078	0.624	0.569	0.503	0.535	0.526	0.585	0.685	0.576
^{243}Cm	0.073	0.055	0.056	0.050	0.114	0.114	0.055	0.061	0.054
^{244}Cm	1.248	0.982	0.853	0.812	1.234	1.192	0.909	1.004	0.898
^{245}Cm	0.120	0.109	0.107	0.102	0.125	0.125	0.107	0.113	0.107
^{246}Cm	0.497	0.640	0.550	0.503	0.938	0.916	0.588	0.671	0.578
^{247}Cm	–	0.138	0.132	–	0.196	0.194	0.134	–	–
^{248}Cm	–	0.599	0.519	–	0.679	0.662	0.566	–	–

Table 4.1.4. One-group fission microscopic cross-sections (barn) in equilibrium core

	ANL (cell)	KAERI (cell)	PSI/CEA (cell)	SCK•CEN (cell)	CIEMAT (core)	JAERI (core)	RIT (core)	PSI/CEA (core)	SCK•CEN (core)
	ENDF	JEF	JEF	JEF	JENDL	JENDL	JEF	JEF	JEF
^{234}U	0.379	0.329	0.368	0.374	0.328	0.339	0.355	0.350	0.356
^{235}U	1.715	1.810	1.791	1.717	1.787	1.792	1.792	1.873	1.786
^{236}U	0.106	0.093	0.108	0.108	0.096	0.099	0.102	0.102	0.103
^{237}Np	0.371	0.315	0.355	0.363	0.341	0.353	0.342	0.336	0.344
^{238}Np	0.355	2.089	3.283	3.172	2.080	2.088	3.291	3.401	3.284
^{238}Pu	1.172	1.101	1.142	1.142	1.119	1.135	1.131	1.135	1.131
^{239}Pu	1.697	1.758	1.776	1.731	1.741	1.753	1.769	1.819	1.765
^{240}Pu	0.423	0.375	0.398	0.418	0.376	0.388	0.400	0.381	0.401
^{241}Pu	2.265	2.397	2.345	2.282	2.399	2.399	2.379	2.445	2.371
^{242}Pu	0.304	0.261	0.279	0.300	0.267	0.277	0.284	0.264	0.285
^{241}Am	0.306	0.252	0.289	0.292	0.269	0.279	0.276	0.273	0.277
^{242m}Am	3.485	2.960	3.093	2.851	2.944	2.948	2.975	3.221	2.965
^{243}Am	0.242	0.195	0.226	0.228	0.194	0.202	0.214	0.212	0.215
^{242}Cm	0.173	0.583	0.629	0.638	0.737	0.753	0.614	0.607	0.615
^{243}Cm	2.350	3.116	3.080	2.980	2.854	2.862	3.092	3.198	3.082
^{244}Cm	0.481	0.419	0.470	0.476	0.431	0.445	0.452	0.449	0.453
^{245}Cm	2.146	2.551	2.571	2.432	2.515	2.521	2.533	2.679	2.525
^{246}Cm	0.306	0.256	0.295	0.299	0.272	0.281	0.281	0.278	0.282
^{247}Cm	1.928	1.917	1.923	1.927	2.203	2.211	1.927	1.924	1.925
^{248}Cm	0.345	0.294	0.334	0.337	0.297	0.308	0.319	0.317	0.321

Table 4.1.5. One-group capture microscopic cross-sections (barn) in equilibrium core

	ANL (cell)	KAERI (cell)	PSI/CEA (cell)	SCK•CEN (cell)	CIEMAT (core)	JAERI (core)	RIT (core)	PSI/CEA (core)	SCK•CEN (core)
	ENDF	JEF	JEF	JEF	JENDL	JENDL	JEF	JEF	JEF
^{234}U	0.491	0.542	0.537	0.494	0.461	0.467	0.538	0.586	0.534
^{235}U	0.441	0.491	0.501	0.442	0.486	0.486	0.479	0.544	0.488
^{236}U	0.364	0.505	0.497	0.466	0.402	0.404	0.504	0.537	0.500
^{237}Np	1.279	1.430	1.384	1.281	1.480	1.481	1.392	1.504	1.385
^{238}Np	0.054	0.392	0.157	0.139	0.388	0.390	0.154	0.173	0.153
^{238}Pu	0.743	0.498	0.493	0.445	0.590	0.591	0.485	0.536	0.482
^{239}Pu	0.378	0.462	0.464	0.406	0.454	0.458	0.455	0.520	0.451
^{240}Pu	0.408	0.504	0.454	0.451	0.520	0.518	0.494	0.502	0.490
^{241}Pu	0.328	0.516	0.427	0.486	0.440	0.438	0.511	0.455	0.509
^{242}Pu	0.360	0.442	0.378	0.393	0.438	0.437	0.428	0.414	0.426
^{241}Am	1.387	1.802	1.755	1.648	1.578	1.580	1.758	1.872	1.751
^{242m}Am	0.301	0.510	0.479	0.430	0.505	0.505	0.451	0.499	0.450
^{243}Am	1.190	1.569	1.500	1.415	1.418	1.418	1.526	1.618	1.519
^{242}Cm	0.238	0.463	0.446	0.403	0.456	0.457	0.451	0.499	0.448
^{243}Cm	0.187	0.194	0.192	0.169	0.341	0.342	0.191	0.215	0.189
^{244}Cm	0.697	0.484	0.480	0.450	0.621	0.613	0.481	0.521	0.479
^{245}Cm	0.265	0.298	0.295	0.267	0.322	0.321	0.291	0.321	0.289
^{246}Cm	0.183	0.208	0.203	0.187	0.304	0.304	0.207	0.224	0.205
^{247}Cm	0.271	0.298	0.285	0.269	0.445	0.442	0.289	0.306	0.288
^{248}Cm	0.198	0.222	0.216	0.199	0.243	0.245	0.226	0.245	0.224

Table 4.1.6. One-group capture to fission microscopic cross-sections (barn) in equilibrium core

	ANL (cell)	KAERI (cell)	PSI/CEA (cell)	SCK•CEN (cell)	CIEMAT (core)	JAERI (core)	RIT (core)	PSI/CEA (core)	SCK•CE (core)
	ENDF	JEF	JEF	JEF	JENDL	JENDL	JEF	JEF	JEF
^{234}U	1.295	1.650	1.461	1.321	1.404	1.377	1.517	1.676	1.501
^{235}U	0.257	0.271	0.280	0.258	0.272	0.271	0.267	0.290	0.273
^{236}U	3.446	5.405	4.597	4.299	4.200	4.068	4.919	5.262	4.858
^{237}Np	3.448	4.538	3.897	3.533	4.336	4.200	4.066	4.471	4.028
^{238}Np	0.151	0.188	0.048	0.044	0.187	0.187	0.047	0.051	0.047
^{238}Pu	0.634	0.453	0.431	0.390	0.527	0.521	0.429	0.472	0.426
^{239}Pu	0.223	0.263	0.261	0.235	0.261	0.261	0.257	0.286	0.256
^{240}Pu	0.965	1.345	1.142	1.078	1.382	1.336	1.235	1.316	1.222
^{241}Pu	0.145	0.215	0.182	0.213	0.184	0.183	0.215	0.186	0.215
^{242}Pu	1.182	1.694	1.356	1.310	1.642	1.580	1.510	1.566	1.497
^{241}Am	4.534	7.142	6.075	5.640	5.866	5.668	6.375	6.863	6.316
^{242m}Am	0.086	0.172	0.155	0.151	0.171	0.171	0.152	0.155	0.152
^{243}Am	4.916	8.046	6.632	6.198	7.297	7.035	7.121	7.618	7.049
^{242}Cm	1.373	0.794	0.709	0.631	0.619	0.606	0.734	0.822	0.728
^{243}Cm	0.079	0.062	0.062	0.057	0.119	0.119	0.062	0.067	0.061
^{244}Cm	1.449	1.156	1.021	0.946	1.440	1.377	1.064	1.161	1.056
^{245}Cm	0.123	0.117	0.115	0.110	0.128	0.127	0.115	0.120	0.115
^{246}Cm	0.596	0.816	0.687	0.627	1.119	1.082	0.738	0.805	0.728
^{247}Cm	0.141	0.156	0.148	0.140	0.202	0.200	0.150	0.159	0.149
^{248}Cm	0.575	0.755	0.646	0.590	0.818	0.795	0.709	0.774	0.698

Table 4.2. Infinite multiplication factor, buckling and migration area

(a) Start-up core

	k_{inf}	B^2	M^2
ANL	1.15894	1.0114E-03	157.15
CIEMAT	1.13732 (±0.00059)	–	–
KAERI	1.13256	6.8650E-04	193.10
PSI/CEA	1.13141	8.6493E-04	214.69
JAERI	1.15920	–	–
RIT	1.14900	–	–
SCK•CEN	1.14729	9.561E-04	154

(b) Equilibrium core

	k_{inf}	B^2	M^2
ANL	1.14420	8.7295E-04	165.21
CIEMAT	1.11629 (±0.00043)	–	–
KAERI	1.13366	6.5130E-04	205.20
PSI/CEA	1.13165	8.5179E-04	230.17
JAERI	1.14192	–	–
RIT	1.15000	–	–
SCK•CEN	1.14884	9.589E-04	155

Table 4.3.1. Main neutronic characteristics of start-up core

Parameters	Organisation						
	ANL	**CIEMAT**	**KAERI**	**PSI/CEA**	**JAERI**	**RIT***	**SCK•CEN**
Library used	ENDF/B-VI	JENDL-3.2	JEF-2.2	JEF-2.2	JENDL-3.2	JEF-2.2	JEF-2.2
k_{eff} at BOL	0.98554	0.9570	0.94546	0.94795	0.9650	0.9590	0.9590
Production to absorption ratio	1.307	1.245	1.226	1.228	1.253	1.220	1.241
Burn-up after 5 cycles (GWd/t_{HM})	175.4	185.7	185.7	185.7	187.3	185.7	185.8
Source strength (n/s)							
BOL	6.10E17	1.65E18	4.11E18	2.26E18	1.25E18	2.54E18	2.29E18
EOL	4.12E18	3.51E18	7.33E18	3.96E18	2.88E18	4.83E18	4.54E18
Coolant void reactivity at BOL/EOL (pcm)							
$k_{eff}^{voided} - k_{eff}^{ref}$	3 161/2 433	3 905/3 214	3 687/2 596	2 870/1 655	3 813/3 048	2 904/1 863	2 896/1 681
$\left(k_{eff}^{voided} - k_{eff}^{ref}\right)/k_{eff}^{ref}$	3 205/2 655	4 078/3 389	3 899/2 866	3 127/1 868	3 952/3 297	3 025/2 020	3 020/1 832
Fuel Doppler effect BOL/EOL (pcm) $\frac{k_{eff}^{980\,K} - k_{eff}^{1580\,K}}{k_{eff}^{980\,K} \cdot k_{eff}^{1580\,K}}$	0/13	38.2/323.7	16.5/27.2	6.2/12.4	20.2/31.9	48/53	11/48
β_{eff} at BOL (pcm)	156	246	–	184.0	173.5	195	–
Median energy of neutron spectrum (keV)	210	212	222	214	162	220	220

** RIT supplementary results: k_{eff} (BOL) using JENDL-3.2: 0.962*
k_{eff} (BOL) using ENDF/B-VI: 0.998

Table 4.3.2. Main neutronic characteristics of equilibrium core

Parameters	Organisation						
	ANL	**CIEMAT**	**KAERI**	**PSI/CEA**	**JAERI**	**RIT**	**SCK•CEN**
Library used	ENDF/B-VI	JENDL-3.2	JEF-2.2	JEF-2.2	JENDL-3.2	JEF-2.2	JEF-2.2
k_{eff} at BOL	0.96895	0.9370	0.94174	0.94374	0.9494	0.9570	0.95509
Production to absorption ratio	1.308	1.241	1.258	1.260	1.258	1.245	1.274
Burn-up after 5 cycles (GWd/t_{HM})	176.1	185.7	185.7	185.7	187.3	193.7	185.8
Source strength (n/s)							
BOL	1.39E18	2.54E18	4.49E18	2.55E18	1.94E18	2.70E18	2.47E18
EOL	3.18E18	2.38E18	5.80E18	2.86E18	2.00E18	3.39E18	2.64E18
Coolant void reactivity at BOL/EOL (pcm)							
$k_{eff}^{voided} - k_{eff}^{ref}$	3 318/2 154	4 511/2 582	3 902/2 034	2 732/1 925	4 138/2 821	3 045/1 605	3 144/1 681
$\left(k_{eff}^{voided} - k_{eff}^{ref}\right)/k_{eff}^{ref}$	3 424/2 308	4 816/2 744	4 144/2 197	2 955/2 276	4 359/2 982	3 183/1 700	3 292/1 831
Fuel Doppler effect BOL/EOL (pcm) $\frac{k_{eff}^{980\,K} - k_{eff}^{1580\,K}}{k_{eff}^{980\,K} \cdot k_{eff}^{1580\,K}}$	20/12	17.1/277.6	23.0/43.7	4.2/5.8	30.4/45.8	45/49	98/103
β_{eff} at BOL (pcm)	116	221	–	155.9	145.2	171	–
Median energy of neutron spectrum (keV)	185	188	181	179	152	188	183

Table 4.4. Effect on k_{eff} of each actinide, ^{15}N, Bi and Pb_{nat} of different libraries

Reference k_{eff} = 1.00007: All ENDF/B-VI data

Exchanged nuclide	JEF-2.2			JENDL-3.2		
	k_{eff}	Δk (pcm)	Δk/atom*	k_{eff}	Δk (pcm)	Δk/atom*
^{237}Np	0.998257	-181	-4.14	0.997425	-265	-6.05
^{241}Am	0.986861	-1 321	-16.34	0.99744	-263	-3.25
^{242m}Am	0.996619	-345	-316.8	0.997574	-250	-229.57
^{243}Am	0.992768	-730	-12.53	0.99502	-505	-8.67
^{238}Pu	1.00073	66	15.62	1.00067	60	14.2
^{242}Cm	1.00008	1	245.16	1.00008	1	245.16
^{243}Cm	1.00102	95	285.63	1.00065	58	174.38
^{244}Cm	1.00118	111	4.68	0.999148	-92	-3.88
^{245}Cm	1.00675	668	211.13	1.00266	259	81.86
^{246}Cm	–	–	–	1.00006	-1	-18.67
^{239}Pu	0.996104	-397	-7.86	0.999828	-24	-0.48
^{240}Pu	0.998555	-152	-6.55	0.997618	-245	-10.56
^{241}Pu	0.999424	-65	-5.28	1.00114	107	8.69
^{242}Pu	1.00007	0	0	1.00007	0	0
^{15}N	0.995843	-423	–	0.99551	-456	–
^{209}Bi	0.99934	-73	–	0.999303	-77	–
Pb_{nat}	1.00687	680	–	0.988994	-1 108	–

** Δk/atom, in units of 1E-24.*

Table 4.5. End of cycle burn-up reactivity drop components (in units of $10^3\Delta k$)

Core	Δk from	ENDF/B-VI	JENDL-3.2			JEF-2.2			
		ANL	CIEMAT	JAERI	RIT	KAERI	PSI/CEA	RIT	SCK•CEN
Start-up	Actinides[a]	28	28	14	22	3	8	4	16
	FPs[b]	41	13	27	34	37	28	35	25
	Total	69	41	41	56	40	36	39	41
Equilibrium	Actinides[a]	-11	-18	-27	–	-27	-26	-27	-17
	FPs[b]	45	14	30	–	43	35	44	22
	Total	36	-4	3	–	16	9	17	5

[a] *Actinide component evaluated from k_{eff} values with FP concentrations set to zero.*
[b] *Evaluated as total effect minus actinide component.*

Table 4.6.1. Production rate in start-up core (reactions/cm^3/sec)

	ENDF/B-VI	JENDL-3.2		JEF-2.2			
	ANL	CIEMAT	JAERI	KAERI	PSI/CEA	RIT	SCK•CEN
^{234}U	–	–	–	–	2.00E+00	–	–
^{235}U	–	–	–	–	8.69E+00	–	–
^{236}U	–	–	–	–	5.99E-01	-	-
^{237}Np	9.66E+11	8.14E+11	1.17E+12	8.11E+11	9.22E+11	9.99E+11	9.91E+11
^{238}Np	–	–	–	–	1.80E+01	–	–
^{238}Pu	3.09E+11	2.67E+11	3.45E+11	2.69E+11	2.99E+11	3.39E+11	3.24E+11
^{239}Pu	5.30E+12	4.72E+12	6.16E+12	4.77E+12	5.29E+12	6.03E+12	5.68E+12
^{240}Pu	6.13E+11	5.12E+11	6.75E+11	5.37E+11	5.93E+11	6.65E+11	6.50E+11
^{241}Pu	1.73E+12	1.56E+12	2.01E+12	1.54E+12	1.69E+12	1.95E+12	1.82E+12
^{242}Pu	1.76E+11	1.51E+11	1.91E+11	1.53E+11	1.65E+11	1.90E+11	1.87E+11
^{241}Am	1.79E+12	1.51E+12	1.71E+12	1.58E+12	1.81E+12	1.94E+12	1.92E+12
^{242m}Am	2.62E+11	1.89E+11	2.18E+11	1.88E+11	2.07E+11	2.35E+11	2.20E+11
^{243}Am	1.06E+12	7.97E+11	8.95E+11	8.33E+11	9.62E+11	1.01E+12	1.02E+12
^{242}Cm	5.61E+07	1.98E+08	2.26E+08	1.62E+08	1.81E+08	2.02E+08	1.96E+08
^{243}Cm	5.72E+10	5.86E+10	6.45E+10	6.30E+10	6.99E+10	7.98E+10	7.49E+10
^{244}Cm	8.82E+11	7.01E+11	7.91E+11	7.31E+11	8.32E+11	9.04E+11	8.91E+11
^{245}Cm	5.17E+11	5.06E+11	5.43E+11	5.50E+11	6.16E+11	6.94E+11	6.52E+11
^{246}Cm	1.30E+09	1.01E+09	1.13E+09	1.13E+09	1.30E+09	1.38E+09	1.38E+09
^{247}Cm	–	–	–	–	1.44E+01	–	–
^{248}Cm	–	–	–	–	2.74E+00	–	–

Table 4.6.2. Absorption rate in start-up core (reactions/cm^3/sec)

	ENDF/B-VI	JENDL-3.2		JEF-2.2			
	ANL	CIEMAT	JAERI	KAERI	PSI/CEA	RIT	SCK•CEN
^{234}U	–	–	–	–	1.83E+00	–	–
^{235}U	–	–	–	–	4.46E+00	–	–
^{236}U	–	–	–	–	1.20E+00	–	–
^{237}Np	1.50E+12	1.38E+12	1.72E+12	1.31E+12	1.49E+12	1.65E+12	1.55E+12
^{238}Np	–	–	0.00E+00	0.00E+00	6.66E+00	–	–
^{238}Pu	1.67E+11	1.31E+11	1.63E+11	1.24E+11	1.39E+11	1.57E+11	1.48E+11
^{239}Pu	2.19E+12	1.97E+12	2.45E+12	1.99E+12	2.23E+12	2.50E+12	2.36E+12
^{240}Pu	4.01E+11	3.75E+11	4.69E+11	3.72E+11	3.98E+11	4.71E+11	4.44E+11
^{241}Pu	6.65E+11	6.15E+11	7.61E+11	6.27E+11	6.68E+11	7.88E+11	7.44E+11
^{242}Pu	1.25E+11	1.15E+11	1.44E+11	1.15E+11	1.20E+11	1.46E+11	1.38E+11
^{241}Am	2.83E+12	2.58E+12	3.21E+12	2.87E+12	3.22E+12	3.60E+12	3.40E+12
^{242m}Am	8.58E+10	6.64E+10	8.23E+10	6.58E+10	7.32E+10	8.25E+10	7.79E+10
^{243}Am	1.73E+12	1.62E+12	2.01E+12	1.75E+12	1.96E+12	2.18E+12	2.06E+12
^{242}Cm	3.50E+07	8.89E+07	1.11E+08	7.81E+07	8.85E+07	9.91E+07	9.34E+07
^{243}Cm	1.76E+10	1.87E+10	2.32E+10	1.93E+10	2.14E+10	2.42E+10	2.29E+10
^{244}Cm	5.80E+11	4.50E+11	5.60E+11	4.07E+11	4.61E+11	5.19E+11	4.89E+11
^{245}Cm	1.58E+11	1.59E+11	1.97E+11	1.57E+11	1.76E+11	1.97E+11	1.86E+11
^{246}Cm	5.47E+08	5.59E+08	7.01E+08	4.79E+08	5.50E+08	6.13E+08	5.77E+08
^{247}Cm	–	–	–	–	4.47E+00	–	–
^{248}Cm	–	–	–	–	1.14E+00	–	–

Table 4.6.3. Production to absorption rate ratio in start-up core

	ENDF/B-VI	JENDL-3.2		JEF-2.2			
	ANL	CIEMAT	JAERI	KAERI	PSI/CEA	RIT	SCK•CEN
^{234}U	–	–	–	–	1.09	–	–
^{235}U	–	–	–	–	1.95	–	–
^{236}U	–	–	–	–	0.50	–	–
^{237}Np	0.64	0.59	0.68	0.62	0.62	0.61	0.64
^{238}Np	–	–	–	–	2.70	–	–
^{238}Pu	1.85	2.04	2.12	2.17	2.16	2.16	2.19
^{239}Pu	2.42	2.40	2.51	2.40	2.37	2.41	2.40
^{240}Pu	1.53	1.36	1.44	1.44	1.49	1.41	1.46
^{241}Pu	2.60	2.53	2.63	2.46	2.53	2.47	2.45
^{242}Pu	1.40	1.31	1.32	1.33	1.37	1.30	1.36
^{241}Am	0.63	0.59	0.53	0.55	0.56	0.54	0.57
^{242m}Am	3.06	2.85	2.65	2.85	2.83	2.84	2.83
^{243}Am	0.61	0.49	0.45	0.48	0.49	0.46	0.49
^{242}Cm	1.60	2.23	2.03	2.07	2.04	2.04	2.10
^{243}Cm	3.24	3.13	2.78	3.27	3.26	3.29	3.27
^{244}Cm	1.52	1.56	1.41	1.80	1.81	1.74	1.82
^{245}Cm	3.27	3.18	2.75	3.51	3.51	3.53	3.51
^{246}Cm	2.38	1.81	1.62	2.36	2.37	2.25	2.39
^{247}Cm	–	–	–	–	3.23	–	–
^{248}Cm	–	–	–	–	2.40	–	–

Table 4.6.4. Production rate in equilibrium core (reactions/cm^3/sec)

	ENDF/B-VI	JENDL-3.2		JEF-2.2			
	ANL	CIEMAT	JAERI	KAERI	PSI/CEA	RIT	SCK•CEN
^{234}U	2.17E+11	1.77E+11	2.90E+11	1.88E+11	2.13E+11	2.36E+11	2.29E+11
^{235}U	1.90E+11	1.70E+11	2.80E+11	1.74E+11	1.96E+11	2.23E+11	2.04E+11
^{236}U	6.01E+09	5.21E+09	8.34E+09	5.41E+09	6.21E+09	6.56E+09	6.57E+09
^{237}Np	6.30E+11	5.23E+11	7.98E+11	5.21E+11	5.90E+11	6.48E+11	6.35E+11
^{238}Np	5.63E+08	2.23E+09	3.53E+09	2.25E+09	4.41E+09	5.11E+09	4.67E+09
^{238}Pu	3.32E+12	2.84E+12	3.88E+12	2.88E+12	3.21E+12	3.68E+12	3.45E+12
^{239}Pu	1.11E+12	9.92E+11	1.37E+12	1.01E+12	1.14E+12	1.30E+12	1.20E+12
^{240}Pu	1.47E+12	1.21E+12	1.69E+12	1.27E+12	1.40E+12	1.60E+12	1.54E+12
^{241}Pu	6.93E+11	6.33E+11	8.57E+11	6.35E+11	7.04E+11	8.18E+11	7.48E+11
^{242}Pu	3.26E+11	2.75E+11	3.70E+11	2.79E+11	3.00E+11	3.50E+11	3.41E+11
^{241}Am	1.14E+12	9.50E+11	1.14E+12	9.95E+11	1.13E+12	1.24E+12	1.21E+12
^{242m}Am	8.30E+11	5.97E+11	7.25E+11	6.01E+11	6.98E+11	7.69E+11	7.07E+11
^{243}Am	8.24E+11	6.08E+11	7.28E+11	6.38E+11	7.32E+11	7.81E+11	7.78E+11
^{242}Cm	1.26E+08	4.54E+08	5.50E+08	3.67E+08	4.12E+08	4.65E+08	4.44E+08
^{243}Cm	6.64E+10	6.88E+10	7.97E+10	7.45E+10	8.34E+10	9.60E+10	8.83E+10
^{244}Cm	1.40E+12	1.10E+12	1.32E+12	1.14E+12	1.30E+12	1.43E+12	1.39E+12
^{245}Cm	1.53E+12	1.49E+12	1.69E+12	1.65E+12	1.89E+12	2.13E+12	1.96E+12
^{246}Cm	1.03E+11	7.95E+10	9.50E+10	8.83E+10	1.01E+11	1.09E+11	1.08E+11
^{247}Cm	5.99E+10	6.43E+10	6.71E+10	4.92E+10	5.90E+10	6.90E+10	6.40E+10
^{248}Cm	3.04E+09	2.21E+09	2.71E+09	2.61E+09	2.99E+09	3.23E+09	3.18E+09

Table 4.6.5. Absorption rate in equilibrium core (reactions/cm^3/sec)

	ENDF/B-VI	JENDL-3.2		JEF-2.2			
	ANL	CIEMAT	JAERI	KAERI	PSI/CEA	RIT	SCK•CEN
^{234}U	2.12E+11	1.68E+11	2.19E+11	1.91E+11	2.19E+11	2.46E+11	2.28E+11
^{235}U	9.79E+10	8.82E+10	1.13E+11	8.94E+10	1.02E+11	1.14E+11	1.06E+11
^{236}U	1.17E+10	1.04E+10	1.34E+10	1.27E+10	1.45E+10	1.64E+10	1.51E+10
^{237}Np	1.09E+12	1.02E+12	1.32E+12	9.88E+11	1.12E+12	1.26E+12	1.17E+12
^{238}Np	2.32E+08	1.04E+09	1.33E+09	1.05E+09	1.64E+09	1.87E+09	1.73E+09
^{238}Pu	1.86E+12	1.45E+12	1.87E+12	1.38E+12	1.56E+12	1.78E+12	1.65E+12
^{239}Pu	4.67E+11	4.25E+11	5.47E+11	4.35E+11	4.95E+11	5.57E+11	5.16E+11
^{240}Pu	1.02E+12	9.69E+11	1.26E+12	9.76E+11	1.05E+12	1.25E+12	1.16E+12
^{241}Pu	2.68E+11	2.52E+11	3.22E+11	2.59E+11	2.81E+11	3.32E+11	3.07E+11
^{242}Pu	2.51E+11	2.34E+11	3.03E+11	2.38E+11	2.47E+11	3.06E+11	2.84E+11
^{241}Am	2.03E+12	1.88E+12	2.43E+12	2.10E+12	2.38E+12	2.68E+12	2.48E+12
^{242m}Am	2.74E+11	2.10E+11	2.70E+11	2.12E+11	2.49E+11	2.71E+11	2.51E+11
^{243}Am	1.52E+12	1.45E+12	1.86E+12	1.58E+12	1.78E+12	2.02E+12	1.87E+12
^{242}Cm	8.83E+07	2.16E+08	2.81E+08	1.94E+08	2.20E+08	2.50E+08	2.31E+08
^{243}Cm	2.06E+10	2.21E+10	2.84E+10	2.30E+10	2.58E+10	2.94E+10	2.72E+10
^{244}Cm	9.87E+11	7.73E+11	9.95E+11	6.85E+11	7.87E+11	8.88E+11	8.23E+11
^{245}Cm	4.70E+11	4.72E+11	6.05E+11	4.76E+11	5.44E+11	6.08E+11	5.63E+11
^{246}Cm	4.59E+10	4.84E+10	6.28E+10	4.09E+10	4.67E+10	5.31E+10	4.91E+10
^{247}Cm	1.87E+10	1.99E+10	2.56E+10	1.54E+10	1.86E+10	2.16E+10	2.00E+10
^{248}Cm	1.35E+09	1.18E+09	1.54E+09	1.18E+09	1.36E+09	1.54E+09	1.43E+09

Table 4.6.6. Production to absorption rate ratio in equilibrium core

	ENDF/B-VI	JENDL-3.2		JEF-2.2			
	ANL	CIEMAT	JAERI	KAERI	PSI/CEA	RIT	SCK•CEN
^{234}U	1.03	1.05	1.32	0.98	0.97	0.96	1.00
^{235}U	1.94	1.93	2.48	1.94	1.92	1.96	1.93
^{236}U	0.51	0.50	0.62	0.43	0.43	0.40	0.43
^{237}Np	0.58	0.51	0.61	0.53	0.52	0.51	0.54
^{238}Np	2.42	2.16	2.65	2.15	2.69	2.73	2.70
^{238}Pu	1.78	1.96	2.07	2.08	2.06	2.07	2.10
^{239}Pu	2.37	2.34	2.50	2.33	2.30	2.34	2.33
^{240}Pu	1.44	1.25	1.35	1.31	1.34	1.27	1.33
^{241}Pu	2.58	2.51	2.66	2.45	2.51	2.46	2.44
^{242}Pu	1.30	1.17	1.22	1.17	1.21	1.14	1.20
^{241}Am	0.56	0.50	0.47	0.47	0.48	0.46	0.49
^{242m}Am	3.03	2.84	2.69	2.83	2.81	2.84	2.82
^{243}Am	0.54	0.42	0.39	0.40	0.41	0.39	0.42
^{242}Cm	1.42	2.10	1.96	1.89	1.87	1.86	1.92
^{243}Cm	3.22	3.11	2.81	3.24	3.23	3.27	3.25
^{244}Cm	1.42	1.42	1.32	1.67	1.65	1.61	1.69
^{245}Cm	3.26	3.17	2.79	3.48	3.47	3.50	3.48
^{246}Cm	2.25	1.64	1.51	2.16	2.17	2.05	2.20
^{247}Cm	3.20	3.22	2.62	3.19	3.18	3.19	3.19
^{248}Cm	2.26	1.88	1.75	2.21	2.20	2.09	2.23

Table 4.7.1. Fission reaction rate relative to ^{239}Pu fission in start-up core

	ENDF/B-VI	JENDL-3.2		JEF-2.2			
	ANL	CIEMAT	JAERI	KAERI	PSI/CEA	RIT	SCK•CEN
^{234}U	–	–	–	–	4.60E-13	–	–
^{235}U	–	–	–	–	1.93E-12	–	–
^{236}U	–	–	–	–	1.36E-13	–	–
^{237}Np	2.01E-01	1.96E-01	1.72E-01	1.91E-01	1.95E-01	2.00E-01	1.99E-01
^{238}Np	–	–	–	–	3.52E-12	–	–
^{238}Pu	5.87E-02	5.69E-02	5.43E-02	5.65E-02	5.66E-02	5.73E-02	5.73E-02
^{240}Pu	1.20E-01	1.13E-01	1.01E-01	1.16E-01	1.14E-01	1.20E-01	1.20E-01
^{241}Pu	3.18E-01	3.22E-01	3.35E-01	3.15E-01	3.12E-01	3.12E-01	3.12E-01
^{242}Pu	3.43E-02	3.21E-02	2.80E-02	3.29E-02	3.19E-02	3.44E-02	3.44E-02
^{241}Am	3.06E-01	2.88E-01	2.49E-01	2.84E-01	2.94E-01	2.98E-01	2.98E-01
^{242m}Am	4.26E-02	3.51E-02	3.64E-02	3.44E-02	3.50E-02	3.43E-02	3.44E-02
^{243}Am	1.75E-01	1.51E-01	1.29E-01	1.60E-01	1.67E-01	1.69E-01	1.68E-01
^{242}Cm	8.80E-06	3.75E-05	3.46E-05	3.11E-05	3.14E-05	3.20E-05	3.20E-05
^{243}Cm	8.89E-03	1.03E-02	1.08E-02	1.12E-02	1.12E-02	1.11E-02	1.11E-02
^{244}Cm	1.40E-01	1.32E-01	1.18E-01	1.35E-01	1.39E-01	1.41E-01	1.41E-01
^{245}Cm	7.61E-02	8.72E-02	9.04E-02	8.60E-02	8.71E-02	8.52E-02	8.53E-02
^{246}Cm	2.03E-04	1.90E-04	1.67E-04	1.93E-04	2.00E-04	2.02E-04	2.02E-04
^{247}Cm	–	–	–	–	2.21E-12	–	–
^{248}Cm	–	–	–	–	4.19E-13	–	–

Table 4.7.2. Capture reaction rate relative to ^{239}Pu fission in start-up core

	ENDF/B-VI	JENDL-3.2		JEF-2.2			
	ANL	CIEMAT	JAERI	KAERI	PSI/CEA	RIT	SCK•CEN
^{234}U	–	–	–	–	5.55E-13	–	–
^{235}U	–	–	–	–	5.14E-13	–	–
^{236}U	–	–	–	–	5.21E-13	–	–
^{237}Np	6.09E-01	6.44E-01	7.31E-01	5.99E-01	6.17E-01	5.82E-01	5.83E-01
^{238}Np	–	–	–	–	1.53E-13	–	–
^{238}Pu	3.35E-02	2.46E-02	2.82E-02	2.01E-02	2.08E-02	1.95E-02	1.95E-02
^{239}Pu	2.00E-01	2.15E-01	2.55E-01	2.12E-01	2.29E-01	2.06E-01	2.06E-01
^{240}Pu	1.03E-01	1.20E-01	1.35E-01	1.11E-01	1.05E-01	1.08E-01	1.08E-01
^{241}Pu	4.41E-02	5.55E-02	6.07E-02	6.64E-02	5.49E-02	6.55E-02	6.56E-02
^{242}Pu	3.55E-02	3.97E-02	4.50E-02	3.79E-02	3.47E-02	3.68E-02	3.67E-02
^{241}Am	1.22E+00	1.28E+00	1.44E+00	1.46E+00	1.48E+00	1.42E+00	1.42E+00
^{242m}Am	3.38E-03	5.76E-03	6.25E-03	5.59E-03	5.20E-03	5.14E-03	5.14E-03
^{243}Am	7.53E-01	8.28E-01	9.33E-01	8.88E-01	9.00E-01	8.64E-01	8.65E-01
^{242}Cm	9.94E-06	1.83E-05	2.08E-05	1.70E-05	1.79E-05	1.64E-05	1.64E-05
^{243}Cm	6.56E-04	1.15E-03	1.28E-03	5.79E-04	6.23E-04	5.59E-04	5.60E-04
^{244}Cm	1.82E-01	1.49E-01	1.64E-01	1.18E-01	1.19E-01	1.15E-01	1.15E-01
^{245}Cm	9.21E-03	1.08E-02	1.15E-02	8.99E-03	9.31E-03	8.74E-03	8.75E-03
^{246}Cm	1.06E-04	1.60E-04	1.83E-04	1.06E-04	1.11E-04	1.03E-04	1.03E-04
^{247}Cm	–	–	–	–	2.94E-13	–	–
^{248}Cm	–	–	–	–	2.94E-13	–	–

Table 4.7.3. Fission reaction rate relative to ^{239}Pu fission in equilibrium core

	ENDF/B-VI	JENDL-3.2		JEF-2.2			
	ANL	CIEMAT	JAERI	KAERI	PSI/CEA	RIT	SCK•CEN
^{234}U	2.43E-01	2.18E-01	2.01E-01	2.26E-01	2.27E-01	2.33E-01	2.32E-01
^{235}U	2.03E-01	2.03E-01	2.09E-01	2.01E-01	2.02E-01	2.00E-01	2.00E-01
^{236}U	6.60E-03	6.34E-03	5.69E-03	6.40E-03	6.54E-03	6.63E-03	6.60E-03
^{237}Np	6.26E-01	6.01E-01	5.54E-01	5.76E-01	5.79E-01	5.97E-01	5.94E-01
^{238}Np	4.41E-04	2.56E-03	2.63E-03	2.53E-03	4.00E-03	4.01E-03	4.01E-03
^{238}Pu	3.02E+00	2.88E+00	2.80E+00	2.84E+00	2.81E+00	2.88E+00	2.87E+00
^{240}Pu	1.38E+00	1.27E+00	1.19E+00	1.30E+00	1.25E+00	1.33E+00	1.33E+00
^{241}Pu	6.12E-01	6.25E-01	6.38E-01	6.11E-01	6.05E-01	6.07E-01	6.08E-01
^{242}Pu	3.04E-01	2.79E-01	2.56E-01	2.82E-01	2.69E-01	2.92E-01	2.91E-01
^{241}Am	9.35E-01	8.67E-01	7.88E-01	8.42E-01	8.55E-01	8.73E-01	8.69E-01
^{242m}Am	6.47E-01	5.28E-01	5.40E-01	5.20E-01	5.50E-01	5.22E-01	5.23E-01
^{243}Am	6.50E-01	5.54E-01	4.99E-01	5.77E-01	5.88E-01	5.99E-01	5.96E-01
^{242}Cm	9.42E-05	4.11E-04	3.91E-04	3.33E-04	3.31E-04	3.41E-04	3.40E-04
^{243}Cm	4.94E-02	5.80E-02	5.95E-02	6.22E-02	6.20E-02	6.18E-02	6.19E-02
^{244}Cm	1.06E+00	9.86E-01	9.21E-01	9.94E-01	1.00E+00	1.03E+00	1.02E+00
^{245}Cm	1.08E+00	1.23E+00	1.26E+00	1.22E+00	1.24E+00	1.21E+00	1.22E+00
^{246}Cm	7.71E-02	7.18E-02	6.60E-02	7.08E-02	7.20E-02	7.33E-02	7.30E-02
^{247}Cm	4.44E-02	4.93E-02	4.95E-02	3.96E-02	4.22E-02	4.33E-02	4.33E-02
^{248}Cm	2.26E-03	2.03E-03	1.88E-03	2.08E-03	2.12E-03	2.15E-03	2.14E-03

Table 4.7.4. Capture reaction rate relative to ^{239}Pu fission in equilibrium core

	ENDF/B-VI	JENDL-3.2		JEF-2.2			
	ANL	CIEMAT	JAERI	KAERI	PSI/CEA	RIT	SCK•CEN
^{234}U	3.17E-01	2.82E-01	2.99E-01	3.22E-01	3.33E-01	3.18E-01	3.18E-01
^{235}U	5.21E-02	5.42E-02	5.74E-02	5.29E-02	5.67E-02	5.18E-02	5.21E-02
^{236}U	2.30E-02	2.35E-02	2.55E-02	2.96E-02	3.02E-02	2.93E-02	2.94E-02
^{237}Np	2.19E+00	2.37E+00	2.57E+00	2.22E+00	2.27E+00	2.18E+00	2.19E+00
^{238}Np	6.67E-05	4.72E-04	4.99E-04	4.61E-04	1.92E-04	1.77E-04	1.78E-04
^{238}Pu	1.91E+00	1.42E+00	1.55E+00	1.17E+00	1.22E+00	1.14E+00	1.15E+00
^{239}Pu	2.21E-01	2.44E-01	2.74E-01	2.44E-01	2.61E-01	2.37E-01	2.40E-01
^{240}Pu	1.35E+00	1.63E+00	1.72E+00	1.51E+00	1.43E+00	1.47E+00	1.49E+00
^{241}Pu	8.83E-02	1.12E-01	1.18E-01	1.31E-01	1.10E-01	1.29E-01	1.30E-01
^{242}Pu	3.63E-01	4.16E-01	4.48E-01	4.04E-01	3.67E-01	3.94E-01	3.97E-01
^{241}Am	4.30E+00	4.60E+00	4.96E+00	5.15E+00	5.21E+00	5.07E+00	5.09E+00
^{242m}Am	5.55E-02	8.94E-02	9.40E-02	8.75E-02	8.52E-02	7.91E-02	7.93E-02
^{243}Am	3.25E+00	3.64E+00	3.91E+00	3.91E+00	3.92E+00	3.83E+00	3.85E+00
^{242}Cm	1.30E-04	2.34E-04	2.54E-04	2.28E-04	2.36E-04	2.21E-04	2.23E-04
^{243}Cm	3.92E-03	6.78E-03	7.26E-03	3.64E-03	3.88E-03	3.54E-03	3.57E-03
^{244}Cm	1.56E+00	1.29E+00	1.38E+00	1.00E+00	1.03E+00	1.00E+00	1.00E+00
^{245}Cm	1.34E-01	1.56E-01	1.62E-01	1.37E-01	1.43E-01	1.34E-01	1.35E-01
^{246}Cm	4.67E-02	7.23E-02	7.89E-02	4.84E-02	4.97E-02	4.75E-02	4.77E-02
^{247}Cm	6.22E-03	9.82E-03	1.01E-02	5.74E-03	6.26E-03	6.13E-03	6.16E-03
^{248}Cm	1.32E-03	1.46E-03	1.58E-03	1.33E-03	1.37E-03	1.31E-03	1.30E-03

Table 4.8.1. Fuel isotopic composition at EOL in start-up core (atoms/barn cm)

	ENDF/B-VI	JENDL-3.2		JEF-2.2			
	ANL	CIEMAT	JAERI	KAERI	PSI/CEA	RIT	SCK•CEN
^{234}U	5.236E-06	5.469E-06	5.721E-06	5.927E-06	6.120E-06	6.053E-06	5.606E-06
^{235}U	3.376E-07	3.160E-07	3.050E-07	3.840E-07	3.727E-07	4.062E-07	2.524E-07
^{236}U	1.506E-07	1.430E-07	1.369E-07	2.242E-08	1.404E-07	1.481E-07	8.712E-09
^{237}Np	2.695E-04	2.648E-04	2.605E-04	2.464E-04	2.658E-04	2.483E-04	2.553E-04
^{238}Np	1.900E-07	1.974E-07	2.051E-07	2.091E-07	–	2.244E-07	–
^{238}Pu	2.328E-04	2.442E-04	2.584E-04	2.730E-04	2.847E-04	2.813E-04	3.328E-04
^{239}Pu	3.025E-04	2.953E-04	2.856E-04	2.664E-04	2.822E-04	2.605E-04	2.703E-04
^{240}Pu	2.639E-04	2.631E-04	2.644E-04	2.610E-04	2.722E-04	2.637E-04	2.176E-04
^{241}Pu	6.522E-05	6.705E-05	6.551E-05	6.175E-05	6.475E-05	6.093E-05	5.919E-05
^{242}Pu	1.162E-04	1.175E-04	1.185E-04	1.159E-04	1.236E-04	1.254E-04	8.449E-05
^{241}Am	4.960E-04	4.912E-04	4.833E-04	4.280E-04	4.555E-04	4.185E-04	4.321E-04
^{242m}Am	3.219E-05	3.585E-05	3.802E-05	3.966E-05	3.202E-05	4.626E-05	2.288E-05
^{243}Am	3.875E-04	3.819E-04	3.785E-04	3.440E-04	3.626E-04	3.420E-04	3.460E-04
^{242}Cm	2.014E-05	2.011E-05	2.103E-05	2.371E-05	2.466E-05	2.397E-05	3.272E-05
^{243}Cm	2.554E-06	3.037E-06	2.896E-06	3.288E-06	3.479E-06	3.172E-06	3.905E-06
^{244}Cm	2.687E-04	2.869E-04	2.918E-04	3.118E-04	3.081E-04	3.178E-04	3.140E-04
^{245}Cm	5.515E-05	4.747E-05	4.675E-05	4.284E-05	4.174E-05	4.293E-05	4.223E-05
^{246}Cm	4.123E-06	4.148E-06	3.857E-06	3.946E-06	3.370E-06	3.760E-06	3.581E-06
^{247}Cm	1.153E-07	1.758E-07	1.418E-07	1.273E-07	9.223E-08	1.102E-07	9.743E-08
^{248}Cm	4.600E-09	1.201E-08	6.865E-09	5.785E-09	2.937E-09	3.947E-09	3.265E-09

Table 4.8.2. Fuel isotopic composition at EOL in equilibrium core (atoms/barn cm)

	ENDF/B-VI	JENDL-3.2		JEF-2.2			
	ANL	CIEMAT	JAERI	KAERI	PSI/CEA	RIT	SCK•CEN
^{234}U	9.140E-05	9.393E-05	9.370E-05	8.815E-05	9.141E-05	8.776E-05	8.967E-05
^{235}U	2.078E-05	1.951E-05	1.971E-05	2.089E-05	2.143E-05	2.123E-05	2.129E-05
^{236}U	1.182E-05	1.176E-05	1.175E-05	1.146E-05	1.178E-05	1.173E-05	1.383E-05
^{237}Np	1.620E-04	1.558E-04	1.529E-04	1.461E-04	1.,563E-04	1.445E-04	1.472E-04
^{238}Np	1.251E-07	1.309E-07	1.345E-07	1.361E-07	–	1.479E-07	1.255E-07
^{238}Pu	3.563E-04	3.826E-04	3.868E-04	3.905E-04	4.126E-04	3.929E-04	4.336E-04
^{239}Pu	1.190E-04	1.024E-04	1.025E-04	9.270E-05	9.584E-05	9.326E-05	9.565E-05
^{240}Pu	4.743E-04	4.650E-04	4.642E-04	4.523E-04	4.739E-04	4.508E-04	3.971E-04
^{241}Pu	5.656E-05	6.234E-05	6.349E-05	6.121E-05	6.094E-05	6.314E-05	5.891E-05
^{242}Pu	1.589E-04	1.595E-04	1.596E-04	1.553E-04	1.644E-04	1.613E-04	1.345E-04
^{241}Am	2.898E-04	2.817E-04	2.770E-04	2.465E-04	2.591E-04	2.364E-04	2.443E-04
^{242m}Am	2.694E-05	3.078E-05	3.157E-05	3.193E-05	2.664E-05	3.482E-05	2.084E-05
^{243}Am	2.880E-04	2.807E-04	2.783E-04	2.534E-04	2.643E-04	2.484E-04	2.510E-04
^{242}Cm	1.295E-05	1.310E-05	1.354E-05	1.490E-05	1.580E-05	1.517E-05	2.084E-05
^{243}Cm	2.187E-06	2.493E-06	2.380E-06	2.618E-06	2.963E-06	2.571E-06	3.188E-06
^{244}Cm	3.118E-04	3.324E-04	3.361E-04	3.545E-04	3.550E-04	3.593E-04	3.587E-04
^{245}Cm	9.057E-05	7.973E-05	7.836E-05	6.923E-05	7.018E-05	6.916E-05	6.938E-05
^{246}Cm	4.271E-05	4.179E-05	4.157E-05	4.187E-05	4.208E-05	4.192E-05	4.193E-05
^{247}Cm	3.841E-06	4.435E-06	4.367E-06	3.804E-06	3.966E-06	3.942E-06	3.951E-06
^{248}Cm	1.217E-06	1.452E-06	1.428E-06	1.233E-06	1.234E-06	1.253E-06	1.245E-06

Table 4.9.1. Group and isotopic components of β_{eff} in start-up core (pcm)

	ANL (ENDF/B-VI)							JAERI (ENDF/B-VI)						
	Group						Total	Group						Total
	1	2	3	4	5	6		1	2	3	4	5	6	
^{237}Np	0.725	4.259	2.887	7.174	3.176	1.140	*19.361*	0.734	4.293	2.917	7.252	3.213	1.159	*19.567*
^{238}Np	0.000	0.000	0.000	0.000	0.000	0.000	*0.000*	0.000	0.000	0.000	0.000	0.000	0.000	*0.000*
^{238}Pu	0.082	0.558	0.344	0.815	0.355	0.114	*2.267*	0.078	0.534	0.330	0.783	0.341	0.110	*2.176*
^{239}Pu	2.066	14.589	10.166	19.595	9.938	3.053	*59.407*	2.044	14.378	10.040	19.366	9.824	3.034	*58.686*
^{240}Pu	0.300	2.554	1.394	3.214	1.709	0.529	*9.700*	0.303	2.568	1.404	3.241	1.724	0.536	*9.775*
^{241}Pu	0.869	11.369	6.533	16.888	9.356	3.289	*48.304*	0.850	11.089	6.384	16.515	9.160	3.231	*47.230*
^{242}Pu	0.118	1.449	0.715	1.960	0.816	0.431	*5.489*	0.119	1.462	0.723	1.983	1.349	0.438	*6.074*
^{241}Am	0.395	3.045	1.725	3.888	1.939	0.518	*11.510*	0.403	3.095	1.757	3.962	1.975	0.531	*11.722*
^{242m}Am	0.000	0.000	0.000	0.000	0.000	0.000	*0.000*	0.066	0.757	0.391	0.908	0.465	0.132	*2.720*
^{243}Am	0.000	0.000	0.000	0.000	0.000	0.000	*0.000*	0.269	3.597	1.686	3.614	1.860	0.553	*11.578*
^{242}Cm	0.000	0.000	0.000	0.000	0.000	0.000	*0.000*	0.000	0.000	0.000	0.000	0.000	0.000	*0.000*
^{243}Cm	0.000	0.000	0.000	0.000	0.000	0.000	*0.000*	0.000	0.000	0.000	0.000	0.000	0.000	*0.000*
^{244}Cm	0.000	0.000	0.000	0.000	0.000	0.000	*0.000*	0.000	0.000	0.000	0.000	0.000	0.000	*0.000*
^{245}Cm	0.000	0.000	0.000	0.000	0.000	0.000	*0.000*	0.089	0.765	0.658	1.533	0.829	0.231	*4.106*
^{246}Cm	0.000	0.000	0.000	0.000	0.000	0.000	*0.000*	0.000	0.000	0.000	0.000	0.000	0.000	*0.000*
Total	*4.554*	*37.824*	*23.763*	*53.534*	*27.288*	*9.075*	***156.038***	*4.961*	*42.561*	*26.265*	*59.088*	*30.712*	*9.947*	***173.534***

Table 4.9.1. Group and isotopic components of β_{eff} in start-up core (pcm) (*cont.*)

	PSI (JEF-2.2)							CIEMAT (JENDL-3.2)
	Group						Total	Total
	1	2	3	4	5	6		
^{237}Np	0.679	4.977	2.397	8.874	4.020	1.618	*22.564*	28.803
^{238}Np	0.000	0.000	0.000	0.000	0.000	0.000	*0.000*	0.000
^{238}Pu	0.114	0.630	0.189	0.678	0.710	0.119	*2.440*	3.489
^{239}Pu	2.258	17.297	12.665	20.558	6.262	2.166	*61.205*	83.345
^{240}Pu	0.261	2.642	1.764	3.437	1.220	0.281	*9.605*	12.679
^{241}Pu	0.452	10.753	7.710	18.584	8.409	0.752	*46.660*	69.745
^{242}Pu	0.111	1.363	0.702	1.950	1.307	0.422	*5.856*	7.467
^{241}Am	0.539	3.640	0.930	2.471	2.976	0.393	*10.948*	17.497
^{242m}Am	0.042	0.734	0.224	0.632	0.312	0.081	*2.025*	3.184
^{243}Am	0.183	4.642	1.886	4.742	1.721	0.589	*13.763*	4.021
^{242}Cm	0.000	0.000	0.000	0.000	0.000	0.000	*0.000*	0.001
^{243}Cm	0.008	0.082	0.042	0.075	0.007	0.023	*0.237*	0.451
^{244}Cm	0.102	1.517	0.563	0.884	1.363	0.172	*4.601*	7.422
^{245}Cm	0.064	1.190	0.636	0.833	1.212	0.176	*4.111*	8.117
^{246}Cm	0.000	0.000	0.000	0.000	0.000	0.000	*0.000*	0.020
Total	*4.812*	*49.466*	*29.707*	*63.717*	*29.520*	*6.792*	***184.015***	***246.2406***

Table 4.9.2. Group and isotopic components of β_{eff} in equilibrium core (pcm)

	ANL (ENDF/B-VI)							JAERI (ENDF/B-VI)						
	Group						Total	Group						Total
	1	2	3	4	5	6		1	2	3	4	5	6	
^{232}U	7.73E-6	1.7E-5	9.47E-6	2.06E-5	6.75E-6	2.16E-6	*6.37E-5*	0.000	0.000	0.000	0.000	0.000	0.000	*0.000*
^{233}U	0.0001	0.0003	0.0002	0.0005	0.0002	0.0001	*0.0014*	0.000	0.000	0.000	0.001	0.000	0.000	*0.001*
^{234}U	0.279	1.067	0.976	2.262	0.745	0.271	*5.599*	0.280	1.065	0.977	2.265	0.746	0.273	*5.606*
^{235}U	0.207	1.125	1.045	2.519	0.997	0.420	*6.313*	0.207	1.123	1.046	2.523	0.999	0.423	*6.320*
^{236}U	0.008	0.047	0.042	0.108	0.048	0.020	*0.273*	0.008	0.049	0.044	0.113	0.050	0.021	*0.285*
^{238}U	0.0000	0.0000	0.0000	0.0002	0.0001	0.0000	*0.0004*	0.0000	0.0000	0.0001	0.0002	0.0001	0.0000	*0.0004*
^{237}Np	0.448	2.663	1.790	4.483	1.975	0.713	*12.072*	0.450	2.660	1.791	4.491	1.979	0.717	*12.088*
^{238}Np	0.000	0.000	0.000	0.000	0.000	0.000	*0.000*	0.000	0.004	0.003	0.008	0.004	0.002	*0.021*
^{238}Pu	0.817	5.651	3.448	8.225	3.563	1.147	*22.851*	0.795	5.476	3.349	7.995	3.461	1.120	*22.197*
^{239}Pu	0.408	2.909	2.005	3.889	1.963	0.607	*11.782*	0.409	2.908	2.008	3.899	1.968	0.611	*11.805*
^{240}Pu	0.684	5.877	3.170	7.354	3.894	1.213	*22.192*	0.686	5.877	3.175	7.375	3.906	1.222	*22.241*
^{241}Pu	0.331	4.359	2.472	6.430	3.552	1.254	*18.399*	0.330	4.336	2.463	6.413	3.545	1.256	*18.343*
^{242}Pu	0.208	2.583	1.258	3.471	1.442	0.766	*9.728*	0.209	2.582	1.260	3.478	2.360	0.770	*10.658*
^{241}Am	0.241	1.871	1.048	2.375	1.178	0.317	*7.030*	0.242	1.879	1.055	2.391	1.185	0.320	*7.073*
^{242m}Am	0.000	0.000	0.000	0.000	0.000	0.000	*0.000*	0.204	2.346	1.196	2.792	1.422	0.408	*8.367*
^{243}Am	0.000	0.000	0.000	0.000	0.000	0.000	*0.000*	0.198	2.667	1.232	2.655	1.360	0.407	*8.519*
^{242}Cm	0.000	0.000	0.000	0.000	0.000	0.000	*0.000*	0.000	0.000	0.000	0.000	0.000	0.000	*0.000*
^{243}Cm	0.000	0.000	0.000	0.000	0.000	0.000	*0.000*	0.000	0.000	0.000	0.000	0.000	0.000	*0.000*
^{244}Cm	0.000	0.000	0.000	0.000	0.000	0.000	*0.000*	0.000	0.000	0.000	0.000	0.000	0.000	*0.000*
^{245}Cm	0.000	0.000	0.000	0.000	0.000	0.000	*0.000*	0.256	2.213	1.880	4.405	2.373	0.665	*11.794*
^{246}Cm	0.000	0.000	0.000	0.000	0.000	0.000	*0.000*	0.000	0.000	0.000	0.000	0.000	0.000	*0.000*
^{247}Cm	0.000	0.000	0.000	0.000	0.000	0.000	*0.000*	0.000	0.000	0.000	0.000	0.000	0.000	*0.000*
^{248}Cm	0.000	0.000	0.000	0.000	0.000	0.000	*0.000*	0.000	0.000	0.000	0.000	0.000	0.000	*0.000*
Total	*3.631*	*28.152*	*17.255*	*41.116*	*19.357*	*6.729*	***116.241***	*4.342*	*35.478*	*21.399*	*50.536*	*25.229*	*8.192*	***145.176***

Table 4.9.2. Group and isotopic components of β_{eff} in equilibrium core (pcm) (*cont.*)

	PSI (JEF-2.2)							CIEMAT (JENDL-3.2)
	Group						Total	Total
	1	2	3	4	5	6		
^{232}U	0.000	0.000	0.000	0.000	0.000	0.000	*0.000*	0.000
^{233}U	0.000	0.000	0.000	0.000	0.001	0.000	*0.001*	0.000
^{234}U	0.252	0.924	0.433	1.706	1.075	0.303	*4.692*	5.496
^{235}U	0.222	1.199	1.077	2.601	1.030	0.440	*6.568*	8.087
^{236}U	0.007	0.050	0.035	0.131	0.050	0.023	*0.297*	0.302
^{238}U	0.0000	0.0001	0.0001	0.0002	0.0001	0.0000	*0.0004*	0.000
^{237}Np	0.414	3.054	1.459	5.441	2.453	0.990	*13.810*	18.269
^{238}Np	0.002	0.030	0.015	0.053	0.020	0.009	*0.129*	0.085
^{238}Pu	1.164	6.479	1.929	6.963	7.263	1.217	*25.014*	37.026
^{239}Pu	0.462	3.567	2.591	4.236	1.284	0.445	*12.586*	17.478
^{240}Pu	0.587	5.993	3.968	7.791	2.751	0.636	*21.726*	29.721
^{241}Pu	0.179	4.289	3.050	7.407	3.335	0.299	*18.560*	28.005
^{242}Pu	0.193	2.379	1.215	3.400	2.269	0.735	*10.191*	13.342
^{241}Am	0.322	2.190	0.555	1.486	1.781	0.236	*6.570*	10.884
^{242m}Am	0.135	2.374	0.718	2.042	1.002	0.261	*6.532*	10.057
^{243}Am	0.133	3.387	1.365	3.457	1.249	0.429	*10.019*	3.007
^{242}Cm	0.000	0.000	0.000	0.000	0.000	0.000	*0.000*	0.003
^{243}Cm	0.009	0.093	0.047	0.086	0.008	0.026	*0.269*	0.521
^{244}Cm	0.151	2.270	0.836	1.321	2.029	0.256	*6.864*	11.709
^{245}Cm	0.188	3.497	1.855	2.447	3.543	0.516	*12.047*	23.619
^{246}Cm	0.000	0.000	0.000	0.000	0.000	0.000	*0.000*	1.773
^{247}Cm	0.000	0.000	0.000	0.000	0.000	0.000	*0.000*	1.955
^{248}Cm	0.000	0.000	0.000	0.000	0.000	0.000	*0.000*	0.093
Total	*4.420*	*41.774*	*21.147*	*50.570*	*31.142*	*6.821*	***155.874***	***221.431***

Table 4.10.1. Activity, decay heat and neutron source strength of irradiated fuel at different cooling times (CIEMAT)

	CIEMAT									
	Start-up core					*Equilibrium core*				
Cooling time (years)	**0**	**2**	**5**	**10**	**100**	**0**	**2**	**5**	**10**	**100**
Activity (Bq)										
– Activation products										
– Actinide and daughters	1.15E+19	1.47E+18	1.21E+18	1.04E+18	2.01E+17	8.87E+18	1.57E+18	1.36E+18	1.16E+18	2.14E+17
– Fission products	2.34E+19	3.15E+17	1.32E+17	8.62E+16	9.96E+15	2.07E+19	2.55E+17	1.06E+17	6.87E+16	7.91E+15
Total	3.50E+19	1.78E+18	1.35E+18	1.12E+18	2.10E+17	2.95E+19	1.83E+18	1.47E+18	1.23E+18	2.22E+17
Decay heat (W)	1.10E+07	1.14E+06	9.26E+05	7.96E+05	1.62E+05	9.40E+06	1.27E+06	1.08E+06	9.28E+05	1.77E+05
Neutron production (n/sec)										
– (α,n)	1.24E+11	3.59E+10	2.91E+10	2.50E+10	4.73E+9	9.83E+10	3.99E+10	3.39E+10	2.92E+10	5.16E+9
– Spontaneous fission	3.76E+12	3.10E+12	2.75E+12	2.28E+12	1.12E+11	4.54E+12	3.98E+12	3.59E+12	3.04E+12	5.30E+11
Total	3.88E+12	3.13E+12	2.78E+12	2.30E+12	1.16E+11	4.63E+12	4.02E+12	3.62E+12	3.07E+12	5.35E+11

Table 4.10.2. Activity, decay heat and neutron source strength of irradiated fuel at different cooling times (PSI/CEA)

	PSI/CEA									
	Start-up core					*Equilibrium core*				
Cooling time (years)	**0**	**2**	**5**	**10**	**100**	**0**	**2**	**5**	**10**	**100**
Activity (Bq)										
– Activation products	5.34E+17	6.36E+16	2.96E+16	8.33E+15	9.91E+12	6.20E+17	6.98E+16	3.25E+16	9.14E+15	1.14E+13
– Actinide and daughters	8.18E+18	1.55E+18	1.28E+18	1.09E+18	2.08E+17	7.91E+18	1.66E+18	1.43E+18	1.22E+18	2.19E+17
– Fission products										
Total	8.71E+18	1.61E+18	1.31E+18	1.10E+18	2.08E+17	8.53E+18	1.73E+18	1.46E+18	1.23E+18	2.19E+17
Decay heat (W)	4.96E+06	1.24E+06	1.01E+06	8.66E+05	1.71E+05	4.40E+06	1.36E+06	1.16E+06	9.96E+05	1.84E+05
Neutron production (n/sec)										
– (α,n)										
– Spontaneous fission	3.95E+14	3.24E+14	2.87E+14	2.37E+14	1.07E+13	4.70E+14	4.11E+14	3.70E+14	3.13E+14	5.18E+13
Total	3.95E+14	3.24E+14	2.87E+14	2.37E+14	1.07E+13	4.70E+14	4.11E+14	3.70E+14	3.13E+14	5.18E+13

Table 4.10.3. Activity, decay heat and neutron source strength of irradiated fuel at different cooling times (JAERI)

	JAERI									
	Start-up core					*Equilibrium core*				
Cooling time (years)	**0**	**2**	**5**	**10**	**100**	**0**	**2**	**5**	**10**	**100**
Activity (Bq)										
– Activation products	6.50E+17	1.34E+16	2.88E+15	6.34E+14	4.45E+12	6.74E+17	1.41E+16	3.03E+15	6.78E+14	4.72E+12
– Actinide and daughters	1.18E+19	1.46E+18	1.22E+18	1.04E+18	2.03E+17	8.77E+18	1.57E+18	1.36E+18	1.17E+18	2.13E+17
– Fission products	5.23E+19	6.03E+17	2.38E+17	1.52E+17	1.73E+16	5.28E+19	6.04E+17	2.38E+17	1.52E+17	1.73E+16
Total	6.47E+19	2.07E+18	1.46E+18	1.19E+18	2.20E+17	6.23E+19	2.19E+18	1.60E+18	1.32E+18	2.31E+17
Decay heat (W)	2.02E+07	1.19E+06	9.46E+05	8.10E+05	1.65E+05	1.96E+07	1.31E+06	1.09E+06	9.35E+05	1.77E+05
Neutron production (n/sec)										
– (α,n)	1.28E+11	3.64E+10	2.94E+10	2.53E+10	4.79E+9	9.98E+10	4.00E+10	3.40E+10	2.92E+10	5.15E+9
– Spontaneous fission	3.80E+12	3.12E+12	2.77E+12	2.29E+12	1.09E+11	4.54E+12	3.99E+12	3.59E+12	3.04E+12	5.24E+11
Total	3.93E+12	3.16E+12	2.80E+12	2.32E+12	1.14E+11	4.64E+12	4.02E+12	3.62E+12	3.07E+12	5.29E+11

Table 4.10.4. Activity, decay heat and neutron source strength of irradiated fuel at different cooling times (RIT)

	RIT									
	Start-up core					*Equilibrium core*				
Cooling time (years)	**0**	**2**	**5**	**10**	**100**	**0**	**2**	**5**	**10**	**100**
Activity (Bq)										
– Activation products										
– Actinide and daughters										
– Fission products										
Total	2.54E+19	2.28E+18	1.59E+18	1.29E+18	2.32E+17	2.28E+19	2.40E+18	1.74E+18	1.41E+18	2.37E+17
Decay heat (W)	6.43E+06	1.30E+06	1.03E+06	8.79E+05	1.70E+05	5.41E+06	1.40E+06	1.16E+06	9.91E+05	1.79E+05
Neutron production (n/sec)										
– (α,n)	1.48E+11	4.00E+10	3.20E+10	2.74E+10	4.96E+9	1.14E+11	4.28E+10	3.61E+10	3.09E+10	5.21E+9
– Spontaneous fission	4.19E+12	3.42E+12	3.04E+12	2.51E+12	1.16E+11	4.97E+12	4.34E+12	3.90E+12	3.29E+12	5.30E+11
Total	4.34E+12	3.46E+12	3.07E+12	2.54E+12	1.21E+11	5.09E+12	4.38E+12	3.93E+12	3.32E+12	5.35E+11

Table 4.10.5. Activity, decay heat, and neutron source strength of irradiated fuel at different cooling times (SCK•CEN)

	SCK•CEN									
	Start-up core					*Equilibrium core*				
Cooling time (years)	**0**	**2**	**5**	**10**	**100**	**0**	**2**	**5**	**10**	**100**
Activity (Bq) – Activation products – Actinide and daughters – Fission products Total	2.19E+12	6.24E+11	5.02E+11	4.28E+11	7.57E+10	1.68E+12	6.60E+11	5.58E+11	4.76E+11	7.93E+10
Decay heat (W)										
Neutron production (n/sec) – (α,n) – Spontaneous fission Total										

Table 4.11. ^{210}Po activity of the target (Bq)

	JAERI	**RIT**
^{210}Po activity of target (Bq)	4.83E+16	3.922E+16

FIGURES

Figure 2.1. R-Z model of accelerator-driven minor actinide burner system

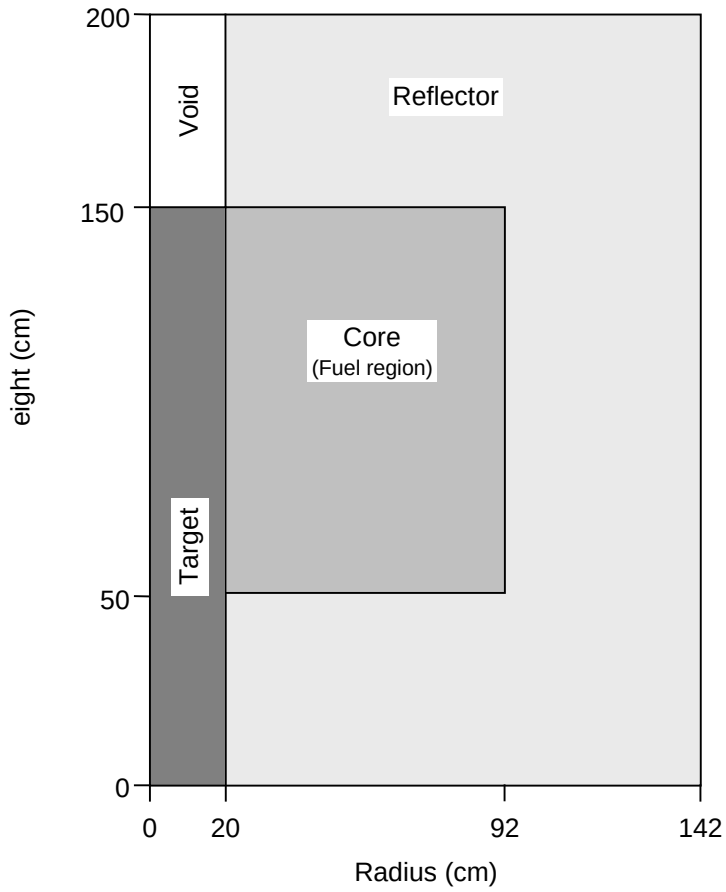

Figure 4.1.1. Start-up core: Capture cross-sections (cell averaged)

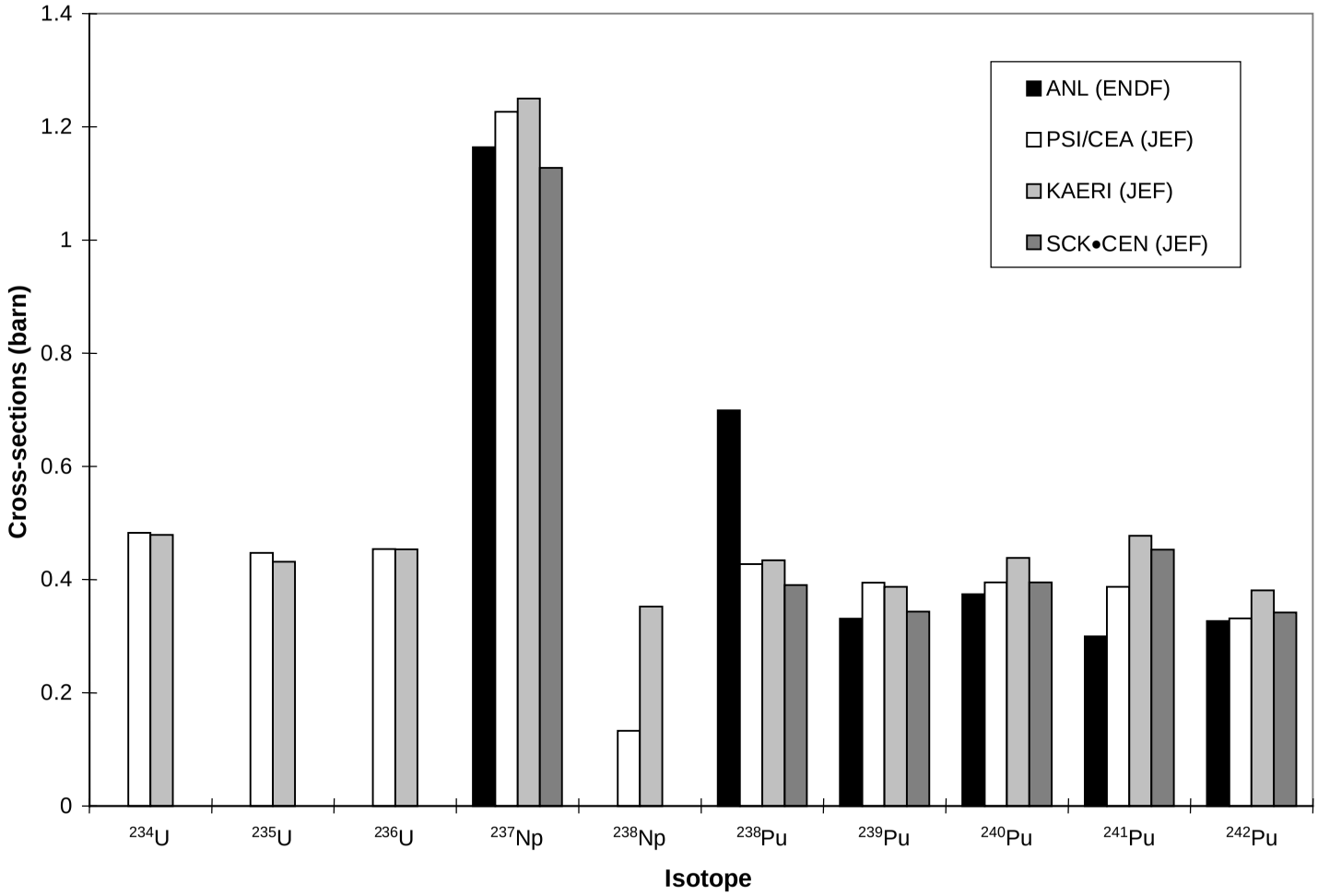

Figure 4.1.2. Start-up core: Capture cross-sections (core averaged)

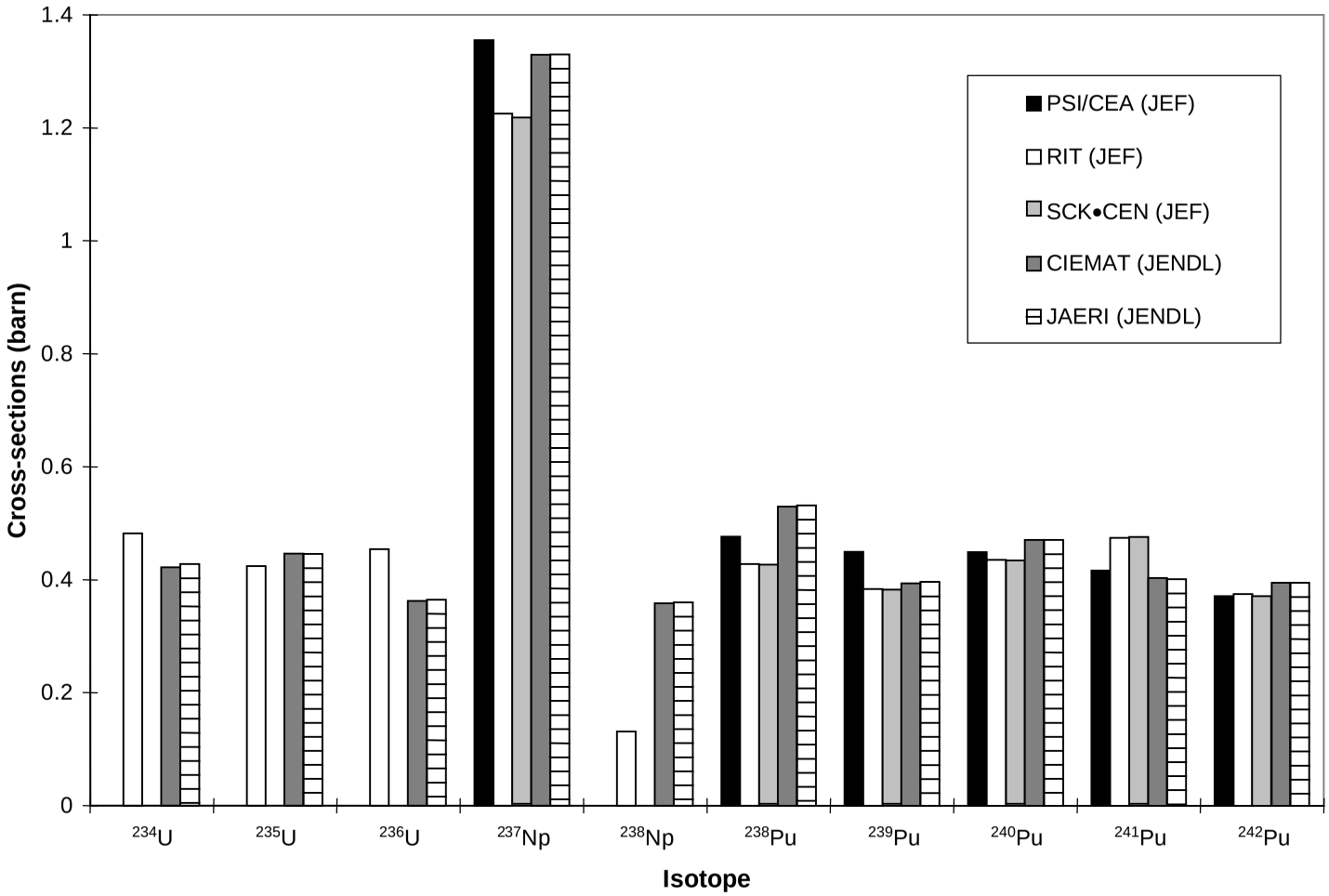

Figure 4.1.3. Start-up core: Capture cross-sections (cell averaged)

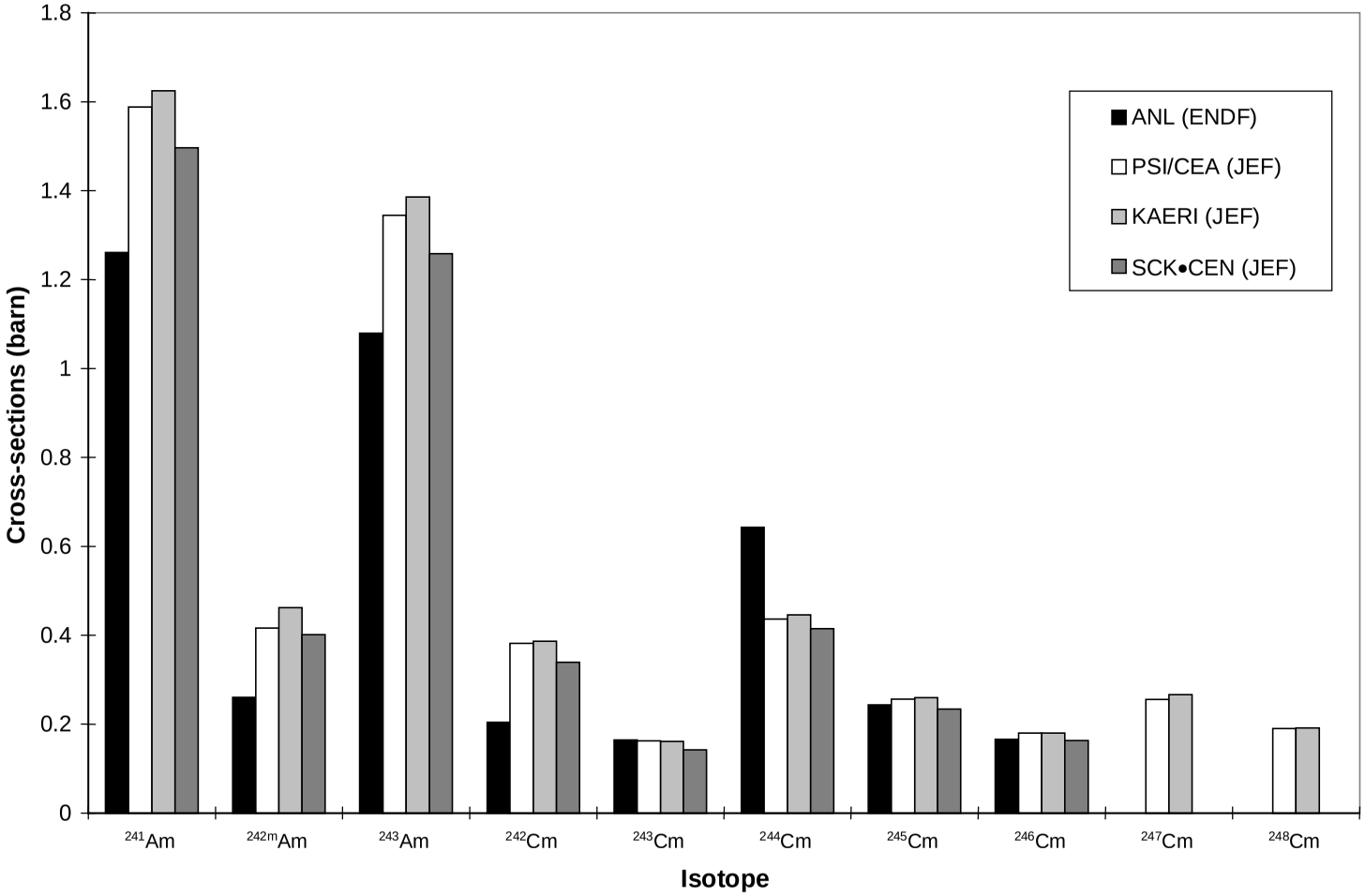

Figure 4.1.4. Start-up core: Capture cross-sections (core averaged)

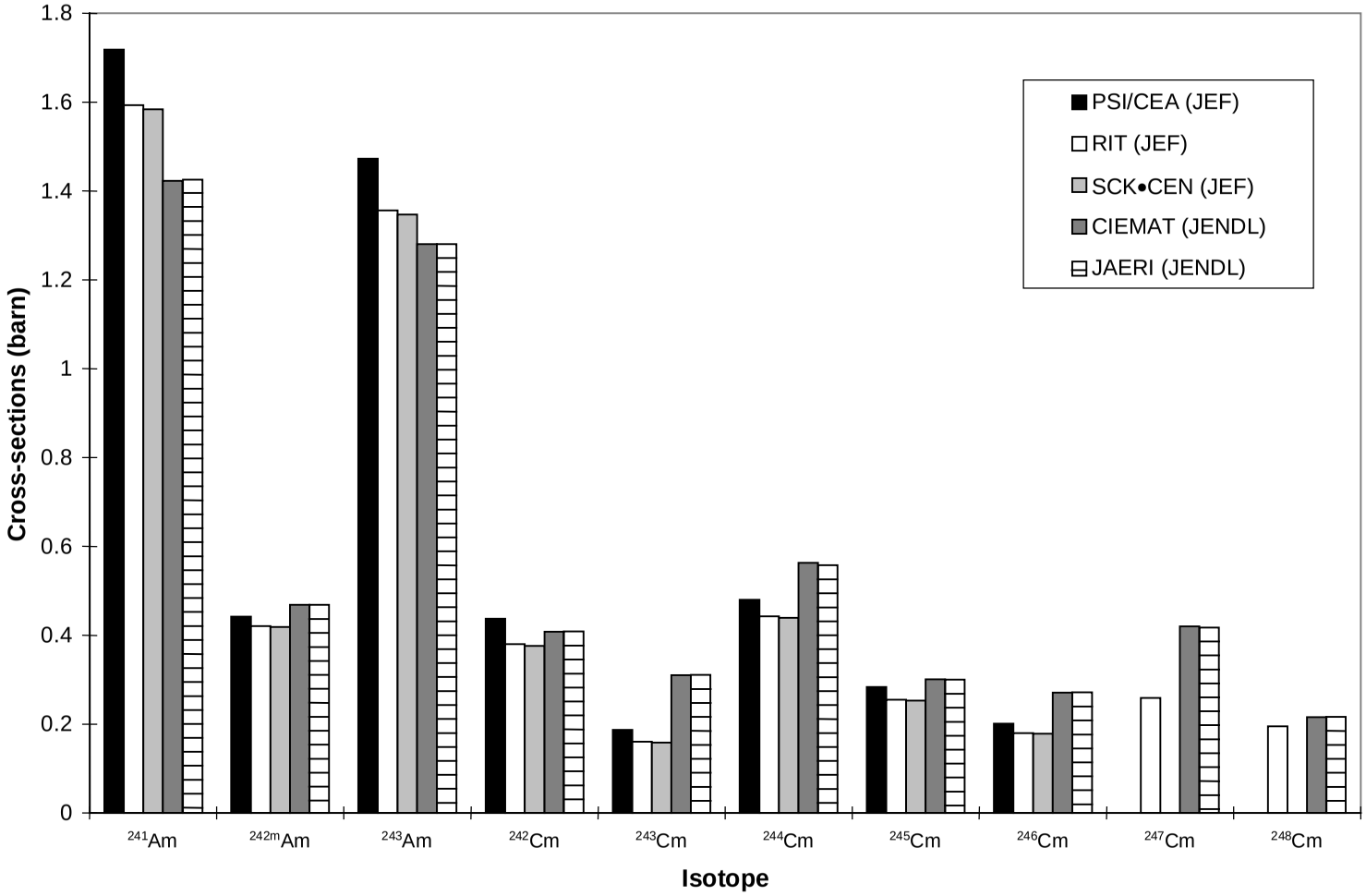

Figure 4.1.5. Equilibrium core: Capture cross-sections (cell averaged)

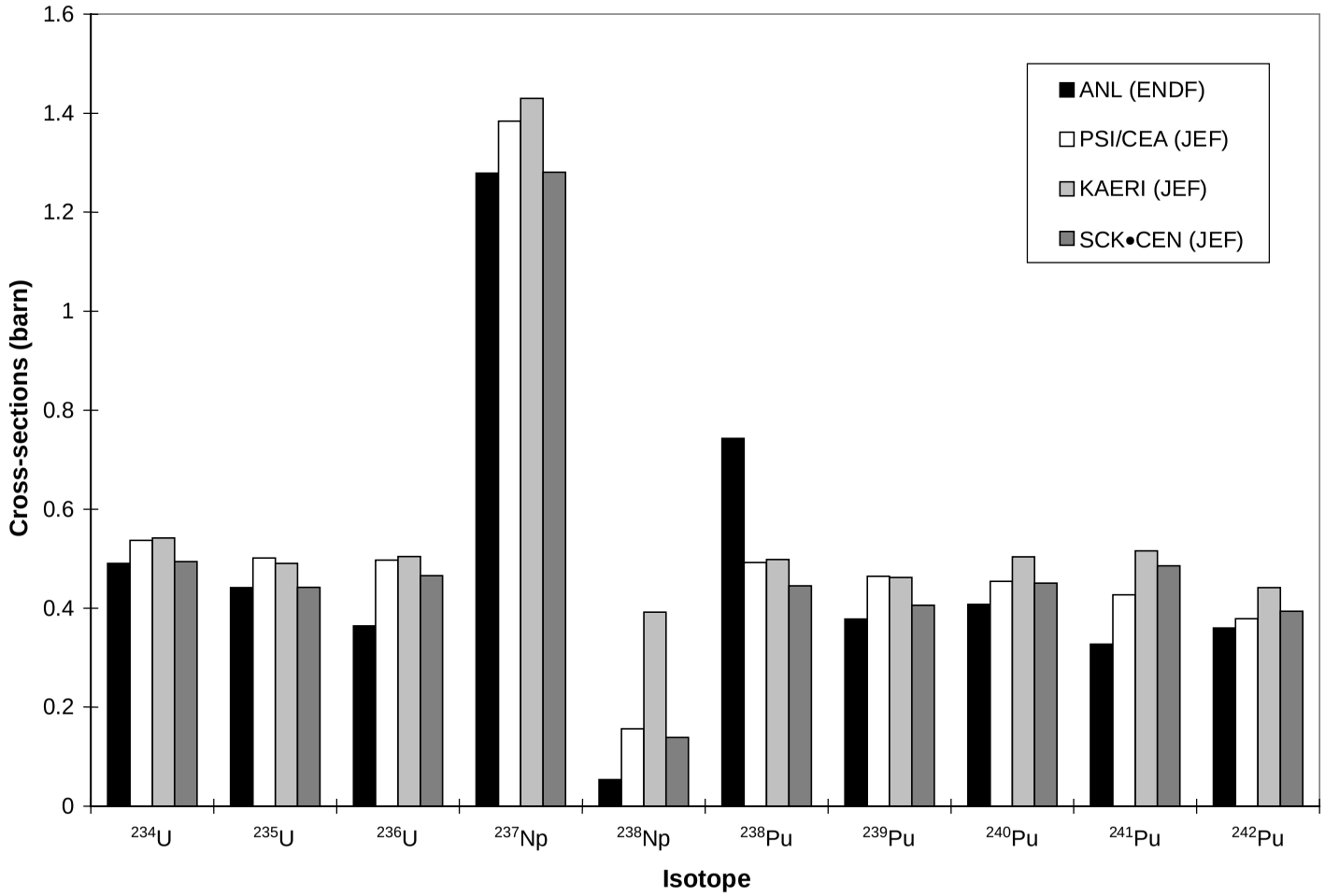

Figure 4.1.6. Equilibrium core: Capture cross-sections (core averaged)

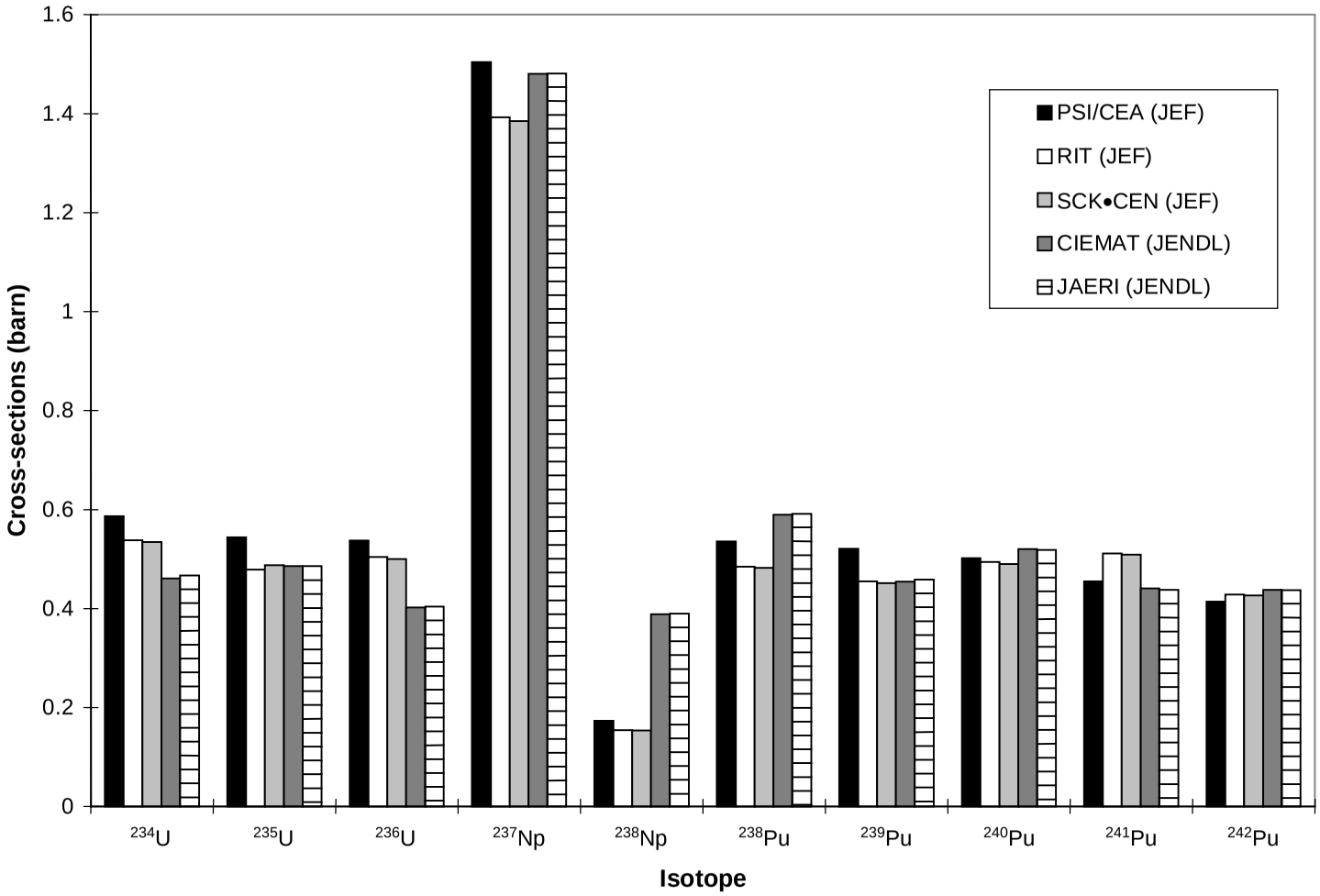

Figure 4.1.7. Equilibrium core: Capture cross-sections (cell averaged)

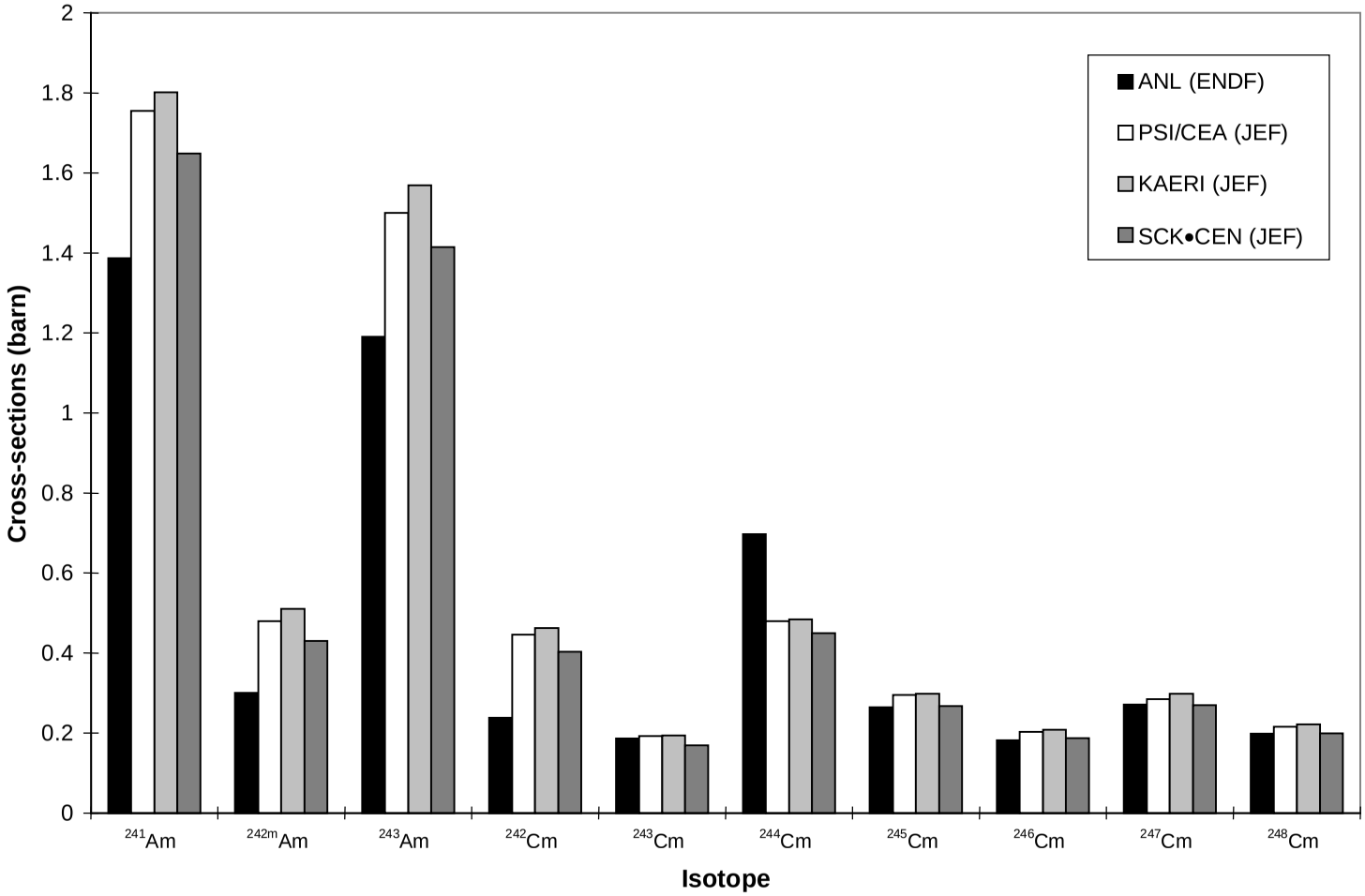

Figure 4.1.8. Equilibrium core: Capture cross-sections (core averaged)

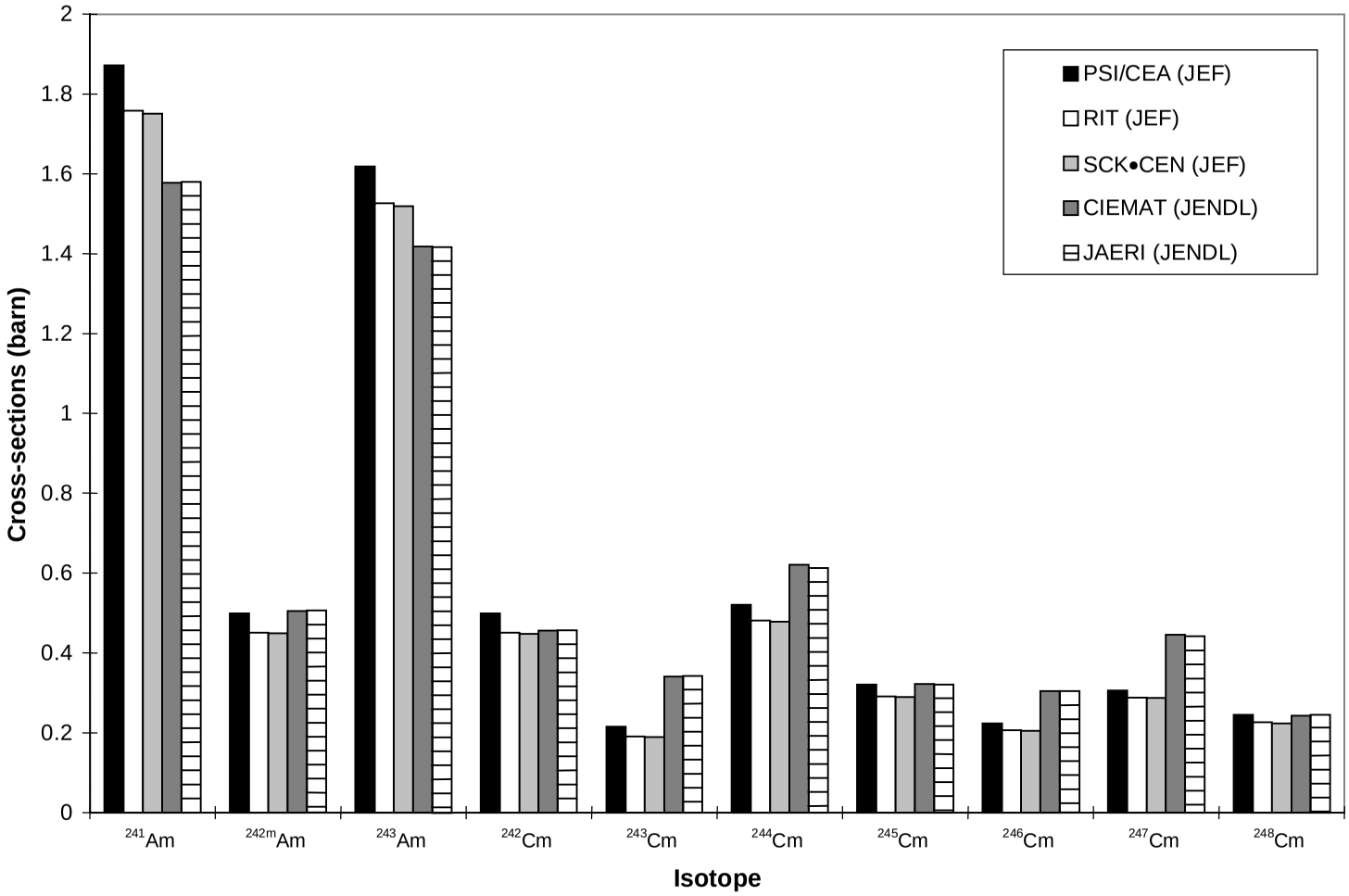

Figure 4.1.9. Start-up core: Fission cross-sections (cell averaged)

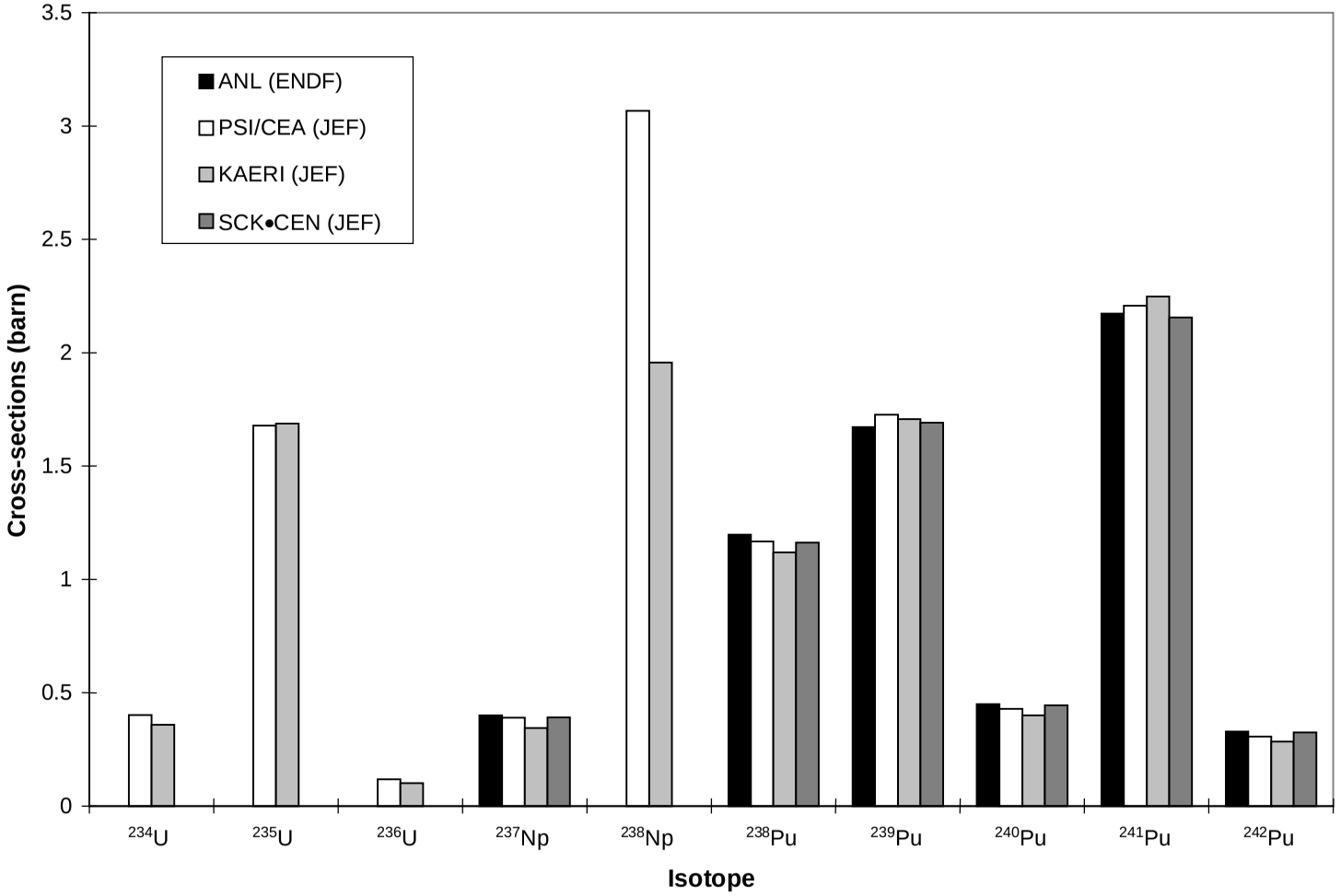

Figure 4.1.10. Start-up core: Fission cross-sections (core averaged)

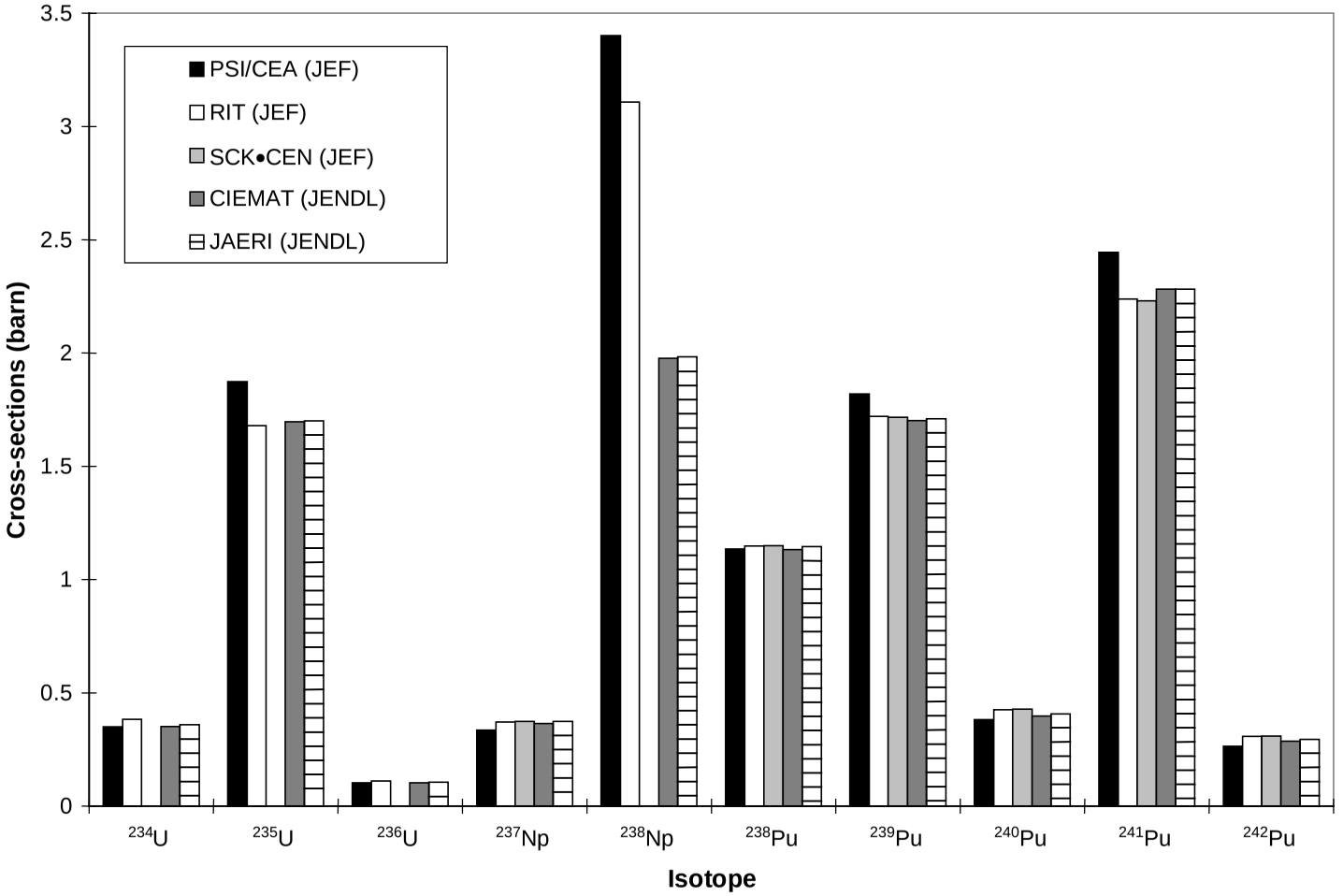

Figure 4.1.11. Start-up core: Fission cross-sections (cell averaged)

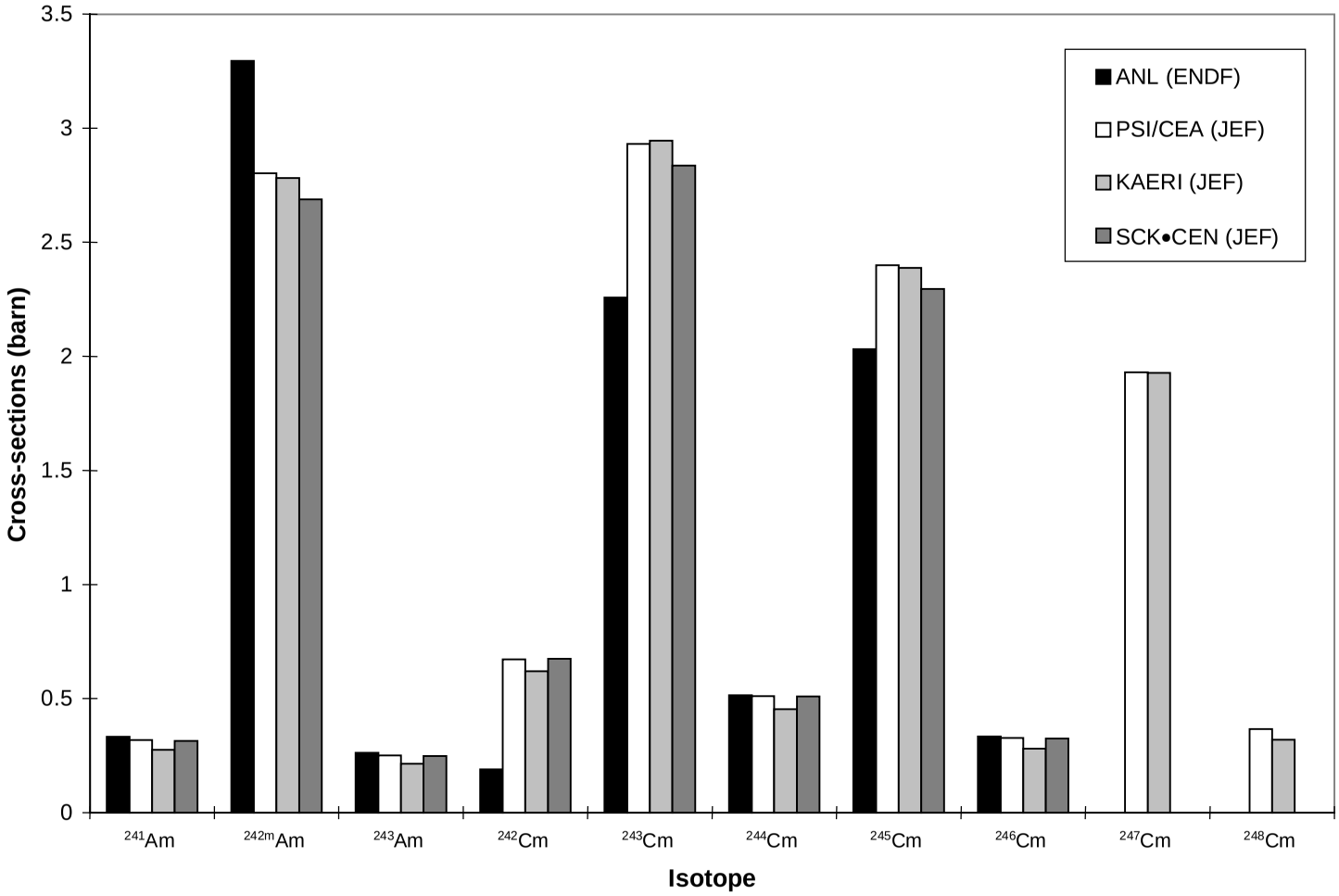

Figure 4.1.12. Start-up core: Fission cross-sections (core averaged)

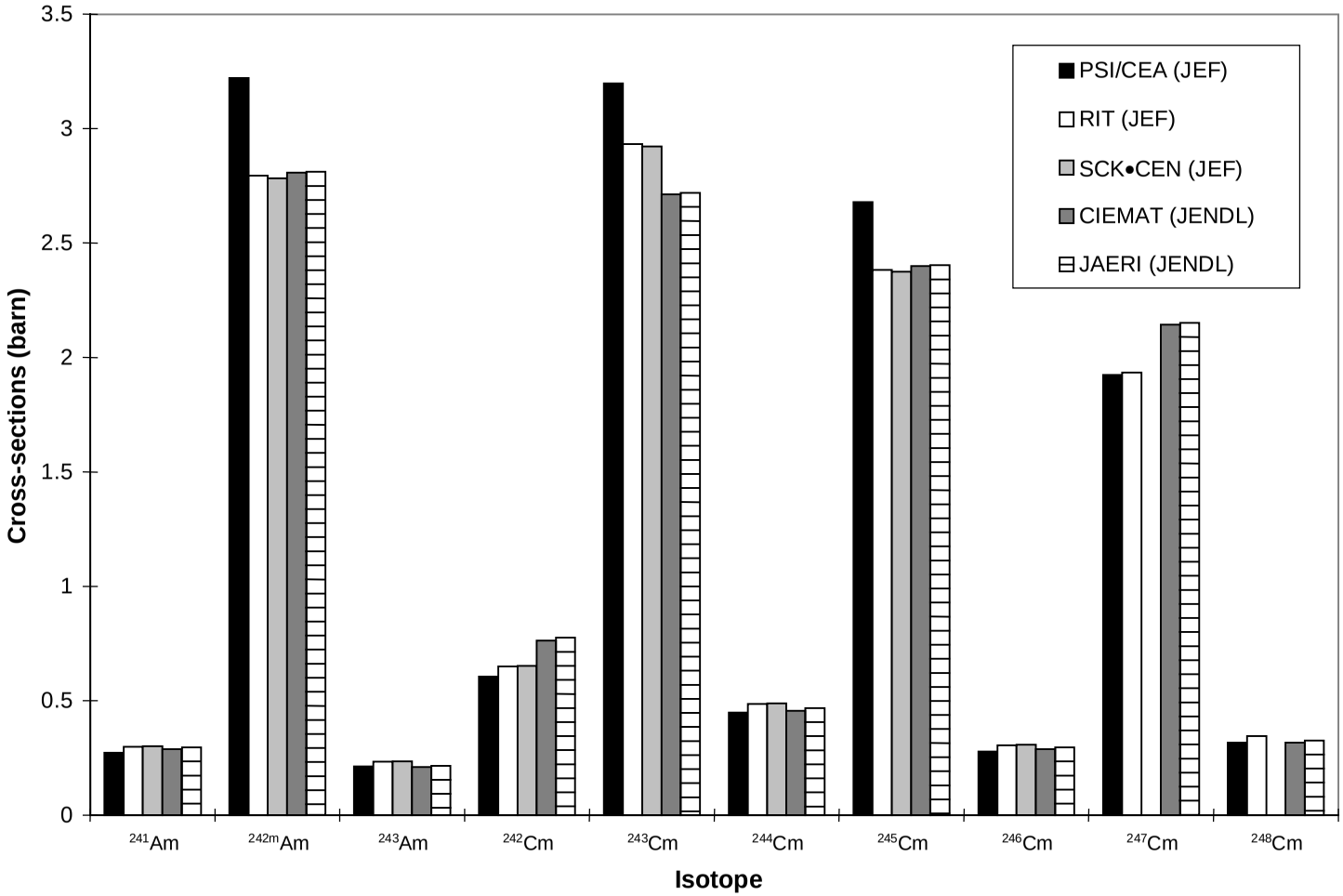

Figure 4.1.13. Equilibrium core: Fission cross-sections (cell averaged)

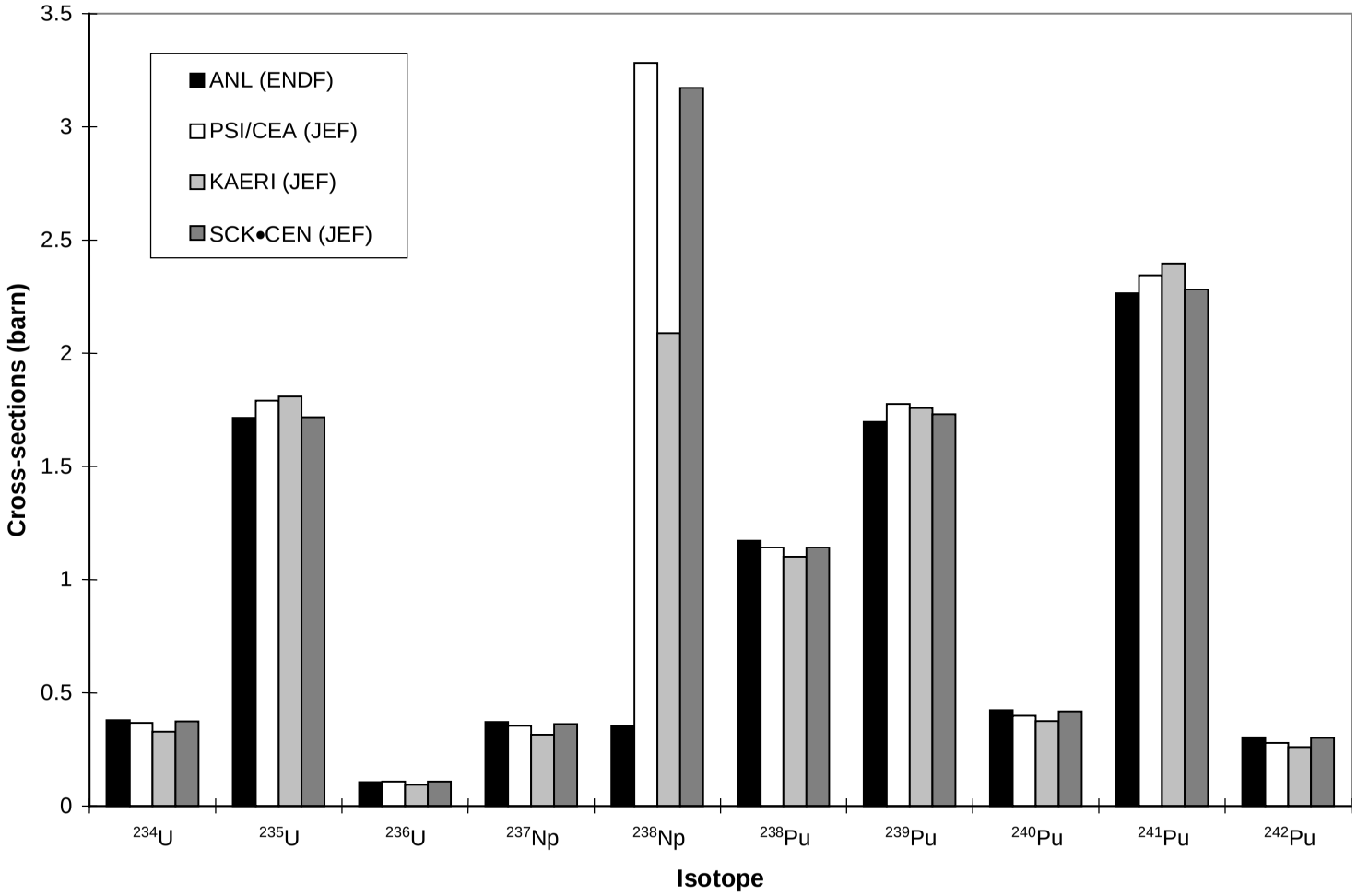

Figure 4.1.14. Equilibrium core: Fission cross-sections (core averaged)

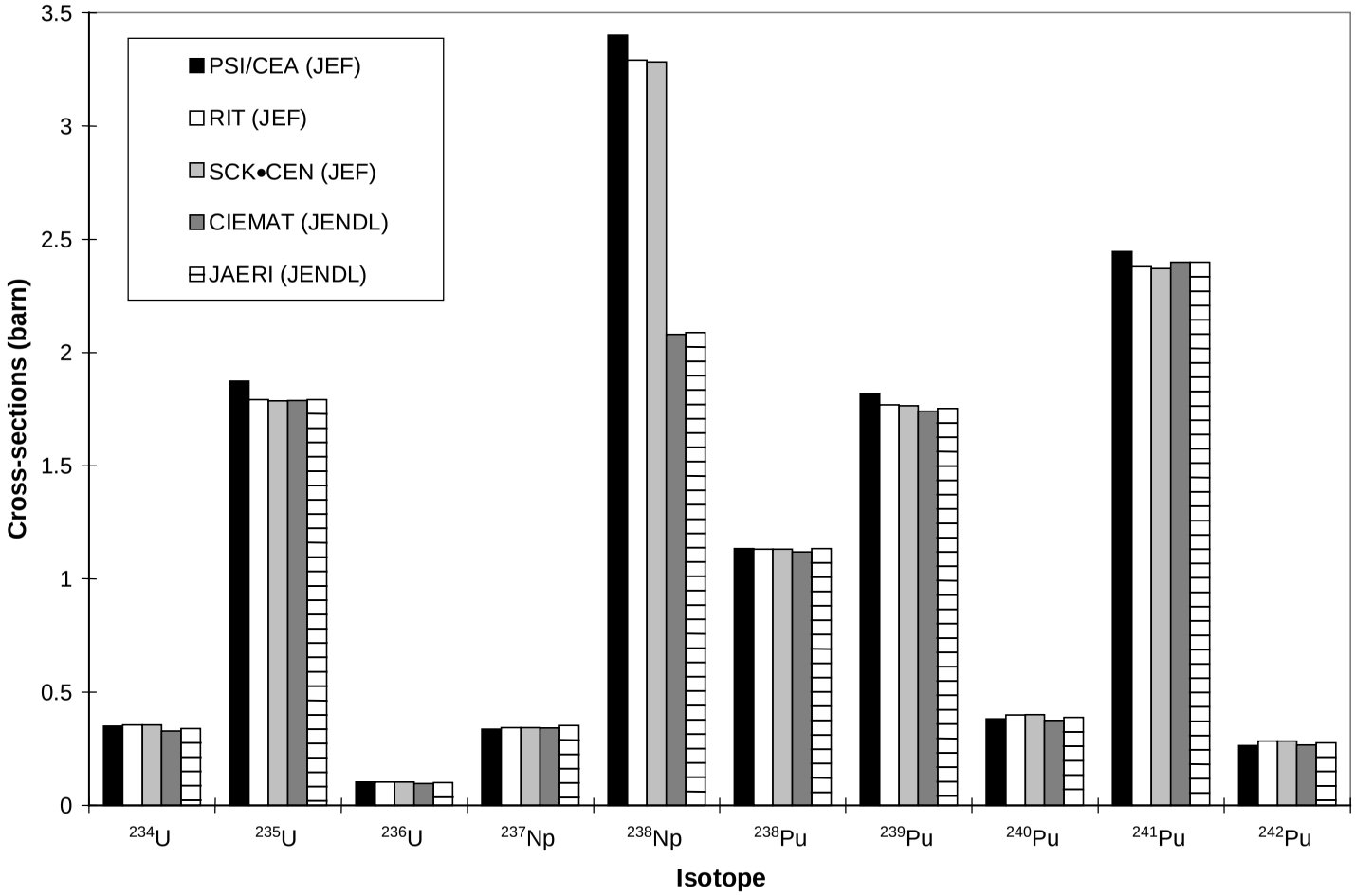

Figure 4.1.15. Equilibrium core: Fission cross-sections (cell averaged)

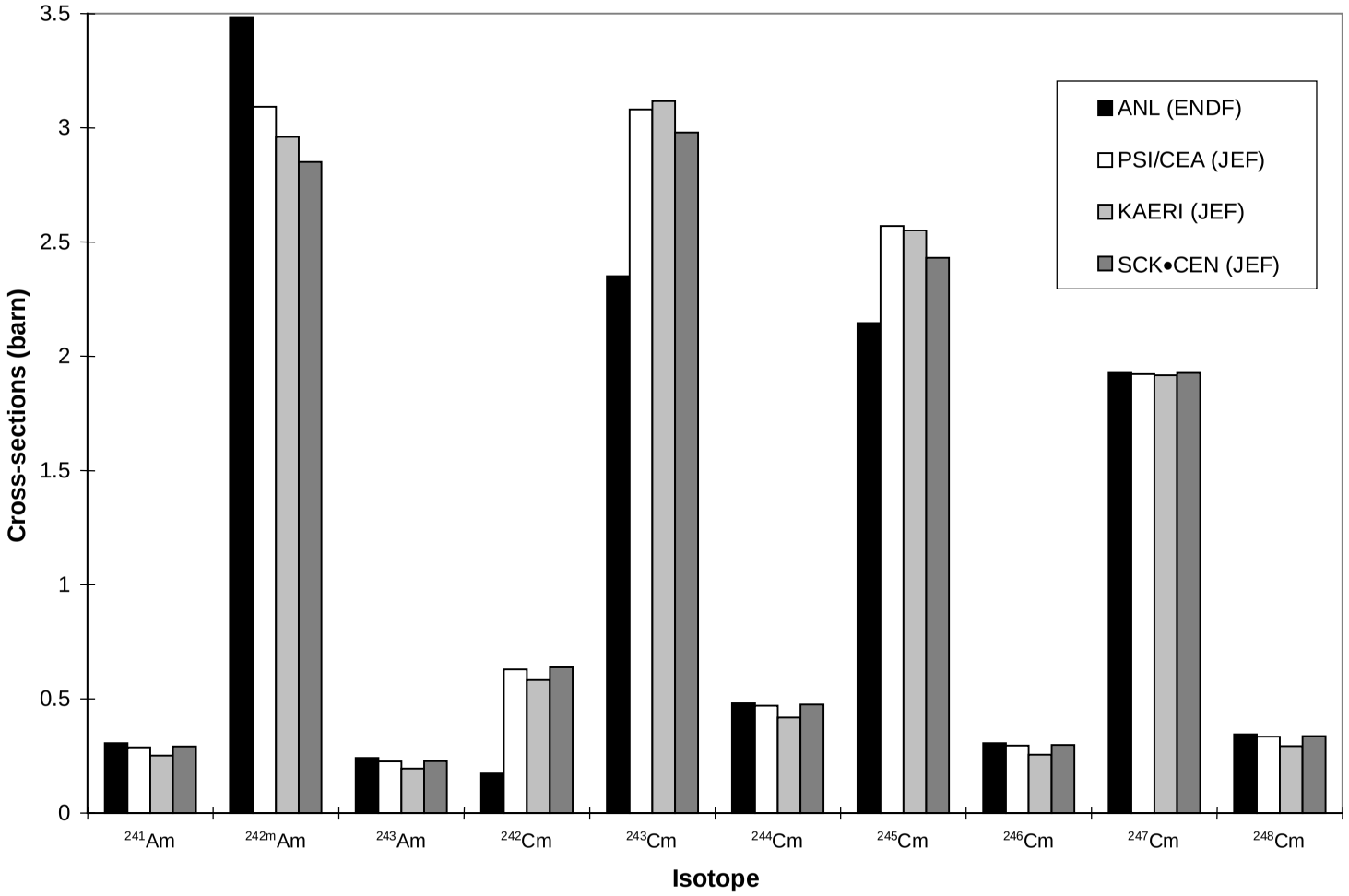

Figure 4.1.16. Equilibrium core: Fission cross-sections (core averaged)

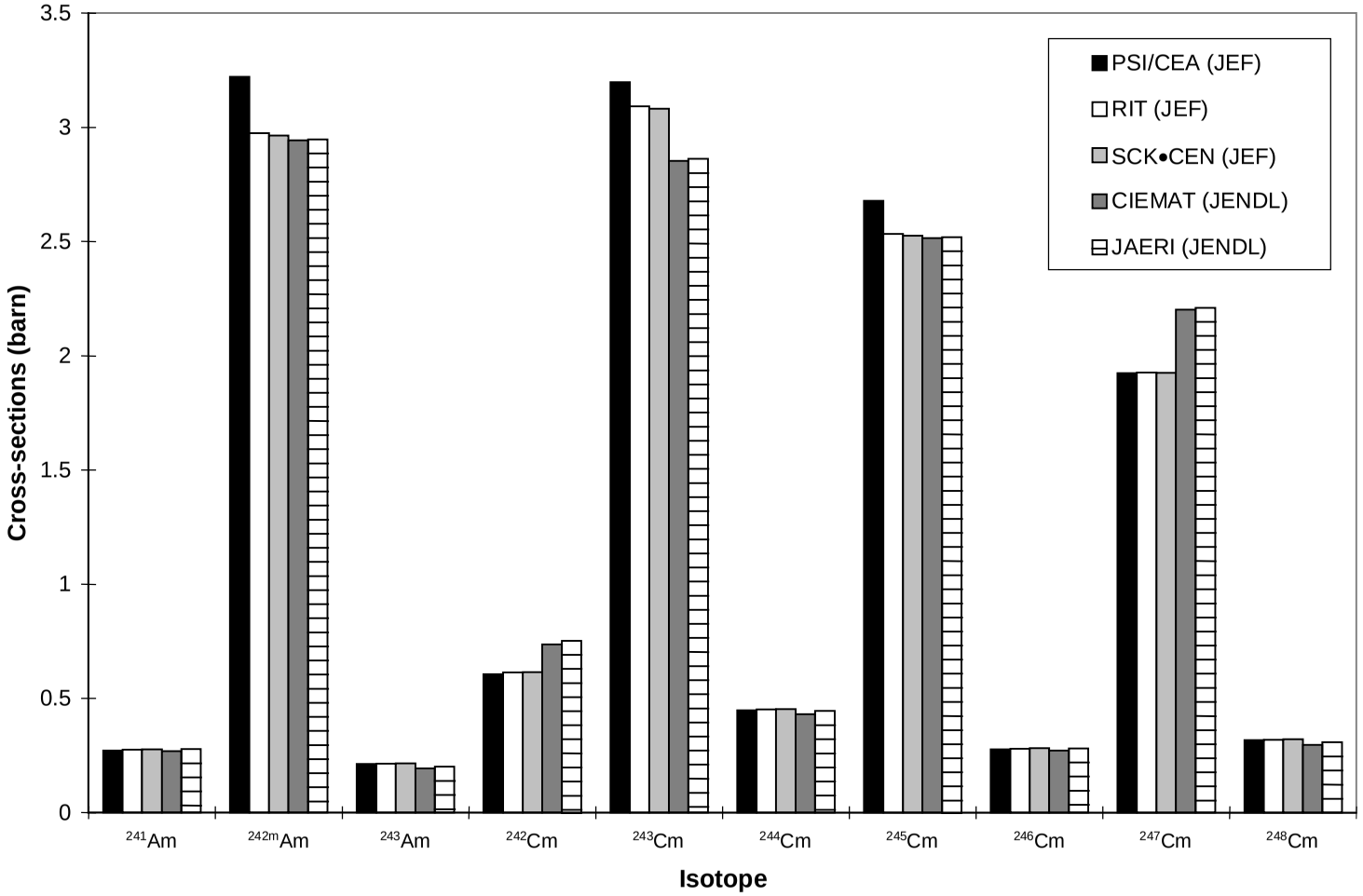

Figure 4.1.17. Comparison of averaging methods for capture cross-sections (equilibrium core)

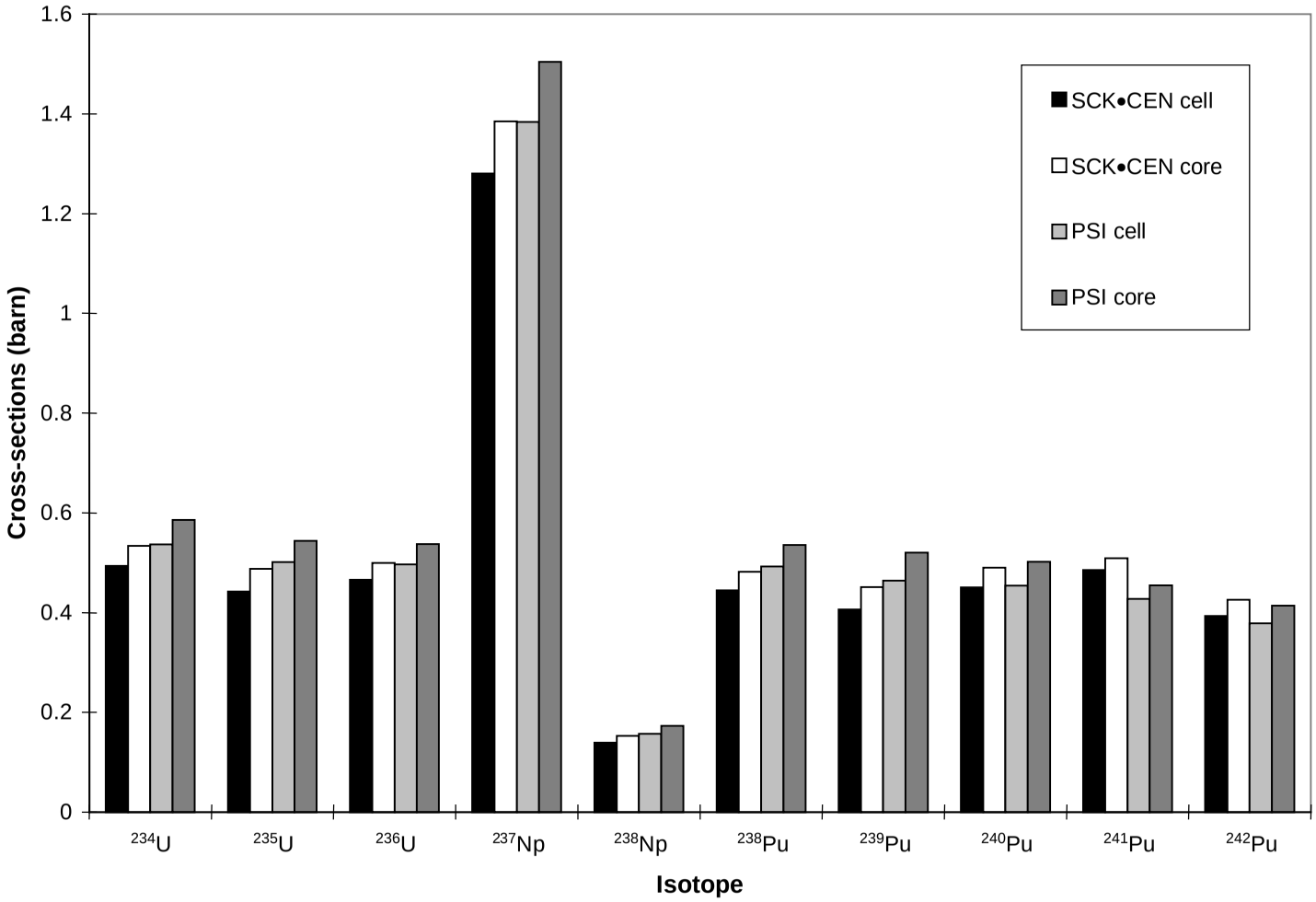

Figure 4.1.18. Comparison of averaging methods for fission cross-sections (equilibrium core)

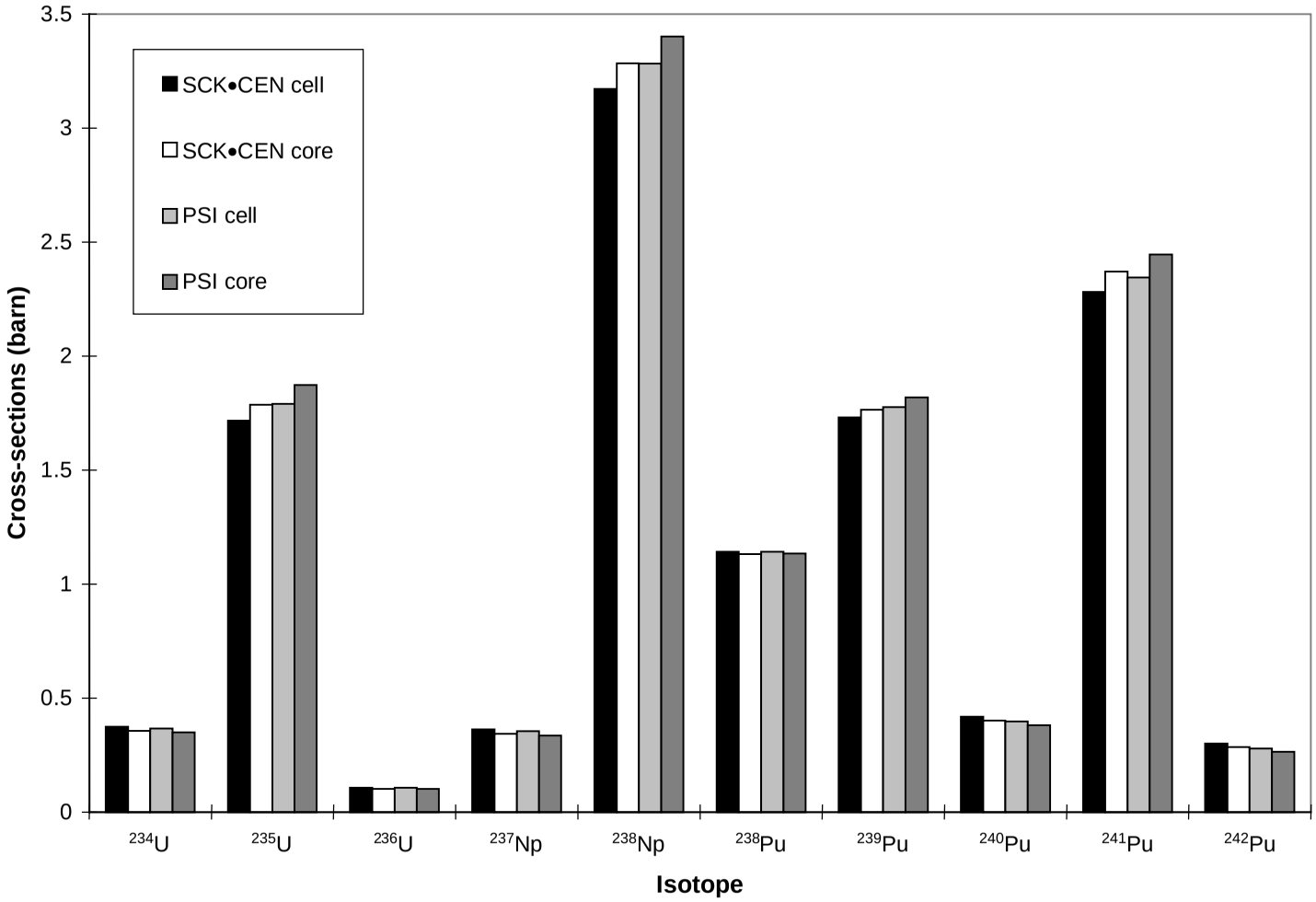

Figure 4.1.19. Comparison of averaging methods for capture cross-sections (equilibrium core)

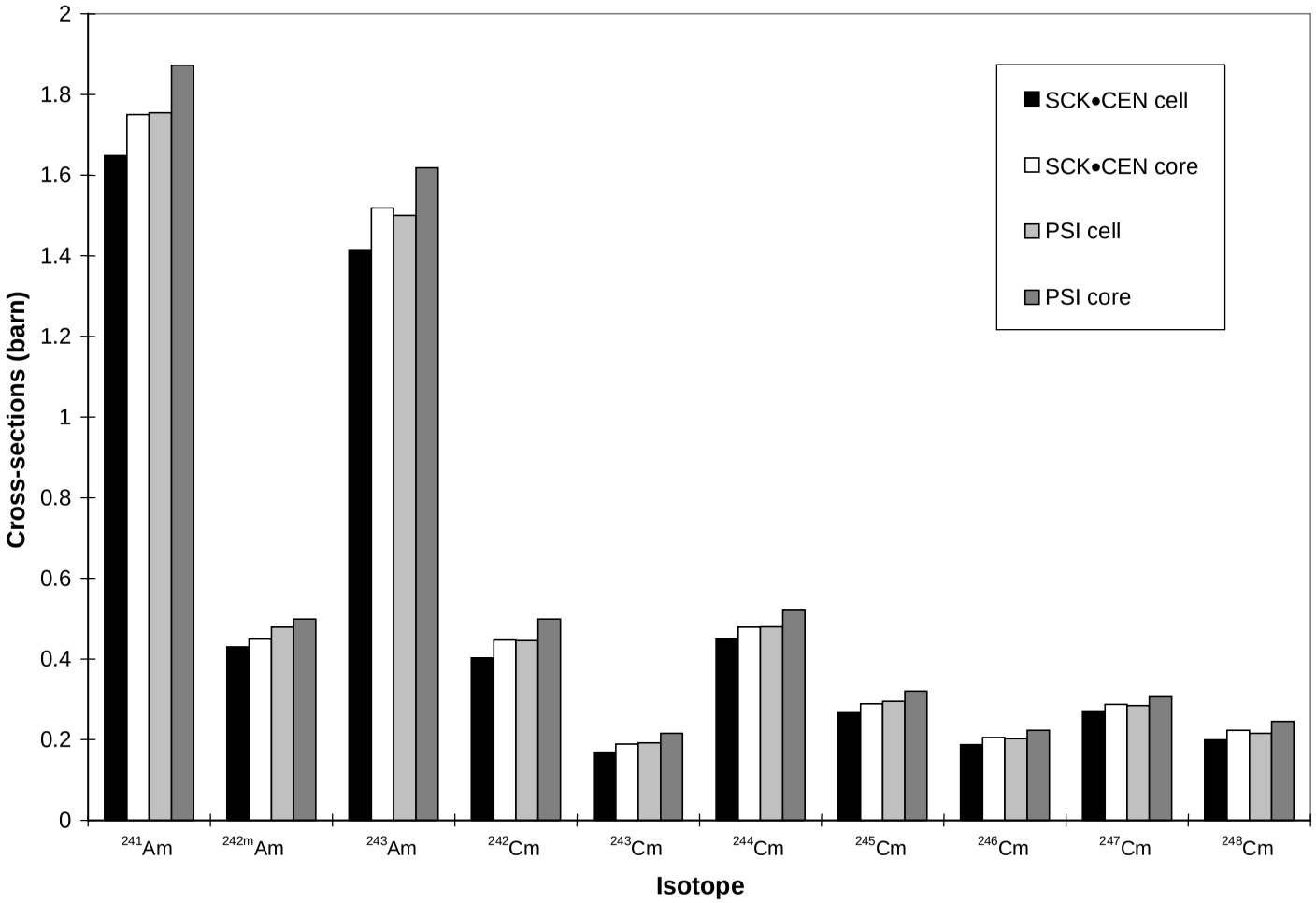

Figure 4.1.20. Comparison of averaging methods for fission cross-sections (equilibrium core)

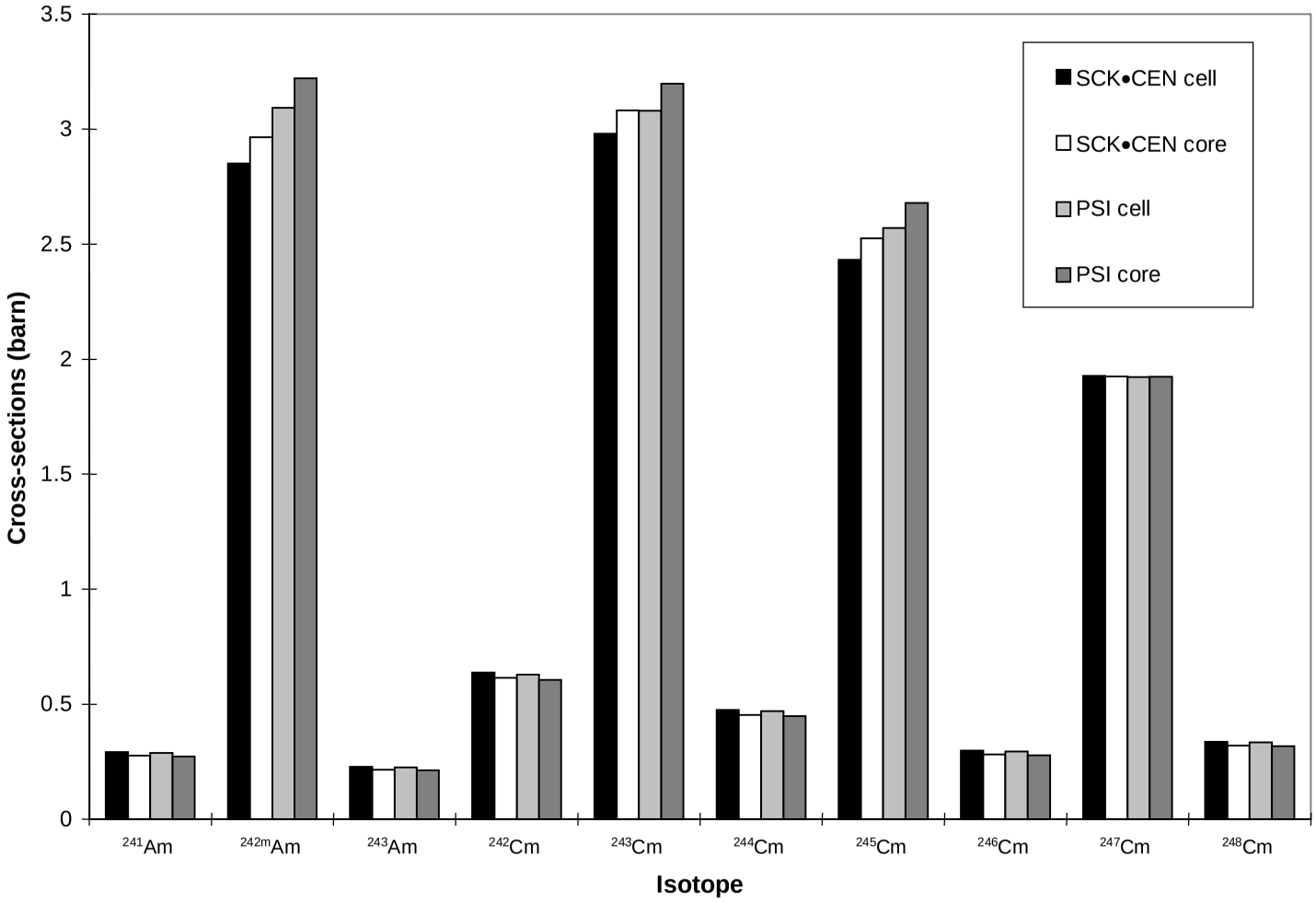

Figure 4.2.1. Start-up core: k_{eff} variation

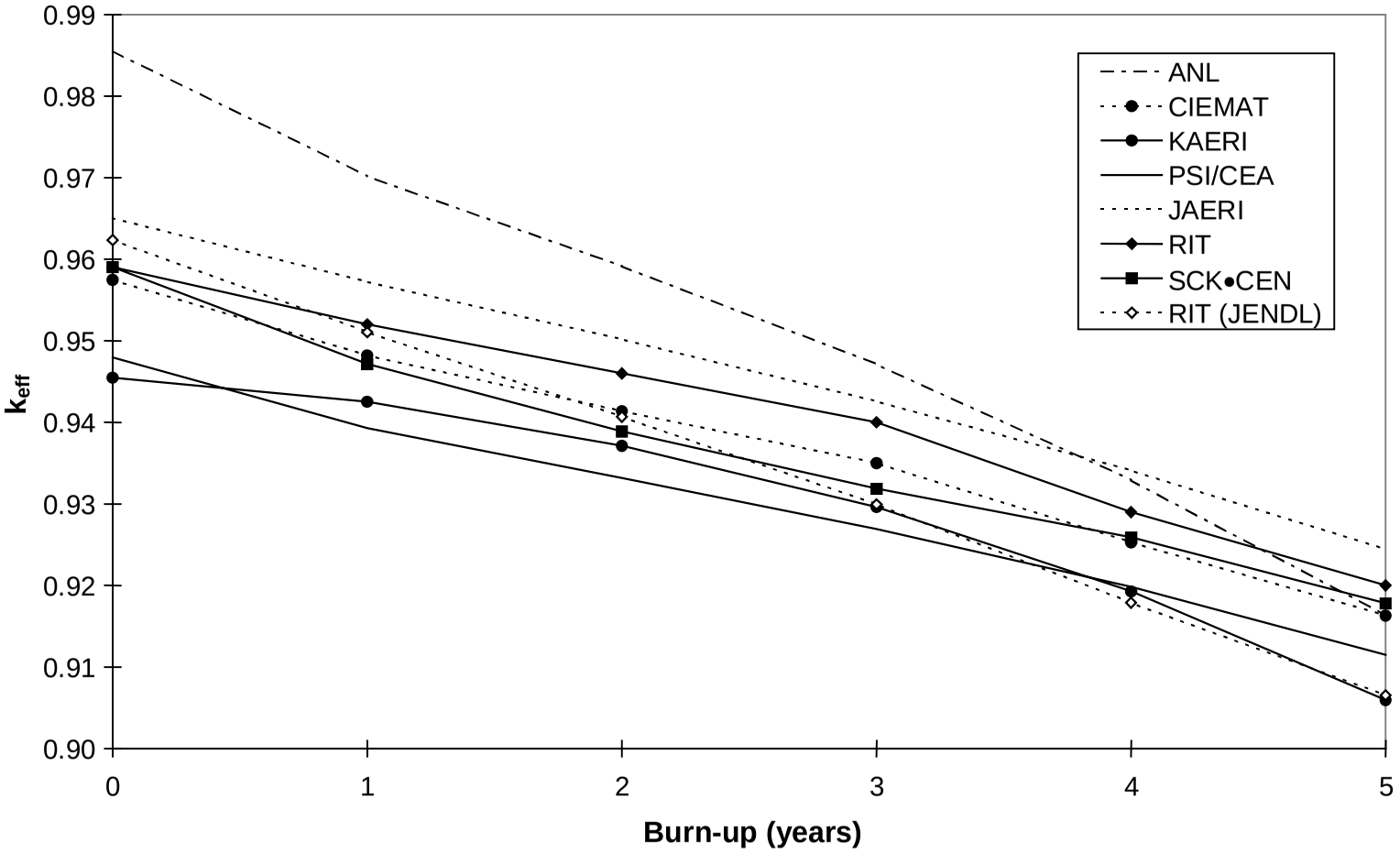

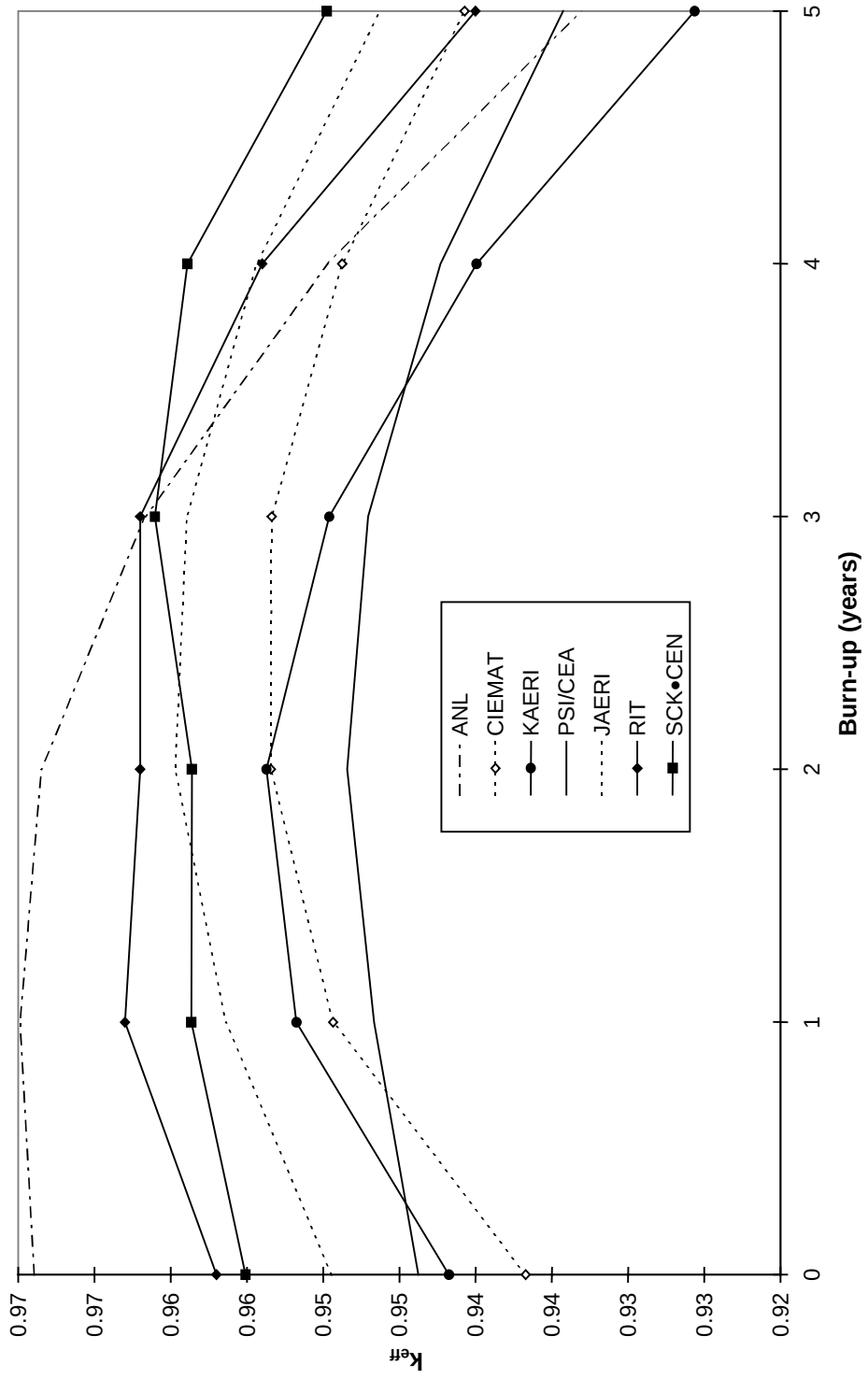

Figure 4.2.2. Equilibrium core: k_{eff} variation

Figure 4.2.3. Effect of burn-up intervals on the reactivity drop: RIT calculation for start-up core

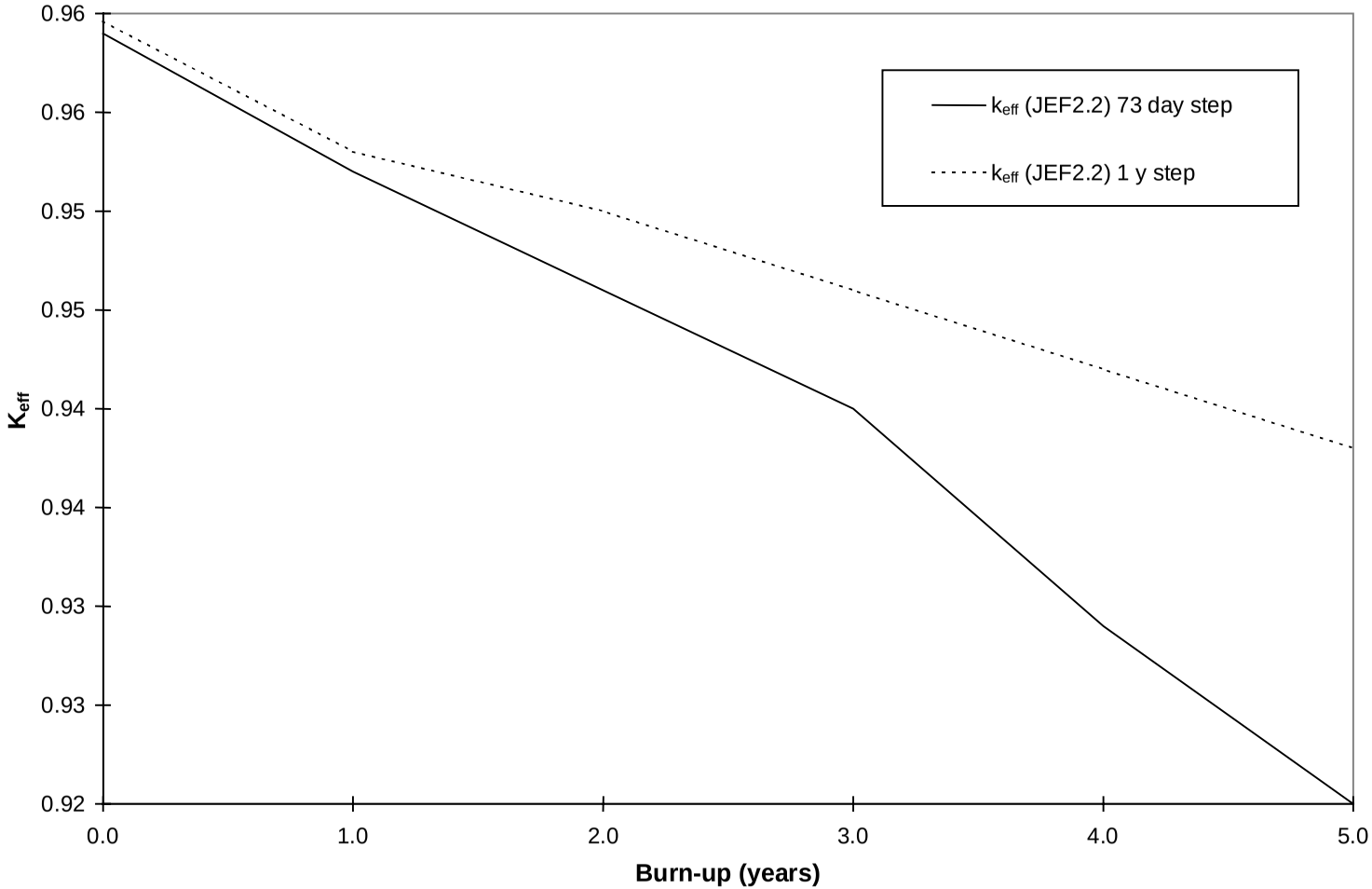

Figure 4.3.1. Neutron spectrum for the start-up core (JEF based solutions)

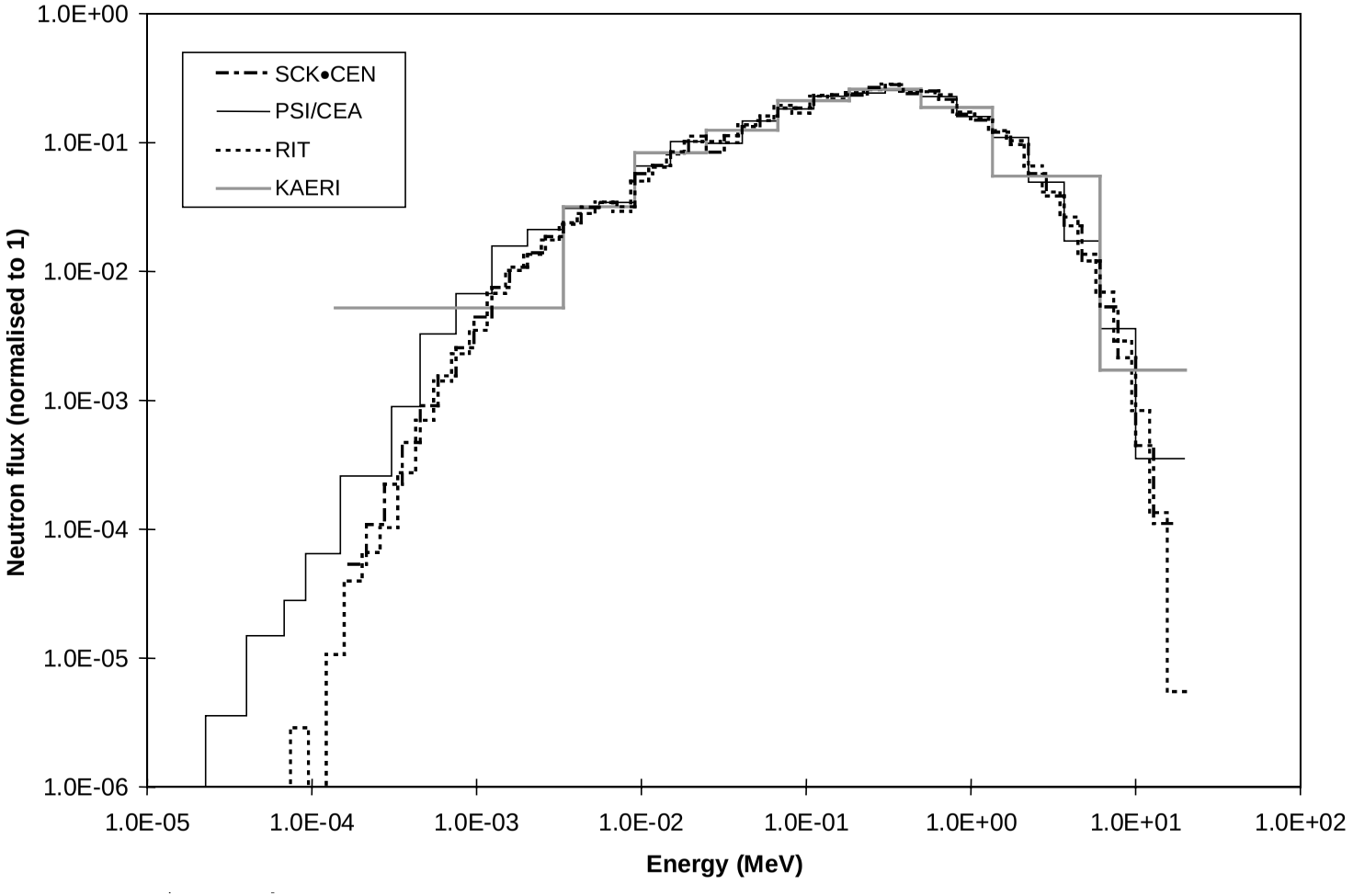

Figure 4.3.2. Neutron spectrum for the start-up core (ENDF and JENDL based solutions)

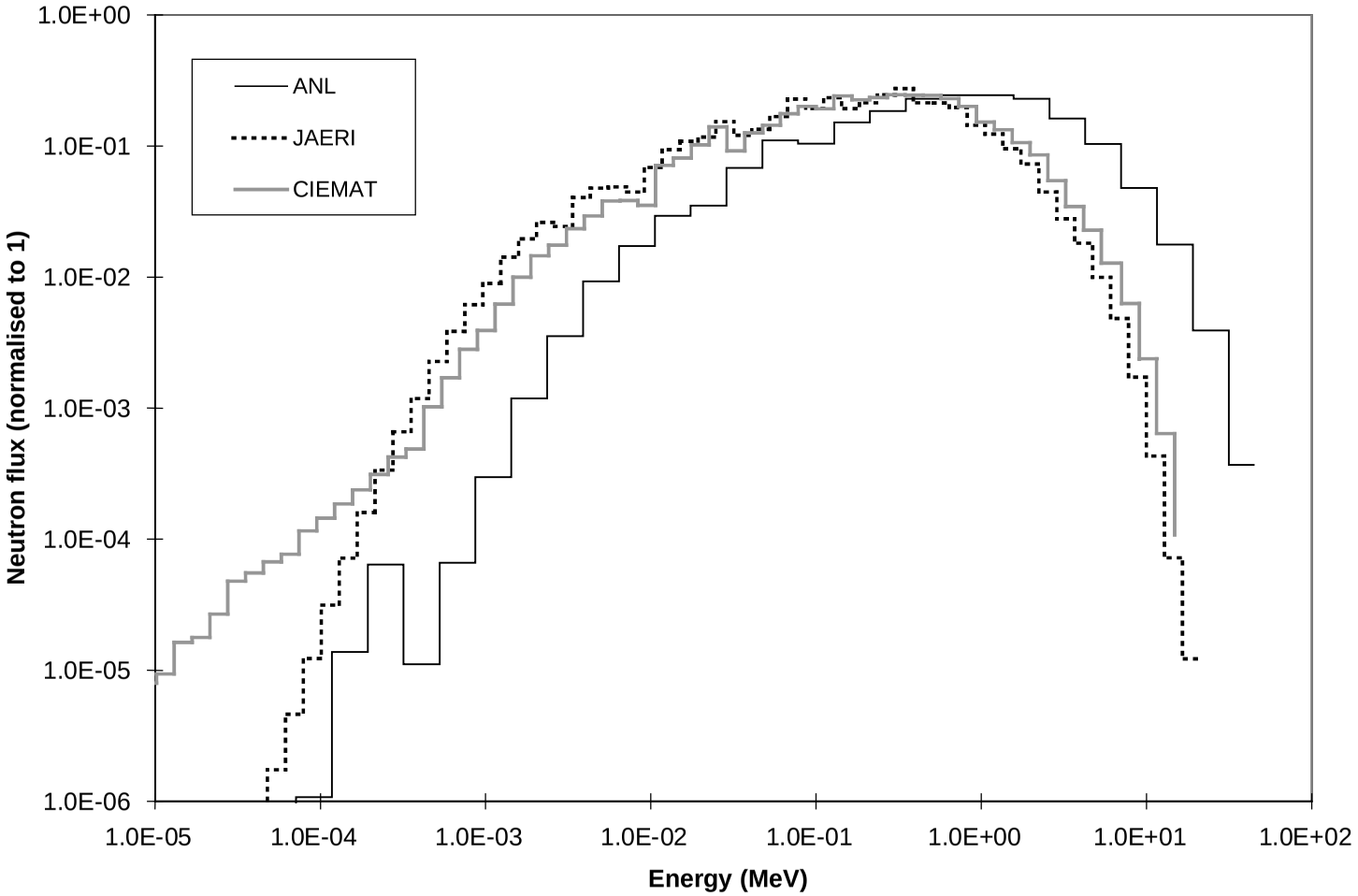

Figure 4.3.3. Neutron spectrum for the equilibrium core (JEF based solutions)

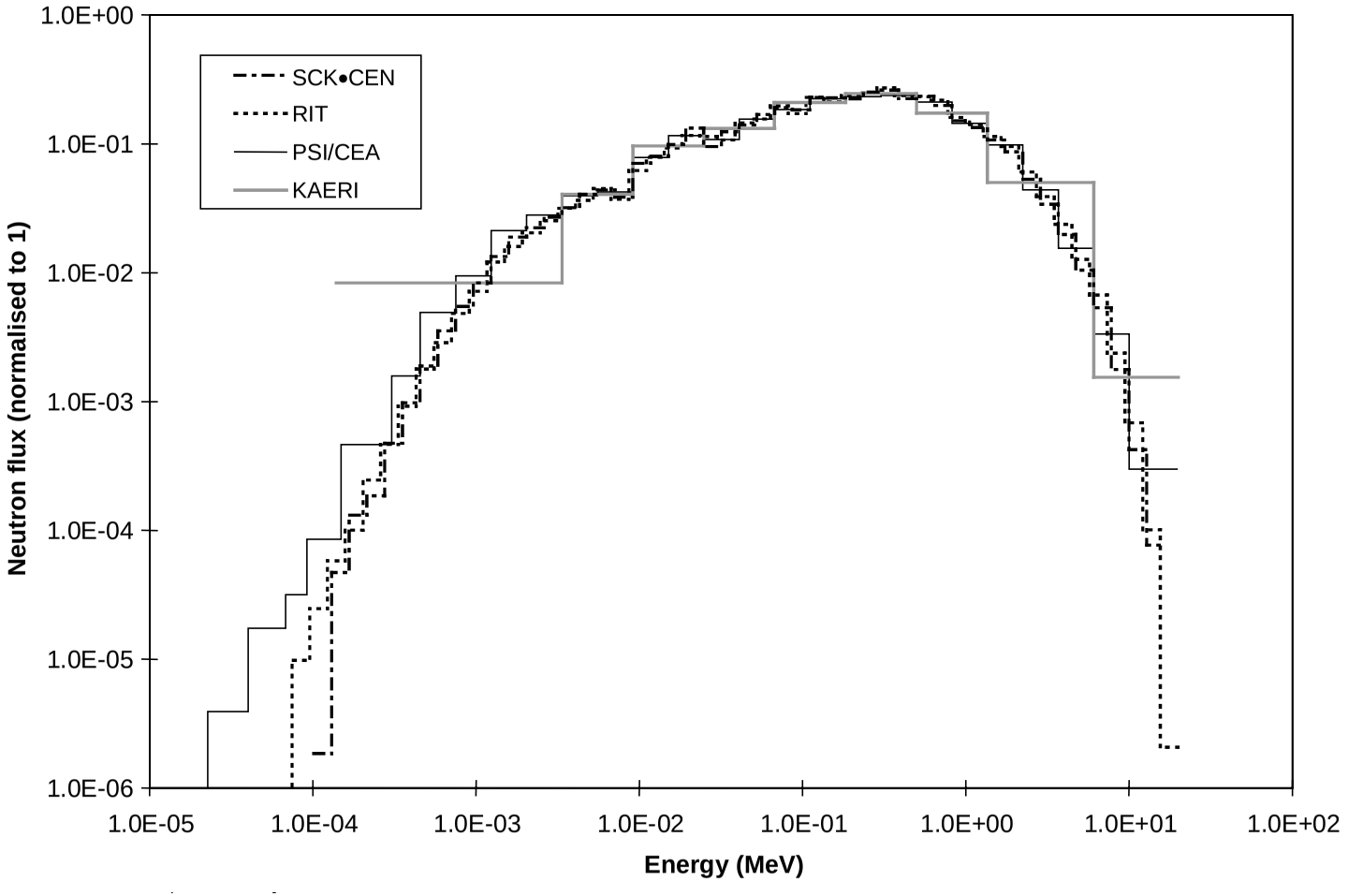

Figure 4.3.4. Neutron spectrum for the equilibrium core (ENDF and JENDL based solutions)

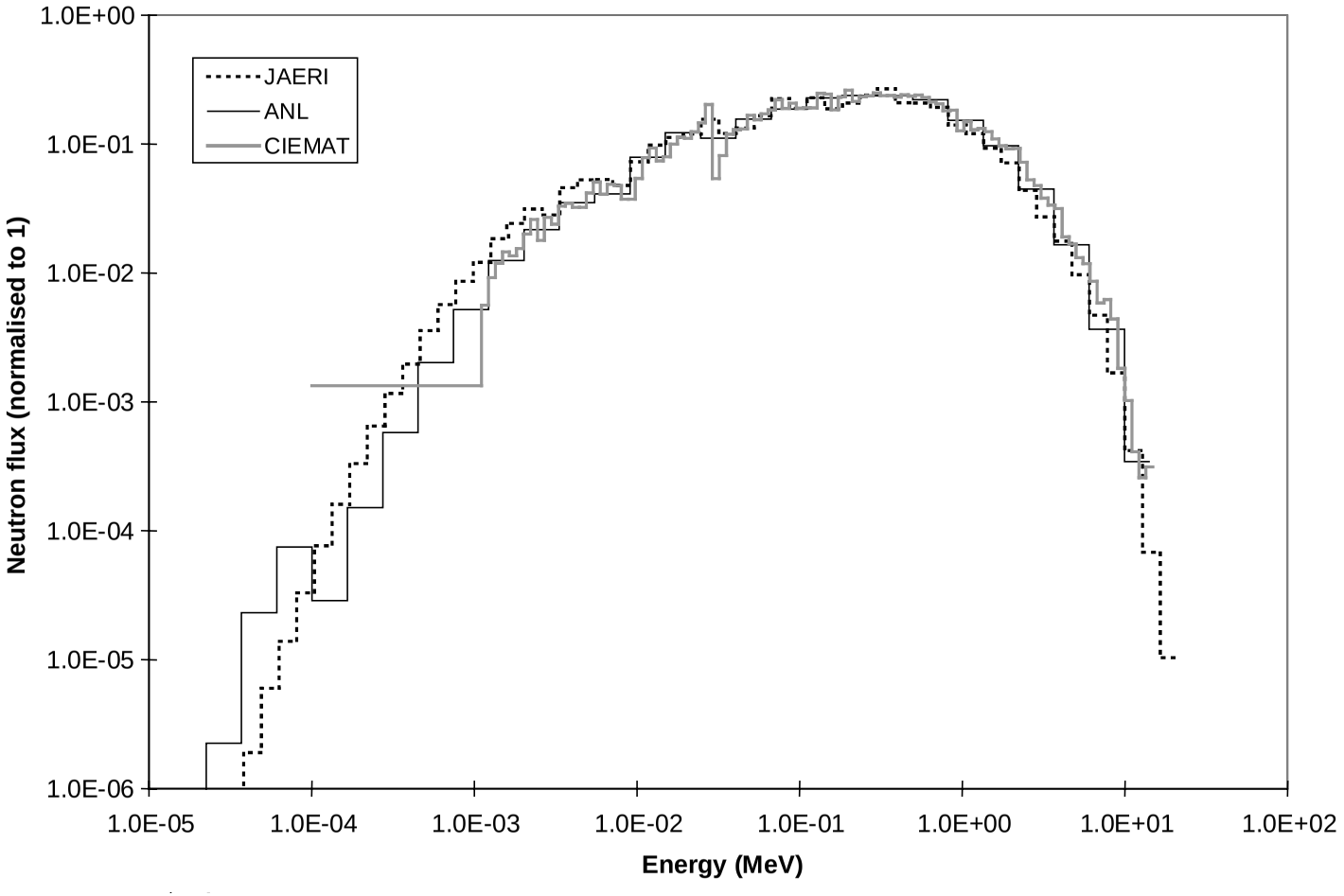

Figure 4.4.1. Start-up core: Axial flux distribution at *R* = 0

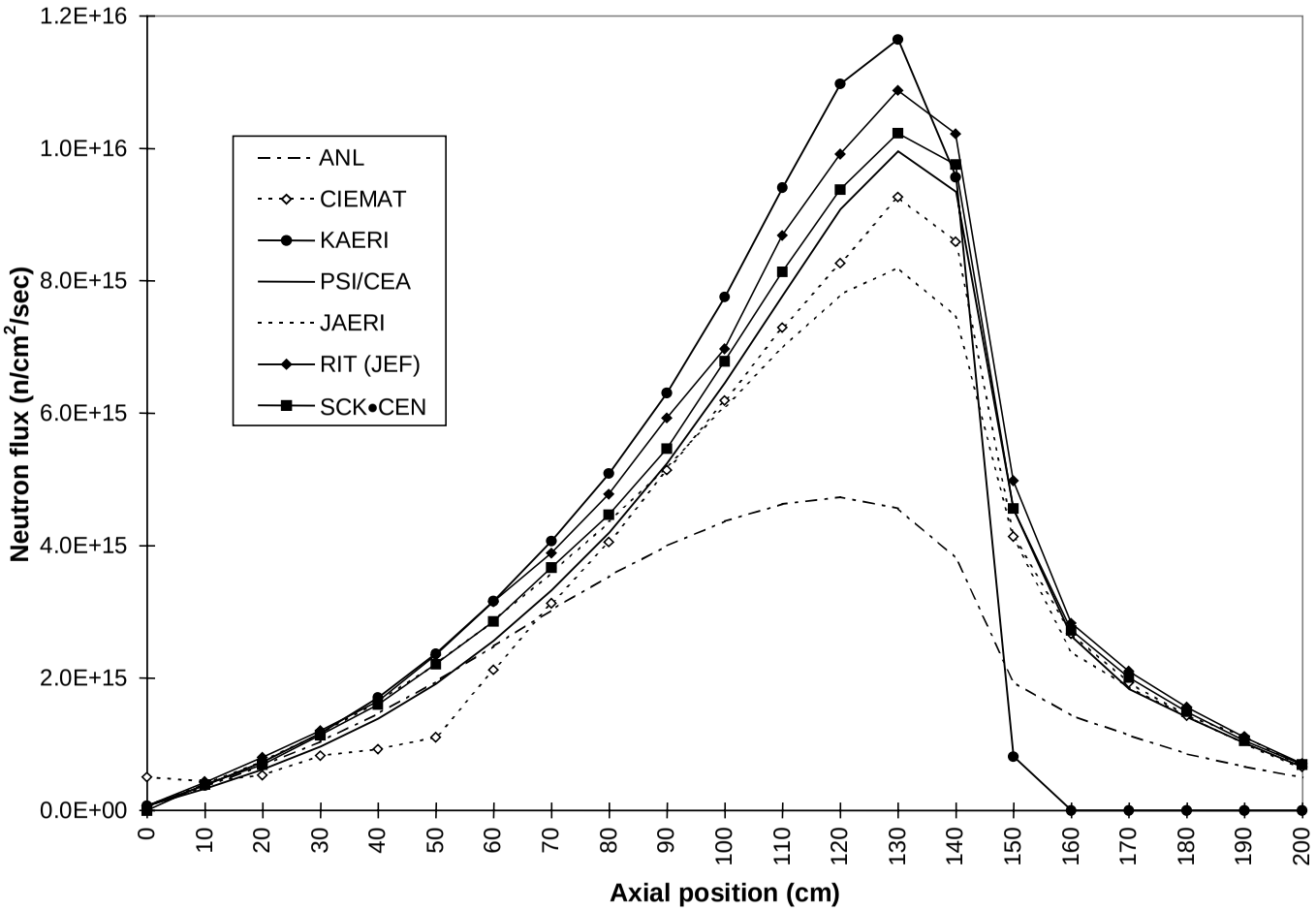

Figure 4.4.2. Equilibrium core: Axial flux distribution at $R = 0$

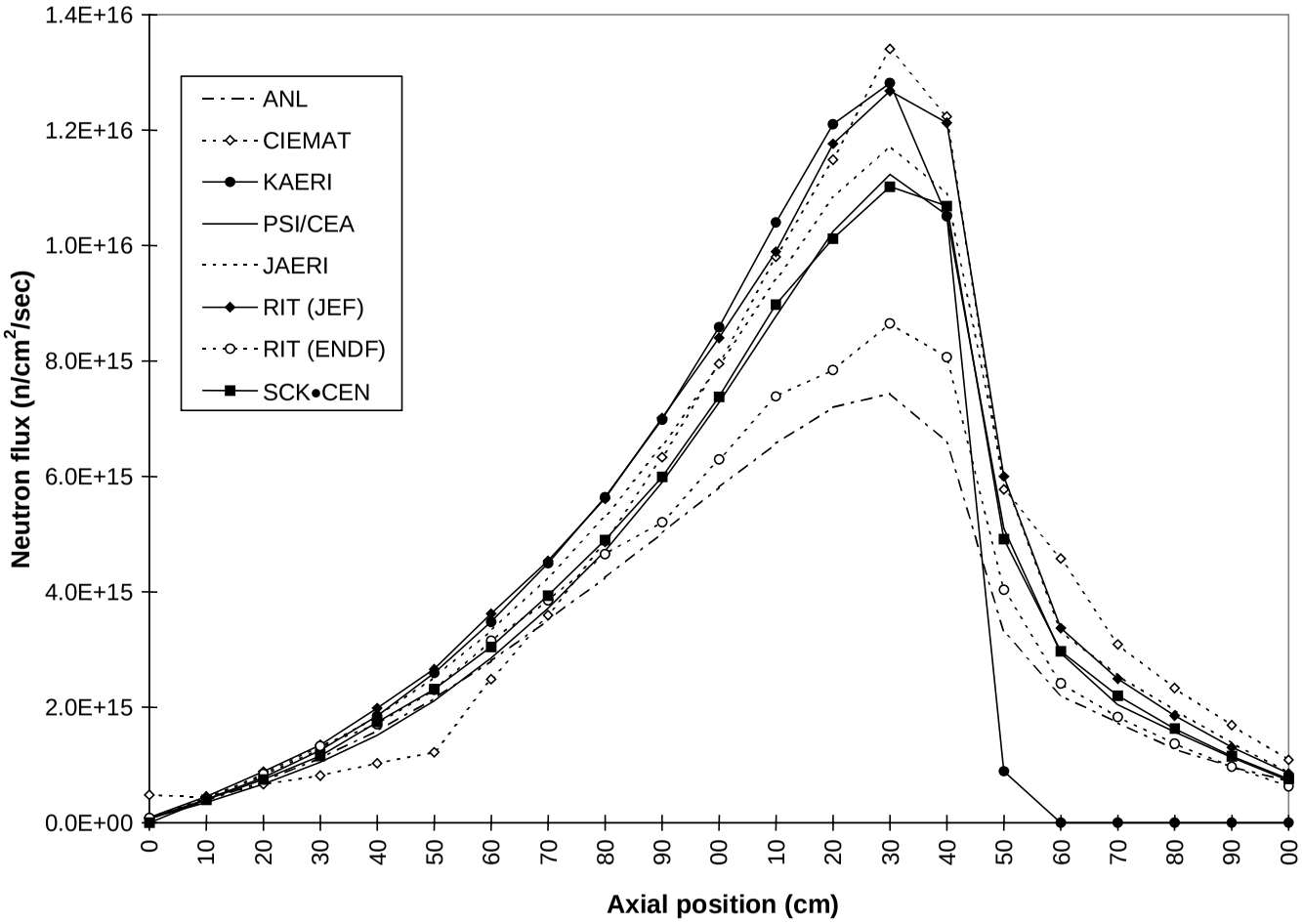

Figure 4.4.3. Start-up core: Axial flux distribution at *R* = 56

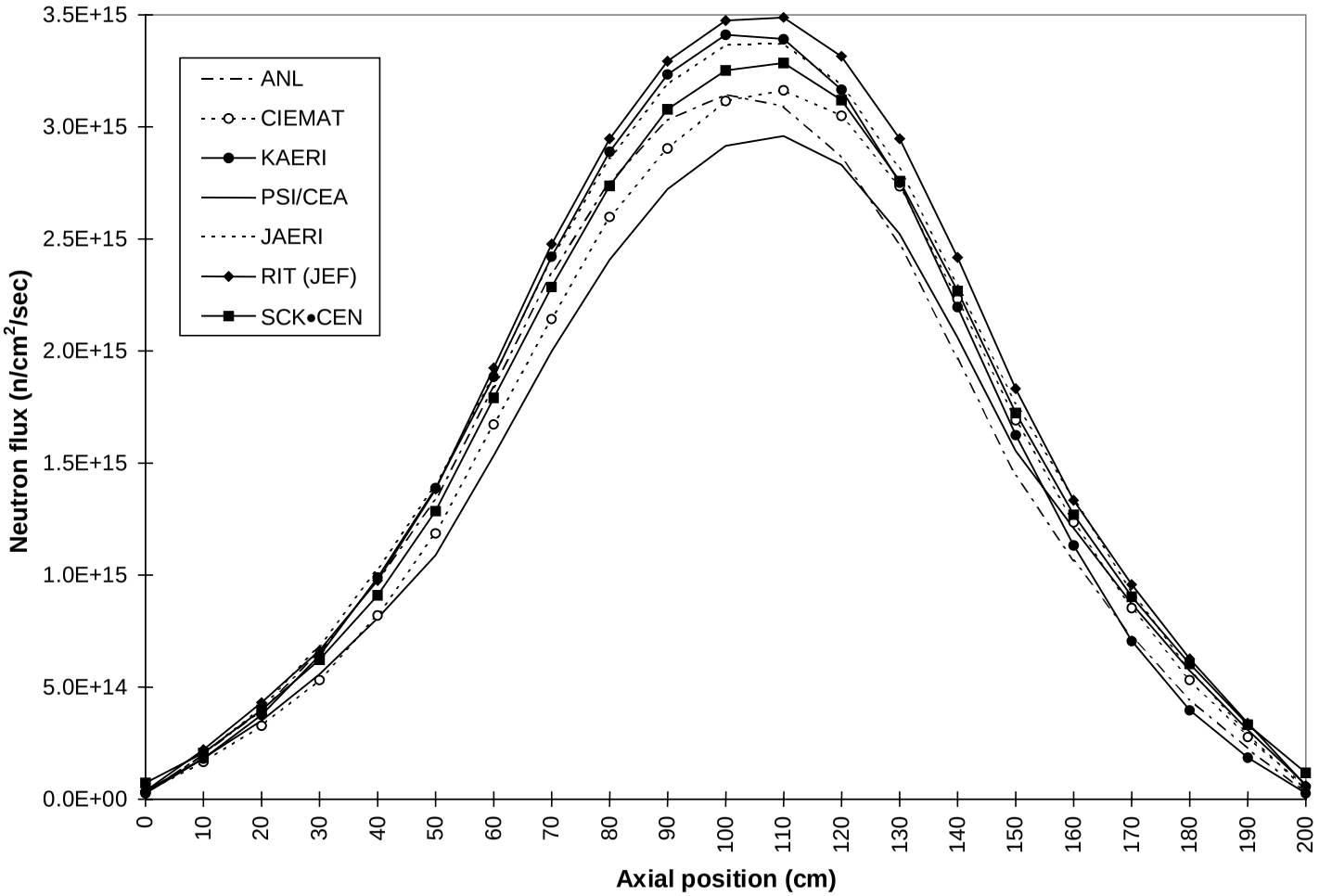

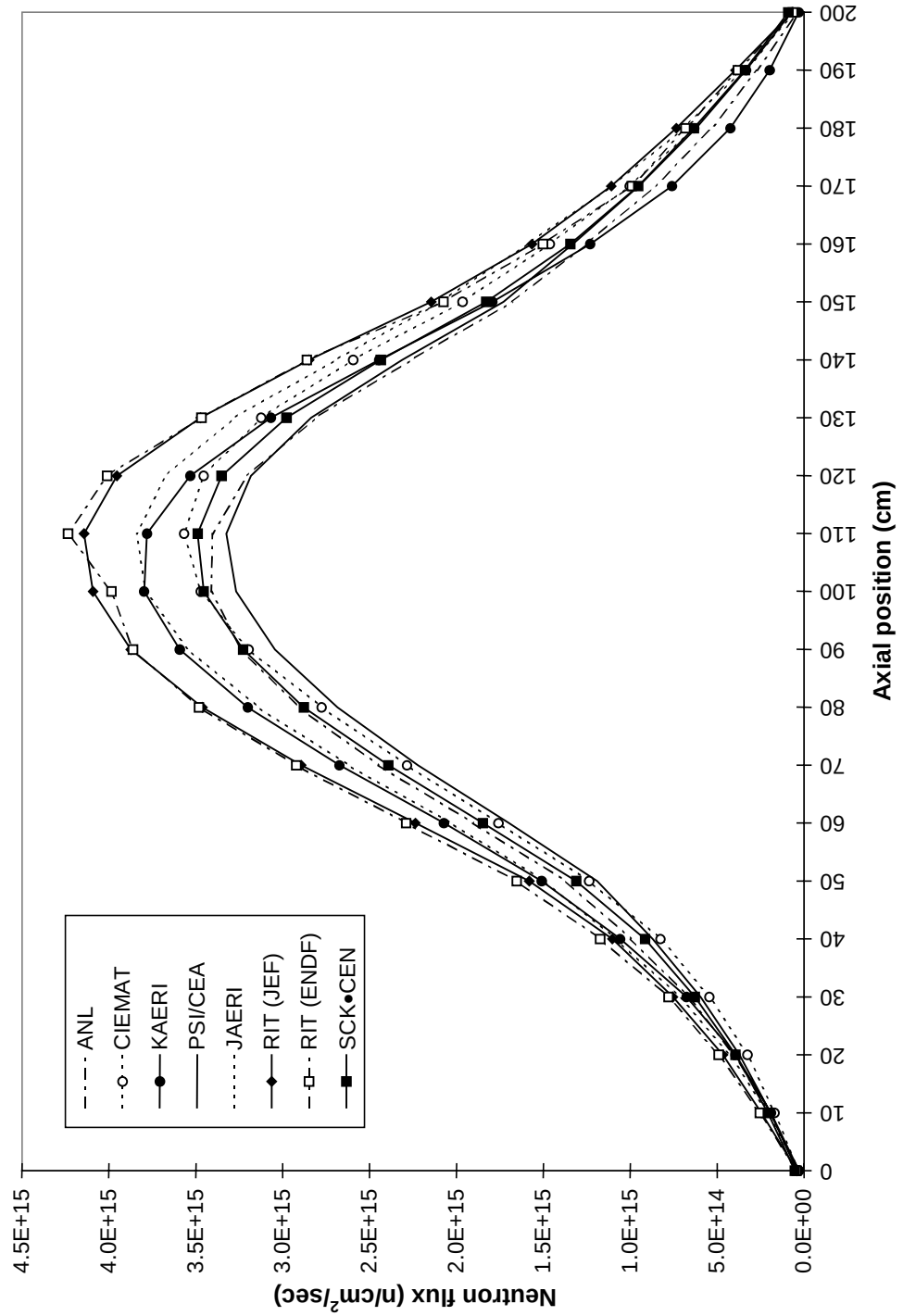

Figure 4.4.4. Equilibrium core: Axial flux distribution at R = 56

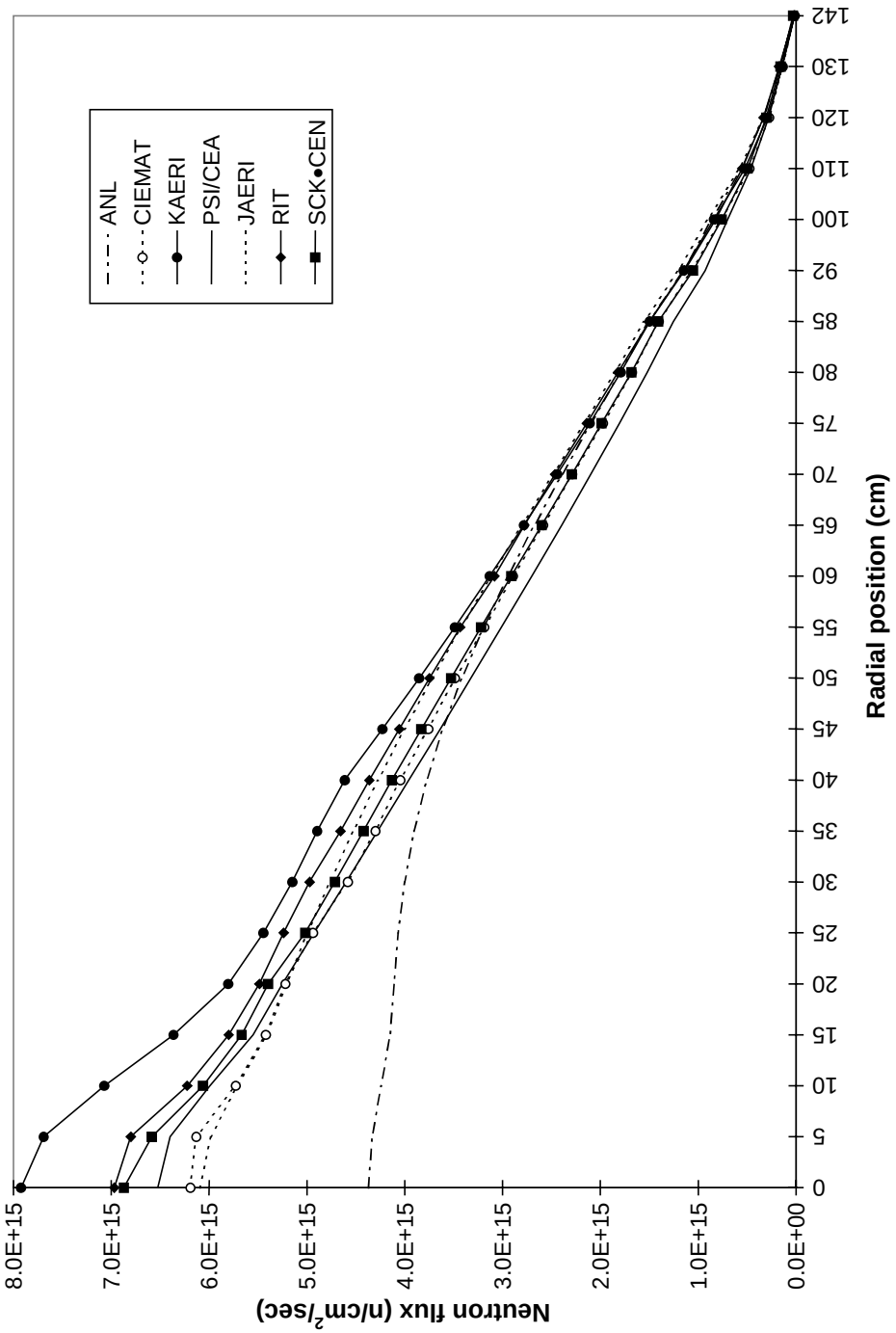

Figure 4.4.5. Start-up core: Radial flux distribution at Z = 100

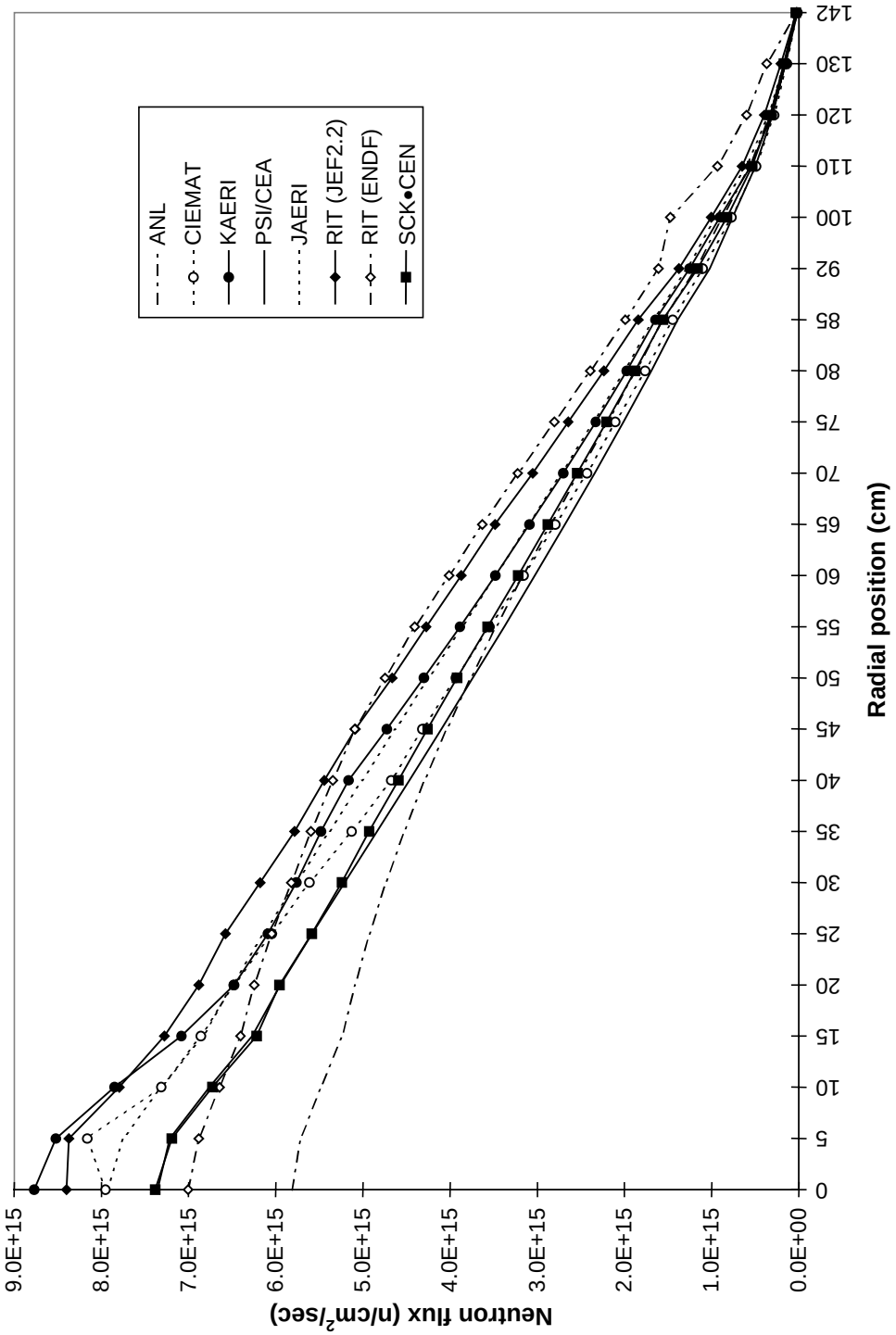

Figure 4.4.6. Equilibrium core: Radial flux distribution at Z = 100

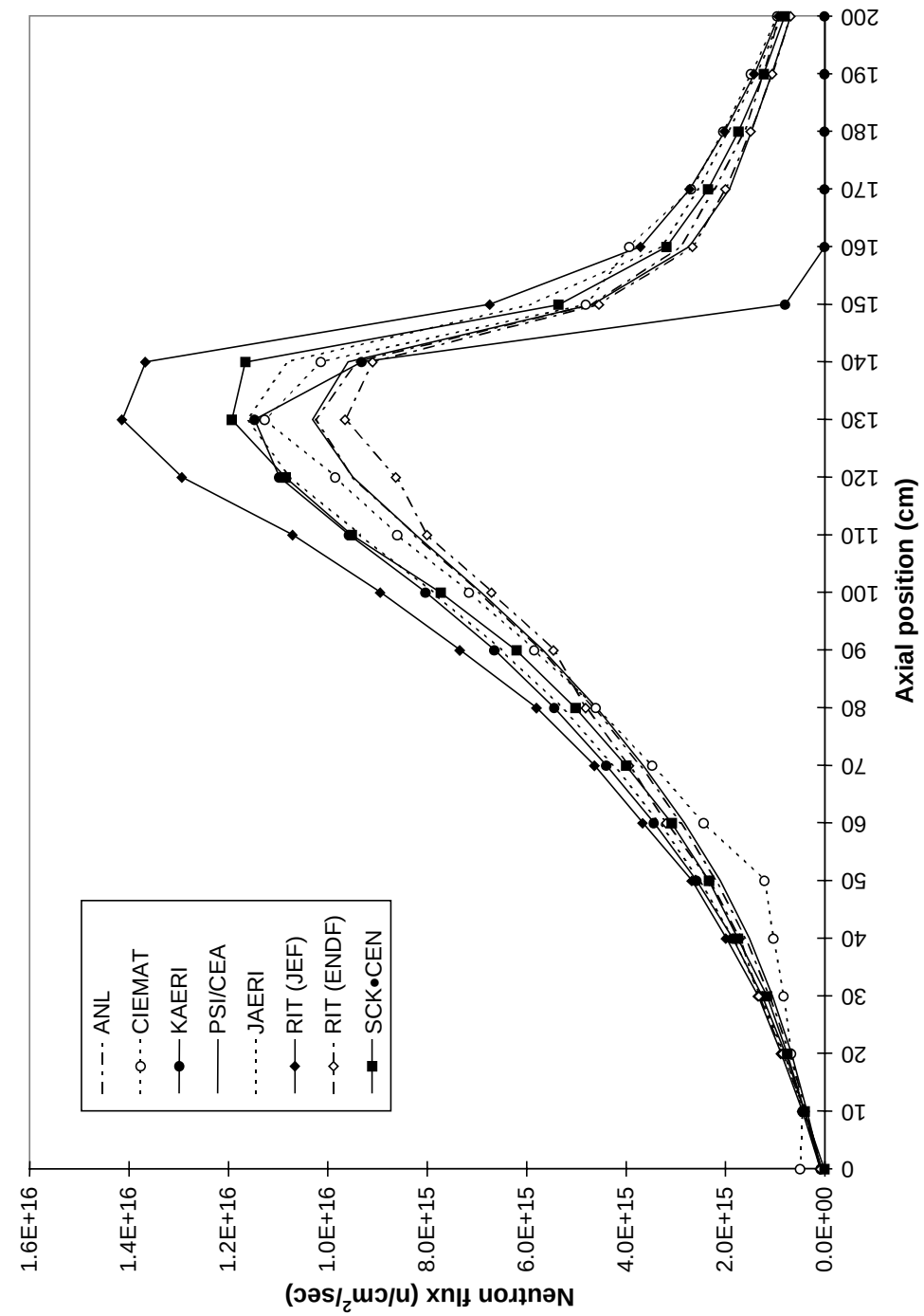

Figure 4.4.7. Axial flux distribution at $R = 0$, values adjusted to $k_{eff} = 0.95$

Figure 4.4.8. Axial flux distribution at *R* = 56, values adjusted to a k_{eff} = 0.95

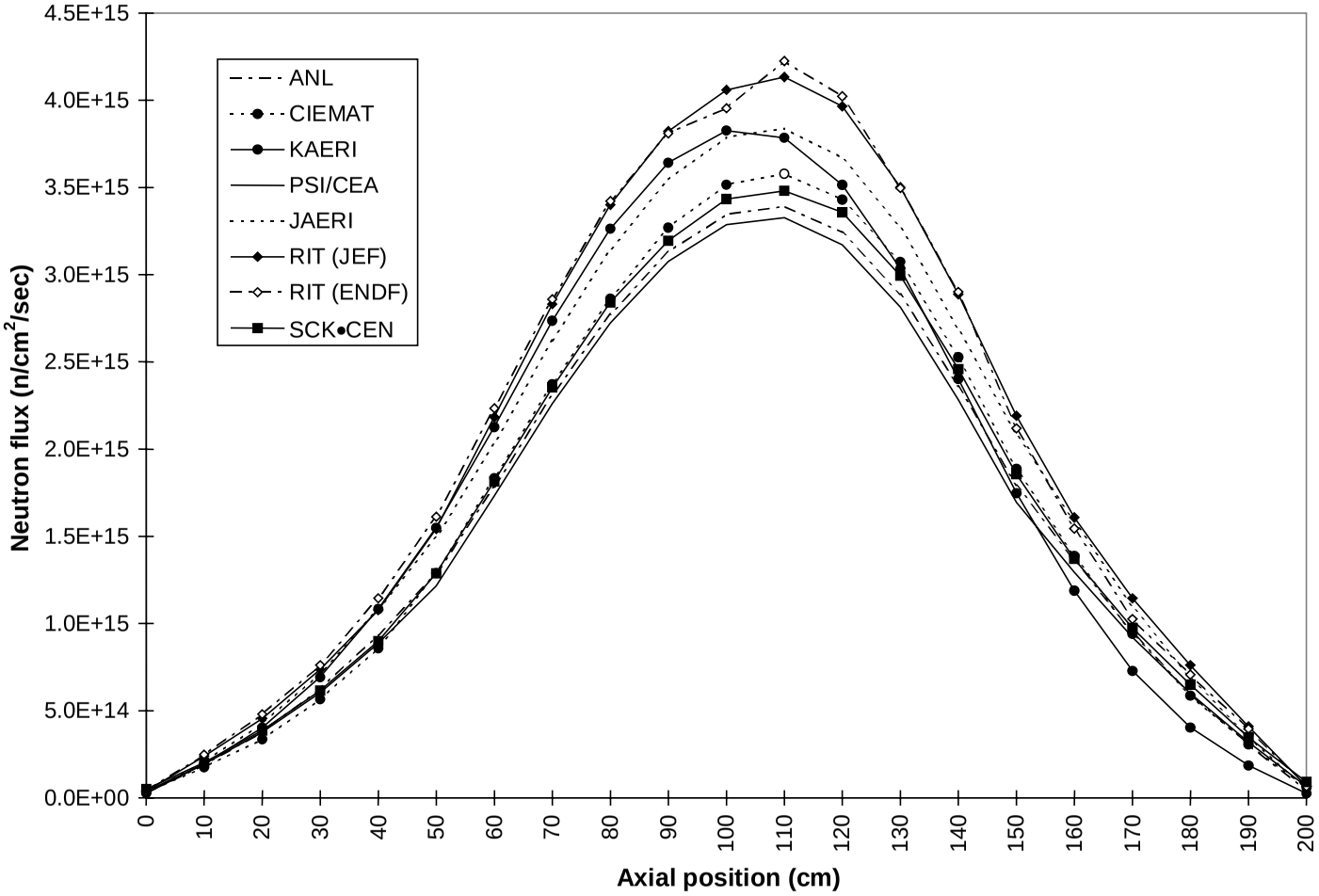

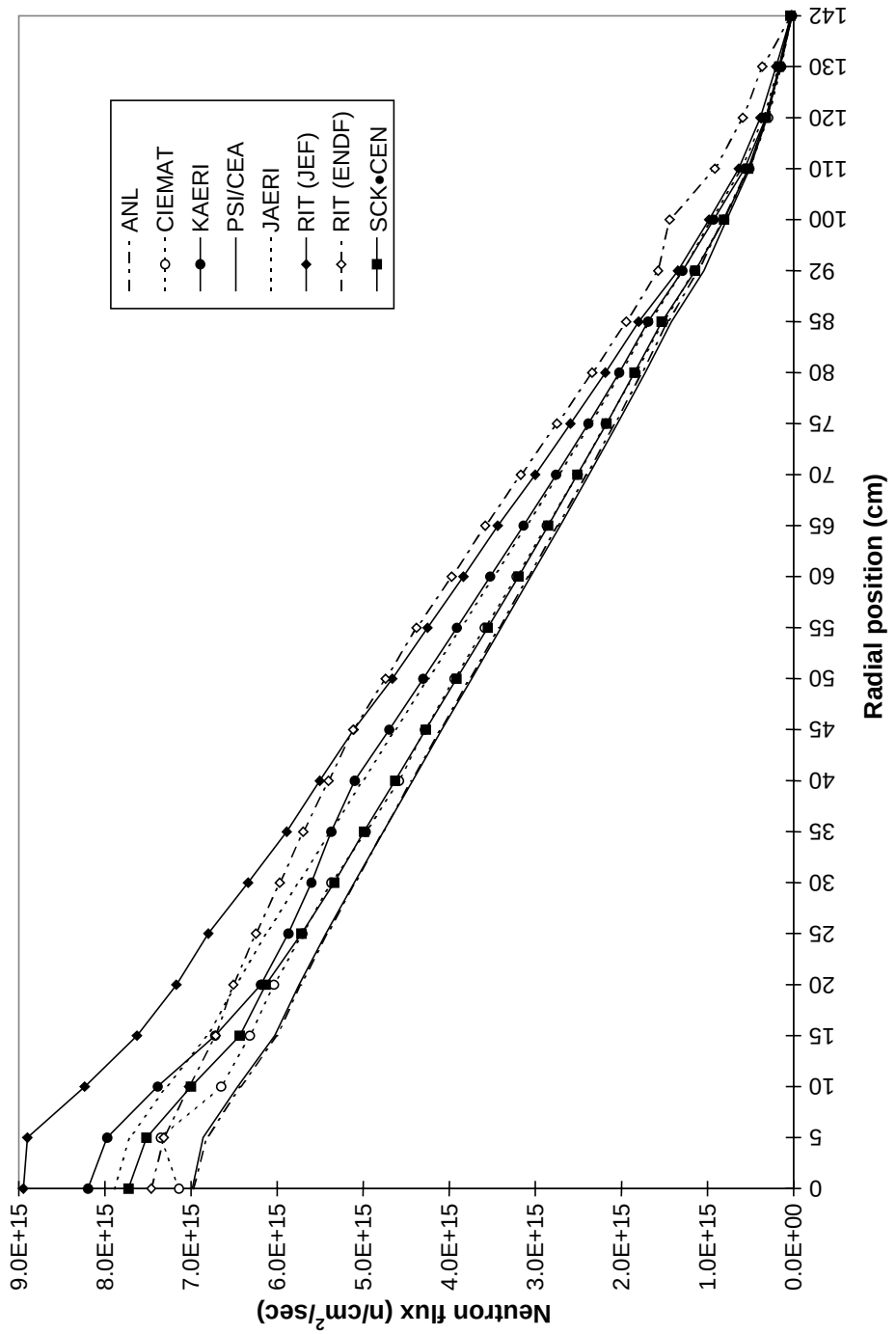

Figure 4.4.9. Radial flux distribution at Z = 100, values adjusted to a k_{eff} = 0.95

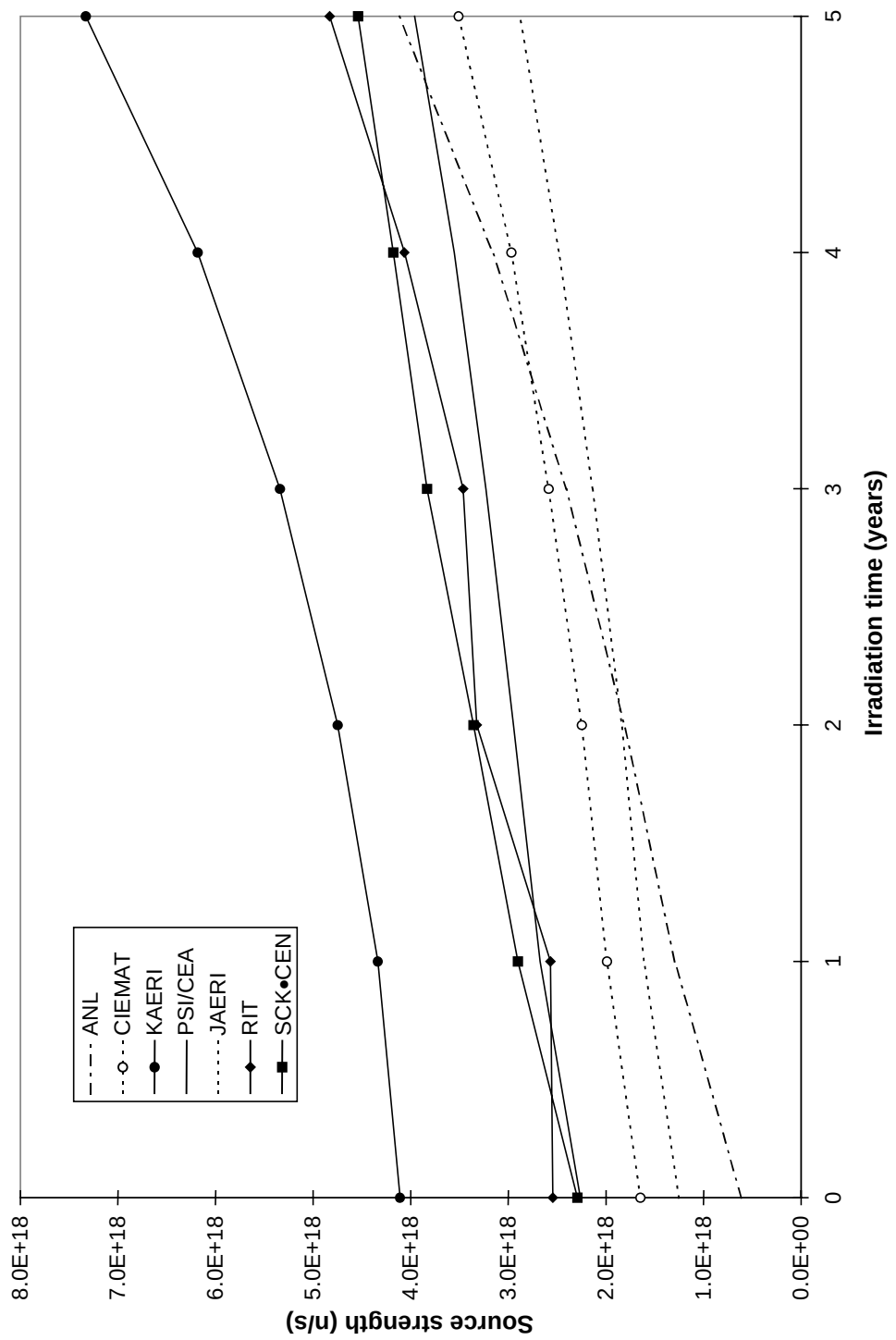

Figure 4.5.1. Source strength for the start-up core

Figure 4.5.2. Source strength for the equilibrium core

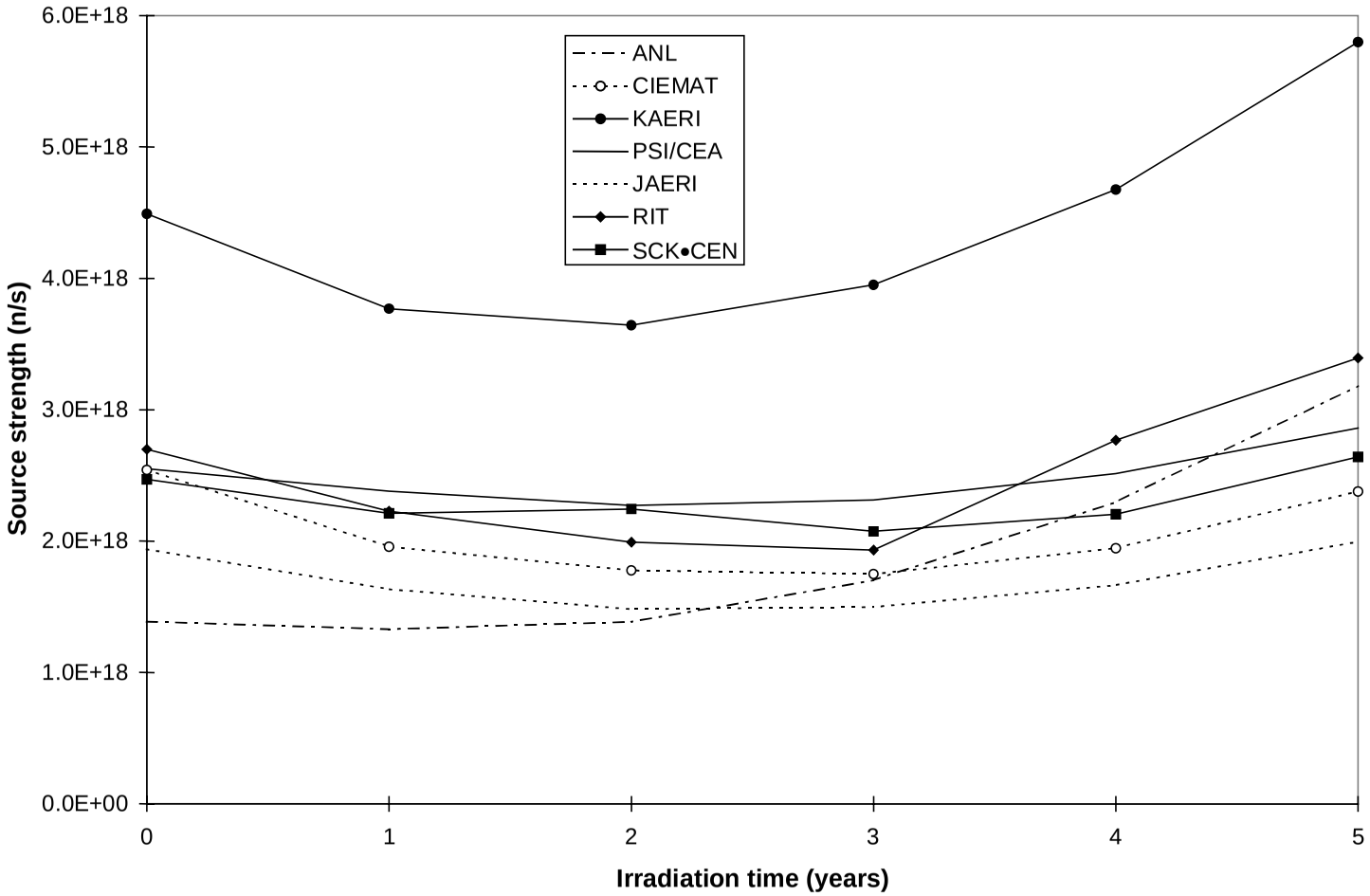

Figure 4.5.3. Source strength for the start-up core (corrected for the k_{eff} effect)

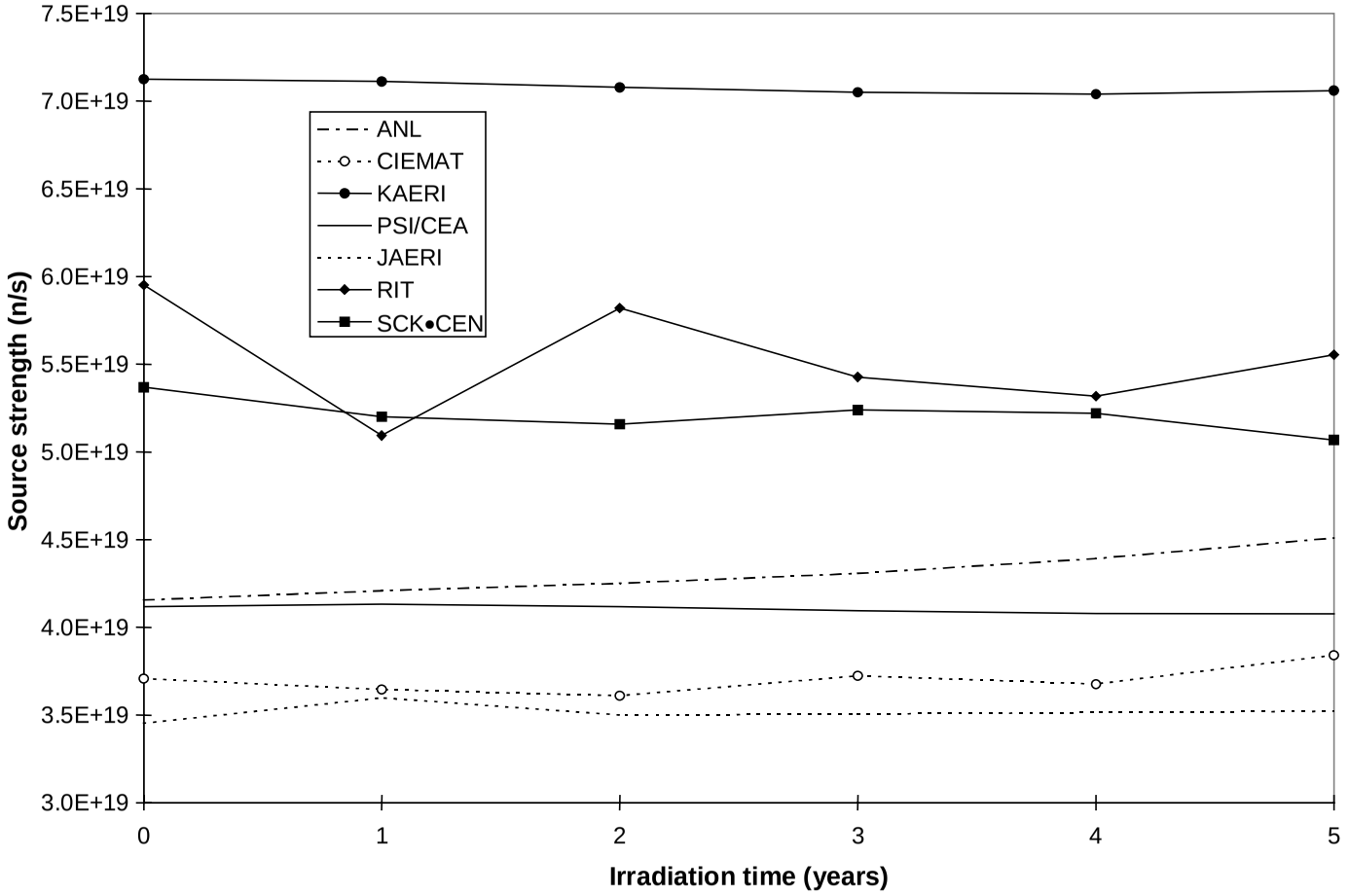

Figure 4.6.1. Total production and absorption reaction rates

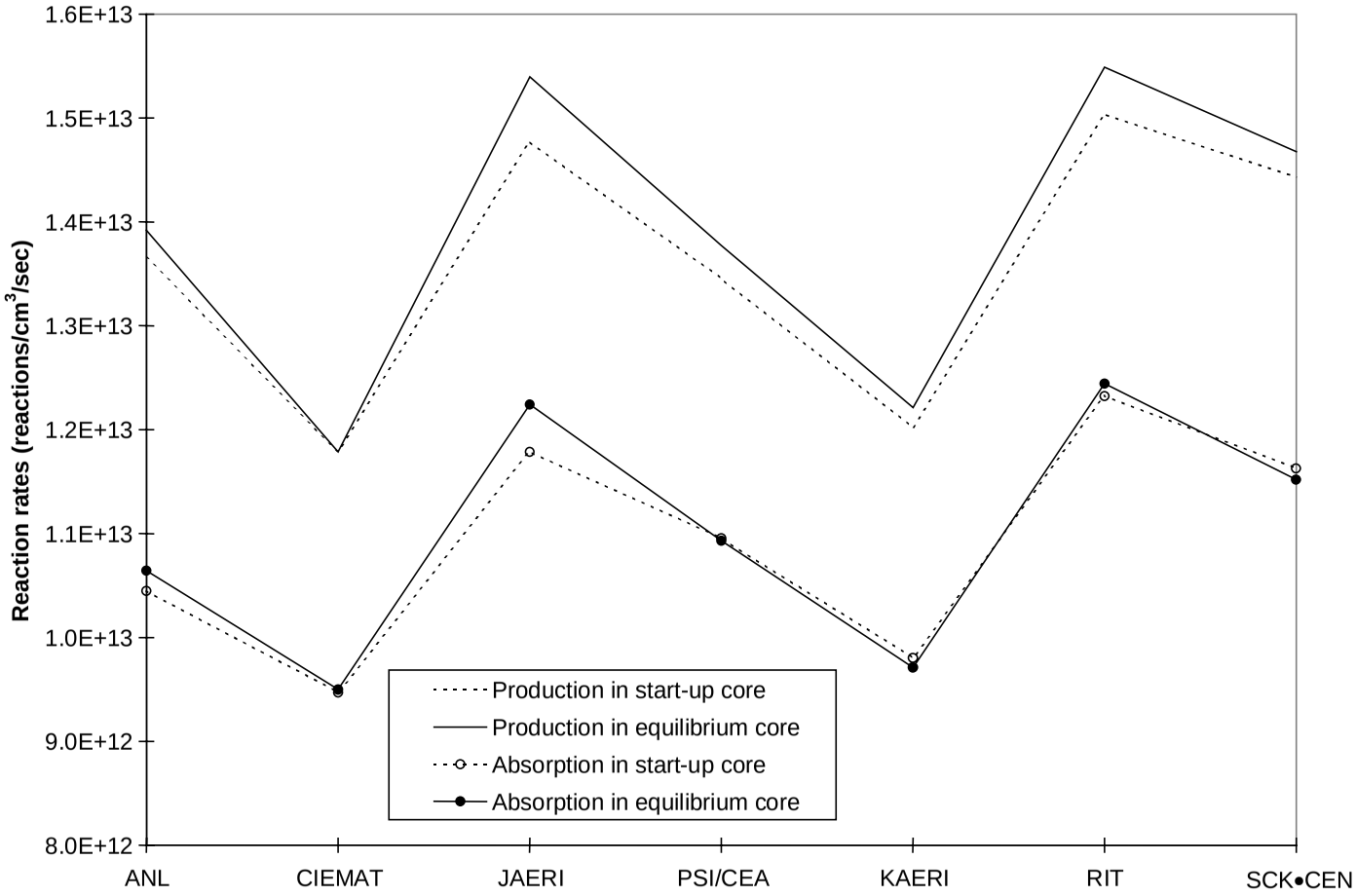

Figure 4.6.2. Production to absorption reaction ratio

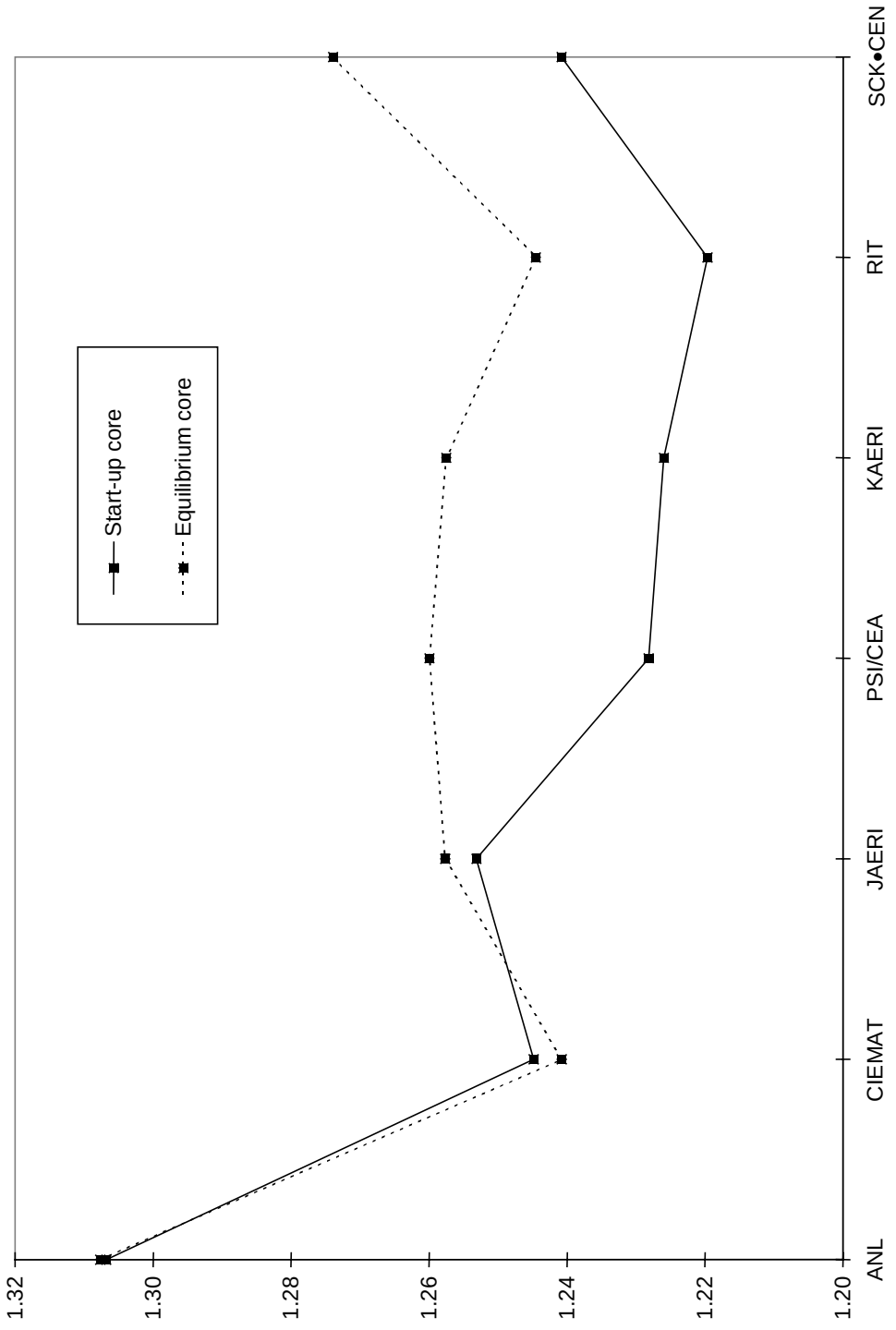

Figure 4.6.3. Start-up core: Absorption reaction rates

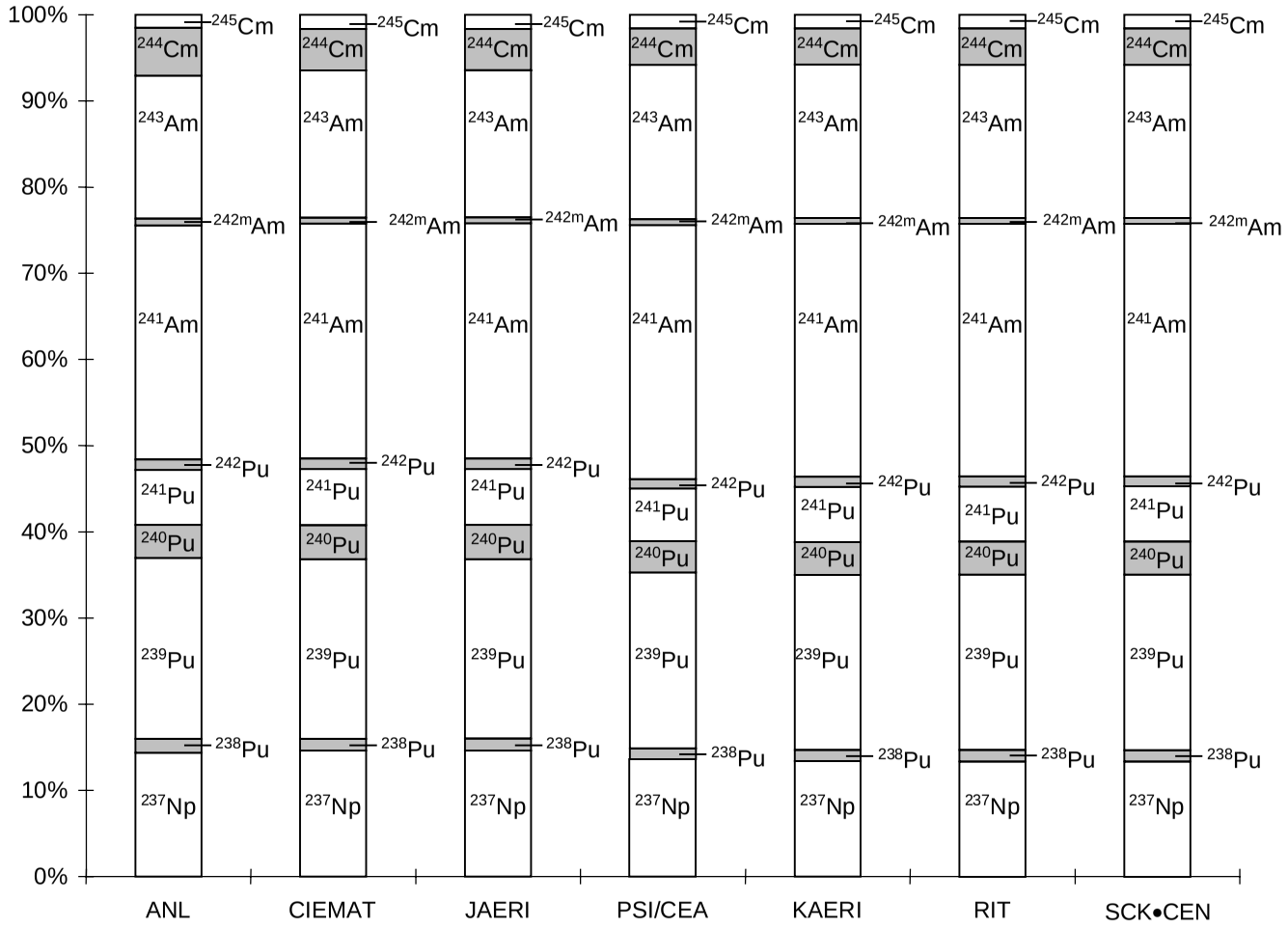

Figure 4.6.4. Equilibrium core: Absorption reaction rates

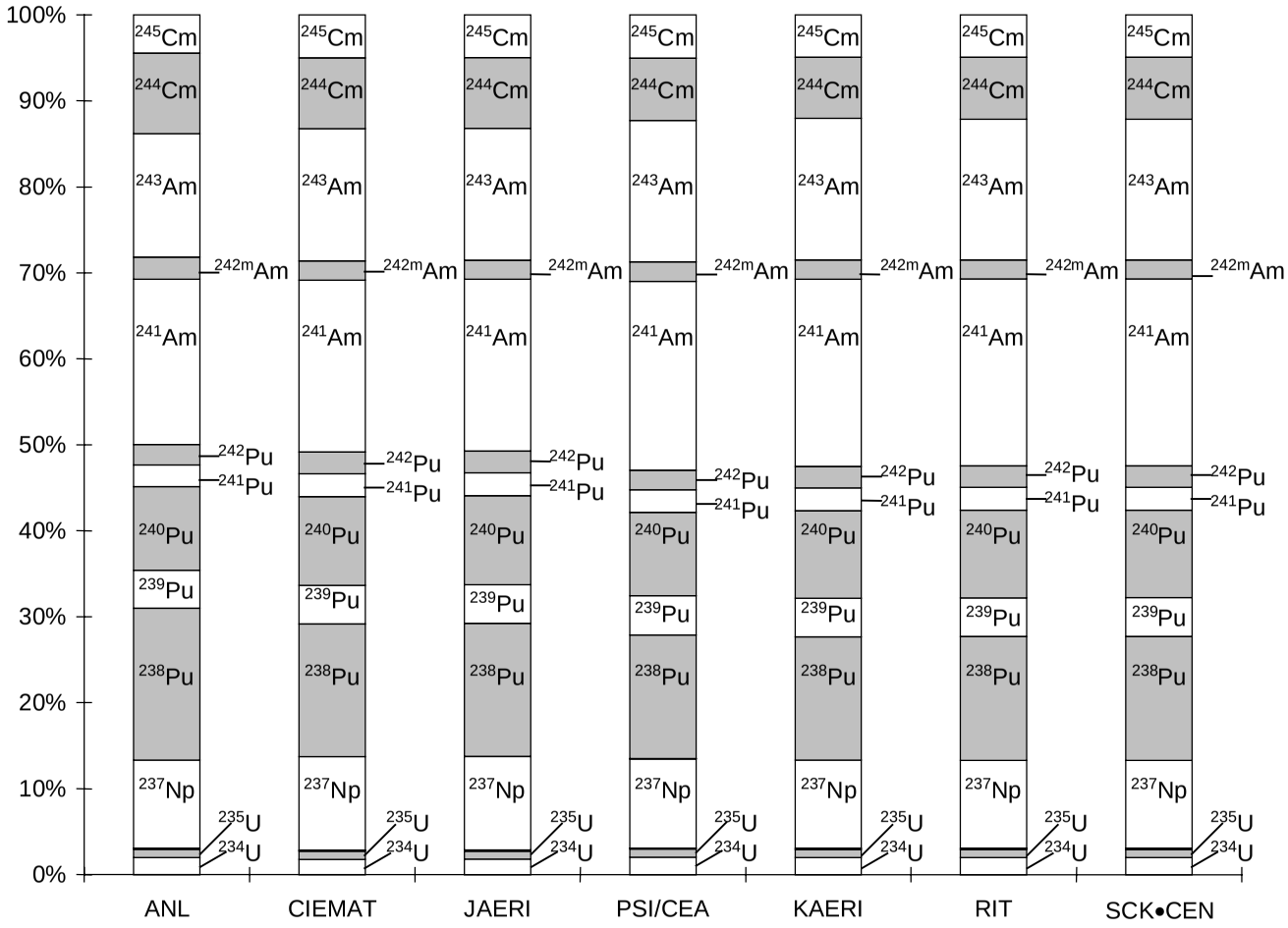

Figure 4.6.5. Start-up core: Production reaction rates

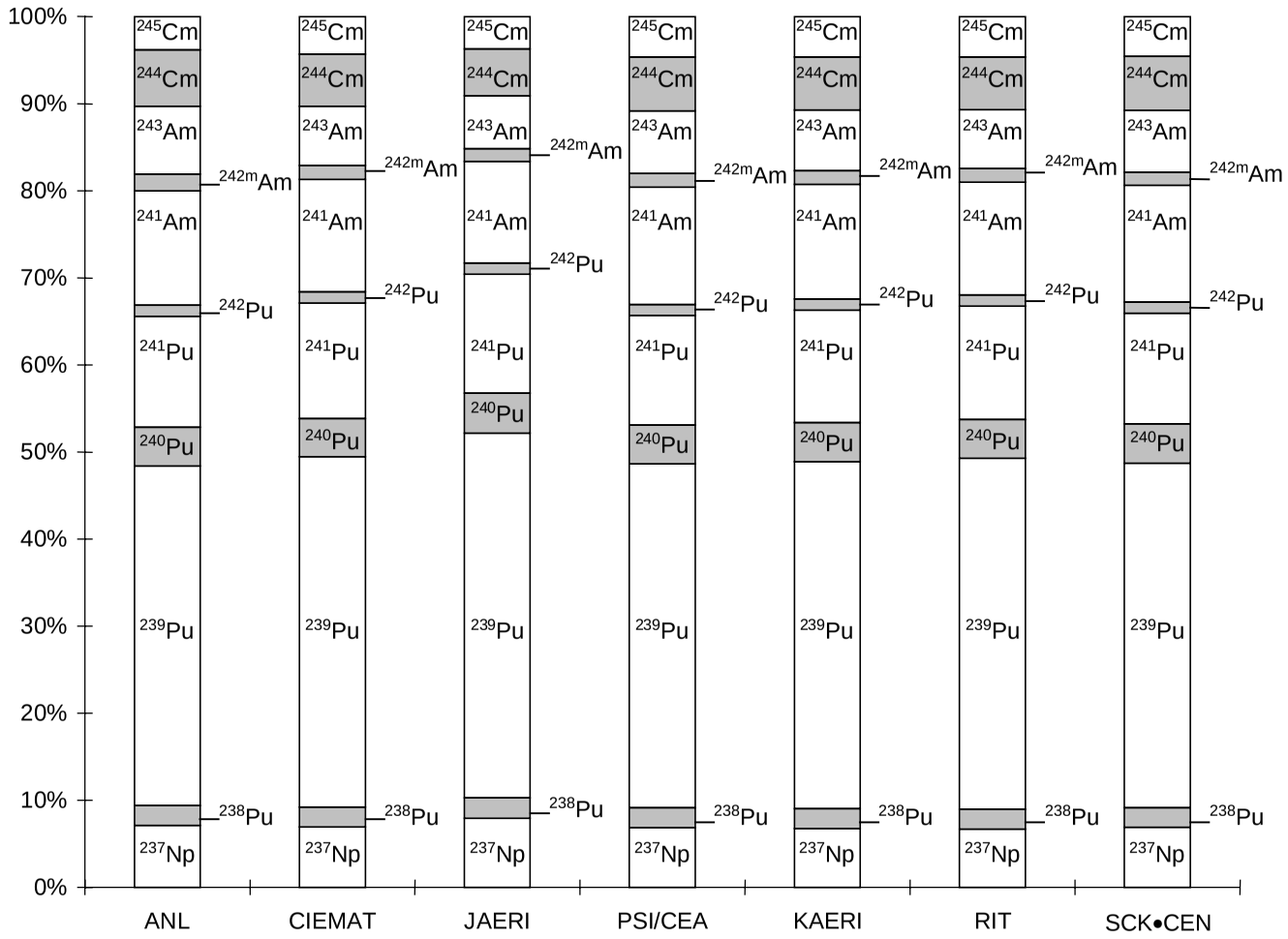

Figure 4.6.6. Equilibrium core: Production reaction rates

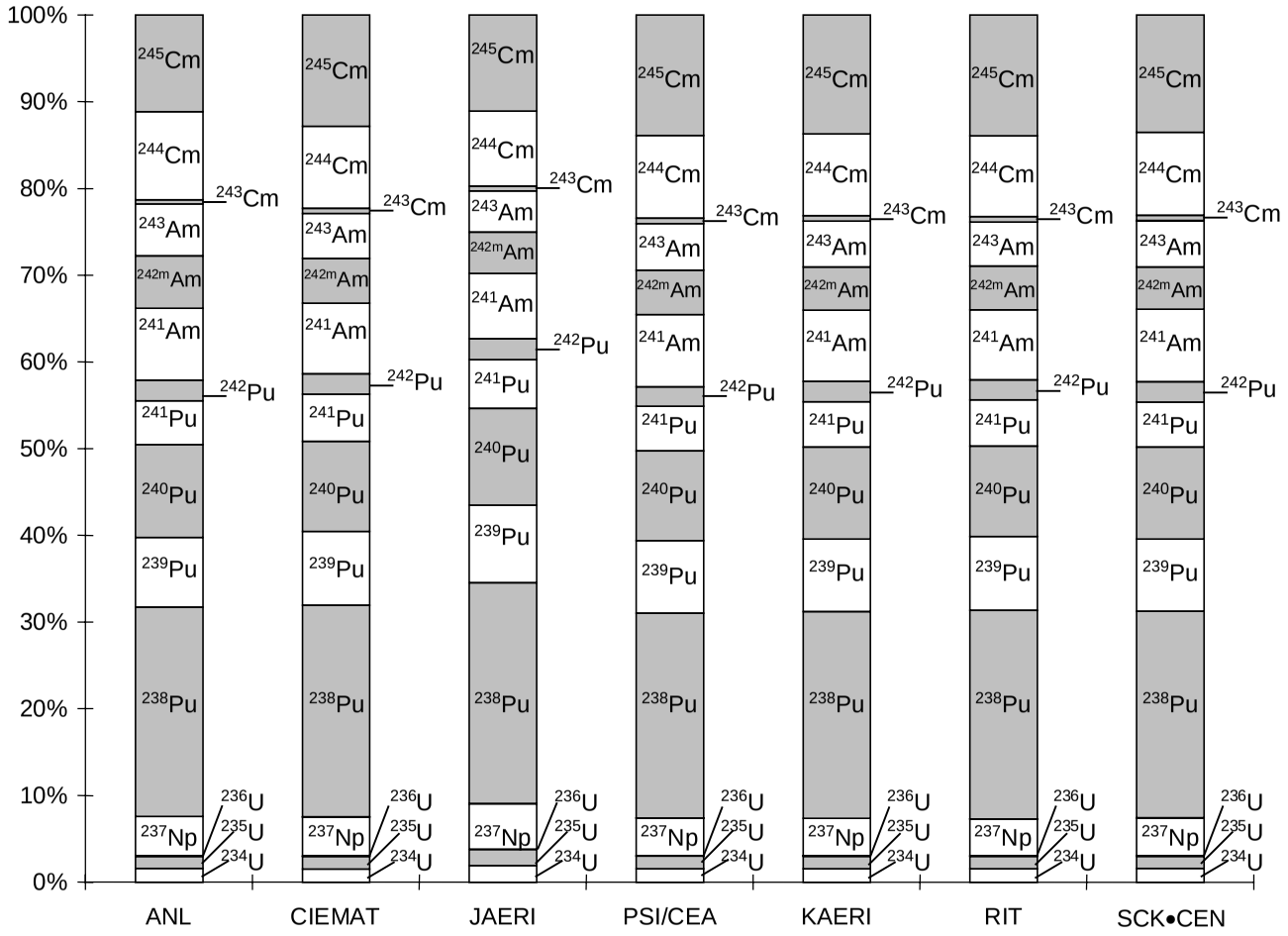

Figure 4.6.7. Start-up core: Absorption reaction rates (normalised to 1)

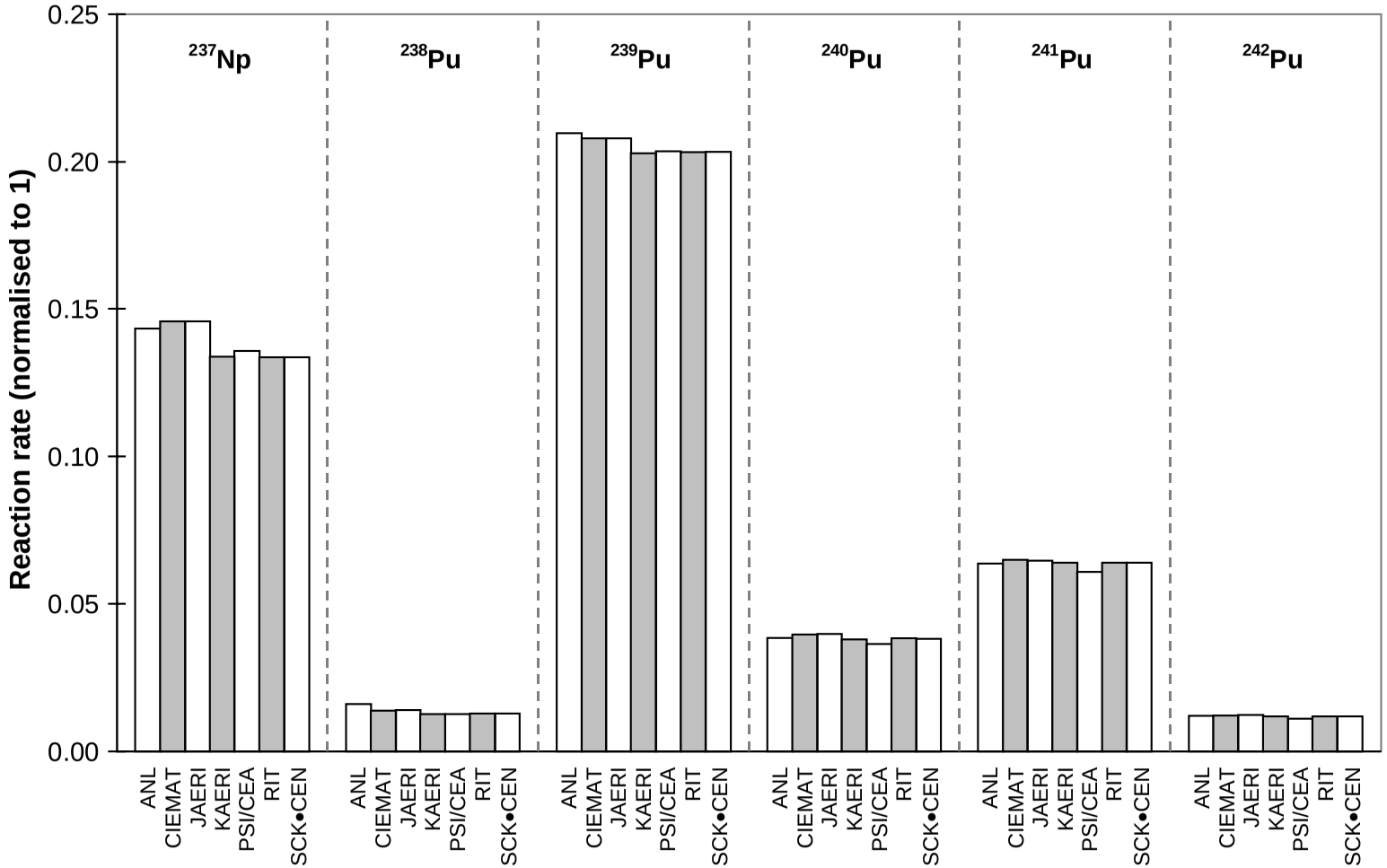

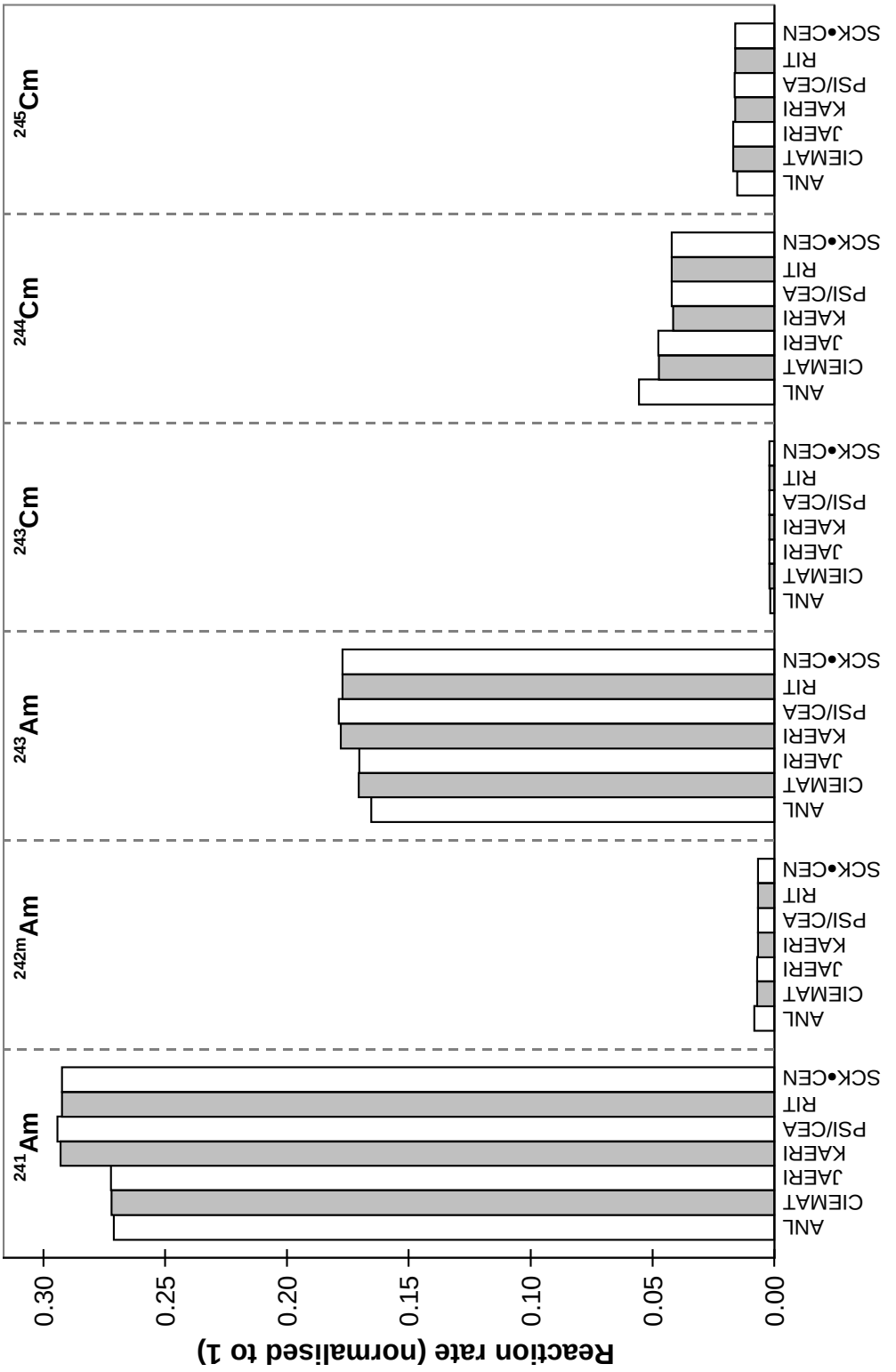

Figure 4.6.7. Start-up core: Absorption reaction rates (normalised to 1) (*cont.*)

Figure 4.6.8. Equilibrium core: Absorption reaction rates (normalised to 1)

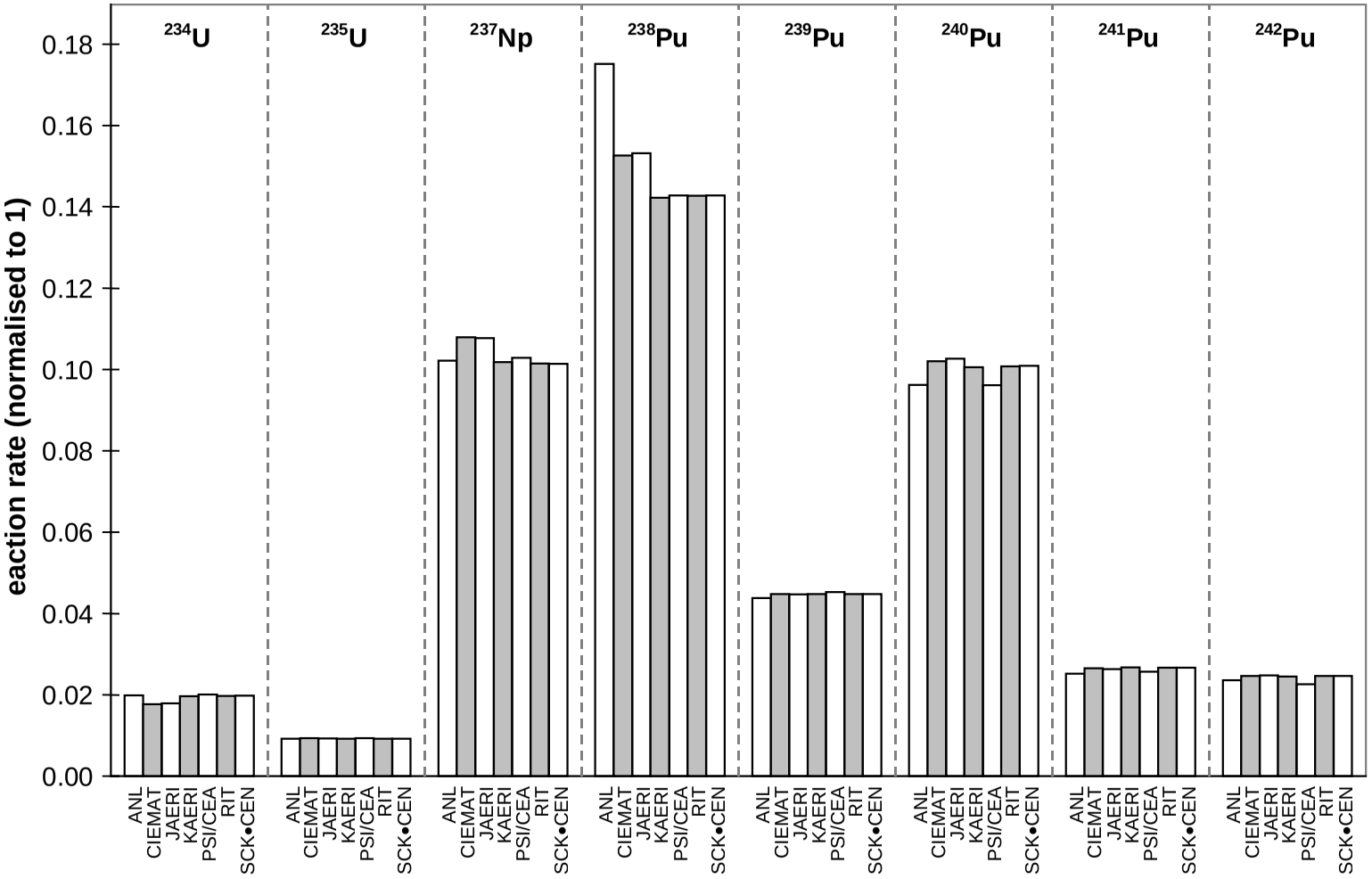

Figure 4.6.8. Equilibrium core: Absorption reaction rates (normalised to 1) (*cont.*)

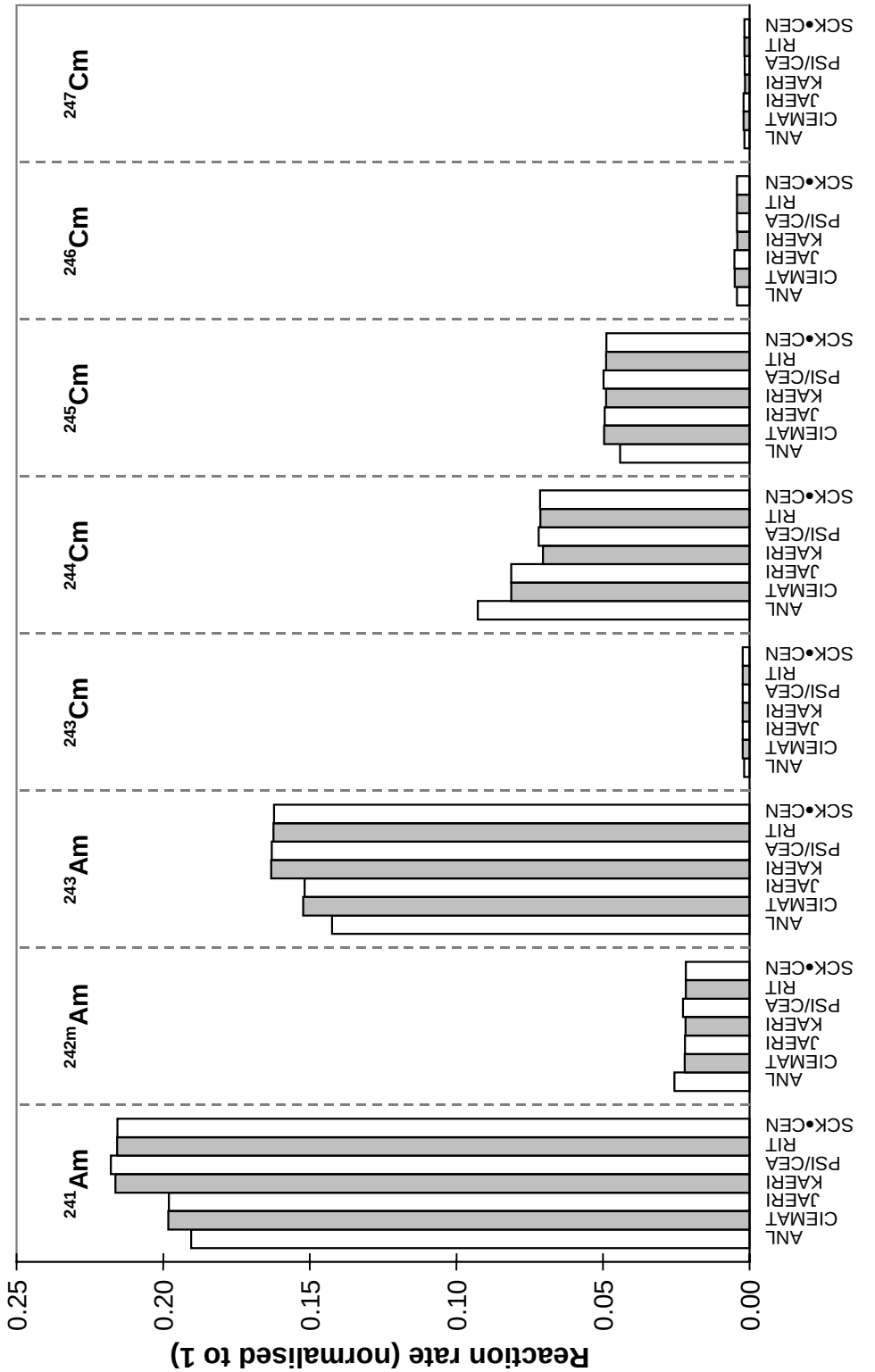

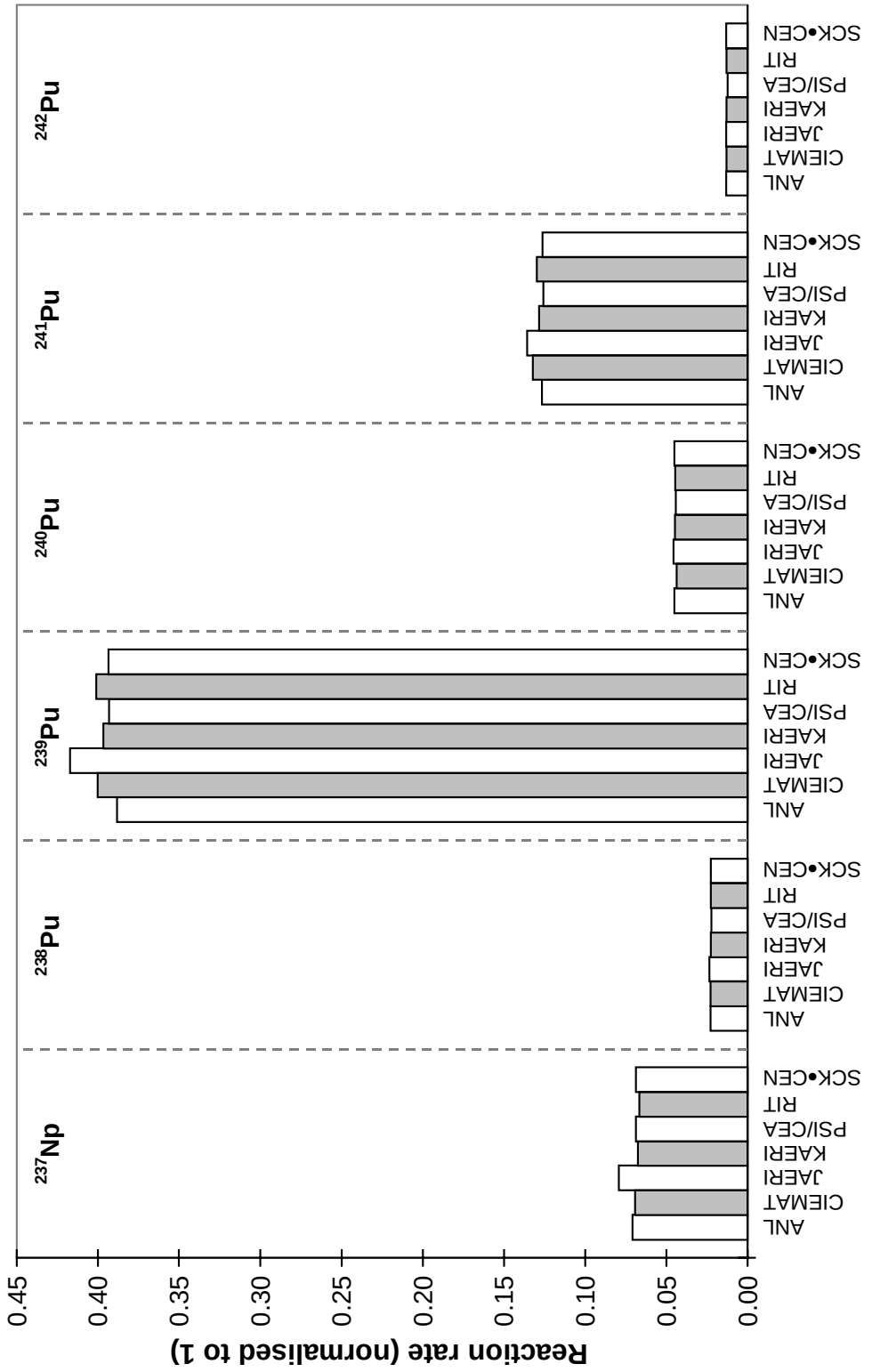

Figure 4.6.9. Start-up core: Production reaction rates (normalised to 1)

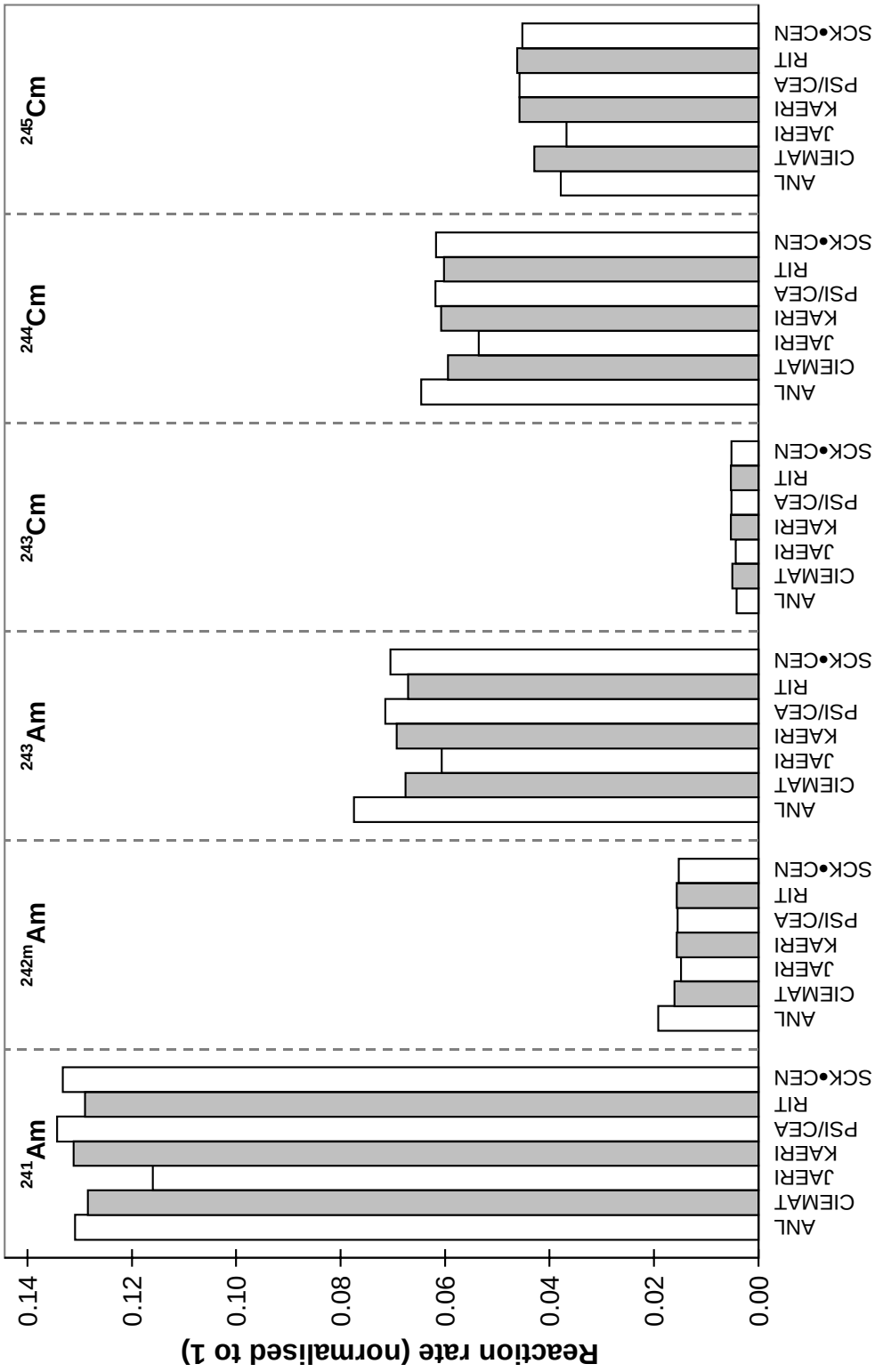

Figure 4.6.9. Start-up core: Production reaction rates (normalised to 1) (*cont.*)

Figure 4.6.10. Equilibrium core: Production reaction rates (normalised to 1)

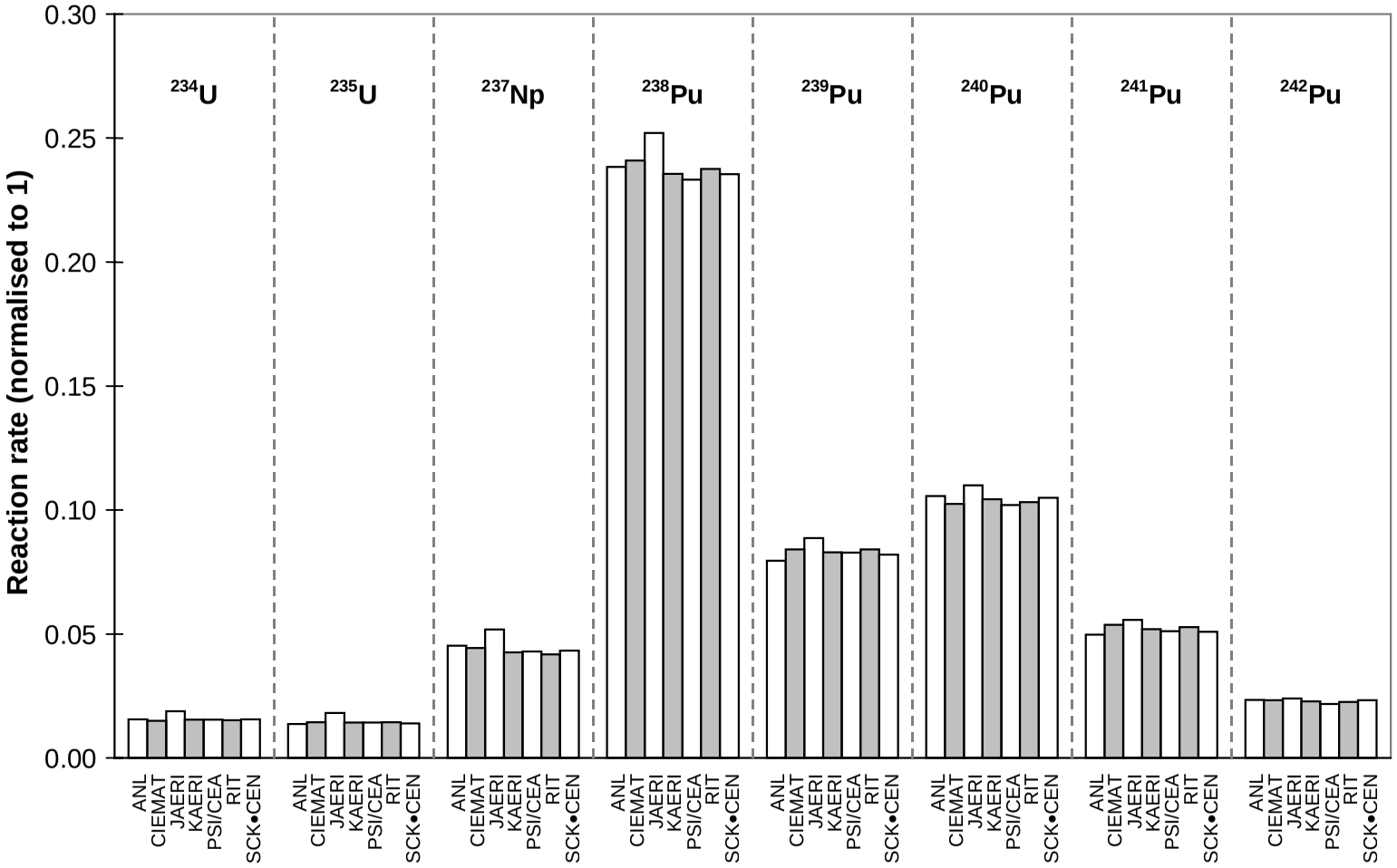

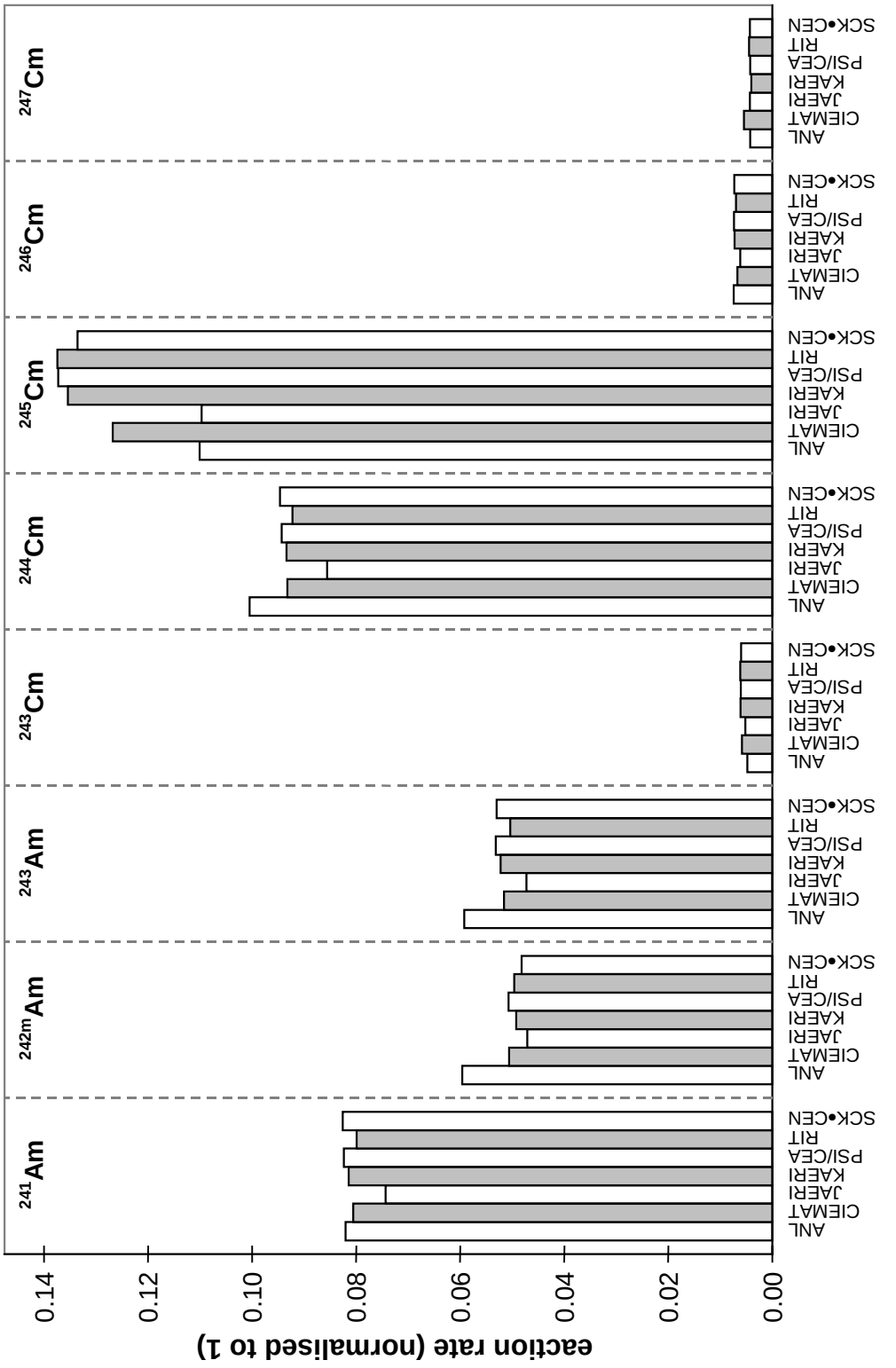

Figure 4.6.10. Equilibrium core: Production reaction rates (normalised to 1) (*cont.*)

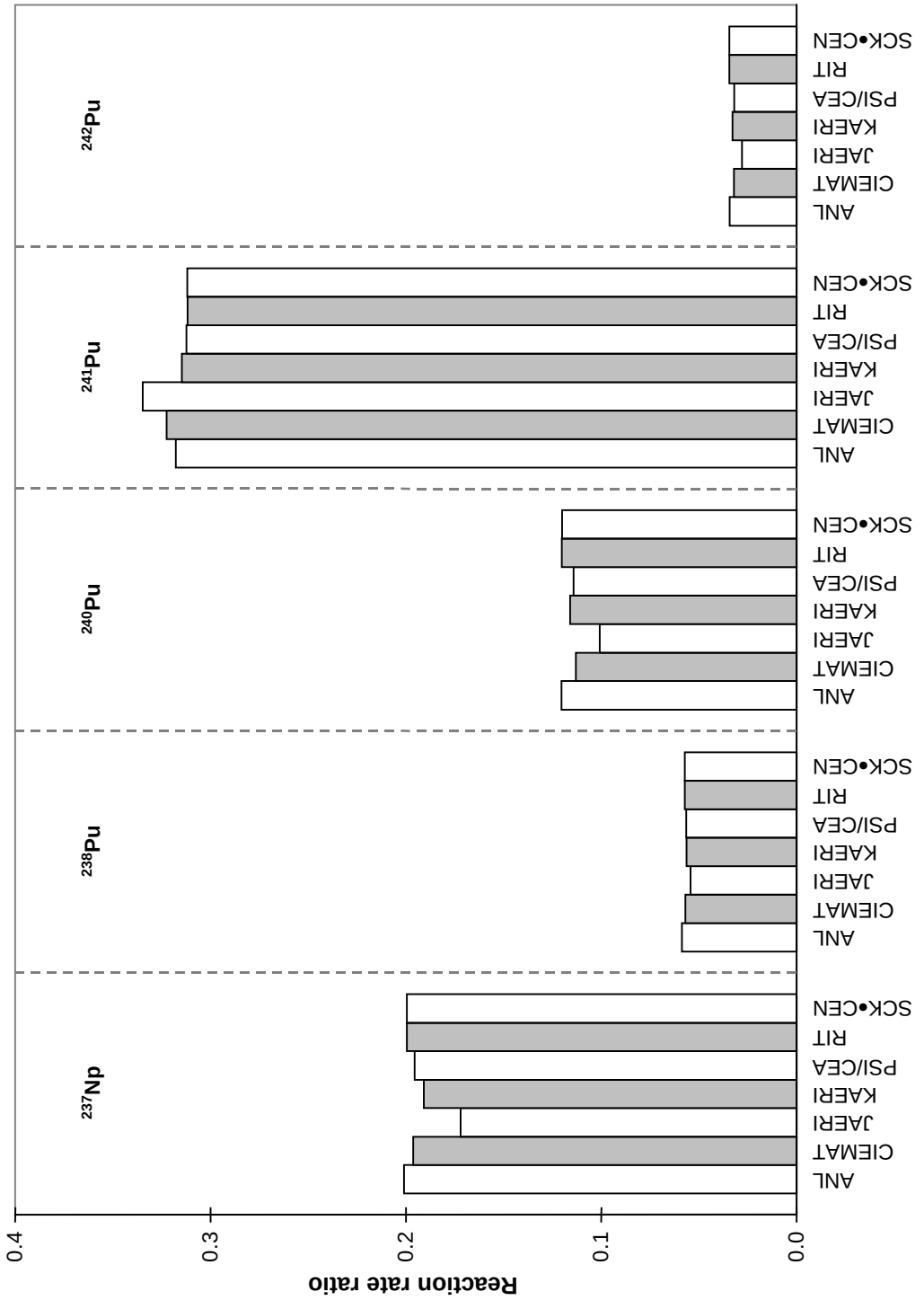

Figure 4.7.1. Start-up core: Fission reaction rate ratio relative to ^{239}Pu fission reaction rate

Figure 4.7.1. Start-up core: Fission reaction rate ratio relative to ^{239}Pu fission reaction rate (*cont.*)

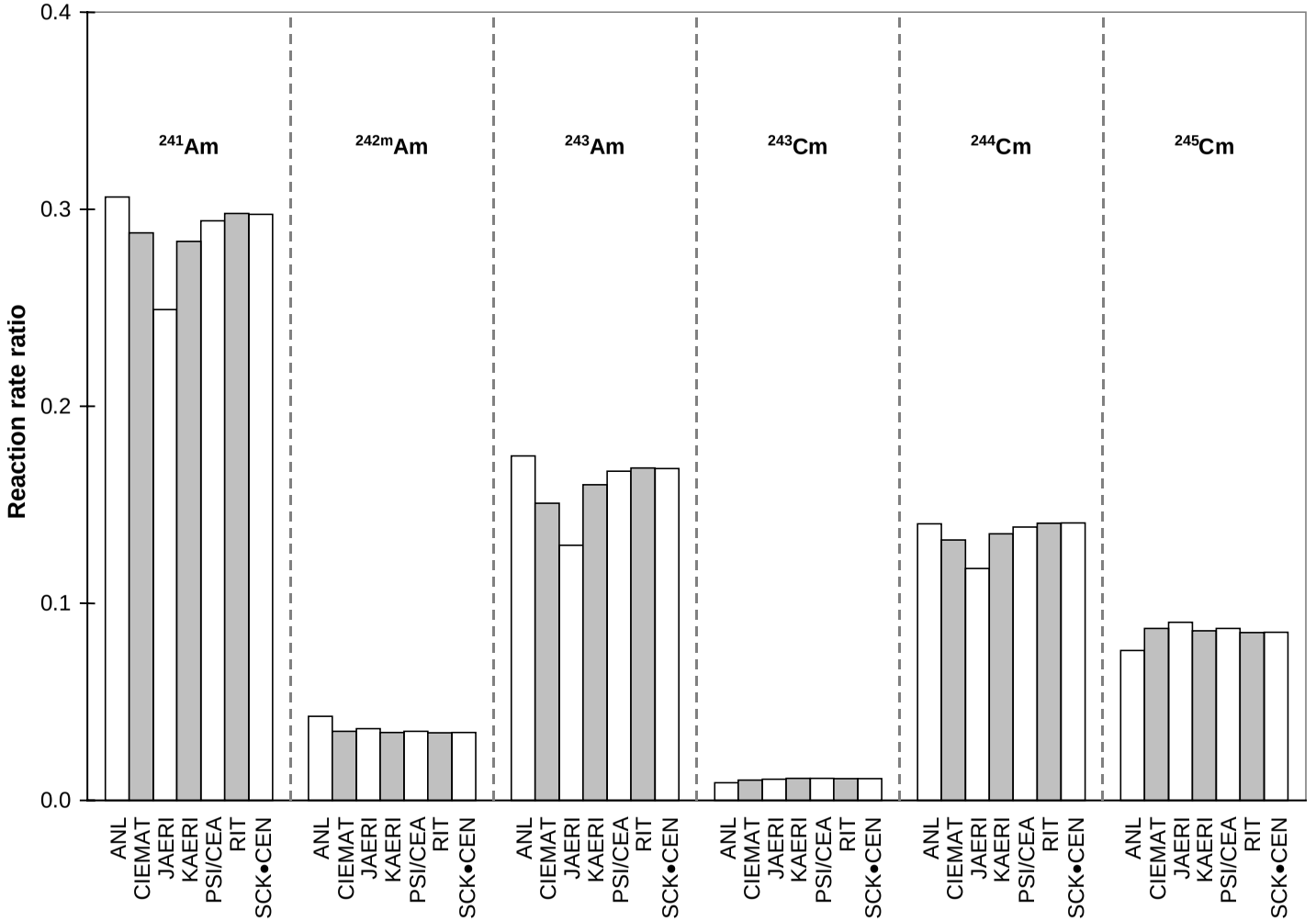

Figure 4.7.2. Start-up core: Capture reaction rate ratio relative to ^{239}Pu fission reaction rate

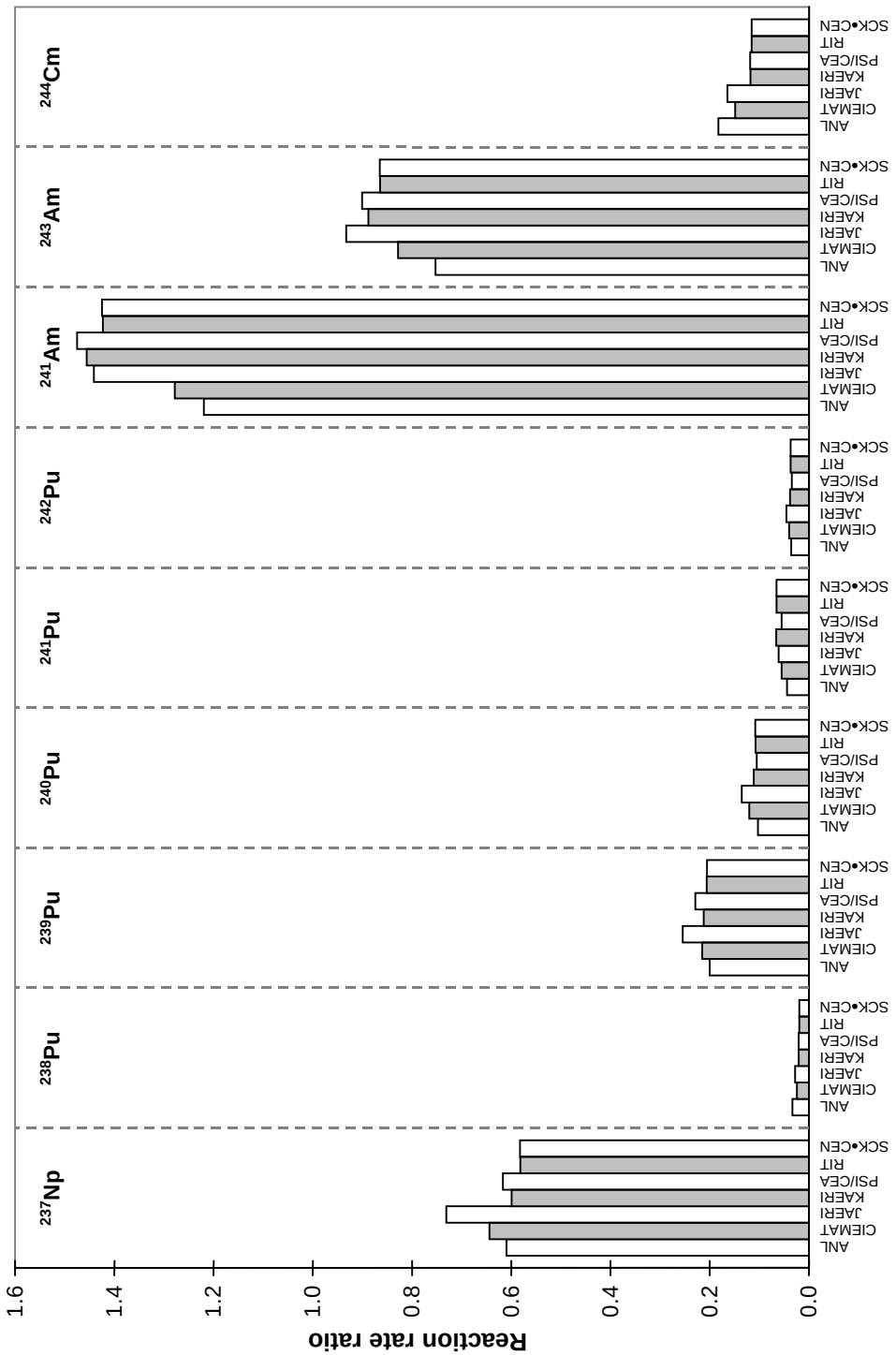

Figure 4.7.3. Equilibrium core: Fission reaction rate ratio relative to ^{239}Pu fission reaction rate

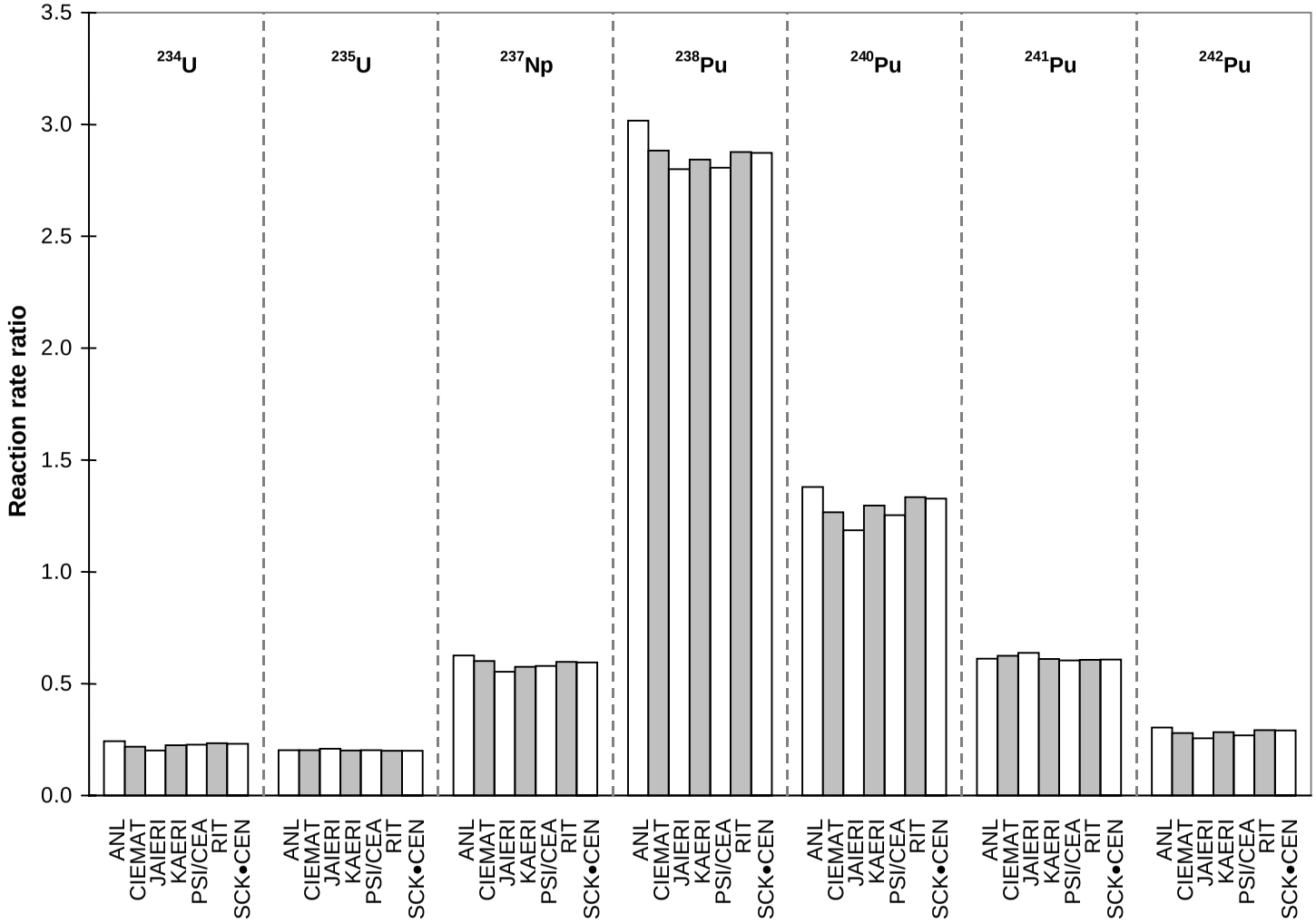

Figure 4.7.3. Equilibrium core: Fission reaction rate ratio relative to ^{239}Pu fission reaction rate (*cont.*)

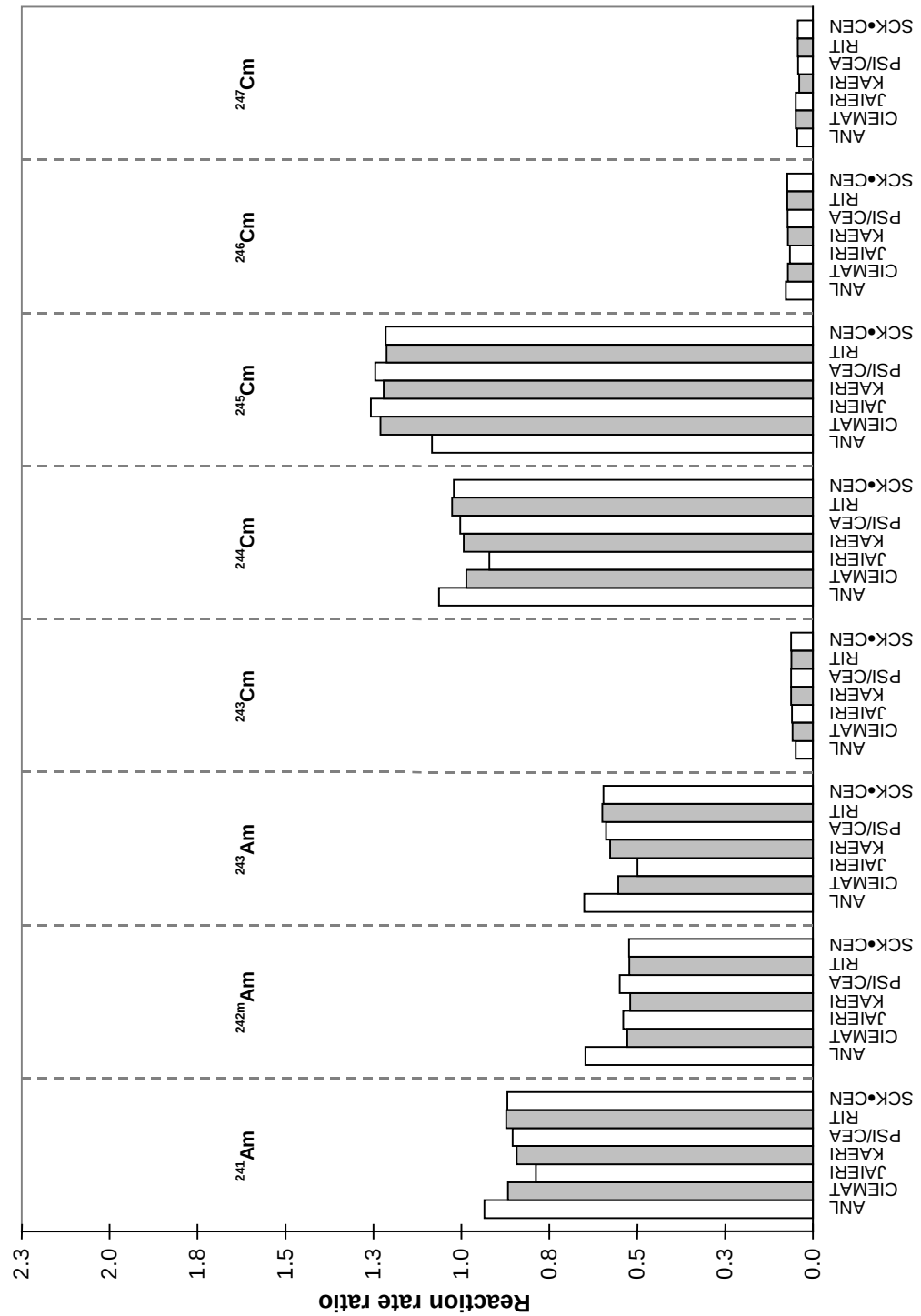

Figure 4.7.4. Equilibrium core: Capture reaction rate ratio relative to ^{239}Pu fission reaction rate

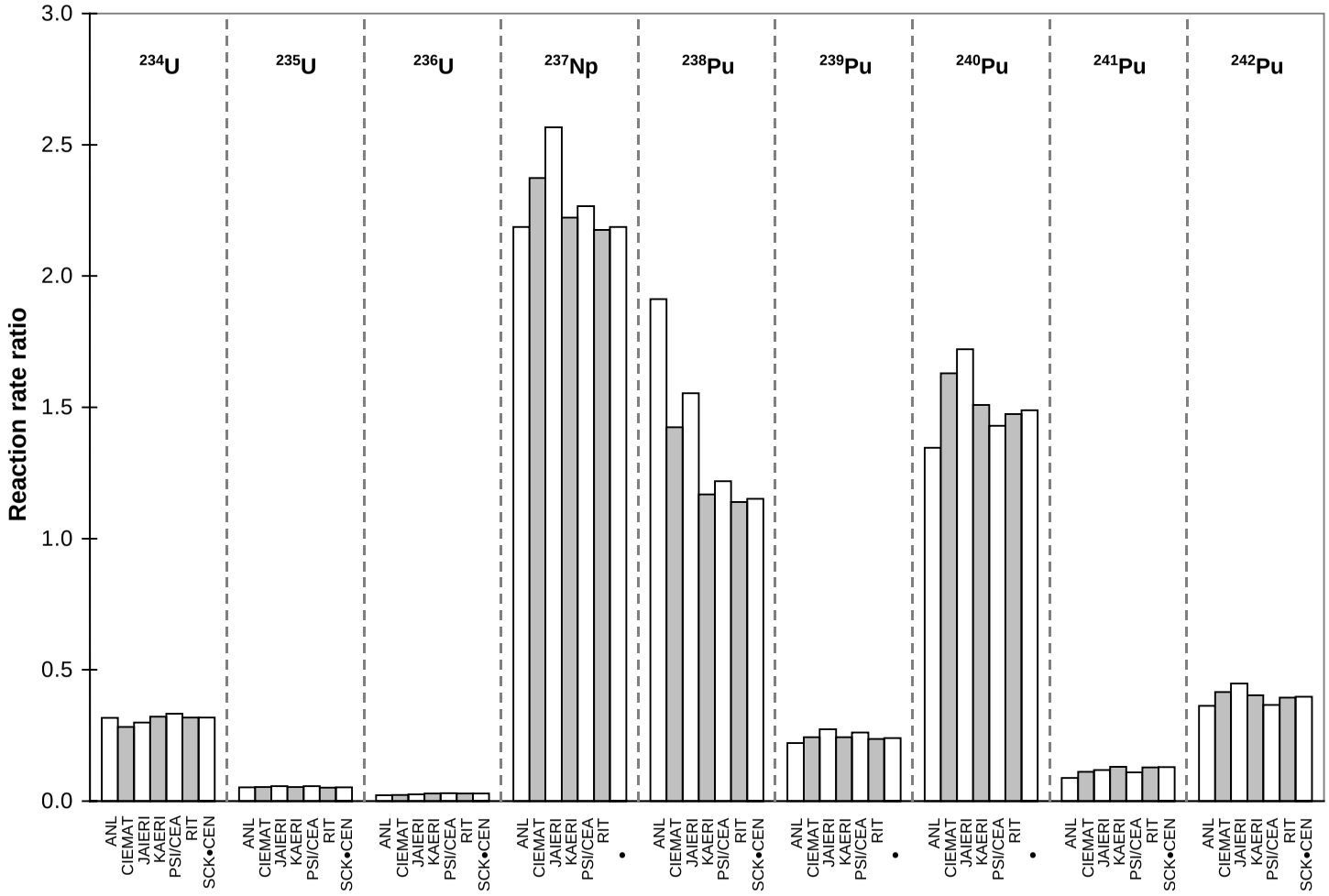

Figure 4.7.4. Equilibrium core: Capture reaction rate ratio relative to ^{239}Pu fission reaction rate (*cont.*)

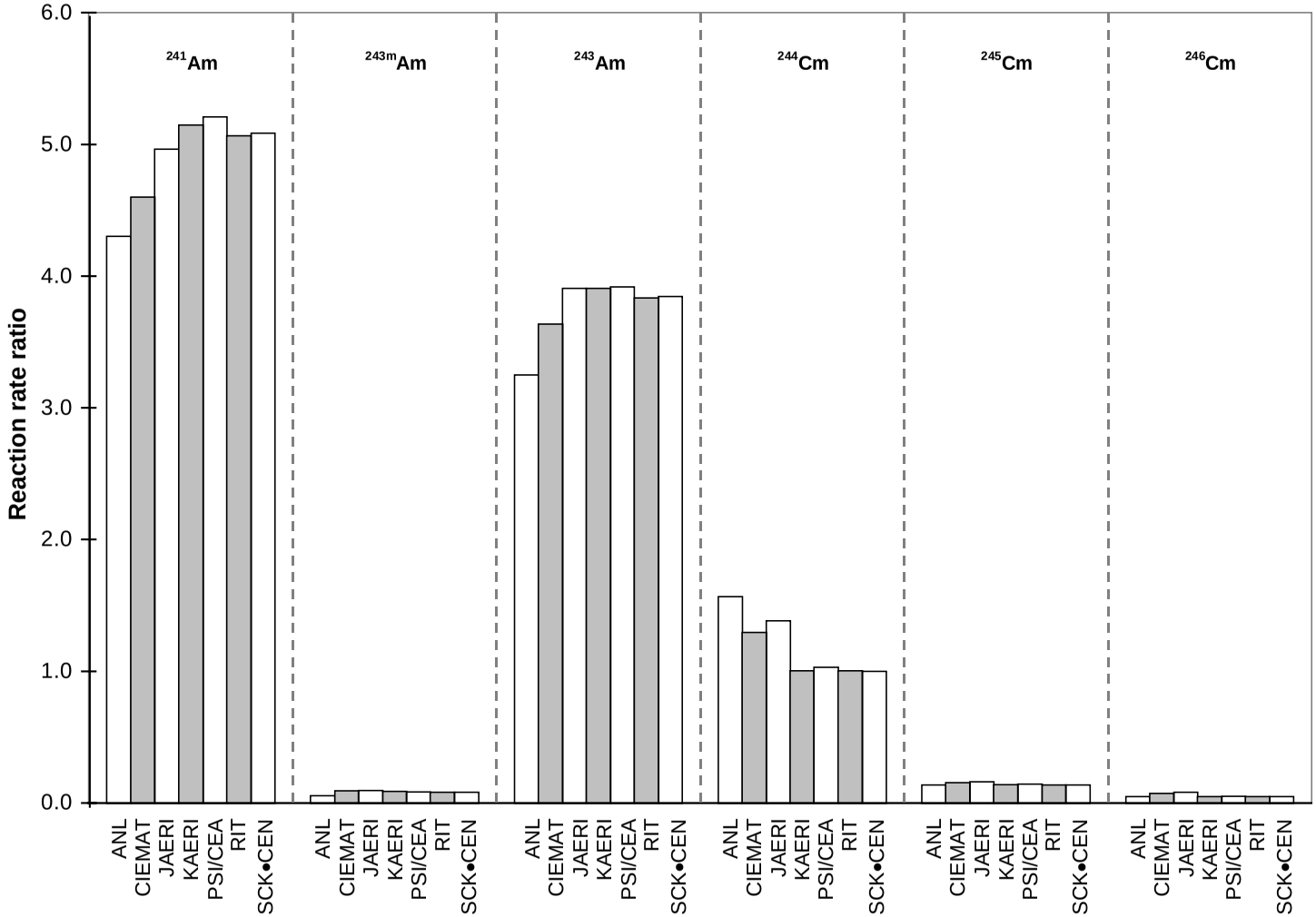

Figure 4.8.1. Start-up core: Isotopic composition at EOL

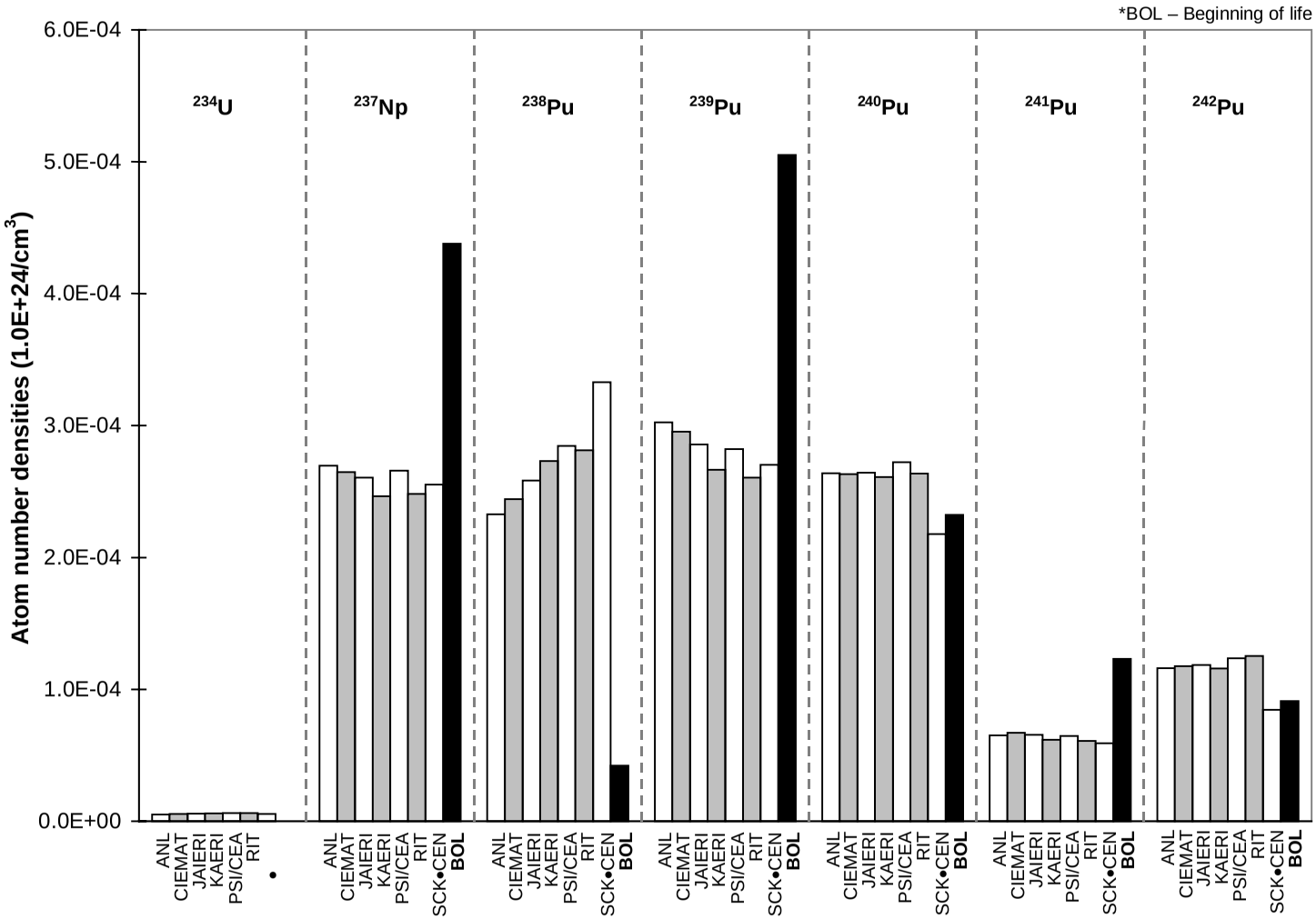

Figure 4.8.1. Start-up core: Isotopic composition at EOL (*cont.*)

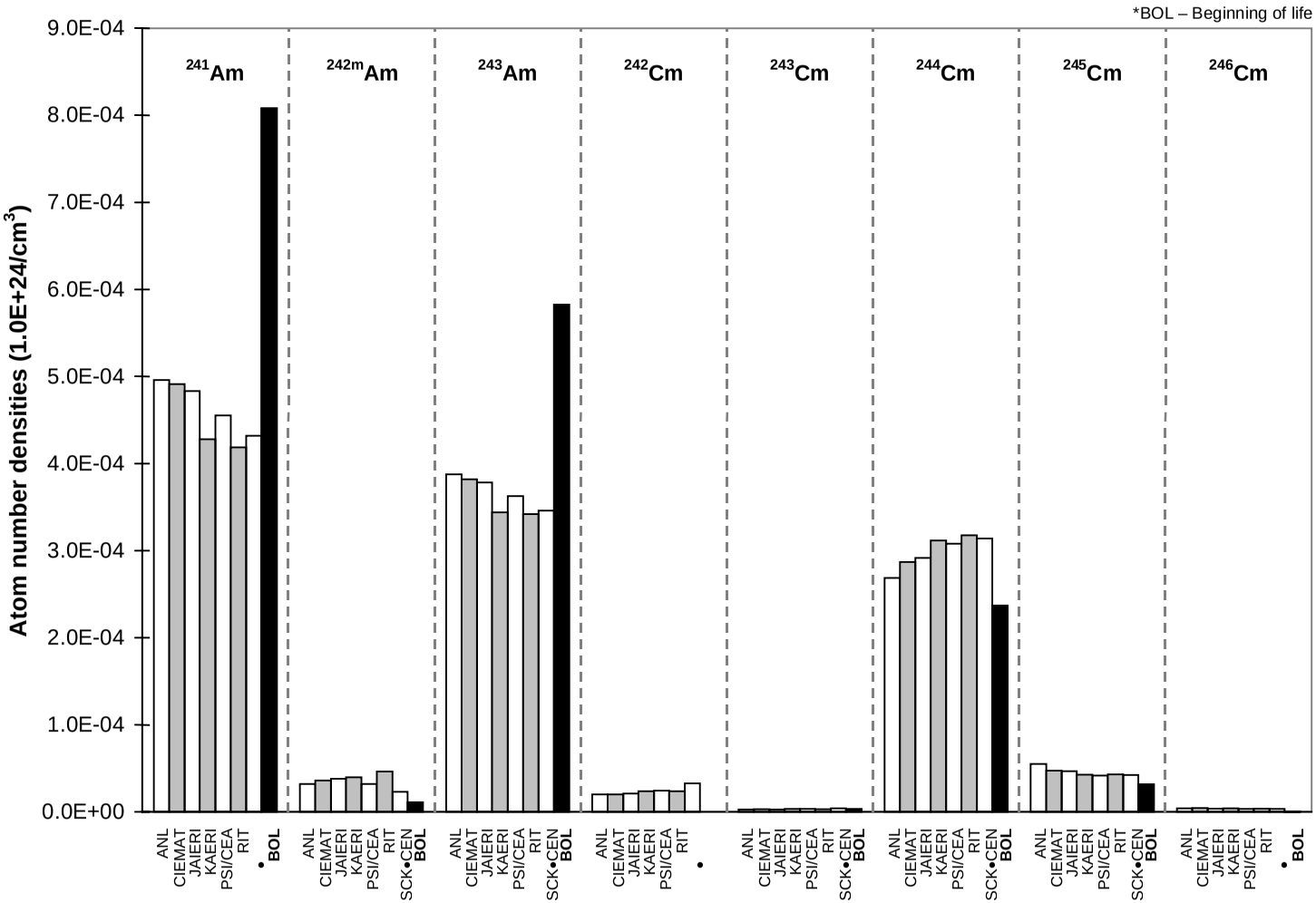

Figure 4.8.2. Equilibrium core: Isotopic composition at EOL

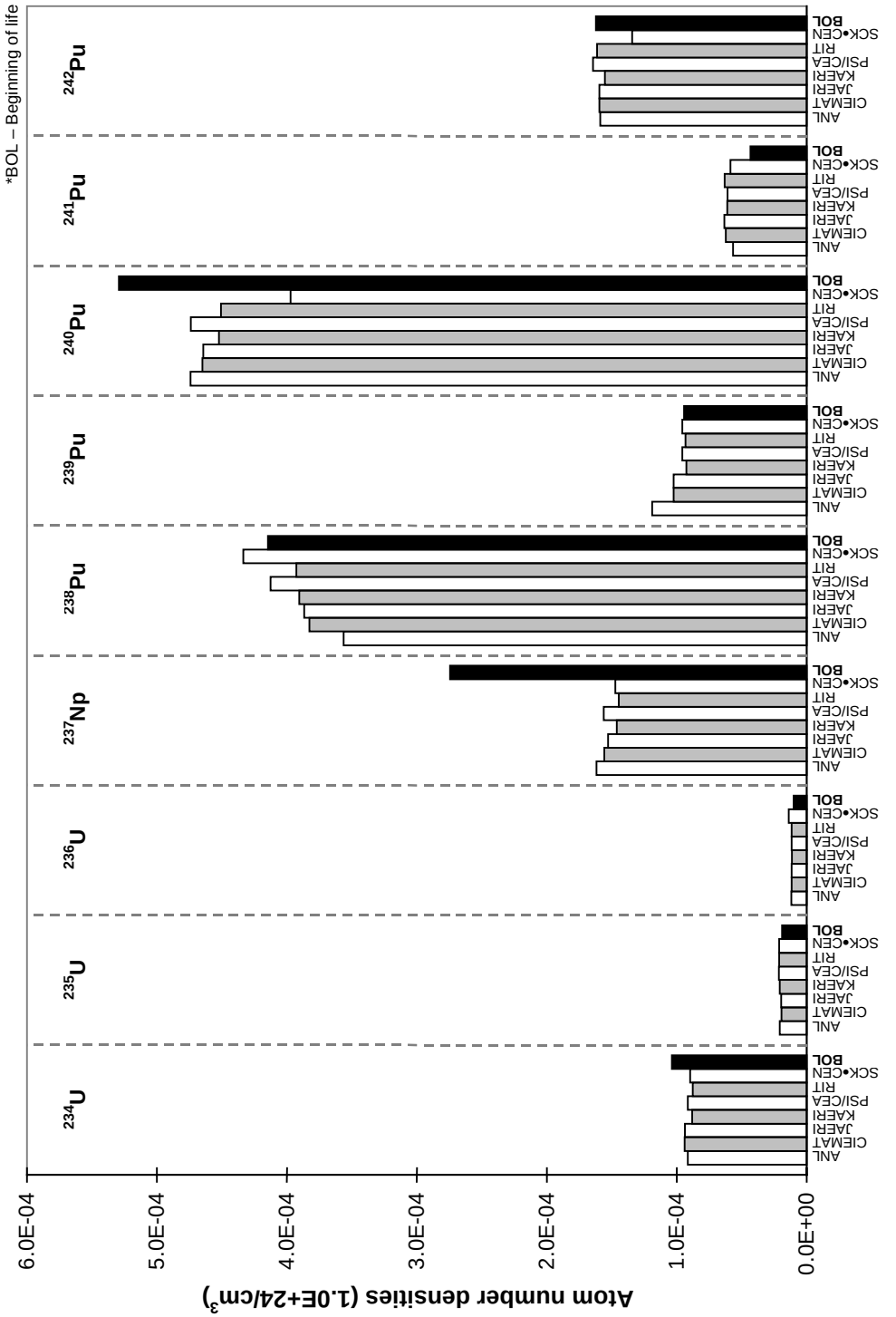

Figure 4.8.2. Equilibrium core: Isotopic composition at EOL (*cont.*)

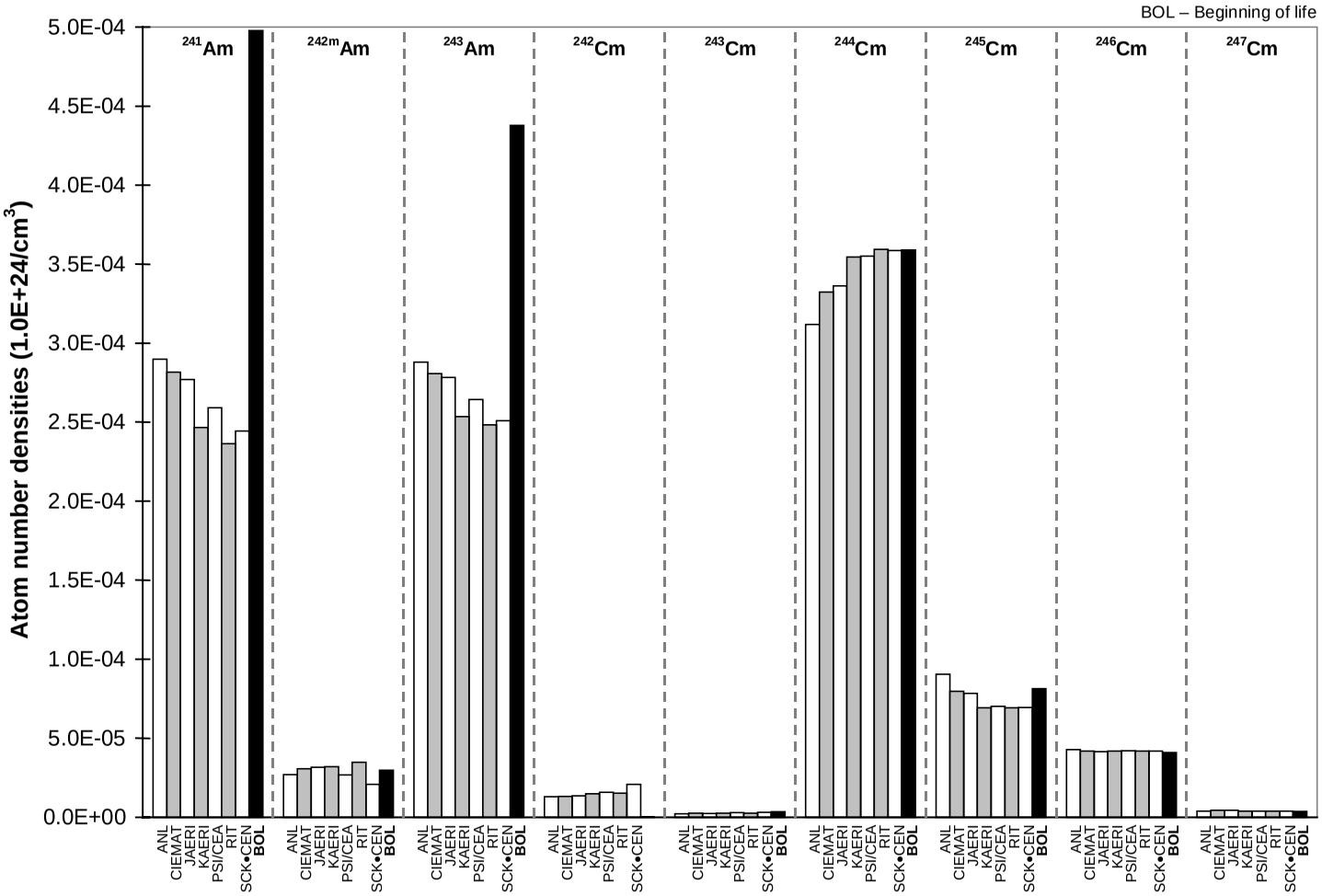

Figure 4.9.1. Activity from activation products

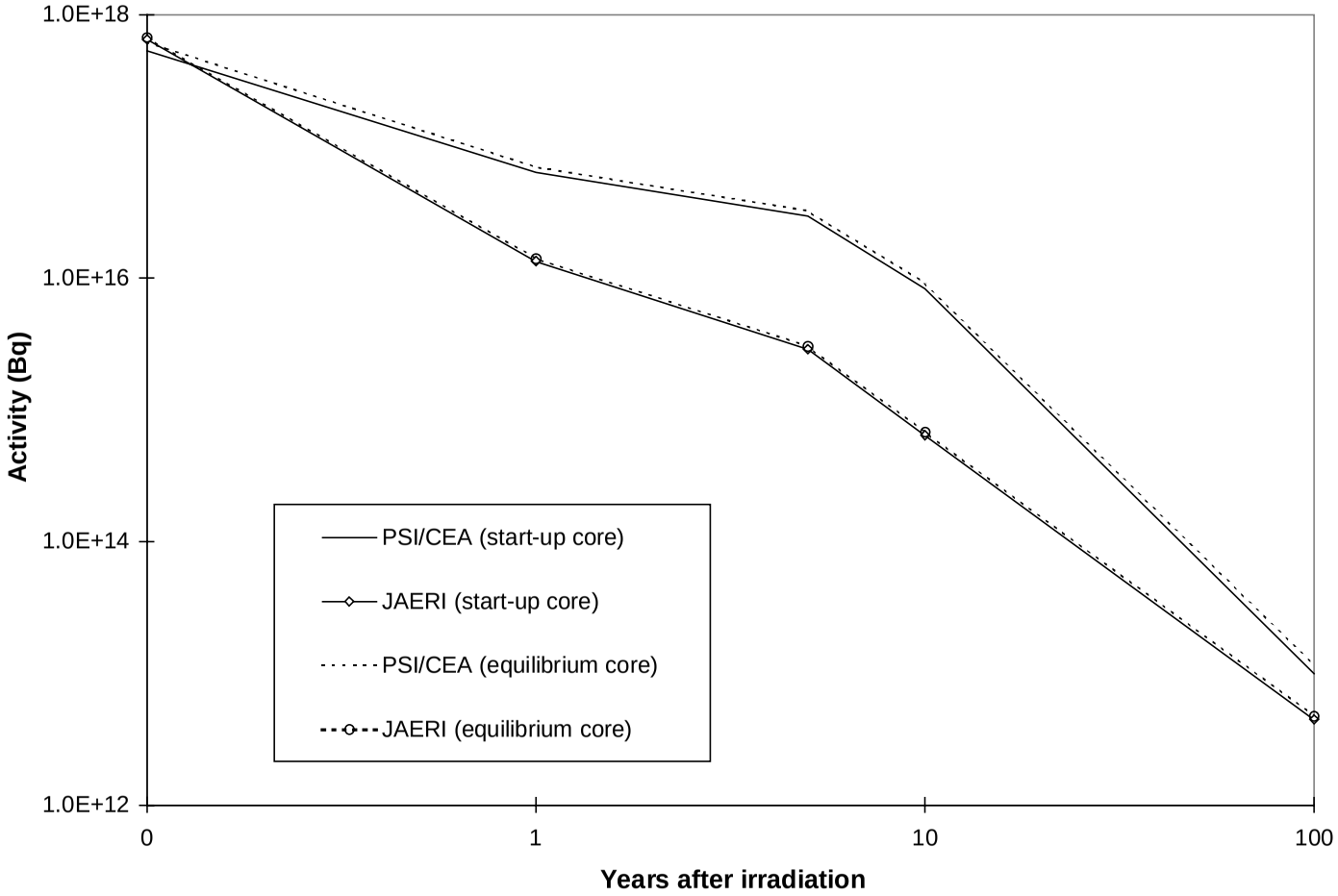

Figure 4.9.2. Start-up core: Activity from actinides

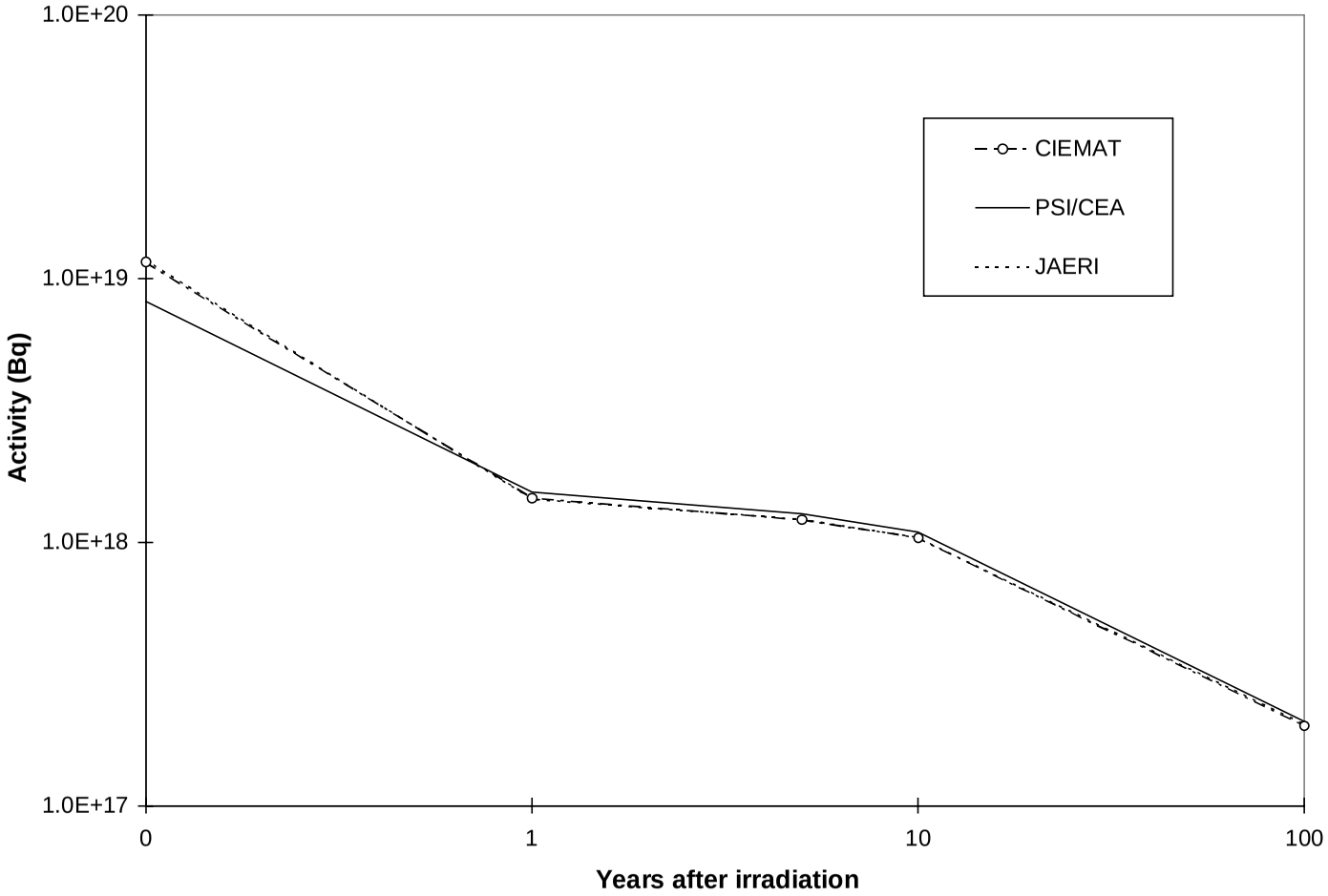

Figure 4.9.3. Equilibrium core: Activity from actinides

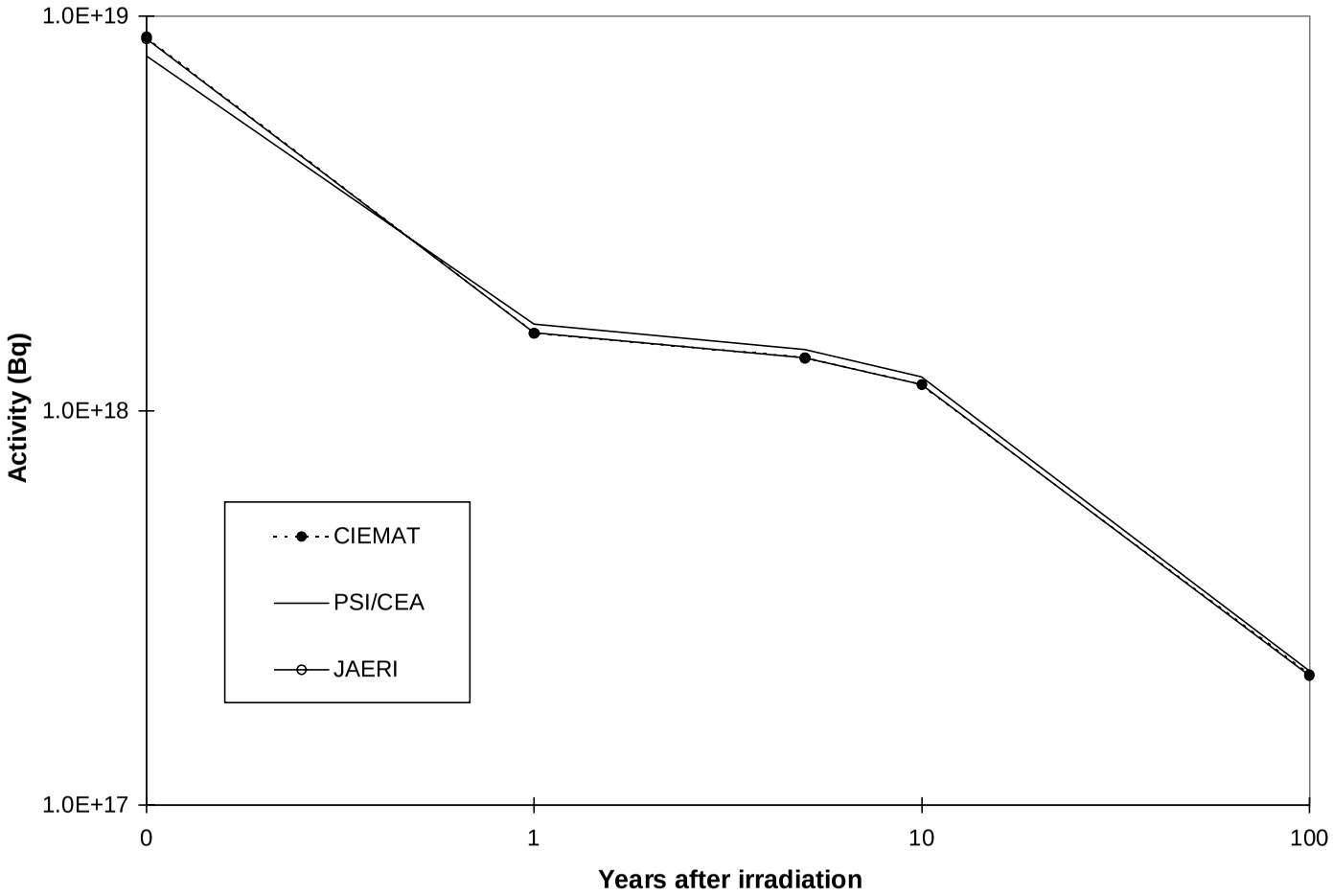

Figure 4.9.4. Activity from fission products

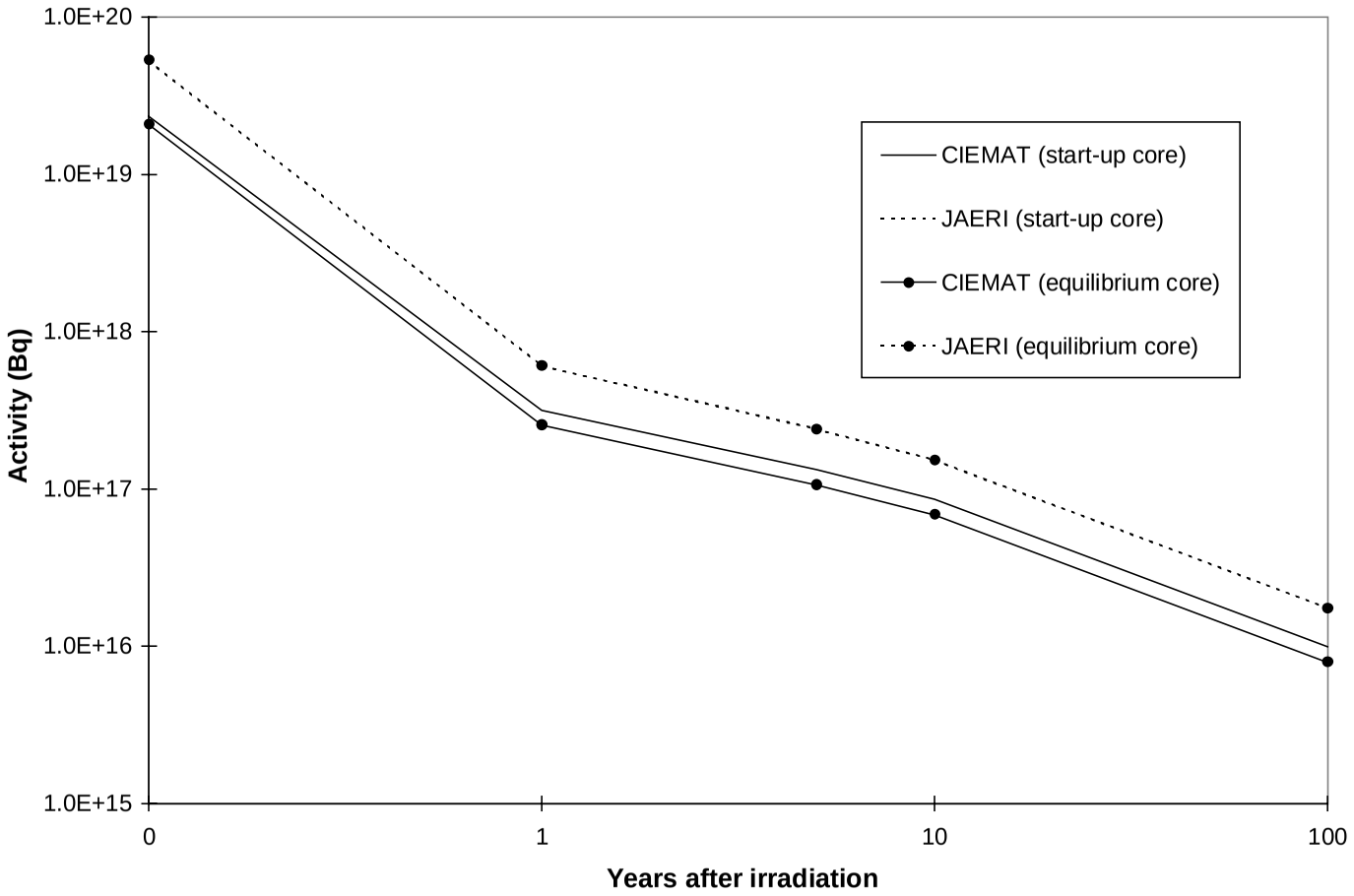

Figure 4.9.5. Start-up core: Total activity

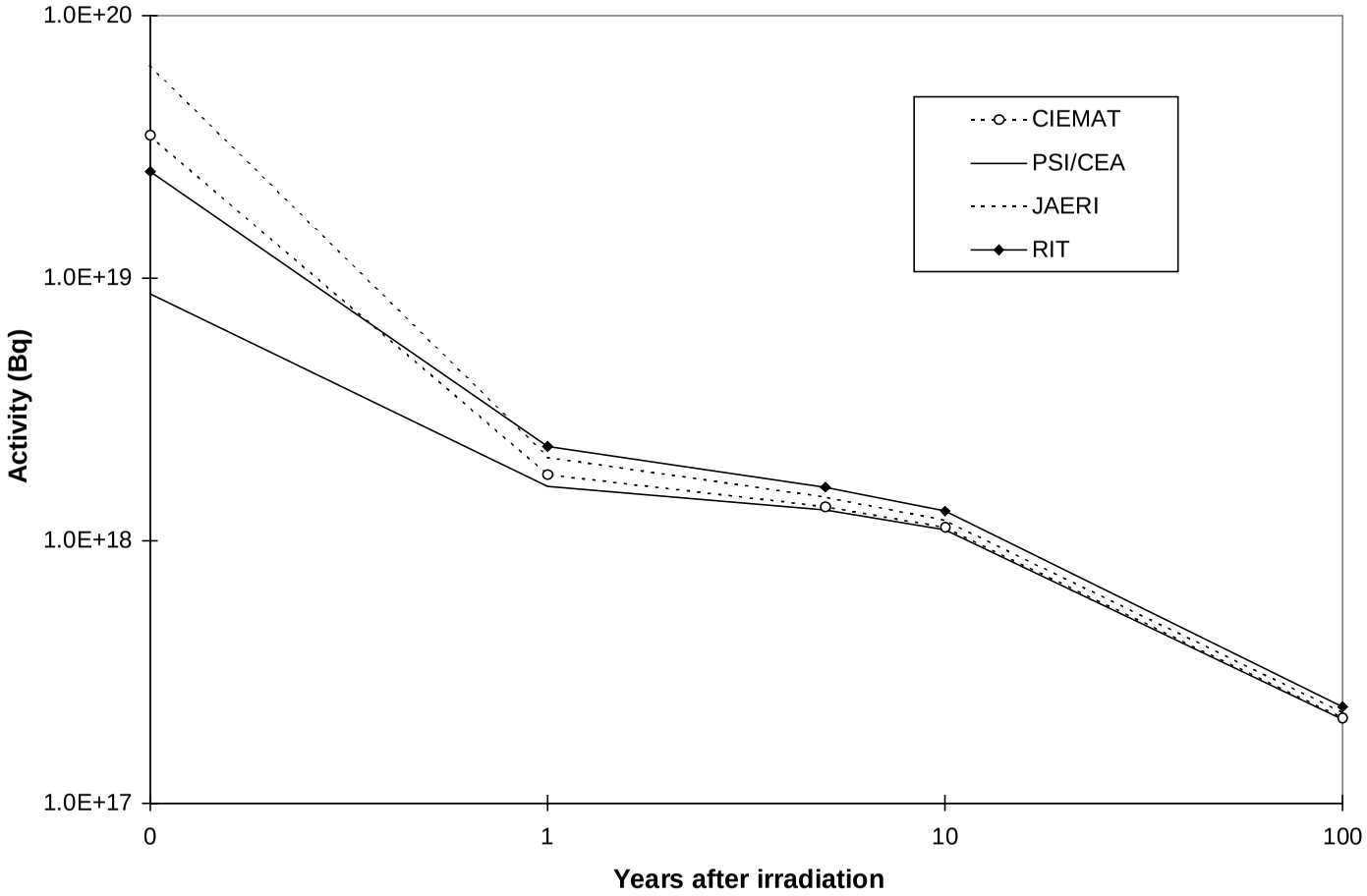

Figure 4.9.6. Equilibrium core: Total activity

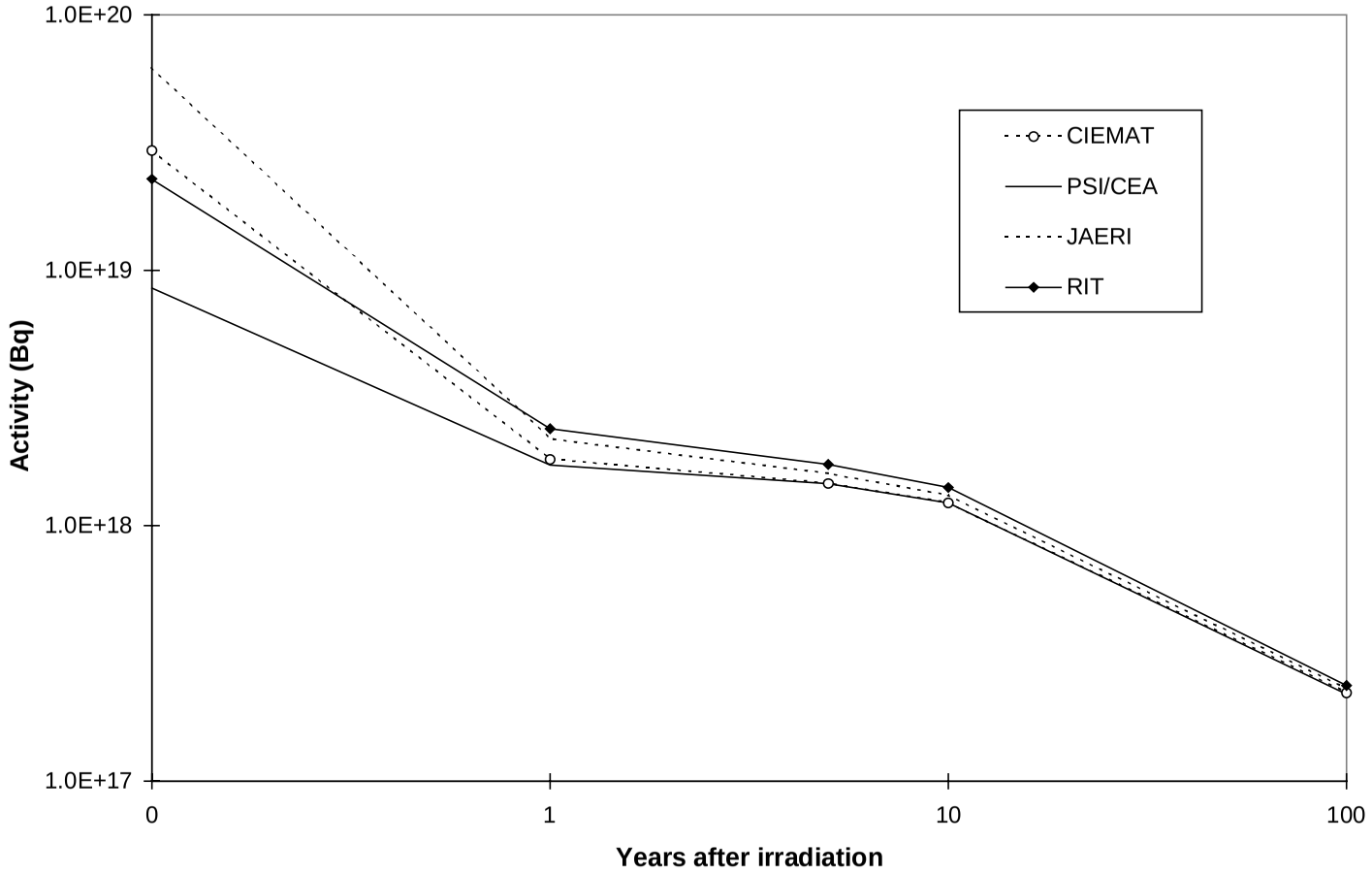

Figure 4.9.7. Start-up core: Decay heat

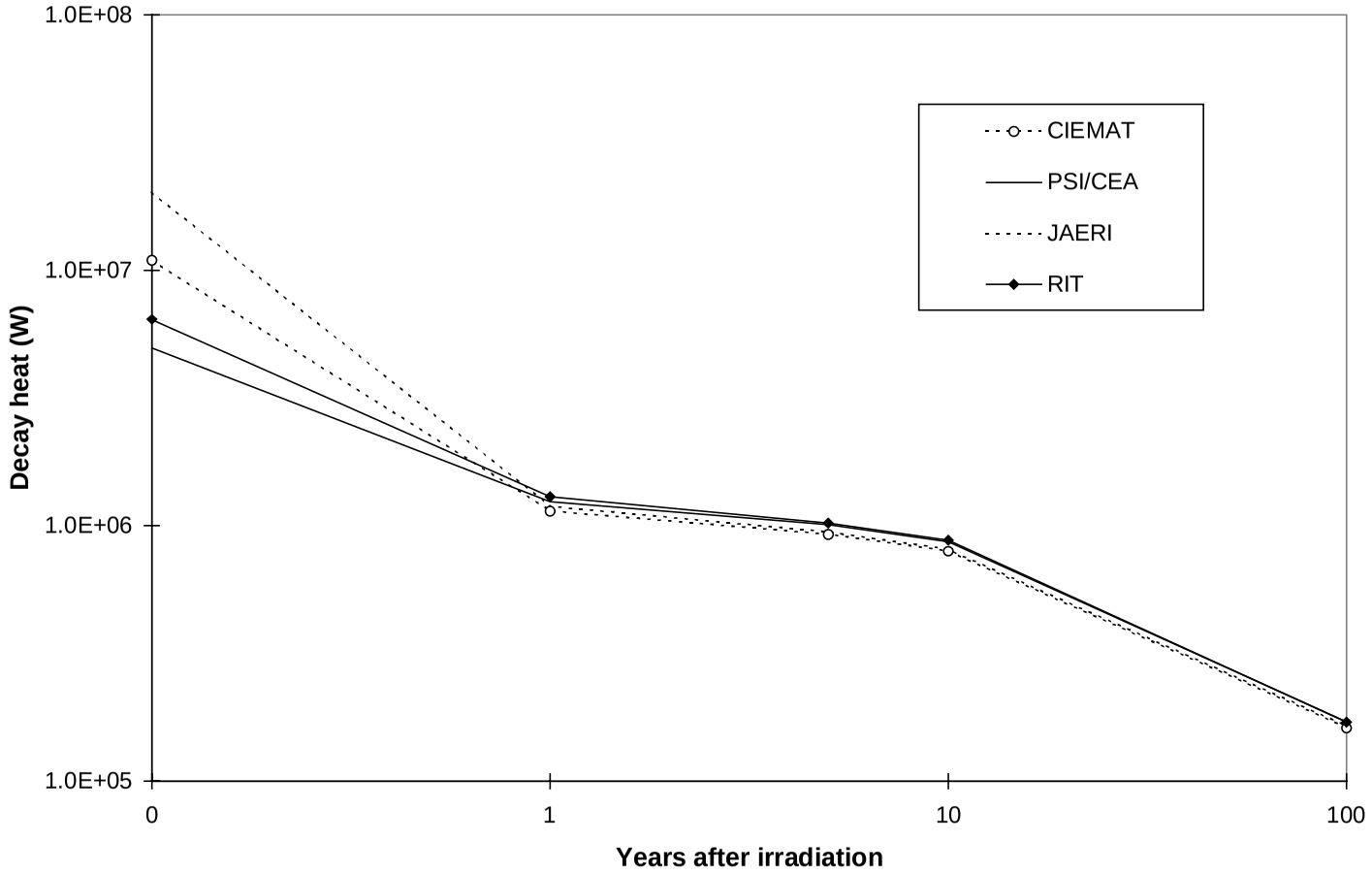

Figure 4.9.8. Equilibrium core: Decay heat

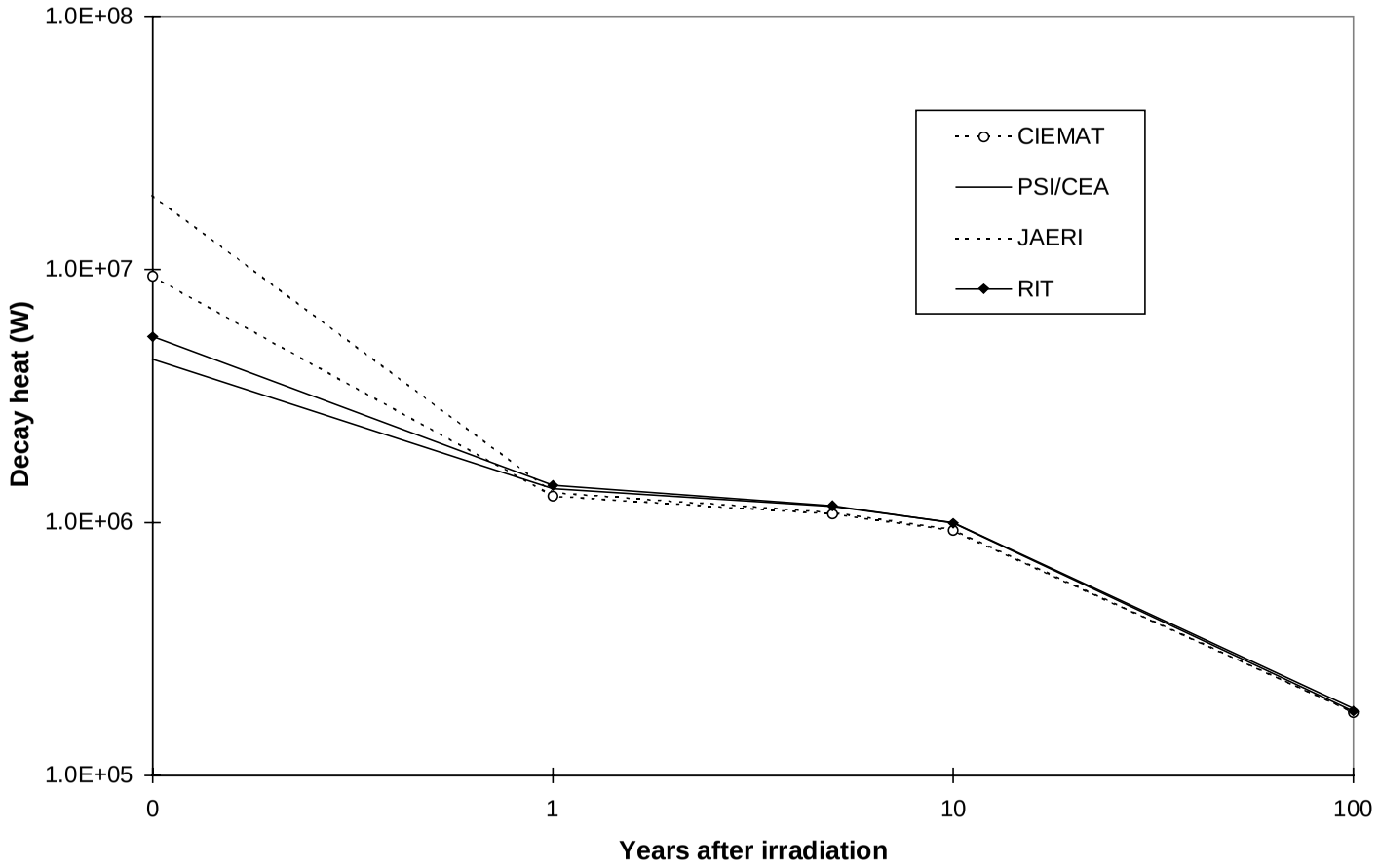

Figure 4.9.9. Start-up core: Neutron produced by (α,n) reactions

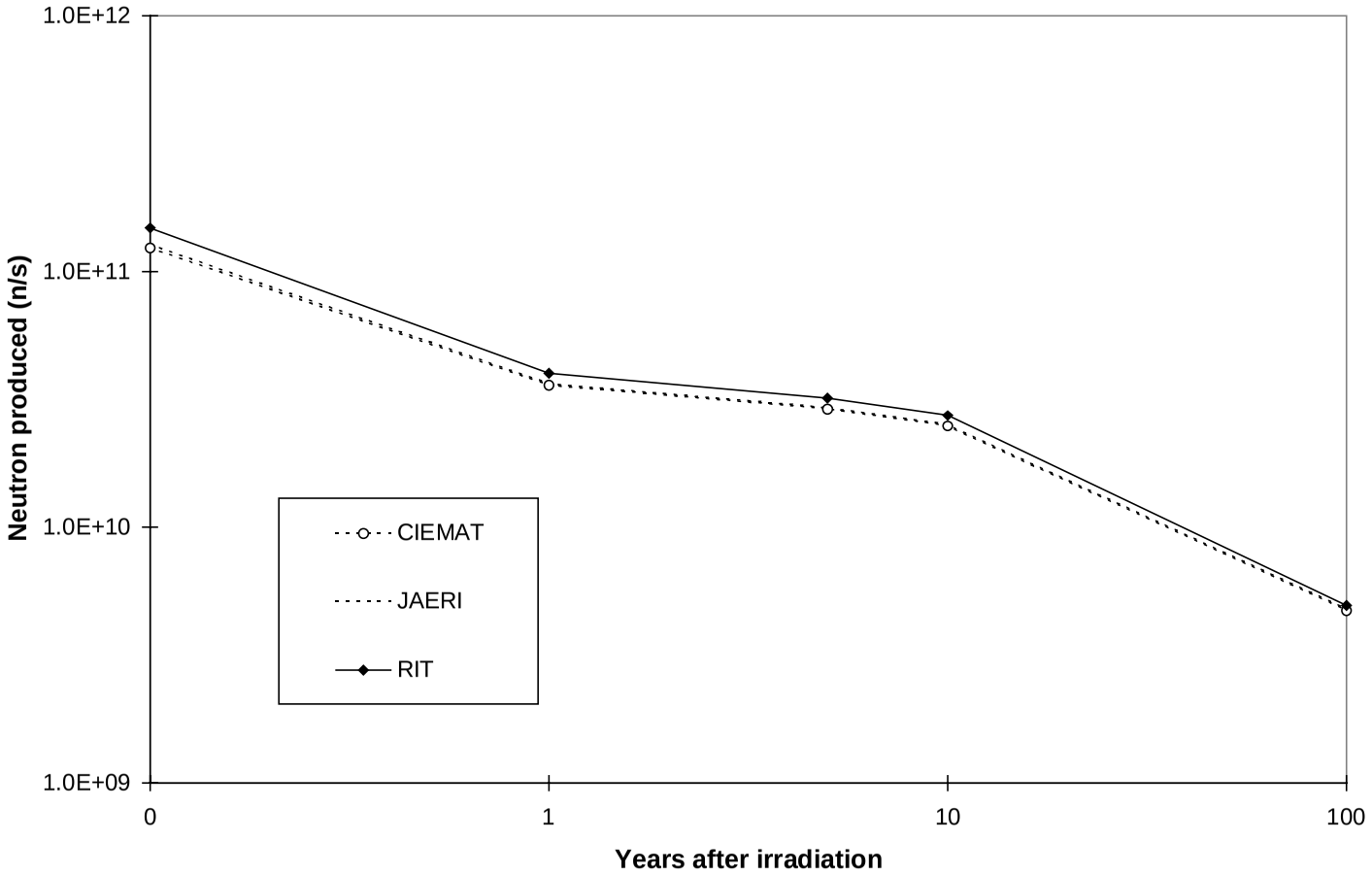

Figure 4.9.10. Start-up core: Neutron produced by spontaneous fission

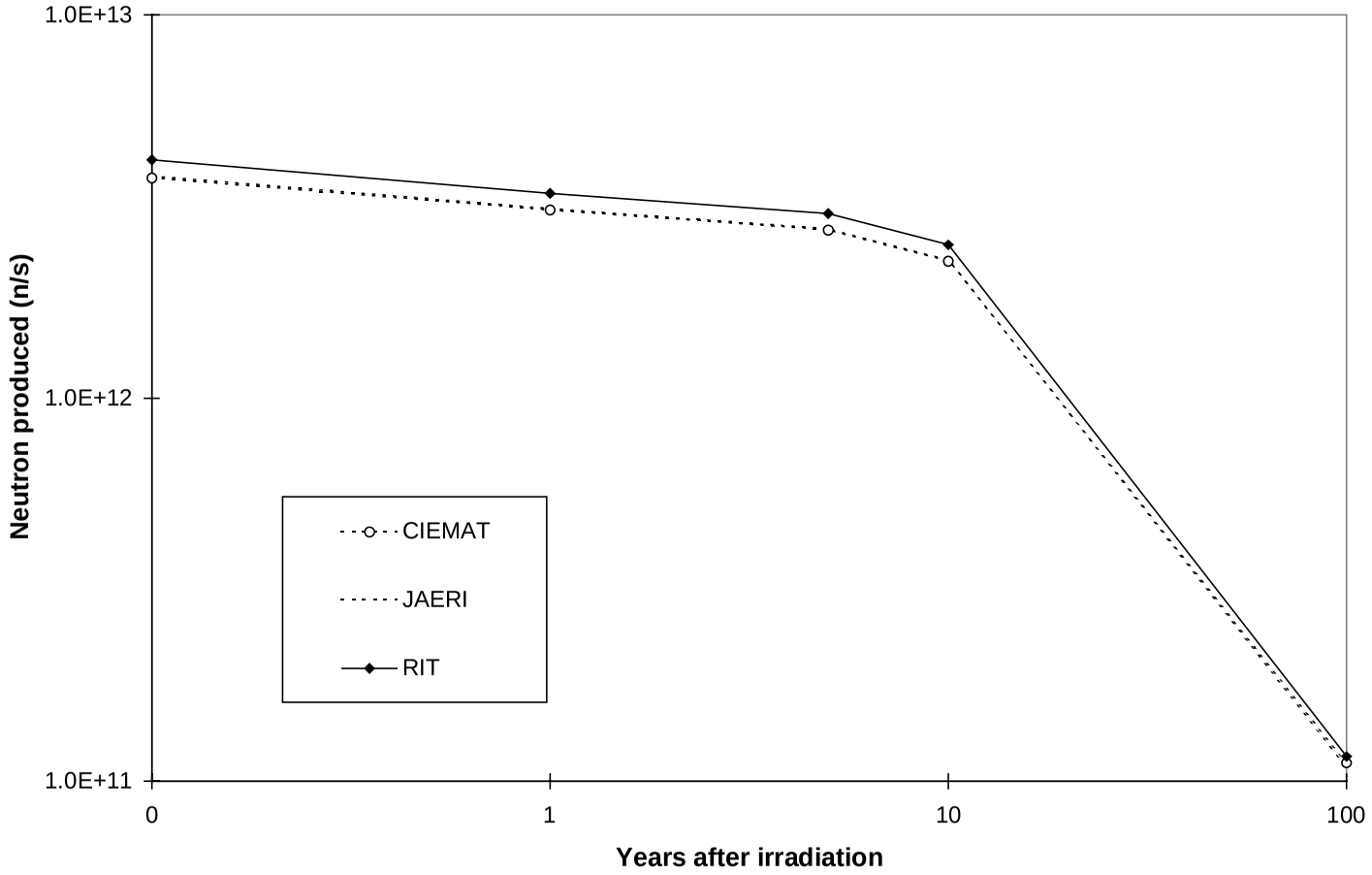

APPENDIX A

Benchmark specification

NEA/NSC/DOC(99)13
(Revised 27 August 1999)

OECD/NEA Nuclear Science Committee

Comparison Calculations for an Accelerator-driven Minor Actinide Burner

1 July 1999

Final Draft

NUCLEAR ENERGY AGENCY
ORGANISATION FOR ECONOMIC CO-OPERATION AND DEVELOPMENT

COMPARISON CALCULATIONS FOR AN ACCELERATOR-DRIVEN MINOR ACTINIDE BURNER

Peter Wydler
PSI

Hideki Takano
JAERI

Background and introduction

In 1994, the NEA Nuclear Science Committee (NSC), through its Task Force on Transmutation, initiated a benchmark exercise on a transmutation strategy based on light water reactors, fast reactors and an accelerator-driven system (ADS). The ADS, a sodium-cooled system with a tungsten target and MA-Pu nitride fuel, was analysed by groups from JAERI, PSI and IPPE. Considerable differences in calculated initial k_{eff} values and burn-up reactivity swings indicated a need for refining the benchmark specification and continuing the exercise with a wider participation [1,2]. This need was strengthened when the participants of the NSC Workshop on Utilisation and Reliability of High Power Accelerators, held in Mito, Japan, from 13-15 October 1998, proposed transient benchmark calculations with emphasis on the beam trip problem of liquid-metal cooled accelerator-driven systems.

The benchmark model described below is suitable for resolving the discrepancies observed in the benchmark exercise of the Task Force on Transmutation and can later be extended for transient applications such as the beam trip problem. The model is similar to that used before, except for the target and the coolant. The choices of a liquid metal target and lead-bismuth coolant reflect the generally increased interest in this technology.

As in the past exercise, emphasis is on the ADS as a component of an advanced nuclear energy system utilising uranium as energy resource. In this context, an obvious role of the ADS is to burn minor actinides in the P&T cycle of a “double strata” fuel cycle strategy [3]. Fuel compositions in the new benchmark exercise are chosen in accordance with this strategy.

The new benchmark exercise was approved by the NSC at its meeting of 2-4 June 1999.

Benchmark specification

General plant concept

For the P&T cycle, the appropriate concept is a modular plant which allows the MA burning capacity to be adjusted flexibly to the requirements of the nuclear park. Considering that a MA burner supports some 15-20 energy producers of the same thermal power and the influence of the size of a module on the overall electricity production cost is therefore small, the module of the **ALMR reference system** has an optimum size. Several features of the ALMR have been incorporated in proposed ADS designs. Adopting this system as the basis for the benchmark calculations has the advantage that a detailed plant concept is available and the performance of the plant with normal cores has already been analysed in great detail, including transient and beyond design basis behaviour [4].

Target/core/reflector geometry and composition

The comparison calculations are carried out for an R-Z model with the dimensions given in Figure 1. The model comprises a central **lead-bismuth target** zone, a void zone in the beam duct region, a multiplying region consisting of homogenised fuel and **lead-bismuth coolant**, and an outer steel reflector zone. The core dimensions are those of the ALMR burner reference core. Reflector and radial shield materials are simulated by an average homogeneous mixture of HT-9 steel (70% by volume) and coolant (remainder). The target and reflector temperature is 650 K. Homogenised atom number densities for the target and the reflector are given in Table 1.

A heavy coolant like lead-bismuth requires a high pumping power. This can be compensated by an increased coolant volume fraction which reduces the pressure drop in the core. In the case of the benchmark reactor, an adequate pitch-to-diameter ratio of 1.6 is achieved by replacing the reference (sodium-cooled) 271 pin subassembly by a 217 pin subassembly. If the pin diameter is preserved, the thermal power reduces proportionally from the 471 MW_{th} of the reference system to 377 MW_{th} for the benchmark reactor.

As for the fuel, dense and non-moderating metals and nitrides are preferable because they improve the neutron economy and the toxicity reduction potential of the system. Reprocessed by the "dry" technique, they are particularly suited for the P&T cycle of the double strata concept. Following Japanese and French project preferences, the comparison calculations concentrate on **nitride fuels**. The nitrogen is assumed to be pure ^{15}N.

Fuel composition and burn-up

Fuel compositions (and hence characteristics) of MA burner cores differ considerably from those of normal MOX cores and also between start-up and equilibrium cores. For determining the composition of the minor actinides transferred to the P&T cycle, the nuclear park is assumed to consist of a mix of UOX-fuelled LWRs (71%), MOX-fuelled LWRs (11%) and CAPRA-type fast reactors which burn the plutonium in a closed cycle after two recycles in the LWRs (18%) [5]. From this MA composition [6], start-up and equilibrium core compositions (cf. Table 1) were determined as follows:

- For the **start-up core**, the MAs are mixed with plutonium from the UOX-fuelled LWRs using a fixed mixing ratio which gives a k_{eff} of about 0.95 at BOL.

- For the **equilibrium core** (fully closed cycle with MA top-up or "feed"), the cycle averaged equilibrium composition was calculated directly using the algorithm described in Ref. [7], and a BOL correction based on an evolution calculation was then applied. MA feed and (BOL) equilibrium composition are compared in Figure 2.

Calculations are performed for both compositions to ensure that the benchmark exercise is representative for a wide range of cores. The operating temperature of the fuel is 980 K.

Because an equilibrium core with undiluted fuel is too reactive, an actinide-zirconium mixture in the form of mono-nitrides is used. The actinide-to-zirconium ratio is set to give a k_{eff} of about 0.95 at BOL. This (fixed) actinide-to-zirconium ratio is also used for the start-up core. Diluting the actinides in an inert matrix has the additional benefit of reducing the activity of the irradiated fuel.

The fuel is irradiated during five years at an average thermal power of 320 MW, corresponding to a load factor of 0.85; at EOL, it reaches a burn-up of approximately 200 GWd/t_{HM}.

External neutron source

A **standard spallation neutron source,** produced with the code HETC by PSI assuming a 1 GeV proton beam, is prescribed. The source is provided in a fine group structure to enable the participants to prepare sources for their own broad group structures. The source data are given in a separate neutron source specification. The target top is set to coincide with the top of the core to reduce possible calculational uncertainties due to the presence of a void in the beam duct region.

Requested results

Homogenous cell calculations

1. One group fission and capture microscopic cross-sections.
2. k_{inf}, B_c^2, M^2.

Reactor calculation (transport theory)

1. Reaction rate balance components (production, absorption, leakage) for fuel zone at BOL, decomposition by nuclide.
2. Radial neutron flux distribution (z = 100 cm), axial neutron flux distributions (r = 0 cm, 56 cm).
3. Neutron spectrum and reaction rate ratios relative to ^{239}Pu fission at r,z = 56 cm, 100 cm.
4. Burn-up (GWd/t_{HM}), k_{eff}, k_{eff} without fission products (set fission-product concentrations to zero), and source strength (neutrons/s at the full power of 377 MW_{th}) for five burn-up step (5×365 d).
5. Fuel isotopic composition at EOL.
6. Pb-Bi void reactivity effect of fuel zone at BOL and EOL, defined as $k_{eff}^{voided} - k_{eff}^{ref}$ and $\left(k_{eff}^{voided} - k_{eff}^{ref}\right)/k_{eff}^{ref}$.
7. Fuel Doppler reactivity effect at BOL and EOL, defined as $\left(k_{eff}^{980\,K} - k_{eff}^{1580\,K}\right)/\left(k_{eff}^{980\,K} \cdot k_{eff}^{1580\,K}\right)$.
8. β_{eff} at BOL.
9. Activity, decay heat, and neutron source strength of irradiated fuel.
10. ^{210}Po activity of target.

To simplify the processing of the results, empty Excel tables are supplied to the participants. The deadline for submitting the tables with the results is **30 September 1999**. The results should be sent to:

Byung Chan NA	Tel: +33 1 45 24 10 91
OECD/NEA	Fax: +33 1 45 24 11 10
Le Seine Saint-Germain	E-mail: na@nea.fr
12, Boulevard des Îles	
F-92130 Issy-les-Moulineaux	
France	

REFERENCES

[1] OECD/NEA NSC Task Force on Physics Aspects of Different Transmutation Concepts, "JAERI Proposal of Benchmark Problem on Method and Data to Calculate the Nuclear Characteristics in Accelerator-based Transmutation System With Fast Neutron Flux" (NSC/DOC(96)10).

[2] H. Takano, *et al.*, Proc. Int. Conf. on the Physics of Nuclear Science and Technology, 5-8 October 1998, Long Island, USA, 1 462.

[3] T. Mukaiyama, *et al*., "R&D Strategy for Partitioning & Transmutation under OMEGA Program and Neutron Science Project of JAERI", 5th OECD/NEA Inf. Exchange Mtg. on Actinide and Fission Product Partitioning and Transmutation, 25-27 November 1998, Mol, Belgium.

[4] Utility Industry Review of the ALMR Plant Design Program, 20-21 May 1993, San Jose, California, USA.

[5] M. Salvatores, "Advanced Options for Transmutation Strategies", 5th OECD/NEA Inf. Exchange Mtg. on Actinide and Fission Product Partitioning and Transmutation, 25-27 Nov. 1998, Mol, Belgium.

[6] J. Tommasi, CEA Cadarache, private communication.

[7] P. Wydler and Y. Kadi, Proc. 3rd OECD/NEA Inf. Exchange Mtg. on Actinide and Fission Product Partitioning and Transmutation, 12-14 December 1994, Cadarache, France, 298 (NEA/P&T Report No. 13).

Figure 1. R-Z model of accelerator-driven minor actinide burner system

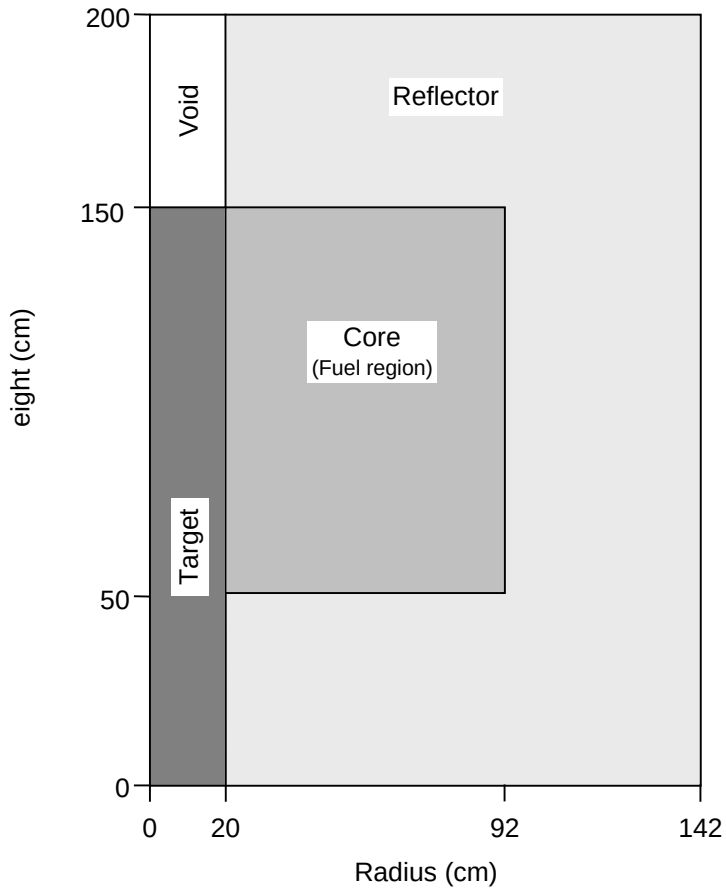

Figure 2. Minor actinide feed and equilibrium composition

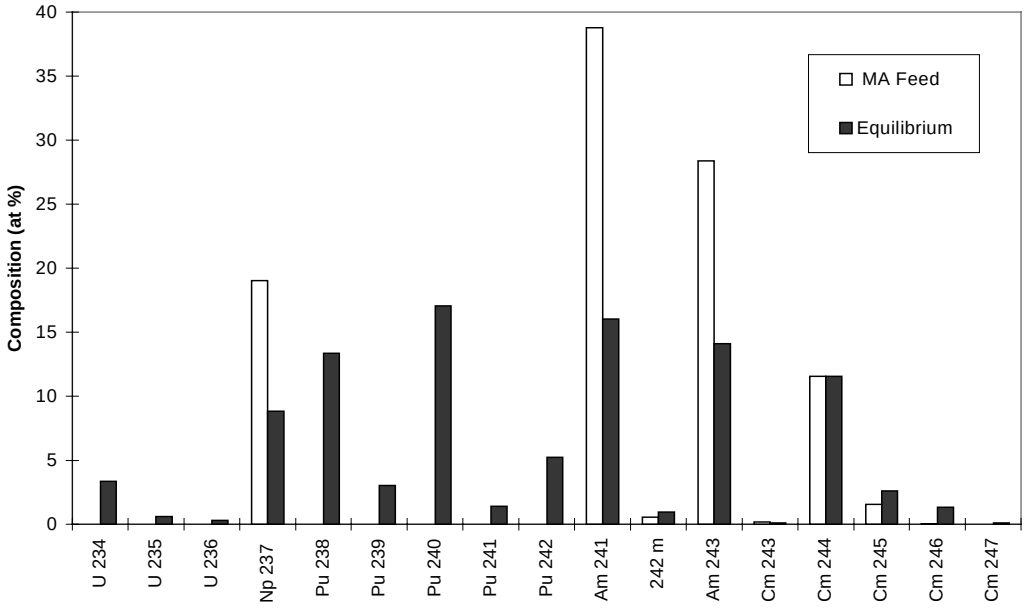

Table 1. Homogenised atom number densities (1.0E+24/cm^3)

Target	
Pb	1.320E-02
^{209}Bi	1.632E-02

Reflector	
^{54}Fe	2.990E-03
^{56}Fe	4.560E-02
^{57}Fe	1.075E-03
^{58}Fe	1.344E-04
^{50}Or	3.458E-04
^{52}Or	6.422E-03
^{53}Or	7.134E-04
^{54}Or	1.741E-04
^{58}Ni	1.977E-04
^{60}Ni	7.305E-05
^{61}Ni	3.111E-06
^{62}Ni	9.724E-06
^{64}Ni	2.388E-06
Mo	3.565E-04
Mn	3.412E-04
^{182}W	2.140E-05
^{183}W	1.155E-05
^{184}W	2.465E-05
^{186}W	2.280E-05
Pb	4.075E-03
^{209}Bi	5.039E-03

Fuel		
	Equilibrium	Start-up
^{232}U	6.214E-10	–
^{233}U	6.524E-09	–
^{234}U	1.039E-04	–
^{235}U	1.895E-05	–
^{236}U	1.018E-05	–
^{237}U	6.214E-09	–
^{238}U	2.019E-08	–
^{237}Np	2.745E-04	4.377E-04
^{238}Np	2.051E-07	–
^{238}Pu	4.147E-04	4.226E-05
^{239}Pu	9.449E-05	5.051E-04
^{240}Pu	5.293E-04	2.321E-04
^{241}Pu	4.330E-05	1.232E-04
^{242}Pu	1.623E-04	9.102E-05
^{241}Am	4.978E-04	8.084E-04
^{242m}Am	2.982E-05	1.089E-05
^{243}Am	4.378E-04	5.827E-04
^{242}Cm	8.855E-08	4.079E-08
^{243}Cm	3.379E-06	3.326E-06
^{244}Cm	3.591E-04	2.371E-04
^{245}Cm	8.122E-05	3.164E-05
^{246}Cm	4.104E-05	5.355E-07
^{247}Cm	3.682E-06	–
^{248}Cm	1.065E-06	–
^{90}Zr	3.847E-03	
^{91}Zr	8.465E-04	
^{92}Zr	1.285E-03	
^{94}Zr	1.292E-03	
^{96}Zr	2.064E-04	
^{15}N	1.058E-02	
^{54}Fe	9.759E-04	
^{56}Fe	1.488E-02	
^{57}Fe	3.507E-04	
^{58}Fe	4.386E-05	
^{50}Cr	1.128E-04	
^{52}Cr	2.096E-03	
^{53}Cr	2.328E-04	
^{54}Cr	5.682E-05	
^{58}Ni	6.451E-05	
^{60}Ni	2.384E-05	
^{61}Ni	1.015E-06	
^{62}Ni	3.173E-06	
^{64}Ni	7.792E-07	
Mo	1.163E-04	
Mn	1.114E-04	
^{182}W	6.984E-06	
^{183}W	3.770E-06	
^{184}W	8.045E-06	
^{186}W	7.439E-06	
Pb	6.360E-03	
^{209}Bi	7.865E-03	

Appendix A

SPALLATION NEUTRON SOURCE SPECTRUM AND A COLLAPSING PROGRAM

The spallation neutron spectrum is given in Table A.1. The calculation was carried out by PSI using the HETC code. A height of 100 cm and a radius of 20 cm of the Pb-Bi spallation target were assumed. The injection proton beam was assumed to have an energy of 1 GeV and a radius of 10 cm. The resulting spallation neutron is the volume averaged one in the region with a radius of 10 cm. ***The collapsed source is in units of neutrons per broad group – normalised to one neutron – and conforms to the definition of the external neutron source in the inhomogeneous neutron transport equation.*** The maximum energy is 20 MeV and lethargy width is 0.1.

Table A.1. Spallation neutron spectrum and energy structure

Group number	Energy boundary (eV)		Spallation spectrum
	Upper	Lower	
1	2.00E+07	1.81E+07	9.078E-03
2	1.81E+07	1.64E+07	1.013E-02
3	1.64E+07	1.48E+07	1.136E-02
4	1.48E+07	1.34E+07	1.274E-02
5	1.34E+07	1.21E+07	1.439E-02
6	1.21E+07	1.10E+07	1.612E-02
7	1.10E+07	9.93E+06	1.801E-02
8	9.93E+06	8.99E+06	2.003E-02
9	8.99E+06	8.13E+06	2.208E-02
10	8.13E+06	7.36E+06	2.418E-02
11	7.36E+06	6.66E+06	2.623E-02
12	6.66E+06	6.02E+06	2.831E-02
13	6.02E+06	5.45E+06	3.012E-02
14	5.45E+06	4.93E+06	3.171E-02
15	4.93E+06	4.46E+06	3.330E-02
16	4.46E+06	4.04E+06	3.449E-02
17	4.04E+06	3.65E+06	3.540E-02
18	3.65E+06	3.31E+06	3.595E-02
19	3.31E+06	2.99E+06	3.623E-02
20	2.99E+06	2.71E+06	3.612E-02
21	2.71E+06	2.45E+06	3.574E-02
22	2.45E+06	2.22E+06	3.503E-02
23	2.22E+06	2.01E+06	3.408E-02
24	2.01E+06	1.81E+06	3.295E-02
25	1.81E+06	1.64E+06	3.156E-02
26	1.64E+06	1.49E+06	3.003E-02
27	1.49E+06	1.34E+06	2.839E-02
28	1.34E+06	1.22E+06	2.669E-02
29	1.22E+06	1.10E+06	2.488E-02
30	1.10E+06	9.96E+05	2.310E-02
31	9.96E+05	9.01E+05	2.138E-02
32	9.01E+05	8.15E+05	1.961E-02
33	8.15E+05	7.38E+05	1.793E-02
34	7.38E+05	6.67E+05	1.633E-02
35	6.67E+05	6.04E+05	1.483E-02
36	6.04E+05	5.46E+05	1.342E-02
37	5.46E+05	4.94E+05	1.210E-02
38	4.94E+05	4.47E+05	1.085E-02
39	4.47E+05	4.05E+05	9.724E-03
40	4.05E+05	3.66E+05	8.681E-03
41	3.66E+05	3.31E+05	7.736E-03
42	3.31E+05	3.00E+05	6.904E-03
43	3.00E+05	2.71E+05	6.129E-03
44	2.71E+05	2.46E+05	5.405E-03
45	2.46E+05	2.22E+05	4.792E-03
46	2.22E+05	2.01E+05	4.242E-03
47	2.01E+05	1.82E+05	3.766E-03
48	1.82E+05	1.65E+05	3.325E-03
49	1.65E+05	1.49E+05	2.907E-03
50	1.49E+05	1.35E+05	2.552E-03
51	1.35E+05	1.22E+05	2.258E-03
52	1.22E+05	1.10E+05	1.988E-03
53	1.10E+05	9.98E+04	1.763E-03
54	9.98E+04	9.03E+04	1.559E-03

Table A.1. Spallation neutron spectrum and energy structure (*cont.*)

Group number	Energy boundary (eV)		Spallation spectrum
	Upper	Lower	
55	9.03E+04	8.17E+04	1.350E-03
56	8.17E+04	7.40E+04	1.196E-03
57	7.40E+04	6.69E+04	1.047E-03
58	6.69E+04	6.06E+04	9.147E-04
59	6.06E+04	5.48E+04	8.183E-04
60	5.48E+04	4.96E+04	7.100E-04
61	4.96E+04	4.49E+04	6.305E-04
62	4.49E+04	4.06E+04	5.552E-04
63	4.06E+04	3.67E+04	4.930E-04
64	3.67E+04	3.32E+04	4.274E-04
65	3.32E+04	3.01E+04	3.778E-04
66	3.01E+04	2.72E+04	3.384E-04
67	2.72E+04	2.46E+04	2.949E-04
68	2.46E+04	2.23E+04	2.648E-04
69	2.23E+04	2.02E+04	2.390E-04
70	2.02E+04	1.82E+04	2.059E-04
71	1.82E+04	1.65E+04	1.847E-04
72	1.65E+04	1.49E+04	1.675E-04
73	1.49E+04	1.35E+04	1.436E-04
74	1.35E+04	1.22E+04	1.295E-04
75	1.22E+04	1.11E+04	1.109E-04
76	1.11E+04	1.00E+04	1.035E-04
77	1.00E+04	9.06E+03	8.915E-05
78	9.06E+03	8.19E+03	7.758E-05
79	8.19E+03	7.41E+03	7.212E-05
80	7.41E+03	6.71E+03	6.270E-05
81	6.71E+03	6.07E+03	5.503E-05
82	6.07E+03	5.49E+03	4.799E-05
83	5.49E+03	4.97E+03	4.213E-05
84	4.97E+03	4.50E+03	3.787E-05
85	4.50E+03	4.07E+03	3.237E-05
86	4.07E+03	3.68E+03	2.959E-05
87	3.68E+03	3.33E+03	2.611E-05
88	3.33E+03	3.01E+03	2.192E-05
89	3.01E+03	2.73E+03	1.910E-05
90	2.73E+03	2.47E+03	1.635E-05
91	2.47E+03	2.23E+03	1.468E-05
92	2.23E+03	2.02E+03	1.280E-05
93	2.02E+03	1.83E+03	1.173E-05
94	1.83E+03	1.65E+03	1.002E-05
95	1.65E+03	1.50E+03	9.417E-06
96	1.50E+03	1.35E+03	7.641E-06
97	1.35E+03	1.23E+03	6.334E-06
98	1.23E+03	1.11E+03	5.563E-06
99	1.11E+03	1.00E+03	5.697E-06
100	1.00E+03	9.08E+02	0.00E+00
101	9.08E+02	8.22E+02	0.00E+00
102	8.22E+02	7.43E+02	0.00E+00
103	7.43E+02	6.73E+02	0.00E+00
104	6.73E+02	6.09E+02	0.00E+00
105	6.09E+02	5.51E+02	0.00E+00
106	5.51E+02	4.98E+02	0.00E+00
107	4.98E+02	4.51E+02	0.00E+00
108	4.51E+02	4.08E+02	0.00E+00
109	4.08E+02	3.69E+02	0.00E+00
110	3.69E+02	3.34E+02	0.00E+00
111	3.34E+02	3.02E+02	0.00E+00
112	3.02E+02	2.73E+02	0.00E+00
113	2.73E+02	2.47E+02	0.00E+00
114	2.47E+02	2.24E+02	0.00E+00
115	2.24E+02	2.03E+02	0.00E+00
116	2.03E+02	1.83E+02	0.00E+00
117	1.83E+02	1.66E+02	0.00E+00
118	1.66E+02	1.50E+02	0.00E+00
119	1.50E+02	1.36E+02	0.00E+00
120	1.36E+02	1.23E+02	0.00E+00
121	1.23E+02	1.11E+02	0.00E+00
122	1.11E+02	1.01E+02	0.00E+00

The spallation neutron source distribution is shown in Table A.2. The incident face of the proton beam is 150 cm.

Table A.2. Relative axial distribution of spallation neutron

Axial mesh boundary (cm)		Axial dependence (normalised to 1)
Higher z	Lower z	
150	140	0.33369
140	130	0.26611
130	120	0.17754
120	110	0.10825
110	100	0.06085
100	90	0.03193
90	80	0.01131
80	70	0.00571
70	60	0.00300
60	50	0.00161

Lower reflector (z < 50 cm): source assumed to be zero.
Radial dependence: flat for r < 10 cm, zero for r > 10 cm.

A collapsing program is given with a sample input. With this program, participants can prepare a broad group source from the given fine group source.

As for the input requirements for the program, two parameters are required as follows:

- Number of broad energy groups needed (NG).
- Broad energy group boundaries (NG + 1 values).

Program

```
C
      DIMENSION SPCF(200),ENGF(200)
      DIMENSION SPCB(200),ENGB(200)
C
C-------------------------------------------------------------------------------
------
C  Argument list
C    SPCF ------ Spallation Neutron Spectrum (Fine Group)
C    ENGF ------ Energy Boundaries (Fine Group)
C                             (max. 20MeV and 0.1 lethargy width)
C    NFMAX ----- Maximum Energy Group in which Spallation Neutron
C                Spectrum Value is not Zero.
C    SPCB ------ Spallation Neutron Spectrum (Broad Group)
C    ENGB ------ Energy Boundaries (Broad Group) (User Defined)
C    NG -------- Number of Broad Energy Group (User Defined)
C-------------------------------------------------------------------------------
------
C    Spallation Neutron Spectrum (Fine Group)
C-------------------------------------------------------------------------------
------
      DATA SPCF /
     1 9.077813E-03,1.012502E-02,1.135525E-02,1.274015E-02,1.438940E-02,
     2 1.612079E-02,1.800880E-02,2.002510E-02,2.207799E-02,2.417684E-02,
```

```
     3 2.622826E-02,2.831017E-02,3.011647E-02,3.171274E-02,3.330298E-02,
     4 3.449215E-02,3.539787E-02,3.594954E-02,3.622908E-02,3.612481E-02,
     5 3.573763E-02,3.502797E-02,3.408120E-02,3.295011E-02,3.156411E-02,
     6 3.003249E-02,2.839161E-02,2.668770E-02,2.487513E-02,2.310057E-02,
     7 2.137692E-02,1.961305E-02,1.792636E-02,1.632955E-02,1.482981E-02,
     8 1.341559E-02,1.209983E-02,1.085395E-02,9.723592E-03,8.681344E-03,
     9 7.736486E-03,6.903799E-03,6.128924E-03,5.405224E-03,4.792020E-03,
     A 4.241554E-03,3.766159E-03,3.324580E-03,2.906963E-03,2.551883E-03,
     B 2.257631E-03,1.987543E-03,1.762664E-03,1.558565E-03,1.349907E-03,
     C 1.195676E-03,1.047209E-03,9.147288E-04,8.182757E-04,7.100258E-04,
     D 6.304973E-04,5.552250E-04,4.930232E-04,4.273694E-04,3.777688E-04,
     E 3.383900E-04,2.948554E-04,2.647934E-04,2.389877E-04,2.059430E-04,
     F 1.846952E-04,1.675025E-04,1.436406E-04,1.294642E-04,1.109311E-04,
     1 1.034575E-04,8.914701E-05,7.758471E-05,7.212194E-05,6.270453E-05,
     2 5.502984E-05,4.799192E-05,4.212699E-05,3.787072E-05,3.237444E-05,
     3 2.959279E-05,2.610734E-05,2.191810E-05,1.910293E-05,1.635479E-05,
     4 1.467909E-05,1.280231E-05,1.172987E-05,1.002066E-05,9.417409E-06,
     5 7.641173E-06,6.334130E-06,5.563309E-06,5.697365E-06,101*0.0/
C
      PARAMETER ( NFMAX = 99 )
C
C-----------------------------------------------------------------------
C     User Defined Broad Energy Group Number
C-----------------------------------------------------------------------
      READ(5,*) NG
C-----------------------------------------------------------------------
C     User Defined Broad Energy Group Boundaries
C-----------------------------------------------------------------------
      READ(5,*) (ENGB(I),I=1,NG+1)
C
C-----------------------------------------------------------------------
C     Define Fine Energy Boudaries
C-----------------------------------------------------------------------
      ENGF(1) = 2.0E+7
      DO 100 I=2,200
         ENGF(I) = ENGF(I-1) / EXP(0.1)
  100 CONTINUE
C-----------------------------------------------------------------------
C     Initialization of Broad Spectrum Values
C-----------------------------------------------------------------------
      DO 101 I=1,NG
        SPCB(I) = 0.0
  101 CONTINUE
C
      NF = 1
      NB = 1
      SUMF = 0.0
C
C-------------------------------------------------------------------------------
-------
C     Procedure to Collapse Spectrum to User Defined Energy Structure
C        NF ----- Index of Fine Energy Group
C        NB ----- Index of Broad Energy Group
C-------------------------------------------------------------------------------
-------
C
      IF ( ENGF(NF) .LE. ENGB(NB) ) THEN
         NF = NF + 1
         GO TO 203
      END IF
C
  201 CONTINUE
      IF ( ENGF(NF) .GT. ENGB(NB) ) THEN
         NF = NF + 1
         GO TO 201
      END IF
C
  202 CONTINUE
```

```
C
      EU = ENGB(NB)
      EL = ENGF(NF)
      IF ( ENGF(NF-1).GT.EU) THEN
         FL1 = LOG(EU/EL)
         FL2 = LOG(ENGF(NF-1)/ENGF(NF))
         FL  = FL1 / FL2
         SPCB(NB) = SPCB(NB) + SPCF(NF-1) * FL
         NF = NF + 1
      END IF
C
C
C-------------------------------------------------------------------------------
--------------
C     Case in which Fine Energy Boudary Exists within Broad Energy Group
C-------------------------------------------------------------------------------
--------------
C
  203 CONTINUE
      IF ( ENGF(NF) .GT. ENGB(NB+1) ) THEN
         SPCB(NB) = SPCB(NB) + SPCF(NF-1)
         NF = NF + 1
         IF ( NF .GT. NFMAX ) THEN
            GO TO 300
         END IF
         EU = ENGF(NF - 1)
         EL = ENGF(NF)
         GO TO 203
C
C-----------------------------------------------------------------------
C     Move to Next Broad Energy Group
C-----------------------------------------------------------------------
C
      ELSE
         EU = ENGF(NF-1)
         EL = ENGB(NB+1)
         FL1 = LOG(EU/EL)
         FL2 = LOG(ENGF(NF-1)/ENGF(NF))
         FL  = FL1 / FL2
         SPCB(NB) = SPCB(NB) + SPCF(NF-1) * FL
      END IF
      NB = NB + 1
      IF ( NB .LE. NG ) GO TO 202
C
  300 CONTINUE
C
C-----------------------------------------------------------------------
C     Normalization of Broad Spectrum to Unity
C-----------------------------------------------------------------------
      SUMB = 0.0
      DO 301 I=1,NG
  301 SUMB = SUMB + SPCB(I)
      DO 302 I=1,NG
  302 SPCB(I) = SPCB(I) / SUMB
C
C-----------------------------------------------------------------------
C     User Defined Broad Energy Group Spectrum Edition
C-----------------------------------------------------------------------
      WRITE(6,'(6E12.5)') (SPCB(I),I=1,NG)
C
      STOP
      END
```

Sample input

```
73
 0.20000E+08 0.16490E+08 0.12840E+08 0.10000E+08 0.77880E+07 0.60653E+07
 0.47237E+07 0.36788E+07 0.28651E+07 0.22313E+07 0.17377E+07 0.13534E+07
 0.10540E+07 0.82085E+06 0.63928E+06 0.49787E+06 0.38774E+06 0.30197E+06
 0.23518E+06 0.18316E+06 0.14264E+06 0.11109E+06 0.86517E+05 0.67380E+05
 0.52475E+05 0.40868E+05 0.31828E+05 0.24788E+05 0.19305E+05 0.15034E+05
 0.11709E+05 0.91188E+04 0.71017E+04 0.55308E+04 0.43074E+04 0.33546E+04
 0.26126E+04 0.20347E+04 0.15846E+04 0.12341E+04 0.96112E+03 0.74852E+03
 0.58295E+03 0.45400E+03 0.35357E+03 0.27536E+03 0.21445E+03 0.16702E+03
 0.13007E+03 0.10130E+03 0.78893E+02 0.61442E+02 0.47851E+02 0.37266E+02
 0.29023E+02 0.22603E+02 0.17604E+02 0.13710E+02 0.10677E+02 0.83153E+01
 0.64760E+01 0.50435E+01 0.39279E+01 0.30590E+01 0.23824E+01 0.18554E+01
 0.14450E+01 0.11253E+01 0.87642E+00 0.68255E+00 0.53157E+00 0.41399E+00
 0.32242E+00 0.10000E-04
```

Appendix B

DETAILS TO BE PROVIDED ABOUT THE CALCULATIONAL SCHEME USED
(*Preferred format is WORD*)

1. Author(s) of the solution.

2. Establishment.

3. Name(s) of code system(s) used.

4. Bibliographic references for the codes used.

5. Origin of cross-section data (ENDF/B-VI, JEF-2.2, JENDL-3.2, etc., describe deviations from standard libraries, e.g. mix from different libraries).

6. Cell calculation and cross-section condensation (describe your scheme, provide details about assumptions made):

    a) Resonance shielding including unresolved resonance treatment and mutual shielding: specify method(s) and energy range depending on nuclides (actinides, clad, fission products, oxygen).

    b) Fission spectra: specify whether only a single spectrum was used or a weighted mix from all fissile nuclides, explain procedure.

    c) Describe how the (n,2n) reaction was treated.

    d) Weighting spectrum for scattering matrices, e.g. correction of the out-scatter and self-scatter terms, considering the differences between original weighting spectrum and realistic cell spectrum.

    e) Method used for spectrum calculation, treatment of leakage.

    f) Number of energy groups used in the different phases.

7. Method(s) used for reactor calculation (source calculation).

8. Burn-up calculation:

    a) Time steps between spectrum calculations.

    b) Actinide and fission product chains.

    c) Fission yields.

9. Method(s) used for decay calculation.

10. Other assumptions and characteristics, comments useful for interpreting correctly the results.

Appendix C

RESULTS TO BE REPORTED
(***Preferred format is EXCEL***)

A. Homogeneous cell calculations

1. One-group fission and capture microscopic cross-sections (barn)

	Start-up core		Equilibrium core	
	Fission	**Capture**	**Fission**	**Capture**
^{234}U				
^{235}U				
^{236}U				
^{237}Np				
^{238}Np				
^{238}Pu				
^{239}Pu				
^{240}Pu				
^{241}Pu				
^{242}Pu				
^{241}Am				
^{242m}Am				
^{243}Am				
^{242}Cm				
^{243}Cm				
^{244}Cm				
^{245}Cm				
^{246}Cm				
^{247}Cm				
^{248}Cm				

2. Infinite multiplication factor and buckling

	Start-up core	Equilibrium core
k_∞		
B^2 (cm^{-2})*		
M^2 (cm^2)		

** B^2: Critical buckling.*

B. Reactor calculations

1. Reaction rate balance components (production, absorption, leakage) for fuel zone at BOL (reactions/cm^3/sec)

	Start-up core at BOL			Equilibrium core at BOL		
	Production	**Absorption***	**Leakage**	**Production**	**Absorption***	**Leakage**
^{234}U						
^{235}U						
^{236}U						
^{237}Np						
^{238}Np						
^{238}Pu						
^{239}Pu						
^{240}Pu						
^{241}Pu						
^{242}Pu						
^{241}Am						
^{242m}Am						
^{243}Am						
^{242}Cm						
^{243}Cm						
^{244}Cm						
^{245}Cm						
^{246}Cm						
^{247}Cm						
^{248}Cm						

* *Absoprtion = Fission + Capture*

2. Neutron flux distribution (neutrons/cm^2/sec)

2.1. Radial distribution at z = 100 cm

Radial position (cm)	Start-up core	Equilibrium core
0.0		
5.0		
10.0		
15.0		
20.0		
25.0		
30.0		
35.0		
40.0		
45.0		
50.0		
55.0		
60.0		
65.0		
70.0		
75.0		
80.0		
85.0		
92.0		
100.0		
110.0		
120.0		
130.0		
142.0		

2.2. Axial distributions (r = 0 cm, 56 cm)

Axial position (cm)	Start-up core		Equilibrium core	
	r = 0 cm	r = 56 cm	r = 0 cm	r = 56 cm
0.0				
10.0				
20.0				
30.0				
40.0				
50.0				
60.0				
70.0				
80.0				
90.0				
100.0				
110.0				
120.0				
130.0				
140.0				
150.0				
160.0				
170.0				
180.0				
190.0				
200.0				

3. Neutron spectrum and reaction rate ratios relative to ^{239}Pu fission at r, z = 56 cm, 100 cm

*3.1. Neutron spectrum [group fluxes, Fi(u)]**

Lower energy boundary (MeV)	Start-up core	Equilibrium core
Emax = Your energy mesh for the reactor calculation (start with Emax)	–	–

** According to your energy group mesh, the size of the table can be modified.*

3.2. Reaction rate ratios relative to ^{239}Pu fission, F(^{239}Pu)

	Start-up core		Equilibrium core	
	Fission/F(^{239}Pu)	**Capture/F(^{239}Pu)**	**Fission/F(^{239}Pu)**	**Capture/F(^{239}Pu)**
^{234}U				
^{235}U				
^{236}U				
^{237}Np				
^{238}Np				
^{238}Pu				
^{239}Pu				
^{240}Pu				
^{241}Pu				
^{242}Pu				
^{241}Am				
^{242m}Am				
^{243}Am				
^{242}Cm				
^{243}Cm				
^{244}Cm				
^{245}Cm				
^{246}Cm				
^{247}Cm				
^{248}Cm				

4. Burn-up (GWd/tHM), k_{eff}, k_{∞} without fission products, and source strength (neutrons/s at the full power of 377 MWth) for 5 burn-up steps (5 × 365 d)

4.1. Start-up core

Parameters	**Start-up core**					
	0.0 (0 d)	**1st step (365 d)**	**2nd step (2 × 365 d)**	**3rd step (3 × 365 d)**	**4th step (4 × 365 d)**	**5th step (5 × 365 d)**
Burn-up (GWd/t)						
k_{eff}						
k_{∞} without FPs*						
Source strength (n/sec)						

** For k_{∞} without FPs, set FP concentrations to zero.*

4.2. Equilibrium core

Parameters	Equilibrium core					
	0.0 (0 d)	**1st step (365 d)**	**2nd step (2 × 365 d)**	**3rd step (3 × 365 d)**	**4th step (4 × 365 d)**	**5th step (5 × 365 d)**
Burn-up (GWd/t)						
k_{eff}						
k_{eff} without FPs*						
Source strength (n/sec)						

** For k_{eff} without FPs, set FP concentrations to zero.*

5. Fuel isotopic composition at EOL (atoms/barn cm)

Isotope	Start-up core at EOL (5 × 365 d)	Equilibrium core at EOL (5 × 365 d)
^{234}U		
^{235}U		
^{236}U		
^{237}Np		
^{238}Np		
^{238}Pu		
^{239}Pu		
^{240}Pu		
^{241}Pu		
^{242}Pu		
^{241}Am		
^{242m}Am		
^{243}Am		
^{242}Cm		
^{243}Cm		
^{244}Cm		
^{245}Cm		
^{246}Cm		
^{247}Cm		
^{248}Cm		

6.7.8. Safety parameters: Coolant void reactivity effect of fuel zone, fuel Doppler reactivity effect and β_{eff}

Parameters	Start-up core		Equilibrium core	
	BOL	EOL	BOL	EOL
Coolant void reactivity effect (pcm) k_{eff} (voided) – k_{eff} (ref) [k_{eff} (voided) – k_{eff} (ref)]/k_{eff} (ref)				
Fuel Doppler effect (pcm) [k_{eff} (980 K) – k_{eff} (1 580 K)]/[k_{eff} (980 K) × k_{eff} (1 580 K)]				
β_{eff} (pcm)		–		–

9. Activity, decay heat and neutron source strength of irradiated fuel at different cooling times

9.1. Start-up core

Parameters	Start-up core				
	0.0	2 years	5 years	10 years	100 years
Activity (Bq) – Activation products – Actinide and daughters – Fission products					
Decay heat (W)					
Neutron source (neutrons/sec) – (α,n) neutron production – Spontaneous fission neutron production					

9.2. Equilibrium core

Parameters	Equilibrium core				
	0.0	2 years	5 years	10 years	100 years
Activity (Bq) – Activation products – Actinide and daughters – Fission products					
Decay heat (W)					
Neutron source (neutrons/sec) – (α,n) neutron production – Spontaneous fission neutron production					

10. ^{210}Po activity of target at the end of irradiation (start-up core at EOL)

^{210}Po activity of target (Bq)	

APPENDIX B

Calculation details supplied by the participants

ANL

1. *Author(s) of the solution.*

   W.S. Yang and C.G. Stenberg

2. *Establishment.*

   Reactor Analysis Division, Argonne National Laboratory

3. *Name(s) of code system(s) used.*

   MC^2-2, TWODANT, REBUS-3

4. *Bibliographic references for the codes used.*

   H. Henryson II, B.J. Toppel and C.G. Stenberg, "MC^2-2: A Code to Calculate Fast Neutron Spectra and Multigroup Cross-sections", ANL-8144, Argonne National Laboratory (1976).

   R.E. Alcouffe, F.W. Brinkley, D.R. Marr and R.D. O'Dell, "User's Guide for TWODANT: A Code Package for Two-dimensional, Diffusion-accelerated, Neutral-particle Transport", LA-10049-M, Los Alamos National Laboratory (1990).

   B.J. Toppel, "A User's Guide to the REBUS-3 Fuel Cycle Analysis Capability", ANL-83-2, Argonne National Laboratory Report (1983).

   R.P. Hosteny, "The ARC System Fuel Cycle Analysis Capability, REBUS-2", ANL-7721, Argonne National Laboratory Report (1978).

5. *Origin of cross-section data (ENDF/B-VI, JEF-2.2, JENDL-3.2, etc., describe deviations from standard libraries, e.g. mix from different libraries).*

   ENDF/B-VI data was used for all isotopes except for lumped fission products. The cross-sections of lumped fission products were generated from ENDF/B-V data for 180 individual fission product isotopes.

6. *Cell calculation and cross-section condensation (describe your scheme, provide details about assumptions made):*

   a) *Resonance shielding including unresolved resonance treatment and mutual shielding: specify method(s) and energy range depending on nuclides (actinides, clad, fission products, oxygen).*

      The resolved resonance integral calculation assumes the narrow resonance approximation, allows for Doppler broadening, and accounts for interference scattering and the effects of overlap with neighbouring resolved resonances (~20). Resonance "screening" procedure determines which resonances are pre-processed and placed into the "smooth" data and which resonances should be modelled by their resonance parameters. ETOE-2, which prepares the MC^2-2 library, pre-processed the wide resonances (which are temperature independent and represented by the ultra-fine-group (i.e. 2 082 groups) MC^2-2 structure) and extremely weak resonances (which do not contribute significantly to the self-shielding or Doppler effects). Self-shielding effects of the remaining resonances are explicitly evaluated in the MC^2-2 calculation.

The unresolved resonance integral calculation assumes a narrow resonance approximation and accounts for interference scattering, the effects of overlap with resonances in other spin sequences, and the effects of self-overlap with resonances of the same spin sequences.

The resolved and unresolved energy range used is specified by the ENDF data and is unique for each nuclide.

b) Fission spectra: specify whether only a single spectrum was used or a weighted mix from all fissile nuclides, explain procedure.

A weighted fission spectrum from all fissionable nuclides was used. In the group condensation, a set-wide fission spectrum vector was obtained by weighting the ultra-fine-group isotopic fission spectra with the fission sources of individual isotopes.

c) Describe how the (n,2n) reaction was treated.

The (n,2n) reaction was treated as a source term in the ultra-fine-group spectrum calculation. For the secondary energy distribution, tabulated function, evaporation spectrum and discrete levels were used. The discrete ultra-fine-group (n,2n) scattering source was approximately treated by neglecting the energy-angle correlation.

d) Weighting spectrum for scattering matrices, e.g. correction of the out-scatter and self-scatter terms, considering the differences between original weighting spectrum and realistic cell spectrum.

The contributions from the ultra-fine-group library and the unresolved resonances were obtained from the ultra-fine-group flux weighting. The contributions from the resolved resonances were determined using the resonance reaction rate and the probability of scattering a neutron by a resonance into a group. The resonance reaction rate is calculated directly from the resonance integrals, which take account of overlap, self-shielding and Doppler broadening effects.

e) Method used for spectrum calculation, treatment of leakage.

For individual materials of given nuclide densities and temperatures, homogeneous ultra-fine-group flux calculations were performed. The consistent P1 method was used with group-independent buckling search for the fundamental mode spectrum calculations performed with 2 082 groups. In these calculations, ^{204}Pb was added to ^{206}Pb since ^{204}Pb data is not available on ENDF/B-VI data.

f) Number of energy groups used in the different phases.

From the homogeneous ultra-fine-group MC^2-2 calculations (2 082 energy groups), 230-group cross-sections were determined for individual materials of given nuclide densities and temperatures. Using these 230-group material-dependent cross-sections, region-dependent 33-group isotopic cross-sections were generated from the 230-group full-core TWODANT calculations. In this 33-group cross-section generation, the fuel was divided into three radial regions and the reflector was divided into top, bottom and radial reflectors. The target was treated as a single region. On the other hand, the 33-group cross-sections of lumped fission products were directly obtained from MC^2-2 calculations for the homogenised atom densities of the equilibrium core.

7. *Method(s) used for reactor calculation (source calculation).*

The flux distributions were computed by solving fixed source problems using the TWODANT transport theory code. An R-Z computational model was employed in these calculations with ~2.5 cm mesh size and vacuum boundary condition. Except for the reactivity effect calculations, the 33-group cross-sections collapsed with the 230-group flux obtained from the full-core TWODANT calculation for the equilibrium core fuel composition was employed. Specifically, this cross-section set was used for all flux and reaction rate calculations at BOL and burn-up calculations. For the reactivity effect evaluations for the start-up core, the 33-group cross-sections were generated by separate TWODANT calculations using the start-up core fuel composition.

8. *Burn-up calculation:*

a) Time steps between spectrum calculations.

Each burn-up interval was one year. However, the fuel zone was divided into 20 burn regions and the region density iteration was performed with a relative convergence criterion of 0.001. That is, the depletion calculation for each region was performed with the average of the beginning and end of time interval fluxes. The end of time interval flux was iteratively computed by iteration on the final nuclide densities. Four region density iterations were typically performed for each burn step to satisfy this convergence criterion.

b) Actinide and fission product chains.

The depletion calculations were performed using burn-up changes for nuclides ranging from ^{232}U to ^{248}Cm. Five lumped fission products were used to represent the fission products. Using the MC^2-2 calculation performed for the equilibrium core fuel composition, 33-group cross-sections were generated for 180 fission products. By weighting these cross-sections with fission yields of ^{235}U, ^{238}U, ^{239}Pu, ^{240}Pu and ^{241}Pu, respectively, 33-group cross-sections of five lumped fission products were generated. These five lumped fission products were named FP35, FP38, FP39, FP40 and FP41, respectively. A dummy isotope was also used to represent the other end products not included in the chains.

Capture, (n,2n), and fission reactions were considered for all actinide isotopes included in the problem specification. In the capture and (n,2n) reactions, short-lived intermediate products were neglected. As a result, the products of capture reactions of ^{238}U, ^{238}Np, ^{242}Pu and ^{243}Am were represented by ^{239}Pu, ^{239}Pu, ^{243}Am and ^{244}Cm, respectively. The capture reaction of ^{241}Am was modelled to yield ^{242}Cm, ^{242m}Am and ^{242}Pu with yield fractions of 0.66, 0.20 and 0.14, respectively. The products of (n,2n) reactions of ^{238}Pu and ^{241}Am were respectively represented by ^{237}N and ^{240}Pu. The (n,2n) reaction of ^{243}Am was assumed to yield ^{2442m}Am, ^{242}Pu and ^{242}Cm with yield fractions of 0.5, 0.086 and 0.414, respectively. ^{242}Cm was assumed to yield ^{241}Am in 99% of its (n,2n) reactions and ^{237}Np in 1%. It was assumed that 37.4% of (n,2n) reactions of ^{237}Np yield ^{236}U and the remaining 62.6% yield a fictitious dummy isotope. The end products of ^{248}Cm capture and ^{232}U (n,2n) reactions were represented by a fictitious dummy isotope.

Important α and β decays of actinide isotopes were also considered. Specifically, α decay was considered for all actinide isotopes except for ^{238}Np and ^{241}Pu. The β^- decays of ^{238}Np, ^{241}Pu, ^{242m}Am and the β^+ decay of ^{242m}Am were also included in the burn chains. The employed decay constants for the β^-, β^+, and α decays of ^{242m}Am were 1.189E-10, 2.487E-11 and 7.225E-13, respectively.

c) Fission yields.

For full reactor depletion calculations, the lumped fission product FP35 was used to represent the fission products of ^{232}U, ^{233}U, ^{234}U, ^{235}U and ^{236}U, while the fission products of ^{237}U, ^{238}U, ^{237}Np, ^{238}Np and ^{238}Pu were represented by FP38. The lumped fission products FP39 and FP40 were respectively used to represent the fission products of ^{239}Pu and ^{240}Pu. The fission products of ^{241}Pu and higher actinides were represented by FP41.

Even though it has not been completed, the decay heat calculation employs much different fission yields. In decay heat calculations performed with the ORIGEN code, much more detailed fission yields are used with the conserved actinide reaction rates of the full core depletion calculation.

9. Method(s) used for decay calculation.

10. *Other assumptions and characteristics, comments useful for interpreting correctly the results.*

The burn-up calculations were performed at the constant power of 377 MW_{th} by adjusting the source intensity.

The reaction rates and flux distributions in Section B were obtained from fixed source calculations. However, the k_{eff} values and reactivity coefficients were calculated using the corresponding homogeneous eigenvalue problems.

CIEMAT

1. *Author(s) of the solution.*

M. Embid, J.M. García-Sanz, E. González, D. Cano-Ott and D. Villamarín
Contact e-mails: jgarcias@ciemat.es, enriques@ciemat.es

2. *Establishment.*

CIEMAT, Nuclear Fission Department, FACET Group
Avda. Complutense, 22
28040 Madrid, Spain

3. *Name(s) of code system(s) used.*

EVOLCODE

4. *Bibliographic references for the codes used.*

[1] E. González, D. Cano, M. Embid, R. Fernández, J. García-Sanz and D. Villamarín, "EVOLCODE: ADS Combined Neutronics and Isotopic Evolution Simulation System", Presented at MC'99 Conference, Madrid, September 1999.

[2] R.E. MacFarlane and D.W. Muir, "The NJOY Nuclear Data Processing System, Version 91" (1994).

[3] "MCNP – A General Monte Carlo N-particle Transport Code, Version 4B" J.F. Briesmeister, ed., LA-12625 M (1997).

[4] M.J. Bell, "ORIGEN – The ORNL Isotope Generation and Depletion Code V", ORNL-4628 (1973).

5. *Origin of cross-section data (ENDF/B-VI, JEF-2.2, JENDL-3.2, etc., describe deviations from standard libraries, e.g. mix from different libraries).*

The cross-section database used in this benchmark for neutron transport calculations and reaction rates calculation is the JENDL-3.2. In total, 245 isotopes have been used at different temperatures (650 K, 980 K, 1 580 K) representing not less than 99% of the total mass inventory at any time. From those 196 are fission fragments. In addition, the EAF3.1 database (about 650 isotopes) has been used for depletion calculations whenever the isotopes considered are not available in the transport library. For this purpose, the EAF3.1 library has been converted to ENDF format.

6. *Cell calculation and cross-section condensation (describe your scheme, provide details about assumptions made):*

The method used is a complete 3-D neutron Monte Carlo simulation with continuous energy cross-sections.

a) *Resonance shielding including unresolved resonance treatment and mutual shielding: specify method(s) and energy range depending on nuclides (actinides, clad, fission products, oxygen).*

Not required for our continuous energy Monte Carlo simulation.

b) *Fission spectra: specify whether only a single spectrum was used or a weighted mix from all fissile nuclides, explain procedure.*

Specific fission used for each fissile isotope according to the JENDL-3.2 database.

c) *Describe how the (n,2n) reaction was treated.*

Continuous energy (n,2n) reaction simulation according to the JENDL-3.2 database.

d) *Weighting spectrum for scattering matrices, e.g. correction of the out-scatter and self-scatter terms, considering the differences between original weighting spectrum and realistic cell spectrum.*

No weighting applied.

e) *Method used for spectrum calculation, treatment of leakage.*

For burn-up calculations, 8 000 bins have been used in the neutron flux energy spectra.

f) *Number of energy groups used in the different phases.*

Continuous energy is used in the transport phases. For burn-up calculations one-group cross-sections are used. They are obtained by weighting each reaction cross-section with the neutron flux energy spectrum (8 000 energy bins) in each cell and each time step (see #7).

7. *Method(s) used for reactor calculation (source calculation).*

See #8.

8. *Burn-up calculation:*

The simulations have been made using the EVOLCODE [1] simulation procedure developed at CIEMAT. The system is a combination of various codes able to perform a coupled neutronic and isotopic time evolution calculation. A scheme of the EVOLCODE system is presented in Figure 1. EVOLCODE combines the following codes:

- NJOY94.61 for nuclear data processing [2]. The cross-section database used in this benchmark for neutron transport calculations and reaction rates calculation is JENDL-3.2. In total, 245 isotopes have been used at different temperatures (650 K, 980 K, 1 580 K) representing not less than 99% of the total mass inventory at any time. From those 196 are fission fragments. In addition, the EAF3.1 database (about 650 isotopes) has been used for depletion calculations whenever the isotopes considered are not available in the transport library. For this purpose, the EAF3.1 library has been converted to ENDF format.

- MCNP4B [3] for the complete 3-D neutron transport simulation. It calculates the neutron multiplication, the energy release by fission, the neutron flux intensity and specific power spatial distributions and the neutron flux energy spectra at different positions.

- ORIGEN2.1 [4], with *ad hoc* cross-sections libraries, for burn-up calculations.

Figure 1. Combined neutronic and isotopic combined time evolution calculation scheme

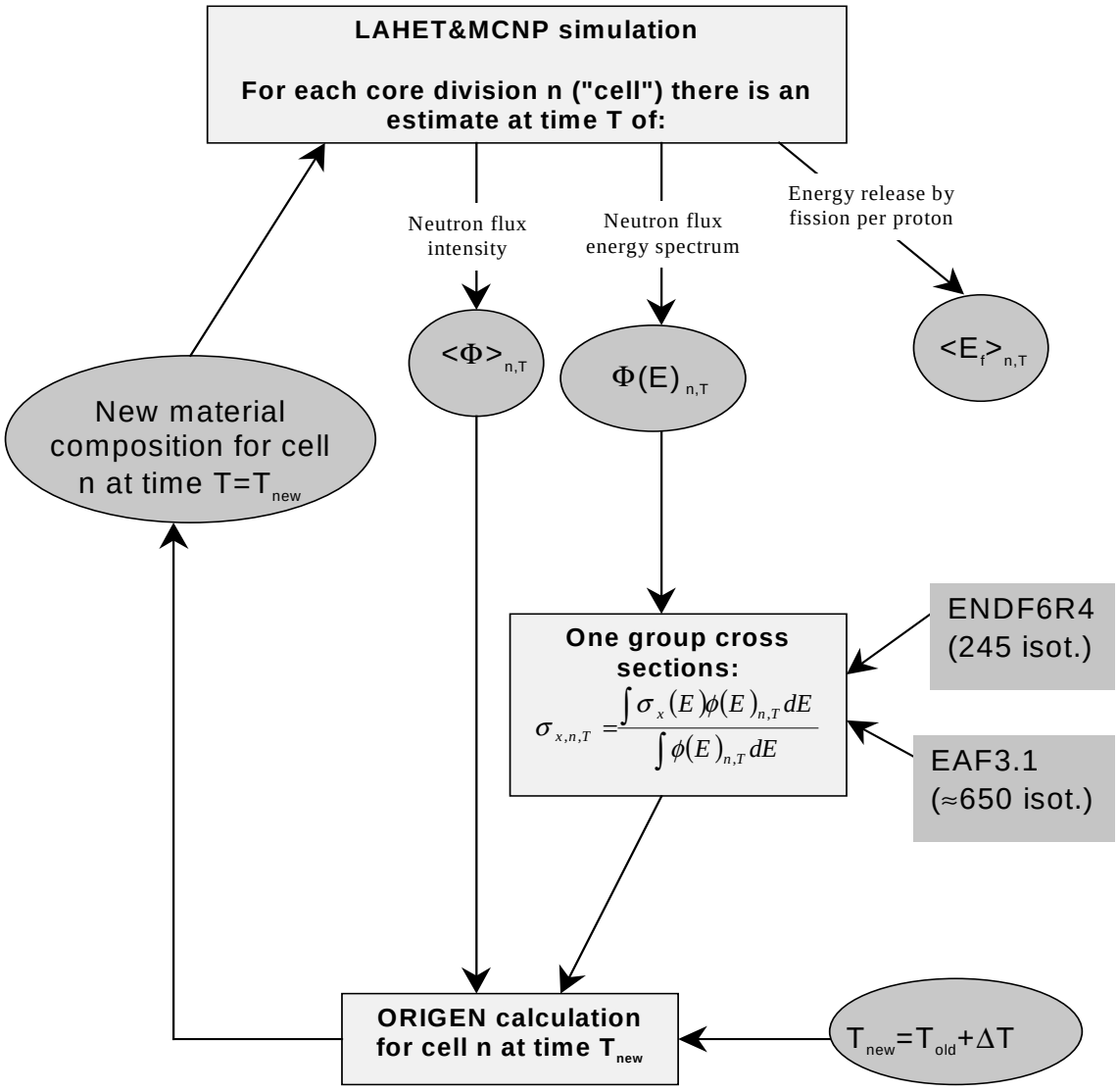

EVOLCODE couples these codes as follows:

- The core has been divided into 90 cells mesh as shown in Figure 2. Each core division will have its own neutron flux estimate, energy release by fission and neutron flux energy spectrum estimators. The target is also divided in 10 cells.

- A MCNP4B complete simulation of the neutron transport in steady state is done using the provided external source, in the BOL configuration of the system.

- The following phase is a set of ORIGEN2.1 burn-up calculations, one for each core division. For this purpose, one-group cross-sections are obtained for each core zone integrating the depletion reaction cross-sections weighted by the neutron flux energy spectra, obtained in the MCNP4B phase. The ORIGEN2.1 calculations use these *ad hoc* one-group cross-sections and the neutron flux intensity corresponding to each cell, normalised to the required total power.

Figure 2. Geometrical description of the ADMAB used for the simulation

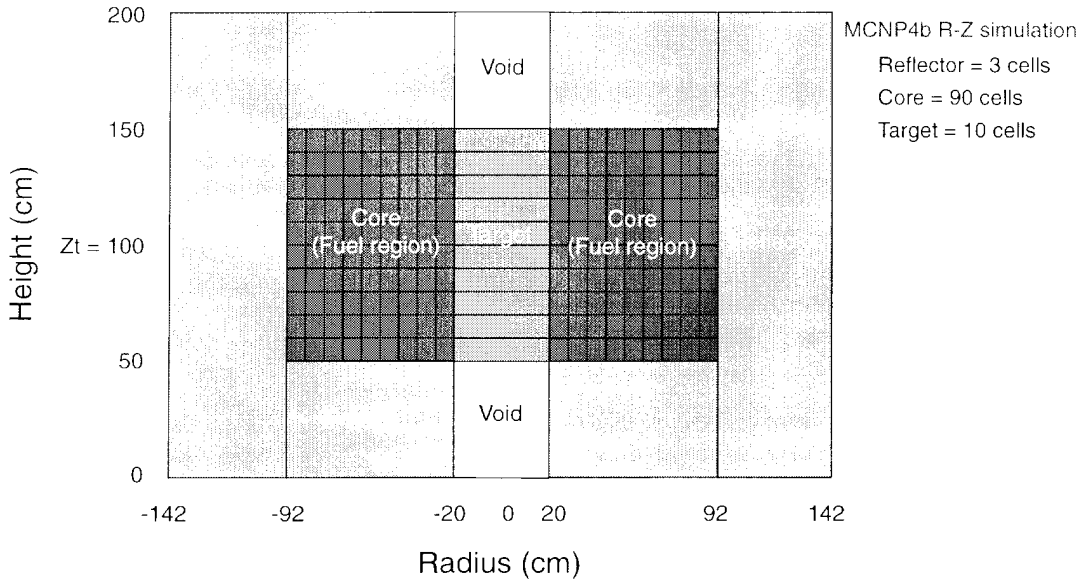

- When all ORIGEN2.1 calculations are finished, the resulting material descriptions are translated from the ORIGEN2.1 format to MCNP4B format, preparing a new MCNP input data file.
- A new time step is performed beginning a new neutron MCNP4B transport simulation.
- This procedure is repeated for each time step.

In burn-up calculations:

a) Time steps between spectrum calculations.

365 days.

b) Actinide and fission product chains.

ORIGEN2.1.

c) Fission yields.

From ENDFB VI R.3 database.

9. *Method(s) used for decay calculation.*

ORIGEN2.1

10. *Other assumptions and characteristics, comments useful for interpreting correctly the results.*

Note: Because of shortage of time to verify quality of data after the last source redefinition not all the requested results are included in the attached Excel file. The remainder will be provided as soon as possible.

KAERI

1. *Author(s) of the solution.*

   Won Seok Park and Yong Nam Kim

2. *Establishment.*

   Korea Atomic Energy Research Institute (KAERI)

3. *Name(s) of code system(s) used.*

   TRANSX 2.15, TWODANT 3.0, DIF3D 7.0, REBUS-3

4. *Bibliographic references for the codes used.*

   R.E. MacFarlane, "TRANSX-2: A Code for Interfacing MATSX Cross-section Libraries to Nuclear Transport Codes", Los Alamos National Laboratory Report LA-12312-MS (1993).

   R. E. Alcouffe, "User's Guide for TWODANT: A Code Package for Two-dimensional, Diffusion-accelerated, Neutron Transport", Los Alamos National Laboratory Report LA-10049-M, LANL (1990).

   K.L. Derstine, "DIF3D: A Code to Solve One-, Two- and Three-dimensional Finite Difference Diffusion Theory Problems", Argonne National Laboratory Report ANL-82-64 (1984).

   K.L. Derstine, "The DIF3D Nodal Neutronics Option for Two- and Three-dimensional Diffusion Theory Calculations in Hexagonal Geometry", Argonne National Laboratory Report ANL-83-1 (1983).

   B.J. Toppel, "A User's Guide for the REBUS-3 Fuel Cycle Analysis Capability", Argonne National Laboratory Report ANL-83-2 (1983).

5. *Origin of cross-section data (ENDF/B-VI, JEF-2.2, JENDL-3.2, etc., describe deviations from standard libraries, e.g. mix from different libraries).*

   Most from JEF-2.2, two for Pb_{nat} and ^{242m}Am from JENDLE-3.2.

6. *Cell calculation and cross-section condensation (describe your scheme, provide details about assumptions made):*

   We have used the cross-section library KAFAX-F22. It was developed not by us but by the team of The Nuclear Data Evaluation Laboratory of KAERI for the burn-up calculation of the Korea Advanced LIquid MEtal Reactor (KALIMER) in 1997. Therefore we have no idea of preparation for cross-section library and cannot give any detailed description of the below items from a) to e), related with treatment of cross-section data, just now. We apologise for this unfaithfulness. We will give a description after obtaining the information, as soon as possible.

   a) *Resonance shielding including unresolved resonance treatment and mutual shielding: specify method(s) and energy range depending on nuclides (actinides, clad, fission products, oxygen).*

b) Fission spectra: specify whether only a single spectrum was used or a weighted mix from all fissile nuclides, explain procedure.

The weighted mix from all fissile nuclide.

c) Describe how the (n,2n) reaction was treated.

Capture cross-section is estimated as the corrected value with subtraction of the cross-section of (n,2n) reaction.

d) Weighting spectrum for scattering matrices, e.g. correction of the out-scatter and self-scatter terms, considering the differences between original weighting spectrum and realistic cell spectrum.

e) Method used for spectrum calculation, treatment of leakage.

f) Number of energy groups used in the different phases.

i) *Stage 1*. Preparation for cross-section library KAFAX-F22 with MATXS format → 80 group.

ii) *Stage 2*. Production of ISOTXS formatted cross-section data using TRANSX as an input data required to solve the neutron transport equation for generation of region-wised group flux and to collapse the fine group data to broad group → 80 group.

iii) *Stage 3*. Cell calculation and generation of region-wised group flux using TWODANT → 80 group.

iv) *Stage 4*. Group collapsing to broad group and production of ISOTXS formatted cross-section data using TRANSX as a lattice parameter required for DIF3D to solve the neutron diffusion equation → 9 group.

v) *Stage 5*. Reactor calculation of steady-state and burn-up parameter using DIF3D/REBUS3 → 9 group.

7. Method(s) used for reactor calculation (source calculation).

Nodal method applied to the neutron diffusion theory.

8. Burn-up calculation:

a) Time steps between spectrum calculations.

One year.

b) Actinide and fission product chains.

^{233}U: (n,r)^{234}U, (n,f)LFPP3 (pseudo(lumped)-fission product from ^{233}U)

^{234}U: (n,r)^{235}U, (n,f)LFPP3

^{235}U: (n,r)^{236}U, (n,f)LFPP5(pseudo(lumped)-fission product from ^{233}U)

^{236}U: (n,r)^{237}Np, (n,f)LFPP3

^{238}U: (n,r)^{239}U, (n,f) LFPP9(pseudo(lumped)-fission product from ^{239}Pu), (n,2n)^{237}Np

^{238}Pu: (n,r)^{239}Pu, (n,f)LFPP9, (alpha-decay)^{234}U

^{237}Np: (n,r)^{238}Pu, (n,f)LFPP9, (n,2n)^{236}U

^{239}Pu: (n,r)^{240}Pu, (n,f)LFPP3, (n,2n)^{238}Pu

^{240}Pu: (n,r)^{241}Pu, (n,f)LFPP9

^{241}Pu: (n,r)^{242}Pu, (n,f)LFPP9

^{242}Pu: (n,r)^{243}Am, (n,f)LFPP9

^{241}Am: (n,r)^{242}Am (20%), ^{242}Cm (66%), ^{242}Pu (14%), (n,f)LFPP9

^{243}Am: (n,r)^{244}Cm, (n,f)LFPP9

^{242}Cm: (n,r)^{243}Cm, (n,f)LFPP9, (alpha-decay)^{238}Pu

^{243}Cm: (n,r)^{244}Cm, (n,f)LFPP9, (alpha-decay)^{239}Pu

^{244}Cm: (n,r)^{245}Cm, (n,f)LFPP9, (alpha-decay)^{240}Pu

^{245}Cm: (n,r)^{246}Cm, (n,f)LFPP9

^{246}Cm: (n,f)LFPP9

c) Fission yields.

As arranged above, we have considered the burn-up chain of the actinide alone, excluding the fission-product chain. In the cross-section library KAFAX-F22 used in this calculation, the cross-section data of fission products is lumped to the pseudo-fission product. This consideration is based on the inference that the nuclides of fission product are not active to the fast neutron spectrum.

9. Method(s) used for decay calculation.

10. Other assumptions and characteristics, comments useful for interpreting correctly the results.

i) We have replaced ^{14}N for ^{15}N, which is not included in KAFAX-F22.

ii) We have excluded ^{237}U, ^{238}Np, ^{247}Cm and ^{248}Cm because the cross-section data is not included in KAFAX-F22. We note that the atomic density of those nuclides in the core is very low compared with the others.

PSI/CEA

1. *Author(s) of the solution.*

   Marco Cometto[1], Peter Wydler[2] and Jean-Christophe Bosq[3]
   [1]CEA on attachment at PSI, [2]PSI, [3]CEA

2. *Establishment.*

   CEA Cadarache/Paul Scherrer Institut

3. *Name(s) of the code system(s) used.*

   ERALIB1/ECCO/ERANOS nuclear data and calculation code system for the cell and reactor calculations.

   ORIHET3 for the activity and decay calculations.

4. *Bibliographic references for the codes used.*

   E. Fort, W. Assal, G. Rimpault, J. Rowlands, P. Smith, R. Soule, "Realisation and Performance of the Adjusted Nuclear Data Library ERALIB1 for Calculating Fast Reactor Neutronics", Proc. Int. Conf. on the Physics of Reactors (PHYSOR'96), Mito, Japan, 16-20 September 1996.

   G. Rimpault, P. Ribon, M. Grimstone, C. Dean, B. Thom, "Validation of New Subgroup Algorithms for Resonance Self-shielding in Heterogeneous Structures", Proc. Topl. Mtg. Advances in Nuclear Engineering Computation and Radiation Shielding, Santa Fe, New Mexico, 9-13 April 1989, American Nuclear Society (1989).

   M.J. Grimstone, J. Tullet, J. Rowlands, B. Thom, G. Rimpault, M. Salvatores, "The Geometrical Treatment in the New European Cell Code ECCO", Proc. Topl. Mtg. Advances in Nuclear Engineering Computation and Radiation Shielding, Santa Fe, New Mexico, 9-13 April 1989, American Nuclear Society (1989).

   G. Rimpault, "Algorithmic Features of the ECCO Cell Code for Treating Heterogeneous Fast Reactor Subassemblies", Proc. Int. Conf. on Mathematics and Computations, Reactors Physics and Environmental Analyses, Portland, Oregon, March-April 1995.

   J.Y. Doriath, C.W. McCallien, E. Kiefhaber, U Wehman, J.Y. Rieunier, "ERANOS1: The Advanced European System of Codes for Reactor Physics Calculation", Proc. Int. Conf. on Mathematical Methods and Supercomputing in Nuclear Applications, Karlsruhe, Germany, 19-23 April 1993.

   G. Palmiotti, J.M. Rieunier, C. Gho, M. Salvatores, "Optimised Two-dimensional Sn Transport (BISTRO)", *Nucl. Sci. Eng.*, 104, 26-33 (1990).

5. *Origin of cross-section data (ENDF/B-VI, JEF-2.2, JENDL-3.2, etc., describe deviations from standard libraries, e.g. mix from different libraries).*

   ERALIB1 multi-group library based on the JEF2.2 evaluated file and processed by the NJOY and CALENDF code systems. In this library, 17 important isotopes for fast neutronic calculations were adjusted, using a statistical process and about 350 integral parameters.

6. *Cell calculation and cross-section condensation (describe your scheme, provide details about assumptions made):*

Homogeneous cell ECCO calculation scheme:

- *First step*. One hundred seventy-two (172) energy groups (estimation of critical B^2)
- *Second step*. One thousand nine hundred sixty-eight (1 968) fine energy groups, using the previously calculated B^2 (spectrum calculation and condensation into 33 energy groups)
- *Third step*. Thirty-three (33) energy groups (critical B^2 calculation and evaluation of the microscopic cross-sections)

a) Resonance shielding including unresolved resonance treatment and mutual shielding: specify method(s) and energy range depending on nuclides (actinides, clad, fission products, oxygen).

The self-shielding effects are treated in ECCO by the subgroup method, using statistical probability tables. ECCO prepares the self-shielded cross-sections and transport matrices combining a precise slowing down treatment in 1 968 energy groups with probability tables in each fine group.

b) Fission spectra: specify whether only a single spectrum was used or a weighted mix from all fissile nuclides, explain procedure.

The fission spectrum is obtained by weighting the fission spectra of all the isotopes by the fission reaction rate.

c) Describe how the (n,2n) reaction was treated.

The (n,2n) reaction is explicitly treated: one neutron disappears and two neutrons appear.

d) Weighting spectrum for scattering matrices, e.g. correction of the out-scatter and self-scatter terms, considering the differences between original weighting spectrum and realistic cell spectrum.

Scattering matrices are condensed using flux weighting and P1 scattering matrices using current weighting.

e) Method used for spectrum calculation, treatment of leakage.

Fundamental mode calculation (spatial variation of the flux assumed to take the form of a buckling mode).

f) Number of energy groups used in the different phases.

Flux calculation performed using a 1 968 fine energy groups scheme, and condensation of cross-sections into 33 energy groups.

7. *Method(s) used for reactor calculation (source calculation).*

Reactor calculations are performed using a two-dimensional (RZ), S_N transport code (BISTRO). The approximation is S4. In order to accelerate the convergence of the transport calculation, inner iterations are accelerated by the DBA diffusion scheme.

8. Burn-up calculation:

a) Time steps between spectrum calculations.

The flux is recalculated every 91.5 days, e.g. 4 times per year. During burn-up the power is kept constant at 320 MW.

b) Actinide and fission product chains.

The decay chain (see table below) includes the following 27 heavy isotopes:

^{232}Th, ^{231}Pa, ^{232}Pa,
^{232}U, ^{233}U, ^{234}U, ^{235}U, ^{236}U, ^{238}U,
^{237}Np, ^{239}Np,
^{238}Pu, ^{239}Pu, ^{240}Pu, ^{241}Pu, ^{242}Pu,
^{241}Am, ^{242m}Am, ^{242}Am, ^{243}Am,
^{242}Cm, ^{243}Cm, ^{244}Cm, ^{245}Cm, ^{246}Cm, ^{247}Cm, ^{248}Cm

Due to their short half-life, some isotopes are not taken into account and their daughters are considered instead: ^{231}U (^{231}Pa), ^{237}U (^{237}Np), ^{239}U (^{239}Np), ^{238}Np (^{238}Pu), ^{240}Np (^{240}Pu), ^{237}Pu (^{237}Np), ^{243}Pu (^{243}Am), ^{244}Am (^{244}Cm), ^{241}Cm (^{241}Am).

Additional data about branching ratios:

1) ^{241}Am + n $\rightarrow$ ^{242m}Am (15%) + ^{242}Am (85%)

2) Decay of ^{242}Am: ^{242}Cm (84%) + ^{242}Pu (16%)

The fission products are replaced by six pseudo fission products corresponding to the following six isotopes (^{235}U, ^{238}U, ^{239}Pu, ^{240}Pu, ^{241}Pu, ^{242}Pu); the following table shows which pseudo fission product is used for each nuclide.

FP ^{235}U: ^{232}Th, ^{231}Pa, ^{232}Pa, ^{232}U, ^{233}U, ^{234}U, ^{235}U, ^{236}U
FP ^{238}U: ^{238}U, ^{237}Np, ^{238}Pu
FP ^{239}Pu: ^{239}Np, ^{239}Pu
FP ^{240}Pu: ^{240}Pu
FP ^{241}Pu: ^{241}Pu, ^{241}Am
FP ^{242}Pu: ^{242}Pu, ^{242m}Am, ^{242}Am, ^{243}Am, ^{242}Cm, ^{243}Cm, ^{244}Cm, ^{245}Cm, ^{246}Cm, ^{247}Cm, ^{248}Cm

c) Fission yields.

The pseudo fission products are based on the JEF-2.2 fission yields. Each pseudo fission product takes into account all the solid fission products: all the gaseous fission products are supposed to migrate immediately to the plenum.

9. Method(s) used for decay calculation.

The code used for decay calculation is ORIHET3, an adaptation of the code ORIGEN. The decay data library is NUBASEX, based on NUBASE data.

As was mentioned earlier, only the heavy isotopes evolove during burn-up, therefore only the concentration of the actinides is known at EOL. However it is possible to estimate the concentration of the activation products in the following way: from the core calculation we can

obtain the averaged flux on the fuel (ϕ), the microscopic cross-sections for each nuclide $\left(\sigma_X^I\right)$ and the number of atoms of each isotope (N_I).

We can calculate the production rate of each isotope *I*, *PR*(*I*) expressed in atoms/sec:

$$PR(I) = \sigma_{n2n}^{I+1} \cdot N^{I+1} \cdot \overline{\phi} + \sigma_{n\gamma}^{I-1} \cdot N^{I-1} \cdot \overline{\phi}$$

Now the concentration of the activation products can be estimated at any time during the burn-up (the production rate takes in account the isotopes produced by neutronic reactions and the decay process) and during the cooling time (production rate set to 0 after 5 years). The use of pseudo fission products does not allow the calculation of the activity.

Consequently the term of decay heat takes in account only the contribution of actinides and activation products.

ORIHET3 does not directly calculate the source of neutron produced by spontaneous fission or by an (α,n) reaction.

The estimation of the neutrons produced by spontaneous fission is made in two steps: knowing the activity of each isotope we can estimate the number of spontaneous fission/sec (*) and multiply it by the averaged number of neutrons per spontaneous fission (**).

References for the nuclear data:

(*) G. Audi, O. Bersillon, J. Blachot and A.W. Wapstra, "The NUBASE Evaluation of Nuclear and Decay Properties", *Nuclear Physics* A, 29 September 1997.

(**) S.F. Mughabghab and D.I. Garber, "Neutron Cross-sections, Vol. I, Resonance Parameters", June 1973.

10. Other assumptions and characteristics, comments useful for interpreting correctly the results.

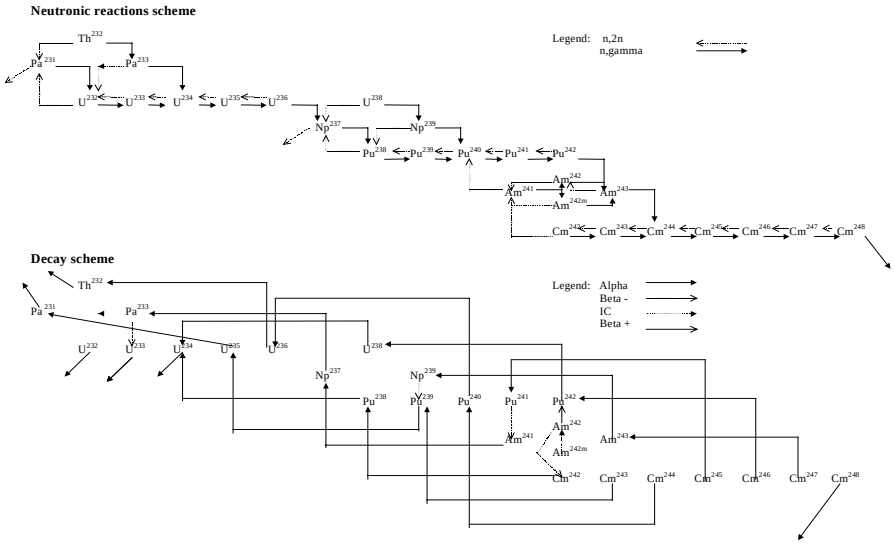

JAERI

1. *Author(s) of the solution.*

   Kenji Nishihara, Kazufumi Tsujimoto and Hideki Takano

2. *Establishment.*

   Japan Atomic Energy Research Institute

3. *Name(s) of the code system(s) used.*

   - Transmutation calculation: ATRAS Code System [1] , which consists of the following components:
     - Preparation of effective cross-sections: SCALE-4.3 [2].
     - Calculation of steady-state neutronics: TWODANT [3].
     - Calculation of burn-up and decay: BURNER [4].
     - Calculation of decay: ORIGEN-2 [5].
   - Calculation of β_{eff}: SRAC95 [6].

4. *Bibliographic references for the codes used.*

   [1] T. Sasa, K. Tsujimoto, T. Takizuka and H. Takano, "Accelerator-driven Transmutation Reactor Analysis Code – ATRAS", JAERI-Data/Code 99-007 (1999).

   [2] "SCALE-4, A Modular Code System for Performing Standarized Computer Analysis for Licensing Evaluation", CCC-545 (1990).

   [3] R.E. Alcouffe, *et al*., "Users Guide for TWODANT: A Code Package for Two-dimensional, Diffusion-accelerated, Neutral-particle Transport", LA-10049-M (1990).

   [4] D.R. Vondy and G.W. Cunningham, "Exposure Calculation Code Module for Reactor Core Analysis: BURNER", ORNL-5180 (1979).

   [5] A.G. Croff, "ORIGEN-2: A Revised and Updated Version of Oak Ridge Isotope Generation and Development Code", ORNL-5621 (1980).

   [6] K. Okumura, K. Kaneko and K. Tsuchihashi, "SRAC95: General Purpose Neutronics Code System", JAERI-Data/Code 96-015 (1996) (in Japanese).

5. *Origin of cross-section data (ENDF/B-VI, JEF-2.2, JENDL-3.2, etc., describe deviations from standard libraries, e.g. mix from different libraries).*

   - Steady-state neutronics calculation: JENDL-3.2.
   - Burn-up calculation: JENDL-3.2.

- Decay calculation: ORIGEN-2 decay library.

- Calculation of β_{eff}: ENDF-B/VI.

6. *Cell calculation and cross-section condensation (describe your scheme, provide details about assumptions made):*

   a) *Resonance shielding including unresolved resonance treatment and mutual shielding: specify method(s) and energy range depending on nuclides (actinides, clad, fission products, oxygen).*

      F-table in multi-group cross-section set for ATRAS [1] was used.

   b) *Fission spectra: specify whether only a single spectrum was used or a weighted mix from all fissile nuclides, explain procedure.*

      Resonance overlapping of ^{238}U was taken into account.

   c) *Describe how the (n,2n) reaction was treated.*

      - 1.4 to 20 MeV: Fission spectrum of ^{239}Pu.

      - 0.8203 eV to 1.4 MeV: 1/E spectrum.

      - Below 0.8203 eV: Maxwellian distribution at 20°C.

   d) *Weighting spectrum for scattering matrices, e.g. correction of the out-scatter and self-scatter terms, considering the differences between original weighting spectrum and realistic cell spectrum.*

   e) *Method used for spectrum calculation, treatment of leakage.*

   f) *Number of energy groups used in the different phases.*

      - Steady-state neutronics calculation: 73 groups.

      - Burn-up calculation: 1 group.

7. *Method(s) used for reactor calculation (source calculation).*

   - *SCALE-4*. Modular code system for performing standardised computer analysis for licensing evaluation. Only BONAMI-S and NITAWL-S codes were used, however, in the present calculation. Hence, these codes were used to prepare effective cross-sections using the f-table method.

   - *TWODANT*. Transport code using finite difference method. Mesh size : about 5 cm for both R and Z directions.

- *BURNER*. One-point one-group burn-up calculation code.
- *ORIGEN-2*. One-point one-group burn-up calculation code.
- *SRAC95*. Cell calculation code using collision probability method. Homogeneous cells to prepare effective cross-sections and function of calculation of kinetic parameter by perturbation theory were used.

8. *Burn-up calculation:*

   a) Time steps between spectrum calculations.

   b) Actinide and fission product chains.

   c) Fission yields.

9. *Method(s) used for decay calculation.*

   Figure 1 shows the calculation scheme.

   The codes SCALE-4, and BURNER were executed at each burn-up step, respectively, to obtain effective cross-sections and compositions of each region.

   TWODANT calculated k_{eff} and 73-group flux of each region, which was then used for collapsing cross-sections in ORILIB.

   The thermal power output was normalised at 377 MW.

   The one-group cross-sections which were calculated by collapsing 73-group microscopic effective cross-section were used in BURNER to update the actinide effective cross-section.

10. *Other assumptions and characteristics, comments useful for interpreting correctly the results.*

    Table A.2: Infinite multiplication factor, buckling and migration area. We indicate only infinite multiplication factors, since buckling values can not be calculated for homogeneous medium.

    Table B.6.7.8: β_{eff}: Delayed neutron data in JENDL-3.2 are completed for a few nuclides (^{233,235,238}U, ^{239,240,241}Pu). So, ENDF-B/VI is used for calculations of β_{eff}.

Figure 1. Calculation scheme of ATRAS code system

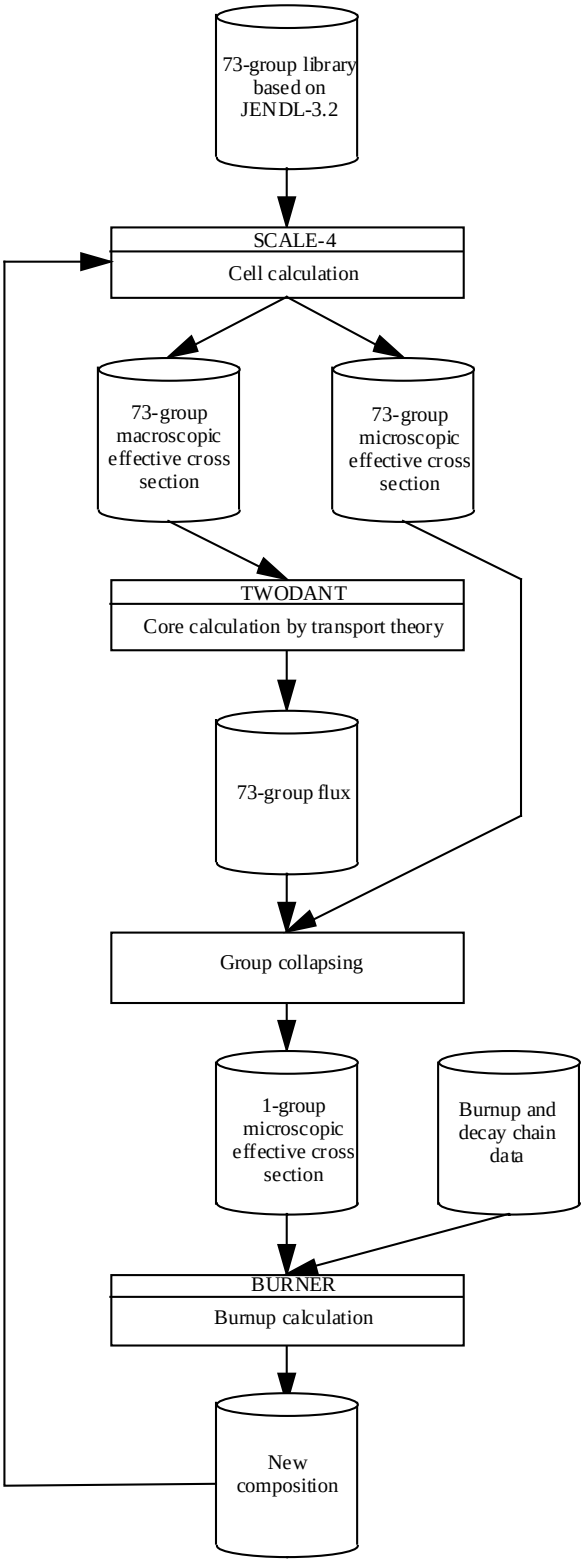

RIT

1. *Author(s) of the solution.*

   Kamil Tucek (kamil@neutron.kth.se), Janne Wallenius and Waclaw Gudowski

2. *Establishment.*

   Royal Institute of Technology
   Dept. of Nuclear & Reactor Physics
   Lindstedtsvägen 24
   S-100 44 Stockholm, Sweden

3. *Name(s) of the code system(s) used.*

   - Neutron transport: MCNP-4B.
   - Burn-up (and neutron transport): MCB.
   - Decay calculations: ORIGEN2.
   - Cross-section treatment: NJOY, versions 91 and 94.

4. *Bibliographic references for the codes used.*

   "MCNP – A General Monte Carlo N-particle Transport Code, Version 4B", Judith F. Briesmeister, ed., LA–12625–M, Los Alamos National Laboratory, New Mexico, USA, March 1997.

   J. Cetnar, J. Wallenius, W. Gudowski, "MCB – A Continuous Energy Monte Carlo Burn-up Code", in Actinide and Fission Product Partitioning and Transmutation, Proc. 5th Int. Information Exchange Meeting, EUR 18898 EN, p. 523, OECD/NEA, 1999.

   A.G.Croff, "A User's Manual for the ORIGEN2 Computer Code", Chemical Technology Division, Oak Ridge National Laboratory, Oak Ridge, Tennessee, USA, July 1980.

   "The NJOY Nuclear Data Processing System, Version 91", R.E. MacFarlane and D.W. Muir, eds., LA–12740–M, Los Alamos National Laboratory, New Mexico, USA, 1994.

5. *Origin of cross-section data (ENDF/B-VI, JEF-2.2, JENDL-3.2, etc., describe deviations from standard libraries, e.g. mix from different libraries).*

   - Default set: JEF–2.2 except for ^{56}Fe, ^{58}Fe and Pb nuclei retrieved from the ENDF/B-VI/5 library and data for ground and isomeric states of ^{244}Am which were taken from the JENDL-3.2 evaluation.
   - Burn-up calculations for start-up core with fission products (Table 4.1) performed also with cross-section sets of ENDFB-VI/5 and JENDL-3.2 evaluations.
   - Temperature adjustment done by NJOY code allowing for temperatures 600 K (assumed for target and reflector), 900 K (fuel) and 1 500 K (Doppler effect calculations).

6. *Cell calculation and cross-section condensation (describe your scheme, provide details about assumptions made).*

   Cell calculations not performed.

7. *Method(s) used for reactor calculation (source calculation).*

   - k_{eff} calculations: MCNP KCODE mode.
   - Source calculations: MCNP source mode.

8. *Burn-up calculation:*

   Calculation of reaction rates and heating done *in flight*.

   a) *Time steps between spectrum calculations.*

      Seventy-three (73) days as default.

   b) *Actinide and fission product chains.*

      Complete set of linear transmutation chains based on available reaction rates obtained from transport and dosimetry cross-section libraries.

   c) *Fission yields.*

      Continuous energy fission yield libraries based on the semi-empirical approach of Wahl and Grashin's non-equilibrium thermodynamical model

9. *Method(s) used for decay calculation.*

   Decay data is for 2 400 nuclides from the Table of Isotopes.

   The Bateman equation is solved by exponential matrix method (default option). The results will also be provided for calculations performed by MCB.

10. *Other assumptions and characteristics, comments useful for interpreting correctly the results.*

    Doppler effect calculations were performed for a change of temperatures of fuel from 900 K to 1 500 K.

    As concerns the void coefficient, only the core region from the coolant is voided.

SCK•CEN

1. *Author(s) of the solution.*

   H. Wienke, Ch. De Raedt, Hamid Ait Abderrahim, Th. Aoust and E. Malambu

2. *Establishment.*

   SCK•CEN
   Boeretang 200,
   B-2400 Mol, Belgium

3. *Name(s) of code system(s) used.*

   MCNP4B [1] – transport calculations.
   NJOY97.95 [2] – cross-section processing.
   ORIGEN-2 – fission-product concentrations.
   BATEMAN2 [3] – burn-up calculations.

4. *Bibliographic references for the codes used.*

   [1] "MCNP – A General Monte Carlo N-particle Transport Code, Version 4B", Judith F. Briesmeister, ed., Los Alamos National Laboratory Report LA-12625-M (1993).

   [2] R.E. MacFarlane, D.W. Muir, "The NJOY Nuclear Data Processing System, Version 91", Los Alamos National Laboratory Report LA-12740-M (1994).

   [3] Ch. De Raedt, BATEMAN2, SCK•CEN, Mol, Belgium, 2000 (unpublished).

5. *Origin of cross-section data (ENDF/B-VI, JEF-2.2, JENDL-3.2, etc., describe deviations from standard libraries, e.g. mix from different libraries).*

   Cross-section data in the MCNP compatible ACE format for the nuclides given in Table 1 of the above report have been derived from JEF-2.2 (except for Pb and ^{233}U which are from ENDF/B-6) using the nuclear cross-section processing code system NJOY97,95 [2]. These cross-section data included Doppler-broadening to the appropriate temperatures of the target, fuel core and reflector, as given in the benchmark description. The cross-section data for the fission products, in so far not available in the MCNP4B cross-section library, also have been derived from JEF-2.2 with NJOY97.

6. *Cell calculation and cross-section condensation (describe your scheme, provide details about assumptions made):*

   a) *Resonance shielding including unresolved resonance treatment and mutual shielding: specify method(s) and energy range depending on nuclides (actinides, clad, fission products, oxygen);*

   b) *Fission spectra: specify whether only a single spectrum was used or a weighted mix from all fissile nuclides, explain procedure.*

c) Describe how the (n,2n) reaction was treated.

d) Weighting spectrum for scattering matrices, e.g. correction of the out-scatter and self-scatter terms, considering the differences between original weighting spectrum and realistic cell spectrum.

e) Method used for spectrum calculation, treatment of leakage.

f) Number of energy groups used in the different phases.

7. Method(s) used for reactor calculation (source calculation).

The reactor calculations (Tables B.1-B.3) were performed with neutron source (sdef card in MCNP4B). The axial and radial flux distributions and spectra were tallied with point detector tallies (at r=0 and axial distances 150, 160, 170, 180, 190 and 200 cm), ring detector tallies (at radial distances 5, 10, 15 and 20 cm) as well as track length tallies (at other axial and radial points). The latter tally results were obtained using spherical (radius 3 cm) and toroidal cells (radius 3 and 2.4 cm).

Reactor calculations have also been performed without source. Although the results are not really relevant, they have been enclosed as well because of their striking similarity with the ones of some participating groups (see "OECD/NEA Comparison Calculations for an Accelerator-driven Minor Actinide Burner: Analysis of Preliminary Results", report presented at the 2nd NEA Workshop on Utilisation and Reliability of High Power Accelerators, Aix-en-Provence, 21-24 November 1999).

8. Burn-up calculation:

The concentrations of the actinides in the fuel at the burn-up steps were obtained using the code BATEMAN2, based upon Bateman equations, developed at SCK•CEN [3], from the reaction rates and average flux calculated with MCNP4B for each step. All important actinide transmutation chains for the problem have been taken into account in the code, except the decay chain $^{244}Cm \rightarrow {}^{240}Pu$ (the decrease of ^{244}Cm by natural decay has been taken into account but not the resulting formation of ^{240}Pu). As a result, the ^{240}Pu concentration is underestimated by about 1% per 0.25 year. This error probably explains the lower ^{240}Pu concentration in the SCK•CEN results with respect to the ^{240}Pu concentrations by the other participants. The concentrations for the fission products at the various burn-up steps were obtained using ORIGEN-2.

a) Time steps between spectrum calculations.

One year.

b) Actinide and fission product chains.

c) Fission yields.

9. Method(s) used for decay calculation.

10. Other assumptions and characteristics, comments useful for interpreting correctly the results.

The strengths of the neutron source was derived from the calculated total number of fissions in the fuel core and the number of fissions per source neutron (weight per source neutron) provided by MCNP4B.

Actinide transmutation chains considered in the SCK•CEN homemade code BATEMAN2

^{234}U (1)
^{234}U (n,γ) ^{235}U (2)
^{234}U (n,γ) ^{235}U (n,γ) ^{236}U (3)
^{234}U (n,γ) ^{235}U (n,γ) ^{236}U (n,γ) ^{237}Np (4)

^{235}U (5)
^{235}U (n,γ) ^{236}U (6)
^{235}U (n,γ) ^{236}U (n,γ) ^{237}U (7)
^{235}U (n,γ) ^{236}U (n,γ) ^{237}U (n,γ) ^{238}Pu (8)
^{235}U (n,2n) ^{234}U (9)

^{236}U (10)
^{236}U (n,γ) ^{237}Np (11)
^{236}U (n,γ) ^{237}Np (n,γ) ^{238}Pu (12)
^{236}U (n,2n) ^{235}U (13)

^{238}U (14)
^{238}U (n,γ) ^{239}Pu (15)
^{238}U (n,γ) ^{239}Pu (n,γ) ^{240}Pu (16)
^{238}U (n,γ) ^{239}Pu (n,γ) ^{240}Pu (n,γ) ^{241}Pu (17)
^{238}U (n,γ) ^{239}Pu (n,γ) ^{240}Pu (n,γ) ^{241}Pu (n,γ) ^{242}Pu (18)
^{238}U (n,γ) ^{239}Pu (n,γ) ^{240}Pu (n,γ) $^{241}Pu^{\beta-} \rightarrow {}^{241}Am$ (19)
^{238}U (n,2n) ^{237}Np (20)

^{237}Np (21)
^{237}Np (n,γ) ^{238}Pu (22)
^{237}Np (n,γ) ^{239}Pu (n,γ) ^{239}Pu (23)

^{238}Pu (24)
^{238}Pu (n,γ) ^{239}Pu (25)
^{238}Pu (n,γ) ^{239}Pu (n,γ) ^{240}Pu (26)
^{238}Pu (n,γ) ^{239}Pu (n,γ) ^{240}Pu (n,γ) ^{241}Pu (27)
^{238}Pu (n,γ) ^{239}Pu (n,γ) ^{240}Pu (n,γ) ^{241}Pu (n,γ) ^{242}Pu (28)
^{238}Pu (n,γ) ^{239}Pu (n,γ) ^{240}Pu (n,γ) $^{241}Pu^{\beta-} \rightarrow {}^{241}Am$ (29)
$^{238}Pu^{\alpha} \rightarrow {}^{234}U$ (30)

^{239}Pu (31)
^{239}Pu (n,γ) ^{240}Pu (32)

$^{239}Pu\ (n,\gamma)\ ^{240}Pu\ (n,\gamma)\ ^{241}Pu$ (33)
$^{239}Pu\ (n,\gamma)\ ^{240}Pu\ (n,\gamma)\ ^{241}Pu\ (n,\gamma)\ ^{242}Pu$ (34)
$^{239}Pu\ (n,\gamma)\ ^{240}Pu\ (n,\gamma)\ ^{241}Pu\ (n,\gamma)\ ^{242}Pu\ (n,\gamma)\ ^{243}Am$ (35)
$^{239}Pu\ (n,\gamma)\ ^{240}Pu\ (n,\gamma)\ ^{241}Pu\ (n,\gamma)\ ^{242}Pu^{\beta-} \rightarrow\ ^{242}Cm$ (36)
$^{239}Pu\ (n,\gamma)\ ^{240}Pu\ (n,\gamma)\ ^{241}Pu^{\beta-} \rightarrow\ ^{241}Am$ (37)
$^{239}Pu\ (n,\gamma)\ ^{240}Pu\ (n,\gamma)\ ^{241}Pu^{\beta-} \rightarrow\ ^{241}Am\ (n,\gamma)\ ^{242m}Am$ (38)
$^{239}Pu\ (n,\gamma)\ ^{240}Pu\ (n,\gamma)\ ^{241}Pu^{\beta-} \rightarrow\ ^{241}Am\ (n,\gamma)\ ^{242}Cm$ (39)
$^{239}Pu\ (n,\gamma)\ ^{240}Pu\ (n,\gamma)\ ^{241}Pu^{\beta-} \rightarrow\ ^{241}Am^{\alpha} \rightarrow\ ^{237}Np$ (40)
$^{239}Pu\ (n,2n)\ ^{238}Pu$ (41)

^{240}Pu (42)
$^{240}Pu\ (n,\gamma)\ ^{241}Pu$ (43)
$^{240}Pu\ (n,\gamma)\ ^{241}Pu\ (n,\gamma)\ ^{242}Pu$ (44)
$^{240}Pu\ (n,\gamma)\ ^{241}Pu\ (n,\gamma)\ ^{242}Pu\ (n,\gamma)\ ^{243}Am$ (45)
$^{240}Pu\ (n,\gamma)\ ^{241}Pu\ (n,\gamma)\ ^{242}Pu\ (n,\gamma)\ ^{243}Am\ (n,\gamma)\ ^{244}Cm$ (46)
$^{240}Pu\ (n,\gamma)\ ^{241}Pu\ (n,\gamma)\ ^{242}Pu^{\beta-} \rightarrow\ ^{242}Cm$ (47)
$^{240}Pu\ (n,\gamma)\ ^{241}Pu^{\beta-} \rightarrow\ ^{241}Am$ (48)
$^{240}Pu\ (n,\gamma)\ ^{241}Pu^{\beta-} \rightarrow\ ^{241}Am\ (n,\gamma)\ ^{242m}Am$ (49)
$^{240}Pu\ (n,\gamma)\ ^{241}Pu^{\beta-} \rightarrow\ ^{241}Am\ (n,\gamma)\ ^{242m}Am\ (n,\gamma)\ ^{243}Am$ (50)
$^{240}Pu\ (n,\gamma)\ ^{241}Pu^{\beta-} \rightarrow\ ^{241}Am\ (n,\gamma)\ ^{242}Cm$ (51)
$^{240}Pu\ (n,\gamma)\ ^{241}Pu^{\beta-} \rightarrow\ ^{241}Am\ (n,\gamma)\ ^{242}Cm\ (n,\gamma)\ ^{243}Cm$ (52)
$^{240}Pu\ (n,\gamma)\ ^{241}Pu^{\beta-} \rightarrow\ ^{241}Am\ (n,\gamma)\ ^{242}Cm^{\alpha} \rightarrow\ ^{238}Pu$ (53)
$^{240}Pu\ (n,\gamma)\ ^{241}Pu^{\beta-} \rightarrow\ ^{241}Am^{\alpha} \rightarrow\ ^{237}Np$ (54)
$^{240}Pu\ (n,2n)\ ^{239}Pu$ (55)

^{241}Pu (56)
$^{241}Pu\ (n,\gamma)\ ^{242}Pu$ (57)
$^{241}Pu\ (n,\gamma)\ ^{242}Pu\ (n,\gamma)\ ^{243}Am$ (58)
$^{241}Pu\ (n,\gamma)\ ^{242}Pu\ (n,\gamma)\ ^{243}Am\ (n,\gamma)\ ^{244}Cm$ (59)
$^{241}Pu\ (n,\gamma)\ ^{242}Pu^{\beta-} \rightarrow\ ^{242}Cm$ (60)
$^{241}Pu^{\beta-} \rightarrow\ ^{241}Am$ (61)
$^{241}Pu^{\beta-} \rightarrow\ ^{241}Am\ (n,\gamma)\ ^{242m}Am$ (62)
$^{241}Pu^{\beta-} \rightarrow\ ^{241}Am\ (n,\gamma)\ ^{242m}Am\ (n,\gamma)\ ^{243}Am$ (63)
$^{241}Pu^{\beta-} \rightarrow\ ^{241}Am\ (n,\gamma)\ ^{242m}Am\ (n,\gamma)\ ^{243}Am\ (n,\gamma)\ ^{244}Cm$ (64)
$^{241}Pu^{\beta-} \rightarrow\ ^{241}Am\ (n,\gamma)\ ^{242}Cm$ (65)
$^{241}Pu^{\beta-} \rightarrow\ ^{241}Am\ (n,\gamma)\ ^{242}Cm\ (n,\gamma)\ ^{243}Cm$ (66)
$^{241}Pu^{\beta-} \rightarrow\ ^{241}Am\ (n,\gamma)\ ^{242}Cm\ (n,\gamma)\ ^{243}Cm\ (n,\gamma)\ ^{244}Cm$ (67)
$^{241}Pu^{\beta-} \rightarrow\ ^{241}Am\ (n,\gamma)\ ^{242}Cm^{\alpha} \rightarrow\ ^{238}Pu$ (68)
$^{241}Pu^{\beta-} \rightarrow\ ^{241}Am\ (n,\gamma)\ ^{242}Cm^{\alpha} \rightarrow\ ^{238}Pu^{\alpha} \rightarrow\ ^{234}U$ (69)
$^{241}Pu^{\beta-} \rightarrow\ ^{241}Am^{\alpha} \rightarrow\ ^{237}Np$ (70)
$^{241}Pu\ (n,2n)\ ^{240}Pu$ (71)

^{242}Pu (72)
$^{242}Pu\ (n,\gamma)\ ^{243}Am$ (73)
$^{242}Pu\ (n,\gamma)\ ^{243}Am\ (n,\gamma)\ ^{244}Cm$ (74)
$^{242}Pu^{\beta-} \rightarrow\ ^{242}Cm$ (75)
$^{242}Pu\ (n,2n)\ ^{241}Pu$ (76)

^{241}Am (77)
$^{241}Am\ (n,\gamma)\ ^{242m}Am$ (78)
$^{241}Am\ (n,\gamma)\ ^{242m}Am\ (n,\gamma)\ ^{243}Am$ (79)

^{241}Am (n,γ) ^{242m}Am (n,γ) ^{243}Am (n,γ) ^{244}Cm (80)
^{241}Am (n,γ) ^{242}Cm (81)
^{241}Am (n,γ) ^{242}Cm (n,γ) ^{243}Cm (82)
^{241}Am (n,γ) ^{242}Cm (n,γ) ^{243}Cm (n,γ) ^{244}Cm (83)
^{241}Am (n,γ) $^{242}Cm^{\alpha} \rightarrow {}^{238}Pu$ (84)
^{241}Am (n,γ) $^{242}Cm^{\alpha} \rightarrow {}^{238}Pu^{\alpha} \rightarrow {}^{234}U$ (85)
$^{241}Am^{\alpha} \rightarrow {}^{237}Np$ (86)
$^{241}Am^{\alpha} \rightarrow {}^{237}Np$ (n,γ) ^{238}Pu (87)

^{242m}Am (88)
^{242m}Am (n,γ) ^{243}Am (89)
^{242m}Am (n,γ) ^{243}Am (n,γ) ^{244}Cm (90)
^{242m}Am (n,2n) ^{241}Am (91)

^{243}Am (92)
^{243}Am (n,γ) ^{244}Cm (93)
^{243}Am (n,γ) ^{244}Cm (n,γ) ^{245}Cm (94)
^{243}Am (n,γ) ^{244}Cm (n,γ) ^{245}Cm (n,γ) ^{246}Cm (95)

^{242}Cm (96)
^{242}Cm (n,γ) ^{243}Cm (97)
^{242}Cm (n,γ) ^{243}Cm (n,γ) ^{244}Cm (98)
$^{242}Cm^{\alpha} \rightarrow {}^{238}Pu$ (99)
$^{242}Cm^{\alpha} \rightarrow {}^{238}Pu^{\alpha} \rightarrow {}^{234}U$ (100)

^{243}Cm (101)
^{243}Cm (n,γ) ^{244}Cm (102)
^{243}Cm (n,γ) ^{244}Cm (n,γ) ^{245}Cm (103)
^{243}Cm (n,γ) ^{244}Cm (n,γ) ^{245}Cm (n,γ) ^{246}Cm (104)
^{243}Cm (n,2n) ^{242}Cm (105)

^{244}Cm (106)
^{244}Cm (n,γ) ^{245}Cm (107)
^{244}Cm (n,γ) ^{245}Cm (n,γ) ^{246}Cm (108)
^{244}Cm (n,γ) ^{245}Cm (n,γ) ^{246}Cm (n,γ) ^{247}Cm (109)
^{244}Cm (n,2n) ^{243}Cm (110)

Chain $^{244}\mathbf{Cm}^{\alpha} \rightarrow {}^{\mathbf{240}}\mathbf{Pu}$ should have been included (the error is about 1% underestimation of the ^{240}Pu concentrations per 3 months)

^{245}Cm (111)
^{245}Cm (n,γ) ^{246}Cm (112)
^{245}Cm (n,γ) ^{246}Cm (n,γ) ^{247}Cm (113)
^{245}Cm (n,γ) ^{246}Cm (n,γ) ^{247}Cm (n,γ) ^{248}Cm (114)

^{246}Cm (115)
^{246}Cm (n,γ) ^{247}Cm (116)
^{246}Cm (n,γ) ^{247}Cm (n,γ) ^{248}Cm (117)

^{247}Cm (118)
^{247}Cm (n,γ) ^{248}Cm (119)

^{248}Cm (120)

APPENDIX C

Questionnaire and summary of the answers

OECD/NEA COMPARISON CALCULATIONS FOR AN ACCELERATOR-DRIVEN MINOR ACTINIDE BURNER: QUESTIONNAIRE

Homogeneous cell calculation

We assume that you prepared broad group cross-sections for the fuel zone with the help of a "cell code" which calculates the fundamental mode neutron spectrum of the cell and that the data in Tables A.1 and A.2 are averaged with this spectrum.

Q1: Please confirm that this assumption is correct; if you supplied data from a different type of calculation, explain how the data were averaged.

Q2: Confirm that the one-group cross-sections in Table A.1 refer to a critical cell, i.e. that they are averaged with a spectrum from a cell calculation with $k_{eff} = 1$ ($B^2 = B^2_{crit}$).

The production-to-absorption reaction ratio for the critical cell can be evaluated as follows: $1 + M^2B^2_{crit}$. *Therefore, in Table A.2, we expect the* k_{inf} *of the cell without leakage.*

Q3: Confirm that you supplied the k_{inf} for the cell without leakage ($B^2 = 0$).

Reactor calculation

Spatial distribution of the neutron source

A revised neutron source specification including a new axial distribution and a new collapsing program for producing a broad group source were circulated in August 1999. Therein, the position and spatial distribution of the source are prescribed as follows:

- *Target top position (impact of proton beam):* $Z_T = 150$ *cm, coinciding with top of the core.*
- *Radial distribution: the source is constant (flat distribution) for* $r < 10$ *cm and 0 for* $r > 10$ *cm.*
- *Axial distribution in the range 150 cm > z > 50 cm (10 cm meshes, starting from top): 0.33369, 0.26611, 0.17754, 0.10825, 0.06085, 0.03193, 0.01131, 0.00571, 0.00300, 0.00161*

Q4: Does the source distribution that you used conform with this specification and have you used the new collapsing program?

Table B.1. Reaction rate balance components

Absorption reaction rates and production rates are defined by $(\Sigma_f + \Sigma_c)\phi$ *and* $\nu\Sigma_f\phi$*, respectively. They should not contain any corrections for* (n,2n) *reactions.*

Q5: Do your results conform with these definitions?

Q6: On request, could you also supply nuclide dependent (n,2n) reaction rates?

Table B.2. Neutron flux distributions

Q7: To which reactor power do your results refer?

Q8: Please specify the radial and axial meshes which you used in the 2-D calculation.

Q9: Have you performed an interpolation to obtain the values in the requested positions?

Table B.3.1. Neutron spectrum

The specification is ambiguous. We expect group fluxes, not group fluxes divided by Δu *. (The values should add up to give the total flux at r,z = 56 cm, 100 cm.)*

Q10: Please confirm that you provided group fluxes.

Tables B.4.1/B.4.2. Burn-up, k_{eff}, k_{eff} without fission products, source strength

By "k_{eff}*" we mean the* k_{eff} *of a homogeneous calculation, i.e. a calculation without the external neutron source. This means that you have to perform a separate* k_{eff} *calculation for each burn-up step. We requested these extra calculations to avoid problems with different definitions of so-called source multiplication factors.*

Q11: Do your k_{eff} values conform with our definition?

The reactor is assumed to run continuously at the constant average thermal power of 320 MW, corresponding to a load factor of 0.85 (see p. 3 of the benchmark specification). In the burn-up calculation with the external source, the thermal power should therefore be kept constant within the one-year burn-up steps, implying an automatic source adjustment within the burn-up steps.

Q12: Confirm that you performed a burn-up calculation with external source; specify the thermal power (or the load factor) and confirm that the power was kept constant within the burn-up steps.

To understand differences in reported burn-up values, we need to know how you calculate power.

Q13: Specify your energy-per-fission values; are they constant or nuclide-dependent? Are the values adjusted for (n,γ) heating, or do you take account of the (n,γ) heating in a different way?

Since the maximum source strength determines the design power of the accelerator, we requested the source strength values in Tables B.4.1/B.4.2 to be normalised to the full power of 377 MWth.

Q14: Specify the thermal power to which your source strength values are normalised.

Numerical approximations, actinide and fission-product chains, fission-product data

Q15: Please specify the number of burn-up regions in the fuel zone (provide a region map).

Q16: How many (2-D) spectrum calculations per 365-day burn-up step have you performed?

Q17: Specify the branching ratios for the $^{241}Am(n,\gamma)^{242/242m}Am$ reaction and the decay of ^{242}Am to ^{242}Cm and ^{242}Pu. Supply any available descriptions of the applied actinide and fission product chains.

Q18: Provide list of explicitly represented fission products.

Q19: Did you use lumped (pseudo) fission products and what are their characteristics?

Q20: Indicate origin of the fission yields.

Table 6.7.8. Safety parameters

Q21: Are coolant void and fuel Doppler reactivity effects evaluated from k_{eff} differences, or did you use other methods as e.g. perturbation theory?

Q22: Confirm that k_{eff} values conform with our definition (cf. Q11).

Q23: Indicate origin of the delayed neutron data used in the β_{eff} calculation.

Name(s) and organisation of the participant(s):

Table C.1. Summary of the answers to the ADS questionnaire*

Institution		ANL	CIEMAT	KAERI	PSI/CEA	JAERI	RIT
Homogeneous cell calculation (Table A.1 and A.2)							
1	1gp XS from fundamental mode cell calc.	Yes	No	Yes	Yes	No	No cell calculation (average of whole core)
2	1gp XS from critical cell calc. (k_{eff} = 1)	Yes	No (avg. whole core)	No	Yes	No	No
3	k_{inf} for no-leakage cell	Yes	Results not provided	Yes	Yes	Yes	Results not provided
Spatial distribution of the neutron source							
4	Source distribution in the spec. & new collaps. program	Yes	Yes	Yes	Yes	Yes	Yes
Reaction rate balance components (Table B.1)							
5	Reaction rates $(\Sigma_f+\Sigma_c)\phi$ and $\nu\Sigma_f\phi$	Yes	Yes	Yes	Yes	Yes	No (n,xn) contributions to abs. and prod.
6	Can supply nuclide dependent (n, 2n) reaction rates	Yes	Yes	Yes	Yes	Yes	Yes (provided)
Neutron flux distributions (Table B.2)							
7	Reactor power level (MW)	377	320	377	377	377	377 (fission power)
8	Radial and axial mesh description	(r,z) = 59 × 80	(r,z) = 40 × 47	(r,z) = 71 × 100	Const. 1 cm mesh	(r,z) = 38 × 40	MC calc.
9	Interpolation for fluxes	Yes	No	Yes	Yes	Yes	No
Neutron spectrum (Table B.3.1)							
10	Group fluxes at r, z = 56, 100 cm	Yes	Yes	Yes	Yes	Yes	Yes

** SCK•CEN had the questionnaire before its participation and some of results have been revised to be conformed to the specification.*

Table C.1. Summary of the answers to the ADS questionnaire (*cont.*)

	Institution	ANL	CIEMAT	KAERI	PSI/CEA	JAERI	RIT
	Burn-up, k_{eff}, k_{eff} without FPs, source strength (Table B.4.1/B.4.2)						
11	Homogeneous k_{eff} calc.	Yes	Yes	Yes	Yes	Yes	Yes
12	• Burn-up calculation with external source • Power level • Constant power	BU calc. with ex. source Const. power 320	BU calc. with ex. source 320	BU calc. with ex. source 320	BU calc. with ex. source Const flux calc normalised to 320	BU calc. with ex. source Const. power 320	BU calc. with ex. source Const. fission power 320
13	• Q values • Const. or nuclide dependent • Adjusted for (n,γ) heating	Nuclide dependent Q/fiss. and Q/capture	Nuclide dependent Q/fiss. adjusted to include (n,γ) heating	Nuclide dependent Q/fiss. and Q/capture (DIF3D)	Nuclide dependent Q/fiss. and Q/capture	Nuclide dependent Q/fiss. (n,γ) heating was not taken into account	Only nuclide dependent Q/fiss. No prompt neutrons and gamma, no (n,γ) heating
14	Power to which the source strength are normalised (MW)	377	377	377	377	377	377
	Numerical approximations, actinide and FP chains, FP data						
15	Number of burn-up regions	20 (r,z = 4 × 5)	90 (r,z = 9 × 10)	20 (r,z = 4 × 5)	1	1	1
16	Number of spectrum calc./ 365 d burn-up step	4	1	1 at BOC	4	1	5
17	• ^{241}Am(n,γ) branching ratio • Decay of ^{242}Am	^{242}Am 80% ^{242m}Am 20% ^{242}Cm 82.7% ^{242}Pu 17.3%	^{242}Am 80% ^{242m}Am 20% ^{242}Cm 82.7% ^{242}Pu 17.3%	^{242}Am 80% ^{242m}Am 20% ^{242}Cm 86% ^{242}Pu 14%	^{242}Am 85% ^{242m}Am 15% ^{242}Cm 84% ^{242}Pu 16%	^{242}Am 80% ^{242m}Am 20% ^{242}Cm 83% ^{242}Pu 17%	^{239}Np 0.0325 ^{237}Np 0.7415 ^{241}Am 0.2255 ^{243}Am 0.88 ^{242}Cm 0.827 ^{242}Pu 0.173
18	Fission product list	None	A list provided	None	None	None (lumped FPs)	A list provided

Table C.1. Summary of the answers to the ADS questionnaire (*cont*.)

	Institution	ANL	CIEMAT	KAERI	PSI/CEA	JAERI	RIT
19	Lumped FPs	Yes 5 LFPs: FP35,38,39, 40, 41	No	Yes 3 LFPs: LFPP3,5,9	Yes (JEF2.2) 6LFPs: FPU5, U8, Pu39, Pu40, Pu41, Pu42	Yes Lumped FPs from ^{232}Th, ^{233,235,238}U, ^{239,241}Pu	No
20	Origin of the FY	ENDF/B-V	ENDF/B-VI (r. 4)	ENDF/B-VI	JEF2.2	JENDL-2	Grashin's non-equilibrium thermodynamical model
	Safety parameters (Table 6.7.8)						
21	Direct calculation for Doppler and void effects	Yes	Yes (large uncertainties)	Yes	Yes	Yes	Yes
22	Homogeneous k_{eff} calc.	Yes	Yes	Yes	Yes	Yes	Yes
23	Origin of the delayed neutron data for β_{eff}	ENDF/B-VI	MCNP calc. (TOTNU & TOTNONU)	Not provided	JEF2.2	ENDF/B-VI	A list provided

APPENDIX D

Sensitivity study on actinide data in ENDF/B-VI, JEF-2.2 and JENDL-3.2 for the ADMAB benchmark system

SENSITIVITY ON ACTINIDE DATA IN ENDF/B-VI, JEF-2.2 AND JENDL-3.2 FOR ADMAB BENCHMARK SYSTEM

Jung-Do Kim and Choong-Sup Gil
Korea Atomic Energy Research Institute

The ENDF/B-VI.5 library is used for all nuclides as the reference and JEF-2.2 and JENDL-3.2 are processed for actinides to generate 175-group (Vitamin-J) MATXS-format libraries using NJOY.

The code used for the start-up core calculation is ONEDANT (P_3 and S_8 approximation) with a one-dimensional core model: spherical geometry keeping the equivalent-volume of 2-D R-Z model. The fission spectrum was directly weighted with the flux in library.

The k_{eff} and reaction rates are calculated by exchanging the data set of actinides from ENDF/B-VI to JEF-2.2 or to JENDL-3.2. The questionable evaluated data in ENDF/B-VI are ^{242}Cm fission data reporting zero values between 30 eV and 10 keV (refer to NEA/WPEC-8, p. 77 Figure 2.31) and ^{242m}Am inelastic data in thermal and epithermal energy range (refer to JEF-Report 14, p. 225). Moreover, there are no (n,3n) reaction data for ^{242}Cm, ^{243}Cm and ^{245}Cm in JEF-2.2. The results are presented in Tables D.1 to D.4. Table D.1 summarises the effects of each actinide from different libraries on k_{eff}. Tables D.2 and D.3 present reaction rates and average ν at the middle of core zone, and energy-dependent reaction-rate distribution, respectively. Table D.4 compares the production, absorption reaction rates and their ratios.

With regard to k_{eff} variation due to actinide data exchange, the following is observed.

ENDF/B-VI to JEF-2.2

1) Negative effect: ^{237}Np, ^{241,242m,243}Am
2) Positive effect: ^{238}Pu, ^{242,243,244,245}Cm
3) Large differences: ^{242m}Am, ^{242,243,245}Cm
4) Maximum difference including Pu isotopes: Over 4 000 pcm

ENDF/B-VI to JENDL-3.2

1) Negative effect: ^{237}Np, ^{241,242m,243}Am, ^{244,246}Cm
2) Positive effect: ^{238}Pu, ^{242,243,245}Cm
3) Large differences: ^{242m}Am, ^{242,243,245}Cm
4) Maximum difference including Pu isotopes: Over 2 000 pcm

As for the differences in reaction rates due to actinide data exchange, the following is observed.

ENDF/B-VI to JEF-2.2

1) Large differences: Inelastic, n2n, n3n
2) Fission: ~20% for ^{242m}Am, ~27% for ^{243}Cm, no idea for ^{242}Cm
3) Capture: ~50% for ^{242m}Am, ~30% for ^{238}Pu, ~70% for ^{242}Cm, ~35% for ^{244}Cm

ENDF/B-VI to JENDL-3.2

1) Large differences: Inelastic, n2n, n3n
2) Fission: ~20% for ^{242m}Am, no idea for ^{242}Cm, ~15% for ^{243}Cm
3) Capture: ~66% for ^{242m}Am, ~80% for ^{242}Cm, ~70% for ^{243}Cm, ~20% for ^{244}Cm, ~45% for ^{246}Cm

The k_{eff} variation and reaction rates due to exchange of ^{15}N, Bi and Pb at the middle position of fuel zone are also studied and presented in Table D.5. The availability of reaction data for ^{15}N, Bi and Pb in ENDF/B-VI, JEF-2.2 and JENDL-3.2 is summarised in Table D.6.

Additional calculations were performed to investigate the influence of fission spectra used in transport calculations. In these calculations, the flux obtained from the previous calculations was used to generate the region-dependent fission spectrum and then used for transport calculations. The results are compared with those of previous calculations in Table D.7.

Table D.1. Effect of each actinide from different libraries on k_{eff} (start-up core)

Reference k_{eff} = 1.00007: All ENDF/B-VI data.

Exchanged nuclide	JEF-2.2			JENDL-3.2		
	k_{eff}	Δk*	Δk/atom**	k_{eff}	Δk*	Δk/atom**
^{237}Np	0.998257	-181	-4.14	0.997425	-265	-6.05
^{241}Am	0.986861	-1321	-16.34	0.99744	-263	-3.25
^{242m}Am	0.996619	-345	-316.8	0.997574	-250	-229.57
^{243}Am	0.992768	-730	-12.53	0.99502	-505	-8.67
^{238}Pu	1.00073	66	15.62	1.00067	60	14.2
^{239}Pu	0.996104	-397	-7.86	0.999828	-24	-0.48
^{240}Pu	0.998555	-152	-6.55	0.997618	-245	-10.56
^{241}Pu	0.999424	-65	-5.28	1.00114	107	8.69
^{242}Pu	1.00007	0	0	1.00007	0	0
^{242}Cm	1.00008	1	245.16	1.00008	1	245.16
^{243}Cm	1.00102	95	285.63	1.00065	58	174.38
^{244}Cm	1.00118	111	4.68	0.999148	-92	-3.88
^{245}Cm	1.00675	668	211.13	1.00266	259	81.86
^{246}Cm	–	–	–	1.00006	-1	-18.67

* Δk values are relative to ENDF/B-VI results, in units of 1E-5.

** Δk/atom, in units of 1E-24.

Table D.2. Reaction rates and average ν at the middle of core zone in start-up core

Reaction	Elastic	Inelastic	n2n	n3n	Fission	Capture	Average ν
^{237}Np							
ENDF/B-VI	6.056E-04	7.656E-05	2.028E-08	3.397E-11	3.009E-05	8.847E-05	2.7093
JENDL-3.2	6.382E-04	7.309E-05	2.002E-08	1.468E-10	3.105E-05	9.119E-05	2.6068
JEF-2.2	6.294E-04	6.410E-05	1.546E-08	6.084E-11	2.998E-05	8.833E-05	2.6134
JENDL/ENDF*	*1.054*	*0.955*	*0.987*	*4.321*	*1.032*	*1.031*	*0.962*
JEF/ENDF	*1.039*	*0.837*	*0.762*	*1.791*	*0.996*	*0.998*	*0.965*
^{241}Am							
ENDF/B-VI	6.483E-04	6.825E-05	4.408E-09	2.454E-12	2.488E-05	9.609E-05	3.3045
JENDL-3.2	6.561E-04	6.646E-05	4.185E-09	1.103E-10	2.485E-05	9.835E-05	3.2887
JEF-2.2	6.241E-04	4.826E-05	1.164E-08	2.438E-11	2.432E-05	1.111E-04	3.3216
JENDL/ENDF	*1.012*	*0.974*	*0.949*	*44.947*	*0.999*	*1.024*	*0.995*
JEF/ENDF	*0.963*	*0.707*	*2.641*	*9.935*	*0.977*	*1.156*	*1.005*
^{242m}Am							
ENDF/B-VI	5.721E-04	7.748E-06	7.288E-08	4.143E-10	2.522E-04	2.000E-05	3.3479
JENDL-3.2	5.720E-04	3.898E-05	2.718E-08	1.783E-10	2.055E-04	3.325E-05	3.361
JEF-2.2	5.528E-04	4.722E-05	7.292E-08	4.293E-10	2.074E-04	3.088E-05	3.2769
JENDL/ENDF	*1*	*5.031*	*0.373*	*0.43*	*0.815*	*1.663*	*1.004*
JEF/ENDF	*0.966*	*6.094*	*1.001*	*1.036*	*0.822*	*1.544*	*0.979*
^{243}Am							
ENDF/B-VI	6.561E-04	8.778E-05	1.939E-08	4.558E-11	1.821E-05	8.539E-05	3.34
JENDL-3.2	6.571E-04	8.838E-05	2.363E-08	3.260E-10	1.806E-05	8.848E-05	3.2796
JEF-2.2	5.987E-04	6.662E-05	3.180E-08	1.300E-10	1.910E-05	9.602E-05	3.1179
JENDL/ENDF	*1.002*	*1.007*	*1.219*	*7.152*	*0.992*	*1.036*	*0.982*
JEF/ENDF	*0.913*	*0.759*	*1.64*	*2.852*	*1.049*	*1.124*	*0.934*

* Ratio JENDL-3.2 to ENDF/B-VI.

** Ratio JEF-2.2 to ENDF/B-VI.

Table D.2. Reaction rates and average ν at the middle of core zone in start-up core (*cont.*)

Reaction	Elastic	Inelastic	n2n	n3n	Fission	Capture	Average ν
^{238}Pu							
ENDF/B-VI	7.058E-04	3.499E-05	2.877E-08	5.970E-10	8.821E-05	4.243E-05	2.9668
JENDL-3.2	8.019E-04	3.059E-05	2.344E-08	1.471E-10	8.928E-05	3.650E-05	2.9682
JEF-2.2	6.585E-04	4.455E-05	5.147E-09	4.955E-11	8.866E-05	3.080E-05	2.9695
JENDL/ENDF	*1.136*	*0.874*	*0.815*	*0.246*	*1.012*	*0.86*	*1*
JEF/ENDF	*0.933*	*1.273*	*0.179*	*0.083*	*1.005*	*0.726*	*1.001*
^{242}Cm							
ENDF/B-VI	6.881E-04	7.566E-05	1.151E-09	2.575E-12	1.419E-05	1.575E-05	3.361
JENDL-3.2	7.022E-04	5.162E-05	1.108E-08	5.263E-11	6.215E-05	2.811E-05	3.336
JEF-2.2	6.606E-04	7.131E-05	7.066E-09	0.00E+00	5.143E-05	2.698E-05	3.2336
JENDL/ENDF*	*1.02*	*0.682*	*9.626*	*20.439*	*4.38*	*1.785*	*0.993*
JEF/ENDF**	*0.96*	*0.943*	*6.139*	*0*	*3.624*	*1.713*	*0.962*
^{243}Cm							
ENDF/B-VI	6.616E-04	9.774E-05	6.955E-08	8.874E-11	1.727E-04	1.268E-05	3.5174
JENDL-3.2	5.978E-04	2.546E-05	9.553E-08	1.623E-10	1.987E-04	2.175E-05	3.52
JEF-2.2	5.528E-04	3.758E-05	2.298E-08	0.000E+00	2.184E-04	1.124E-05	3.4766
JENDL/ENDF	*0.904*	*0.26*	*1.374*	*1.829*	*1.151*	*1.715*	*1.001*
JEF/ENDF	*0.836*	*0.384*	*0.33*	*0*	*1.265*	*0.886*	*0.988*
^{244}Cm							
ENDF/B-VI	6.951E-04	5.216E-05	2.402E-08	4.846E-10	3.875E-05	4.920E-05	3.5502
JENDL-3.2	7.248E-04	5.782E-05	2.929E-08	1.694E-10	3.858E-05	3.946E-05	3.3466
JEF-2.2	7.055E-04	4.504E-05	2.906E-08	6.372E-11	3.912E-05	3.249E-05	3.3439
JENDL/ENDF	*1.043*	*1.109*	*1.219*	*0.35*	*0.996*	*0.802*	*0.943*
JEF/ENDF	*1.015*	*0.863*	*1.21*	*0.131*	*1.01*	*0.66*	*0.942*
^{245}Cm							
ENDF/B-VI	6.078E-04	8.500E-05	1.248E-07	5.586E-10	1.550E-04	1.861E-05	3.6987
JENDL-3.2	6.056E-04	4.382E-05	1.051E-07	1.906E-10	1.757E-04	2.127E-05	3.6015
JEF-2.2	5.937E-04	4.433E-05	2.503E-08	0.000E+00	1.772E-04	1.834E-05	3.9115
JENDL/ENDF	*0.996*	*0.516*	*0.842*	*0.341*	*1.134*	*1.143*	*0.974*
JEF/ENDF	*0.977*	*0.522*	*0.201*	*0*	*1.143*	*0.985*	*1.058*
^{246}Cm							
ENDF/B-VI	7.259E-04	7.629E-05	3.208E-08	1.265E-09	2.495E-05	1.279E-05	3.5752
JENDL-3.2	7.526E-04	7.134E-05	3.153E-08	3.421E-10	2.462E-05	1.876E-05	3.2953
JEF-2.2	7.259E-04	7.629E-05	3.208E-08	1.265E-09	2.495E-05	1.279E-05	3.5752
JENDL/ENDF	*1.037*	*0.935*	*0.983*	*0.27*	*0.987*	*1.467*	*0.922*
JEF/ENDF	*1.000*	*1.000*	*1.000*	*1.000*	*1.000*	*1.000*	*1.000*

* Ratio JENDL-3.2 to ENDF/B-VI.
** Ratio JEF-2.2 to ENDF/B-VI.

Table D.3. Energy-dependent reaction rate distribution in start-up core (%)

Upper energy limit		20 MeV	1 MeV	0.1 MeV	10 keV	1 keV	0.1 keV
^{237}Np							
ENDF/B-VI	Fission	54.14	44.94	0.79	0.13	0.01	0.00
JEF-2.2		53.81	45.27	0.80	0.12	0.00	0.00
JENDL-3.2		53.21	44.72	1.68	0.36	0.02	0.00
ENDF/B-VI	Capture	1.00	29.49	45.28	22.18	1.85	0.18
JEF-2.2		1.01	29.50	45.27	22.18	1.85	0.18
JENDL-3.2		0.96	25.94	47.69	23.34	1.91	0.17
^{238}Pu							
ENDF/B-VI	Fission	25.21	52.76	14.93	6.72	0.37	0.00
JEF-2.2		25.41	52.71	16.56	4.91	0.41	0.00
JENDL-3.2		25.32	52.63	16.60	5.05	0.39	0.00
ENDF/B-VI	Capture	2.71	33.36	39.96	21.96	1.96	0.04
JEF-2.2		1.34	28.55	45.19	22.67	2.19	0.06
JENDL-3.2		2.07	27.05	44.57	23.81	2.45	0.05
^{241}Am							
ENDF/B-VI	Fission	72.83	25.35	1.27	0.50	0.04	0.00
JEF-2.2		74.20	23.87	1.25	0.62	0.05	0.00
JENDL-3.2		73.64	24.54	1.28	0.50	0.04	0.00
ENDF/B-VI	Capture	0.20	29.71	45.69	22.51	1.74	0.14
JEF-2.2		1.01	37.16	42.80	17.52	1.39	0.12
JENDL-3.2		1.21	30.05	44.19	22.50	1.93	0.13
^{242m}Am							
ENDF/B-VI	Fission	8.85	40.19	31.67	17.76	1.43	0.11
JEF-2.2		8.31	43.98	33.17	13.47	0.99	0.08
JENDL-3.2		8.58	45.07	32.27	13.12	0.88	0.08
ENDF/B-VI	Capture	0.40	12.89	46.64	36.77	3.05	0.24
JEF-2.2		0.75	42.52	42.71	13.02	0.93	0.07
JENDL-3.2		2.67	36.30	42.43	17.22	1.28	0.10
^{243}Am							
ENDF/B-VI	Fission	79.17	18.96	1.29	0.54	0.04	0.00
JEF-2.2		79.26	20.00	0.61	0.12	0.01	0.00
JENDL-3.2		80.29	18.53	0.82	0.33	0.03	0.00
ENDF/B-VI	Capture	1.13	27.12	47.84	21.93	1.84	0.13
JEF-2.2		1.42	31.13	45.17	20.46	1.70	0.12
JENDL-3.2		1.15	27.11	47.68	22.13	1.79	0.13
^{242}Cm							
ENDF/B-VI	Fission	84.46	14.77	0.76	0.01	0.00	0.00
JEF-2.2		38.77	50.63	9.50	1.08	0.02	0.00
JENDL-3.2		35.82	51.46	9.19	3.34	0.19	0.01
ENDF/B-VI	Capture	1.05	16.80	38.60	39.39	3.84	0.31
JEF-2.2		0.20	19.82	48.20	28.92	2.67	0.19
JENDL-3.2		1.89	26.04	46.76	22.99	2.16	0.17
^{243}Cm							
ENDF/B-VI	Fission	13.54	41.77	28.43	14.85	1.29	0.12
JEF-2.2		9.98	43.79	33.20	12.13	0.84	0.06
JENDL-3.2		10.08	42.70	32.31	13.87	0.94	0.10
ENDF/B-VI	Capture	0.45	19.01	46.32	31.08	2.86	0.28
JEF-2.2		0.77	22.35	44.59	29.10	2.93	0.25
JENDL-3.2		4.48	30.31	41.63	21.81	1.68	0.10

Table D.3. Energy-dependent reaction rate distribution in start-up core (%) (*cont.*)

Upper energy limit		20 MeV	1 MeV	0.1 MeV	10 keV	1 keV	0.1 keV
^{244}Cm							
ENDF/B-VI	Fission	50.84	44.98	3.24	0.86	0.07	0.00
JEF-2.2		50.85	45.44	3.11	0.45	0.15	0.00
JENDL-3.2		49.58	45.22	3.51	1.62	0.07	0.00
ENDF/B-VI	Capture	1.50	29.85	47.91	19.03	1.69	0.02
JEF-2.2		1.91	33.87	52.41	9.11	2.67	0.03
JENDL-3.2		3.39	28.87	44.56	20.95	2.19	0.03
^{245}Cm							
ENDF/B-VI	Fission	13.24	33.52	35.06	16.79	1.27	0.11
JEF-2.2		11.92	40.56	33.13	13.29	1.01	0.09
JENDL-3.2		10.13	43.63	32.33	12.89	0.93	0.09
ENDF/B-VI	Capture	1.14	30.42	49.65	17.36	1.31	0.11
JEF-2.2		1.76	29.31	43.43	23.38	1.96	0.16
JENDL-3.2		1.96	38.90	42.50	15.26	1.26	0.12
^{246}Cm							
ENDF/B-VI	Fission	71.12	28.71	0.04	0.10	0.02	0.00
JEF-2.2		71.12	28.71	0.04	0.10	0.02	0.00
JENDL-3.2		66.94	28.67	3.02	1.28	0.09	0.00
ENDF/B-VI	Capture	2.64	31.33	39.82	23.48	2.69	0.03
JEF-2.2		2.64	31.33	39.82	23.48	2.69	0.03
JENDL-3.2		2.63	24.86	45.00	25.34	2.15	0.02

Table D.4. Production, absorption reaction rates and their ratios in start-up core

	Production	Absorption	Production/Absorption
^{237}Np			
ENDF/B-VI	8.152E-05	1.186E-04	0.688
JENDL-3.2	8.094E-05	1.222E-04	0.662
JEF-2.2	7.835E-05	1.183E-04	0.662
JENDL/ENDF	*0.993*	*1.031*	*0.963*
JEF/ENDF	*0.961*	*0.998*	*0.963*
^{241}Am			
ENDF/B-VI	8.222E-05	1.210E-04	0.680
JENDL-3.2	8.172E-05	1.232E-04	0.663
JEF-2.2	8.078E-05	1.354E-04	0.597
JENDL/ENDF	*0.994*	*1.018*	*0.976*
JEF/ENDF	*0.983*	*1.119*	*0.878*
^{242m}Am			
ENDF/B-VI	8.443E-04	2.722E-04	3.102
JENDL-3.2	6.907E-04	2.388E-04	2.893
JEF-2.2	6.796E-04	2.383E-04	2.852
JENDL/ENDF	*0.818*	*0.877*	*0.933*
JEF/ENDF	*0.805*	*0.875*	*0.920*

Table D.4. Production, absorption reaction rates and their ratios in start-up core (*cont.*)

	Production	Absorption	Production/Absorption
^{243}Am			
ENDF/B-VI	6.082E-05	1.036E-04	0.587
JENDL-3.2	5.923E-05	1.065E-04	0.556
JEF-2.2	5.955E-05	1.151E-04	0.517
JENDL/ENDF	*0.974*	*1.028*	*0.947*
JEF/ENDF	*0.979*	*1.111*	*0.881*
^{238}Pu			
ENDF/B-VI	2.617E-04	1.306E-04	2.003
JENDL-3.2	2.650E-04	1.258E-04	2.107
JEF-2.2	2.633E-04	1.195E-04	2.204
JENDL/ENDF	*1.013*	*0.963*	*1.052*
JEF/ENDF	*1.006*	*0.914*	*1.100*
^{242}Cm			
ENDF/B-VI	4.769E-05	2.994E-05	1.593
JENDL-3.2	2.073E-04	9.026E-05	2.297
JEF-2.2	1.663E-04	7.841E-05	2.121
JENDL/ENDF	*4.347*	*3.015*	*1.442*
JEF/ENDF	*3.487*	*2.619*	*1.331*
^{243}Cm			
ENDF/B-VI	6.075E-04	1.854E-04	3.277
JENDL-3.2	6.994E-04	2.205E-04	3.173
JEF-2.2	7.593E-04	2.296E-04	3.306
JENDL/ENDF	*1.151*	*1.189*	*0.968*
JEF/ENDF	*1.250*	*1.239*	*1.009*
^{244}Cm			
ENDF/B-VI	1.376E-04	8.795E-05	1.564
JENDL-3.2	1.291E-04	7.804E-05	1.654
JEF-2.2	1.308E-04	7.161E-05	1.827
JENDL/ENDF	*0.939*	*0.887*	*1.058*
JEF/ENDF	*0.951*	*0.814*	*1.168*
^{245}Cm			
ENDF/B-VI	5.733E-04	1.736E-04	3.302
JENDL-3.2	6.328E-04	1.970E-04	3.213
JEF-2.2	6.931E-04	1.955E-04	3.545
JENDL/ENDF	*1.104*	*1.135*	*0.973*
JEF/ENDF	*1.209*	*1.126*	*1.073*
^{246}Cm			
ENDF/B-VI	8.920E-05	3.774E-05	2.364
JENDL-3.2	8.113E-05	4.338E-05	1.870
JEF-2.2	8.920E-05	3.774E-05	2.364
JENDL/ENDF	*0.910*	*1.149*	*0.791*
JEF/ENDF	*1.000*	*1.000*	*1.000*

Table D.5. k_{eff} and reaction rates of ^{15}N, Bi and Pb at the middle position of fuel zone in start-up core

Reaction	elas	inela	n2n	nna	nnp	ng	np	nd	nt	na	k_{eff}
^{15}N											
ENDF/B-VI	2.736E-04	6.300E-08	1.481E-10	3.449E-11	7.582E-11	9.946E-10	8.261E-11	3.233E-10	5.147E-11	4.193E-10	1.00007
JEF-2.2	2.842E-04	3.632E-08	9.132E-11	1.947E-11	7.256E-11	3.558E-11	1.105E-10	2.604E-10	5.702E-11	3.695E-10	0.995843
JENDL-3.2	2.854E-04	3.632E-08	9.129E-11	1.946E-11	7.253E-11	3.556E-11	1.105E-10	2.603E-10	5.700E-11	3.695E-10	0.99551
^{209}Bi											
ENDF/B-VI	6.375E-04	6.352E-06	3.511E-08	4.000E-11	1.961E-13	6.115E-12	2.610E-07	4.933E-11	1.350E-12	1.006E-10	
JEF-2.2	6.684E-04	6.549E-06	3.761E-08	4.952E-11			3.756E-07	2.166E-12		4.767E-12	0.99934
JENDL-3.2	6.289E-04	6.451E-06	3.101E-08	5.021E-11	3.000E-13	3.959E-13	2.677E-07	2.430E-12	1.966E-12	6.817E-12	0.999303
Pb_{nat}											
JEF-2.2	6.268E-04	7.331E-06	3.006E-08	4.826E-11			2.995E-07				1.00687
JENDL-3.2	6.223E-04	9.156E-06	3.414E-08	2.699E-11	8.423E-15	2.821E-13	3.155E-07	4.047E-12		3.604E-12	0.988994

Table D.6. Partial reactions included in files

	nelas	ninel	n2n	n3n	nna	n2na	nnp	nnd	nnt	n2np	ng	np	nd	nt	nh	na
^{15}N																
ENDF/B-VI	o	o	o		o		o				o	o	o	o		o
JEF-2.2	o	o	o		o		o	o	o		o	o	o	o		o
JENDL-3.2	o	o	o		o		o	o	o		o	o	o	o		o
^{209}Bi																
ENDF/B-VI	o	o	o	o	o		o	o	o		o	o	o	o	o	o
JEF-2.2	o	o	o	o							o	o				o
JENDL-3.2	o	o	o	o	o		o				o	o	o			o
Pb_{nat}																
ENDF/B-VI																
JEF-2.2	o	o	o	o			o				o					
JENDL-3.2	o	o	o	o	o		o				o	o				o
^{206}Pb																
ENDF/B-VI	o	o	o	o							o	o		o		o
^{207}Pb																
ENDF/B-VI	o	o	o	o							o	o		o		o
^{208}Pb																
ENDF/B-VI	o	o	o	o	o	o	o	o	o	o	o	o	o	o		o

Table D.7. Influence of different fission spectra on k_{eff} differences

(1) 1-D results using fission spectrum weighted with the flux in library.
(2) 1-D results using fission spectrum weighted with the first calculated flux.
Reference k_{eff} (all ENDF/B-VI): (1) 1.00007, (2) 1.00249.

Exchanged nuclide (JEF-2.2)	(1)		(2)		Δk(2)/Δk(1)	Δk/atom**
	k_{eff}	Δk*	k_{eff}	Δk*		
^{237}Np	0.998257	-181	0.999802	-269	1.49	-6
^{241}Am	0.986861	-1321	0.985743	-1675	1.27	-21
^{242m}Am	0.996619	-345	0.999052	-344	1	-316
^{243}Am	0.992768	-730	0.993266	-922	1.26	-16
^{238}Pu	1.00073	66	1.00316	67	1.02	16
^{239}Pu	0.996104	-397	1.00039	-210	0.53	-4
^{240}Pu	0.998555	-152	1.00103	-146	0.96	-6
^{241}Pu	0.999424	-65	1.00176	-73	1.12	-6
^{242}Pu	1.00007	0	1.00248	-1	–	–
^{242}Cm	1.00008	1	1.0025	1	1	245
^{243}Cm	1.00102	95	1.00343	94	0.99	283
^{244}Cm	1.00118	111	1.00361	-112	1.01	5
^{245}Cm	1.00675	668	1.00944	695	1.04	220
^{246}Cm	–	–	–	–	–	–

Exchanged nuclide (JENDL-3.2)	(1)		(2)		Δk(2)/Δk(1)	Δk/atom**
	k_{eff}	Δk*	k_{eff}	Δk*		
^{237}Np	0.997425	-265	0.999514	-298	1.12	-7
^{241}Am	0.99744	-263	0.997273	-522	1.98	-6
^{242m}Am	0.997574	-250	0.999376	-311	1.24	-286
^{243}Am	0.99502	-505	0.995927	-656	1.3	-11
^{238}Pu	1.00067	60	1.00318	69	1.15	16
^{239}Pu	0.999828	-24	1.00213	-36	1.5	-1
^{240}Pu	0.997618	-245	1.00094	-155	0.63	-7
^{241}Pu	1.00114	107	1.00346	97	0.91	8
^{242}Pu	1.00007	0	1.00248	-1	–	–
^{242}Cm	1.00008	1	1.0025	1	1	245
^{243}Cm	1.00065	58	1.00306	57	0.98	171
^{244}Cm	0.999148	-92	1.0021	-39	0.42	-2
^{245}Cm	1.00266	259	1.00533	284	1.1	90
^{246}Cm	1.00006	-1	1.00248	-1	1	-19

* Δk values are relative to ENDF/B-VI results, in units of 1E-5.
** Δk/atom, in units of 1E-24.

LIST OF CONTRIBUTORS

Authors	
Marco Cometto (PSI, Switzerland) Peter Wydler (Switzerland)	Byung-Chan Na (OECD/NEA)

Secretariat
Byung-Chan Na (OECD/NEA)

Problem specification	
Peter Wydler (Switzerland)	Hideki Takano (JAERI, Japan)

Reviewers	
Tomas Lefvert (RIT, Sweden) Toshitaka Osugi (JAERI, Japan)	Giuseppe Gherardi (ENEA, Italy) Arjan Koning (NRG, The Netherlands)

Benchmark participants	
W.S. Yang (ANL, USA) C.G. Stenberg (ANL, USA) M. Embid (CIEMAT, Spain) J.M. García-Sanz (CIEMAT, Spain) E. González (CIEMAT, Spain) D. Cano-Ott (CIEMAT, Spain) D. Villamarín (CIEMAT, Spain) W.S. Park (KAERI, Korea) Y.N. Kim (KAERI, Korea) M. Cometto (PSI, Switzerland) P. Wydler (Switzerland) J-Ch. Bosq (CEA, France)	K. Nishihara (JAERI, Japan) K. Tsujimoto (JAERI, Japan) H. Takano (JAERI, Japan) K. Tucek (RIT, Swden) J. Wallenius (RIT, Swden) W. Gudowski (RIT, Swden) H. Wienke (SCK•CEN, Belgium) Ch. De Raedt (SCK•CEN, Belgium) H. Ait Abderrahim (SCK•CEN, Belgium) Th. Aoust (SCK•CEN, Belgium) E. Malambu (SCK•CEN, Belgium)

Sensitivity analysis	
Jung-Do Kim (KAERI, Korea)	Choong-Sup Gil (KAERI, Korea)

ALSO AVAILABLE

NEA Publications of General Interest

2000 Annual Report (2001) *Free: paper or Web.*

NEA News
ISSN 1605-9581 Yearly subscription: € 37 US$ 45 GBP 26 ¥ 4 800

Geologic Disposal of Radioactive Waste in Perspective (2000)
ISBN 92-64-18425-2 Price: € 20 US$ 20 GBP 12 ¥ 2 050

Nuclear Science

Fission Gas Behaviour in Water Reactor Fuels (2002)
ISBN 92-64-19715-X Price: € 120 US$ 107 GBP 74 ¥ 12 100

Shielding Aspects of Accelerators, Targets and Irradiation Facilities – SATIF 5 (2001)
ISBN 92-64-18691-3 Price: € 84 US$ 75 GBP 52 ¥ 8 450

Nuclear Production of Hydrogen (2001)
ISBN 92-64-18696-4 Price: € 55 US$ 49 GBP 34 ¥ 5 550

Forsmark 1 & 2 Boiling Water Reactor Stability Benchmark(2001)
ISBN 92-64-18669-4 *Free on request.*

Pyrochemical Separations (2001)
ISBN 92-64-18443-0 Price: € 77 US$ 66 GBP 46 ¥ 7 230

Evaluation of Speciation Technology (2001)
ISBN 92-64-18667-0 Price: € 80 US$ 70 GBP 49 ¥ 7 600

Core Monitoring for Commercial Reactors: Improvements in Systems and Methods (2000)
ISBN 92-64-17659-4 Price: € 74 US$ 71 GBP 44 ¥ 7 450

3-D Radiation Transport Benchmarks for Simple Geometries with Void Regions
(2000) ISBN 92-64-18274-8 *Free on request.*

Benchmark Calculations of Power Distribution Within Fuel Assemblies
Phase II: Comparison of Data Reduction and Power Reconstruction Methods in Production Codes
(2000) ISBN 92-64-18275-6 *Free on request.*

Benchmark on the VENUS-2 MOX Core Measurements (2000) ISBN 92-64-18276-4 *Free on request.*

Calculations of Different Transmutation Concepts: An International Benchmark Exercise
(2000) ISBN 92-64617638-1 *Free on request.*

Prediction of Neutron Embrittlement in the Reactor Pressure Vessel: VENUS-1 and VENUS-3 Benchmarks
(2000) ISBN 92-64-17637-3 *Free on request.*

Pressurised Water Reactor Main Steam Line Break (MSLB) Benchmark
(2000) ISBN 92-64-18280-2 *Free on request.*

International Evaluation Co-operation *(Free on request)*

Volume 1: *Comparison of Evaluated Data for Chromium-58, Iron-56 and Nickel-58* (1996)
Volume 2: *Generation of Covariance Files for Iron-56 and Natural Iron* (1996)
Volume 3: *Actinide Data in the Thermal Energy Range* (1996)
Volume 4: *^{238}U Capture and Inelastic Cross-Sections* (1999)
Volume 5: *Plutonium-239 Fission Cross-Section between 1 and 100 keV* (1996)
Volume 8: *Present Status of Minor Actinide Data* (1999)
Volume 10: *Evaluation Method of Inelastic Scattering Cross-sections for Weakly Absorbing Fission-product Nuclides* (2001)
Volume 12: *Nuclear Model to 200 MeV for High-Energy Data Evaluations* (1998)
Volume 13: *Intermediate Energy Data* (1998)
Volume 14: *Processing and Validation of Intermediate Energy Evaluated Data Files* (2000)
Volume 15: *Cross-Section Fluctuations and Shelf-Shielding Effects in the Unresolved Resonance Region* (1996)
Volume16: *Effects of Shape Differences in the Level Densities of Three Formalisms on Calculated Cross-Sections* (1998)
Volume 17: *Status of Pseudo-Fission Product Cross-Sections for Fast Reactors* (1998)
Volume 18: *Epithermal Capture Cross-Section of ^{235}U* (1999)

Order form on reverse side.

ORDER FORM

OECD Nuclear Energy Agency, 12 boulevard des Iles, F-92130 Issy-les-Moulineaux, France
Tel. 33 (0)1 45 24 10 15, Fax 33 (0)1 45 24 11 10, E-mail: nea@nea.fr**, Internet: www.nea.fr**

Qty	Title	ISBN	Price	Amount
			Total	

❑ Payment enclosed (cheque or money order payable to OECD Publications).

Charge my credit card ❑ VISA ❑ Mastercard ❑ Eurocard ❑ American Express

Card No.	Expiration date	Signature
Name		
Address	Country	
Telephone	Fax	
E-mail		

OECD PUBLICATIONS, 2 rue André-Pascal, 75775 PARIS CEDEX 16
Printed in France.